Dynamics and stability of self-organized atomic crystals in optical cavities

Dissertation
zur Erlangung des Grades
des Doktors der Naturwissenschaften
der Naturwissenschaftlich-Technischen Fakultät
der Universität des Saarlandes

von

Stefan Schütz

Saarbrücken

2016

Tag des Kolloquiums:	10.01.2017
Dekan:	Univ.-Prof. Dr. G. Kickelbick
Mitglieder des Prüfungsausschusses:	
Vorsitzender:	Univ.-Prof. Dr.-Ing. M. Vielhaber
Gutachter:	Univ.-Prof. Dr. G. Morigi
	Univ.-Prof. Dr. Dr. K. Kruse
	Prof. Dr. S. Diehl
Akad. Mitarbeiterin:	Dr. N. Kukharchyk

Eidesstattliche Versicherung

Hiermit versichere ich an Eides statt, dass ich die vorliegende Arbeit selbstständig und ohne Benutzung anderer als der angegebenen Hilfsmittel angefertigt habe. Die aus anderen Quellen oder indirekt übernommenen Daten und Konzepte sind unter Angabe der Quelle gekennzeichnet. Die Arbeit wurde bisher weder im In- noch im Ausland in gleicher oder ähnlicher Form in einem Verfahren zur Erlangung eines akademischen Grades vorgelegt.

Ort, Datum

Unterschrift

Zusammenfassung

Diese Arbeit befasst sich mit der Theorie von Atomen, die an das Quantenlichtfeld eines optischen Resonators koppeln und durch Laser getrieben werden. Die Untersuchungen behandeln einen Bereich, in dem die Atome oberhalb eines kritischen Wertes der Laserintensität spontan regelmäßige räumliche Strukturen bilden, die durch die mechanischen Effekte des Lichtes stabilisiert werden. Die Dynamik, die zu selbstorganisierten Mustern führt, wird systematisch und im semiklassischen Grenzfall beschrieben, wohingegen das Resonatorfeld als Quantenvariable behandelt wird. Die Eigenschaften im Gleichgewicht und außerhalb des Gleichgewichtes werden untersucht, die experimentellen Observablen werden charakterisiert. Es wird gezeigt, dass diese Systeme eine eindrucksvolle Plattform bilden, um Kritikalität in getriebenen dissipativen Systemen mit langreichweitigen Wechselwirkungen zu untersuchen, die in diesem Fall durch mehrfache Photonenstreuung zwischen den Atomen hervorgerufen werden. Die Anwendbarkeit auf eine große Anzahl an Atomen bei ultrakalten Temperaturen wird im Kontext andauernder Experimente diskutiert.

Abstract

This work deals with the theory of atoms coupled to the quantum light field of an optical resonator and driven by lasers. The studies address a regime where, above a critical value of the laser intensity, the atoms spontaneously form regular spatial structures, stabilized by the mechanical effects of the light. A systematic description of the dynamics leading to self-organized patterns is provided in the semiclassical limit, whereas the resonator field is treated as a quantum variable. The equilibrium and out-of-equilibrium properties are determined, the experimental observables are characterised. It is shown that these systems constitute a formidable platform to study criticality in driven-dissipative systems characterized by long-range interactions, which here arise from multiple photon scattering between the atoms. Applications for large atomic samples at ultralow temperatures are discussed in the context of ongoing experiments.

Contents

Introduction

Research context

The control of mechanical effects of light on matter is the basis of several techniques for manipulating the quantum state of physical systems in the microsopic (and also in the mesoscopic) realm [1, 2]. This is a result of the astonishing achievements in cooling and trapping atoms with laser light [3, 4, 5] at the end of the 20th century, being awarded by the Nobel Prize in Physics [6, 7, 8]. Prominent examples are the creation and manipulation of crystalline structures of atoms due to the interaction with a light field [9, 10] that shows, for instance, a periodically modulated intensity (optical lattice) [11]. Recently, the strong coupling of atoms and molecules to the field of a resonator (cavity) has been achieved, opening novel perspectives of control [12, 13, 14, 15, 16, 17]. In this scenario, usually, the quantum light field can not be considered as an independent component of the dynamics, as it is strongly affected by the presence of the atoms. Vice versa, the cavity field acts back on the atomic motion by the mechanical effects of the light (cavity backaction). This, in total, constitutes a prototype of an optomechanical system [18, 19, 20]. This thesis aims at providing a theoretical framework for studying those dynamics, that is based on the effective interactions between atoms, mediated by a common atomic coupling to the field inside the resonator [14, 21].

The optomechanical dynamics of photons and atoms in a cavity is known to give rise to intriguing pheonomena, such as bistability [22, 23, 24], synchronization [25, 26] and self-ordering [27, 28, 29, 30]. Those effects are mostly triggered by the long-range interactions [31] that are mediated by multiple photon scattering and which induce collective phenomena. By this means, atom-cavity setups can be shown to share several analogies with extensively studied long-range interacting systems [32, 33, 34], such

as gravitational clusters, plasmas or coupled oscillators [35, 36]. In fact, in certain limits, the observed collective effects in cavities can be reduced to a long-range Hamiltonian which reflects the observed phenomenon [37, 38]. Nevertheless, in general, one deals with an open system, as cavity photons are lost via the mirrors [39]. For instance, dissipation can be used to tailor processes in which kinetic energy is extracted from the atoms and by this cool matter, known as cavity cooling [40, 41, 42, 43, 44]. Photon losses can be compensated for by an external laser pumping on the system. This might be realized by driving the atoms and/or the cavity by laser light. Here, the strength of the drive can determine whether strong collective effects emerge or not. Indeed, in several scenarios, there exists a critical value of the pump strength which separates two distinct phases of matter (and/or the light field), for instance non-synchronized (unordered) from synchronized (ordered), reminiscent of a phase transition [27, 45, 46, 47, 48].
One of the main questions that arises in such a driven-dissipative long-range interacting many-body quantum system is related to the characterization of the steady state that the system adopts, in particular, whether it can be described by thermal equilibrium [49, 50, 51, 52]. Further interest is dedicated to the aspects of relaxation towards steady state [53]. In long-range interacting (Hamiltonian) systems it is known that long-lived metastable states may emerge, in which the system may reside for a long time before reaching the steady state [35, 54, 55, 56, 57, 58]. Recent studies investigate the robustness of these out-of-equilibrium states and the possible modifications of the relaxation processes in such systems in the presence of noise and dissipation or specific perturbations [59, 60, 61, 62, 63]. The atom-cavity setup, discussed in the following and mainly considered throughout this thesis, constitutes a driven long-range interacting system, in which dissipation and noise are intrinsically present. It therefore represents a remarkable platform to study the out-of-equilibrium dynamics of long-range interacting systems in a noisy environment [64].

Self-organization and state-of-the-art

In this thesis, we consider the interaction of N atoms with the electric field of a cavity mode, see Fig. 1. Individual processes of atom-photon interactions rely on the absorption/emission or virtual scattering of photons by the atoms. Each photon (elementary bosonic excitations of the light field) carries a momentum of the amount $\hbar k$ [65] which is exchanged with the atom, with $\hbar$ Planck's constant and k the wavevector of the light field. Here, we restrict to a regime in which this field is far-detuned from any atomic dipolar transition (dispersive regime), giving rise to an effective optomechanical atom-field coupling [18], in which the atoms redistribute photons by virtual scattering. The setup includes an additional far-off-resonance transverse laser drive (frequency ω_L) for the atoms (dipole-field coupling

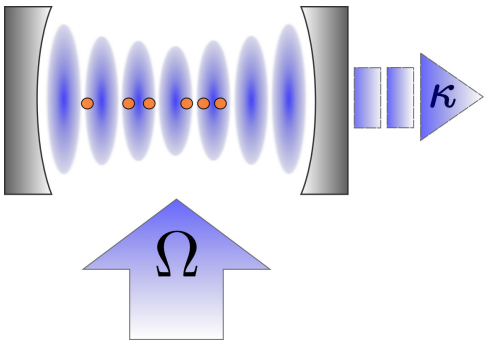

Figure 1: Atoms in a single-mode standing-wave cavity and driven by a transverse laser can spontaneously form ordered patterns when the laser intensity Ω exceeds the rate of photon losses, here due to cavity decay at rate κ. In this regime the atoms experience a long-range interaction mediated by the cavity photons and their motion becomes strongly correlated. Taken from Ref. [64].

Ω) [45, 66]. Those sustain the intracavity field by scattering photons from the laser into the cavity mode (with frequency ω_c , $\omega_L \approx \omega_c$) by Rayleigh scattering. This gain in cavity photons competes with photon losses (with rate 2κ) due to a finite transmittivity of the cavity mirrors. Those processes characterize the presented system as a driven-open one. Some of the central aspects, addressed in this thesis, concern the out-of-equilibrium dynamics and the thermodynamical properties of this system, including detailed studies on the spatial structure that the atoms adopt due to the forces associated with the mechanical effects of the light [14].

In the setup of Fig. 1, for a homogeneous atomic distribution along the cavity axis, the mean intracavity field vanishes (destructive interference of the scattered photons) and with it the mean force: force fluctuations arise from finite density fluctuations and the quantum fluctuations of the light field [67]. When the atoms, instead, form atomic Bragg gratings (interparticle distance of multiples of the cavity wavelength $\lambda = 2\pi/k$) at the antinodes of the cavity mode (positions of maximal coupling), the scattered photons constructively interfere. Those configurations can be stabilized by the mechanical effects of the cavity light field, provided that the laser drive Ω exceeds a threshold value, such that collective atomic photon scattering overcomes the photon losses. The atoms organize in the scattered potential [68]. This phenomenon is referred to as self-organization.

Self-organization has been theoretically predicted in [45], with first experimental evidence found in [69]. These findings set the starting point for many subsequent theoretical and experimental studies on self-organization, for both a thermal cloud of atoms [43, 48, 66] and atomic ensembles in the ultracold realm [37, 38, 39, 47, 50, 67, 70, 71, 72, 73]. This

thesis provides theoretical results on self-organization for thermal atoms – and thus in the semiclassical regime of atomic motion [74] – delivering new insight and results which concern, amongst others, the following points: **(i)** Several theoretical studies impose a semiclassical limit or mean-field description on the cavity field, valid for large photon numbers [43, 45, 66, 75]. The present work delivers an approach in which the cavity field is treated fully quantum-mechanically [74]. This allows for consistent results also in the homogeneous phase, in which field fluctuations can not be discarded, see Chapter 1 (Ref. [74]). **(ii)** The transition to spatially ordered patterns has often been regarded as a second-order phase transition, conjectures were mostly drawn with mean-field treatments or methods of stability analysis [43, 66]. We confirm this hypothesis by an explicit mapping of the free energy to a Landau model at steady state [76, 77], which is analysed in detail, see Chapter 3 (Ref. [77]). **(iii)** The long-range character for the atom-atom interactions, mediated by the cavity field, is well-known [18]. We draw explicit connections to studies in long-range interacting systems [54] and show related relaxation dynamics by performing quenches across the phase transition [64, 78]. Our findings reveal the emergence of long-lived metastable states which are out-of-equilibrium, go beyond a mean-field description, and, surprisingly, are induced by dissipation [79], as discussed in Chapter 6.

Outline of the thesis and internal context

Chapter 1 (Ref. [74]) describes the nonlinear atom-field dynamics for laser-driven atoms in an optical cavity in a regime for which a time-scale separation between field and atomic dynamics applies ($\kappa \gg \omega_r$, the latter being the recoil frequency). In this regime, the cavity field can be eliminated quasi-adiabatically, the atomic motion is treated semiclassically by using a consistent perturbative expansion in $\sqrt{\omega_r/\kappa}$. The resulting time evolution for the atomic phase-space distribution function [80] for N atoms adopts the form of a Fokker-Planck Equation (FPE) [81], that can be simulated by numerically integrating equivalent Stochastic Differential Equations (SDEs) [82, 83]. In the regime of low laser drive, the cooling rate and final temperature for the atomic ensemble are studied, comparing the results with findings in the literature [43]. This optomechanical cooling mechanism [12, 16, 43, 75, 84, 85] is denoted as cavity cooling and is, in general, applicable to any polarizable particles, including molecules [86].
Chapter 2 (Ref. [64]) contains the analysis of the FPE for the atomic motion, derived in Chapter 1, for arbitrary pump intensities and thus in both phases (homogeneous and ordered). In particular, it provides an analytical solution for the (thermal) steady state in the regime far from bistability (small cavity shifts). Furthermore, the effective atom-atom long-range interactions are identified [35, 54], while the observed out-of-equilibrium

dynamics (prethermalization) will be further studied in Chapter 6.
Chapter 3 (Ref. [77]) analyses the steady state, presented in the previous chapter, in more detail. On the one hand, the stability of the Bragg gratings is investigated by numerical simulations. On the other hand, the properties of the cavity light field are determined, including the mean intracavity photon number, the photon statistics and the spectrum at the cavity output [67, 72]. This chapter contains an explicit mapping of the free energy of the atoms to a Landau model (that describes a second-order phase transition) for a convenient order parameter Θ [66], identifying the two stable (equally probable) Bragg configurations [$\Theta \approx 1$ (even) and $\Theta \approx -1$ (odd)] with a magnetization.
An imbalance in the emergence of those even and odd patterns can be induced by an additional (horizontal) laser drive of the cavity mode, which is only taken into account and discussed in **Chapter 4** (Ref. [87]). These studies include a temporal change of the phase of the cavity laser drive, allowing for a switching between the two configurations and deterministically choosing one desired pattern ('pattern seeding').
Chapter 5 (Ref. [88]) contains a mean-field description for laser-driven atoms in optical cavities (see Fig. 1) that imposes a factorization ansatz for the atomic N-particle distribution function of the previous chapters (Chapter 1-3). The transition to spatially ordered patterns is well reproduced within this formalism. We show that the latter, instead, fails in correctly predicting all the dynamical features that are observed after performing a quench (sudden temporal change of the control parameter) across the driven-dissipative phase transition.
Chapter 6 (Ref. [78]) focuses on such quenches from the disordered ($\Theta \approx 0$) to the ordered ($|\Theta| \approx 1$) phase and, by this, on the onset of self-organization due to the interplay of dispersive and dissipative long-range forces. We verify that the mean-field approach of the previous chapter is (only) suitable for describing the short-time dynamics. Indeed, several dynamical stages are identified and analysed, drawing analogy to long-range interacting systems [35, 54], in which long-lived prethermalized states are found [58]. While in many recent studies those metastable states have been verified to being destroyed by noise [59, 62, 63], it is shown that, in our case, the peculiar long-range character of the intrinsically present noise [89] can further extend the prethermalized stage and substantially modify relaxation [90].
Chapter 7 (Ref. [91]) deals with studies on a setup, in which the coherent laser drive is replaced by an incoherent drive, allowing for population inversion in the effective two-level atomic spins with an ultranarrow transition. In fact, the internal atomic degrees are crucial for the discussed phenomena in this chapter: dipole-dipole interactions, induced by the common coupling to a lossy cavity mode [46, 92], can lead to synchronization [36] among the dipoles. Associated mechanical effects have been studied [93, 94, 95], but still are to some extent unexplored and especially addressed in this chapter:

we report on giant frictional forces on the atoms due to cavity-induced spin-spin correlations.

This thesis is closed by the conclusions, providing a summary and an outlook with open questions that could be addressed in future studies.

Contributions of the author of this dissertation

This cumulative thesis contains 7 manuscripts/publications, organized in chapters. The following list solely aims at specifying the aspects to which the author of this dissertation contributed in the manuscripts, it does *not* imply that the other authors had no contribution to these points. A more detailed statement, describing the contributions to the respective manuscript of all the authors, can be found on the first page of the respective chapters.

Chapter 1 (Ref. [74])
development of theoretical model; design and performance of numerical simulations; derivation of analytical results; checking, discussing and analysing the calculations and results; writing of the article

Chapter 2 (Ref. [64])
development of theoretical model; design and performance of numerical simulations; checking, discussing and analysing the calculations and results; writing of the article

Chapter 3 (Ref. [77])
development of theoretical model; performance of analytical calculations; design and performance of numerical simulations; checking, discussing and analysing the calculations and results; writing of the article

Chapter 4 (Ref. [87])
checking, discussing and analysing the calculations and results

Chapter 5 (Ref. [88])
development of the theoretical model; performance of numerical simulations; checking, discussing and analysing the calculations and results; writing of the article

Chapter 6 (Ref. [78])
development of the theoretical model; performance of analytical and numerical calculations; checking, discussing and analysing the calculations and results; writing of the article

Chapter 7 (Ref. [91])
development of the theoretical model; checking, discussing and analysing the calculations and results

CHAPTER 1

Cooling of atomic ensembles in optical cavities: Semiclassical limit

Cooling of atomic ensembles in optical cavities: Semiclassical limit

PHYSICAL REVIEW A **88**, 033427 (2013)

DOI: 10.1103/PhysRevA.88.033427

Authors: Stefan Schütz,[1,*] Hessam Habibian,[1,2,3] and Giovanna Morigi[1]

[1] *Theoretische Physik, Universität des Saarlandes, D-66123 Saarbrücken, Germany*
[2] *Departament de Física, Universitat Autònoma de Barcelona, E-08193 Bellaterra, Spain*
[3] *ICFO – Institut de Ciències Fotòniques, Mediterranean Technology Park, E-08860 Castelldefels (Barcelona), Spain*
[*] *stefan.schuetz@physik.uni-saarland.de*

Author Contributions:
The theoretical model was developed by S. Schütz, H. Habibian, and G. Morigi. Numerical simulations were designed and performed by S. Schütz. Analytical results were derived by S. Schütz. The calculations and results were checked, discussed and analysed by all three authors. The article was majorly written by G. Morigi and S. Schütz.

Abstract:
The semiclassical dynamics of atoms, when the atoms are confined inside a standing-wave high-finesse resonator, is theoretically studied. The atoms are

cooled by scattering processes in which the photons of a transverse laser are coherently scattered into the cavity mode. We derive a Fokker-Planck equation for the atomic center-of-mass variables which allows us to determine the equations of motion in the semiclassical limit for any value of the intensity of the laser field. We extract its prediction for the dynamics when the resonator is essentially in the vacuum state and the atoms are cooled by scattering photons into the cavity mode, which then decays. Its predictions for the stationary atomic distribution are compared with the ones of the Fokker-Planck equation by Domokos et al. [J. Phys. B **34**, 187 (2001)], which has been derived under different assumptions. We find full agreement in the considered parameter regime.

PHYSICAL REVIEW A **88**, 033427 (2013)

Cooling of atomic ensembles in optical cavities: Semiclassical limit

Stefan Schütz,[1,*] Hessam Habibian,[1,2,3] and Giovanna Morigi[1]

[1]*Theoretische Physik, Universität des Saarlandes, D-66123 Saarbrücken, Germany*

[2]*Departament de Física, Universitat Autònoma de Barcelona, E-08193 Bellaterra, Spain*

[3]*ICFO — Institut de Ciències Fotòniques, Mediterranean Technology Park, E-08860 Castelldefels (Barcelona), Spain*

(Received 10 July 2013; published 30 September 2013)

The semiclassical dynamics of atoms, when the atoms are confined inside a standing-wave high-finesse resonator, is theoretically studied. The atoms are cooled by scattering processes in which the photons of a transverse laser are coherently scattered into the cavity mode. We derive a Fokker-Planck equation for the atomic center-of-mass variables which allows us to determine the equations of motion in the semiclassical limit for any value of the intensity of the laser field. We extract its prediction for the dynamics when the resonator is essentially in the vacuum state and the atoms are cooled by scattering photons into the cavity mode, which then decays. Its predictions for the stationary atomic distribution are compared with the ones of the Fokker-Planck equation by Domokos *et al.* [J. Phys. B **34**, 187 (2001)], which has been derived under different assumptions. We find full agreement in the considered parameter regime.

DOI: 10.1103/PhysRevA.88.033427 PACS number(s): 37.10.Vz, 37.30.+i, 42.50.Pq, 03.65.Sq

I. INTRODUCTION

The possibility of cooling and trapping the atomic motion by means of electromagnetic radiation has been remarkably advanced in atomic physics and quantum optics, which was officially recognized with the Nobel Prize in physics in 1997 [1]. In a nutshell, radiative scattering can cool the motion of atoms by means of the mechanical effects of atom-photon interactions. This is achieved by scattering processes, in which the transition rate to states with lower mechanical energy is enhanced by suitably driving an atomic transition, so that the frequency of the absorbed photon is, on average, smaller than that of the emitted one [2,3]. In the presence of high-finesse optical resonators, these processes can be tailored using the strong coupling with the cavity field [4–9].

A remarkable property of the mechanical effects of light inside a high-finesse resonator is the collective phenomena due to multiple scattering of photons, which mediate an effective interaction between the atoms. They give rise to nonlinear dynamics, such as bistability induced by the nonlinear coupling with the motional degrees of freedom [10], synchronization [11], and collective-atomic recoil lasing [12]. In single-mode standing-wave cavities, they can lead to the formation of spatially ordered structures [13–17]. This phenomenon is found in a setup, such as the one sketched in Fig. 1, where the atoms are confined inside a resonator and are driven by a transverse laser. It exhibits a threshold, which is mainly determined by the intensity of the laser. Above threshold, ordered atomic structures (Bragg gratings) form, which coherently scatter photons into the cavity resonator and, vice versa, the cavity field stably traps the atoms in the grating [14,15,17].

The theory of self-organization in laser-cooled atomic ensembles coupled to cavities has been pioneered by Ritsch and coworkers [18], who derived a Fokker-Planck equation describing the coupled dynamics of cavity field and atoms in the limit in which the atomic and field variables can be treated semiclassically [19]. On this basis, the self-organization threshold has been determined [17] and numerical simulations of the system dynamics were performed [18]. This theoretical model does not describe, however, the properties of the cavity field, which is treated in the semiclassical limit. The semiclassical approximation, in fact, breaks down when the intracavity field is small, namely, below and close to the self-organization threshold. Close to threshold, when the patterns are formed, in particular, fluctuations are expected to become larger and larger [13,17]. This calls for developing a unifying theoretical formalism which allows one to describe the coupled atom-field dynamics below, at, and above the self-organization threshold.

In this work, we derive the Fokker-Planck equation governing the atomic dynamics, which is valid for any value of the intracavity field amplitude. This is obtained by following the procedure developed in Refs. [20–22], which allows us to derive an effective Fokker-Planck equation for the atomic motion, in which the cavity field is treated quantum mechanically. This treatment leads to equations of motion which can be simulated by means of stochastic differential equations [19,23,24]. The numerical simulations allow for a reliable description of the dynamics without further assumptions on the state of the intracavity field. As an example, we determine the momentum distribution when the loss rates are much larger than the pump rate, so that the intracavity field is essentially in the vacuum. We then compare the predictions of our model on the atomic distribution with the predictions extracted with the model in Refs. [19,25]. This article is organized as follows. In Sec. II, the theoretical model is introduced and the effective master equation, describing the coupled dynamics of cavity and atoms, is obtained after eliminating the excited state of the atoms in second-order perturbation theory. The Fokker-Planck equation for the atomic dynamics is derived in Sec. III, and the numerical simulations of the center-of-mass motion dynamics are reported and discussed in Sec. IV. The conclusions are drawn in Sec. V. The appendices report details of the calculations in Secs. III and IV.

*stefan.schuetz@physik.uni-saarland.de

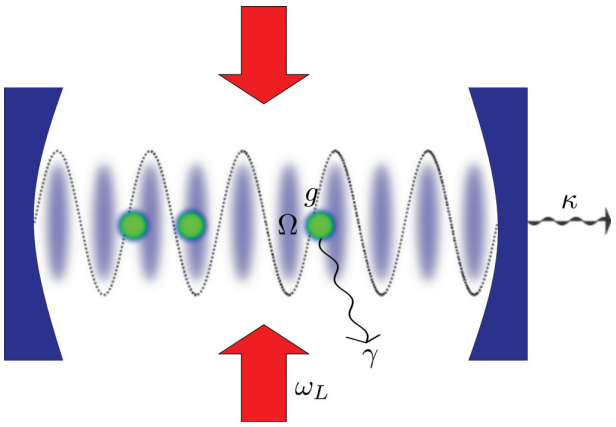

FIG. 1. (Color online) A gas of atoms is confined within a standing-wave resonator and is illuminated by a transverse laser. A dipolar transition of the atoms couples quasiresonantly with the fields and scatters photons from the laser into the cavity. We analyze the dynamics of the atomic center-of-mass motion and steady state in the semiclassical regime.

II. THEORETICAL MODEL

In this section, we derive the master equation which is at the basis of the semiclassical treatment in Sec. III. This effective master equation is obtained for a system of atoms inside the cavity and illuminated by a transverse pump, in the limit in which the atomic transition is driven below saturation. It thus describes the coupled dynamics of atomic center-of-mass motion and cavity field.

A. The system

The physical system is illustrated in Fig. 1: N atoms are confined inside a resonator and their dipolar transitions scatter photons of a transverse laser and of the mode of a standing-wave cavity. The atoms are sufficiently hot to be considered distinguishable. For the sake of generality, we also assume that they can be of different species. We denote by m_j the mass of atom $j = 1,\ldots,N$, and by $|g\rangle_j$ and $|e\rangle_j$ we denote the ground and excited state of the corresponding dipolar transition, whose frequency ω_j is quasiresonantly coupled with the laser and with the cavity field (the position dependence of the transition frequency also takes into account possible spatial inhomogeneities). The laser is here assumed to be a classical standing-wave field with frequency ω_L and wave vector perpendicular to the cavity axis, while the cavity mode is a quantum field of frequency ω_c and wave vector k. The cavity and laser field have the same linear polarization, so that they both drive the atomic dipolar transitions. We denote by $\hat{a}$ and $\hat{a}^\dagger$ the annihilation and creation operators, respectively, of a cavity photon, with $[\hat{a},\hat{a}^\dagger] = 1$.

The center-of-mass motion of the atoms is restricted to the cavity axis, which here corresponds to the x axis. The position and canonically conjugated momentum of atom j are given by the operators $\hat{x}_j$ and $\hat{p}_j$, such that $[\hat{x}_j,\hat{p}_k] = i\hbar\delta_{jk}$, with δ_{jk} as the Kronecker delta. Internal and external degrees of freedom of the atoms couple via the mechanical effects of atom-photon interactions. Our purpose is to provide a theoretical description of the scattering dynamics leading to cooling of the atomic motion.

We start with the master equation for the density matrix $\hat{\rho}$ for the cavity and for the atoms' internal and external degrees of freedom, which reads

$$\frac{\partial}{\partial t}\hat{\rho} = -\frac{i}{\hbar}[\hat{\mathcal{H}},\hat{\rho}] + \mathcal{L}_\kappa\hat{\rho} + \mathcal{L}_\gamma\hat{\rho} \quad (1)$$

$$\equiv \mathcal{L}\rho, \quad (2)$$

where $\mathcal{L}$ is the corresponding Lindbladian. Master equation (1) is reported in the reference frame rotating at the laser frequency ω_L. Here, the coherent dynamics are governed by the Hamiltonian

$$\hat{\mathcal{H}} = \sum_{j=1}^{N}\frac{\hat{p}_j^2}{2m_j} - \hbar\Delta_c\hat{a}^\dagger\hat{a} - \sum_{j=1}^{N}\hbar\Delta_j\hat{\sigma}_j^\dagger\hat{\sigma}_j + \sum_{j=1}^{N}\hbar g_j(\hat{x}_j)(\hat{a}^\dagger\hat{\sigma}_j + \hat{\sigma}_j^\dagger\hat{a}) + \sum_{j=1}^{N}\hbar\Omega_j(\hat{\sigma}_j^\dagger + \hat{\sigma}_j), \quad (3)$$

where $\hat{\sigma}_j = |g\rangle_j\langle e|$ and $\hat{\sigma}_j^\dagger$ is its adjoint, $\Delta_c = \omega_L - \omega_c$ and $\Delta_j = \omega_L - \omega_j$ are the detunings of the laser frequency from the cavity frequency ω_c and from the atomic transition frequency ω_j, respectively; Ω_j is the real-valued coupling strength of atom j with the laser, and $g_j(\hat{x}_j) = g_j\cos(k\hat{x}_j)$ is the real-valued coupling of the atomic transition, with g_j the vacuum Rabi frequency for the atom j and $\cos(kx)$ the spatial mode function.

The incoherent dynamics is assumed to be due to cavity losses, at rate κ, and to radiative decay of the atoms excited states, at rate γ_j. They are described by the superoperators

$$\mathcal{L}_\kappa\hat{\rho} = -\kappa(\hat{a}^\dagger\hat{a}\hat{\rho} + \hat{\rho}\hat{a}^\dagger\hat{a} - 2\hat{a}\hat{\rho}\hat{a}^\dagger), \quad (4)$$

$$\mathcal{L}_\gamma\hat{\rho} = -\sum_{j=1}^{N}\frac{\gamma_j}{2}(\hat{\sigma}_j^\dagger\hat{\sigma}_j\hat{\rho} + \hat{\rho}\hat{\sigma}_j^\dagger\hat{\sigma}_j) + \mathcal{J}\hat{\rho}\,, \quad (5)$$

where

$$\mathcal{J}\hat{\rho} = \sum_{j=1}^{N}\gamma_j\int_{-1}^{1}duN_j(u)|g\rangle\langle e|_j e^{-ik_j u\hat{x}_j}\hat{\rho}e^{ik_j u\hat{x}_j}|e\rangle\langle g|_j. \quad (6)$$

This term describes the jump from $|e\rangle_j$ to $|g\rangle_j$ due to spontaneous decay and takes into account the momentum transfer along the cavity axis to the atom due to spontaneous emission [26]. Here, the dipole radiation pattern $N_j(u)$ is normalized and symmetric about $u = 0$. For later convenience, we define its second moment by $(\overline{u^2})_j$, such that

$$\int_{-1}^{1}duN_j(u)u^2 = (\overline{u^2})_j\,. \quad (7)$$

B. Adiabatic elimination of the excited state

We now proceed in deriving the master equation for the cavity field and atoms' center-of-mass motion when the occupation of the atomic excited states can be neglected. Let us first assume that the particles do not move. In this case, their coupling g_j with the cavity field is fixed, and the excited

state can be eliminated in second order in an expansion in the parameter $1/|\Delta_j|$, assuming that $|\Delta_j| \gg \gamma_j/2, \Omega_j$ and $|\Delta_j| \gg |\Delta_c|, \kappa, g_j\sqrt{\bar{n}}$, with $\bar{n}$ is the mean photon number in the cavity. For N atoms, the condition on the coupling strengths becomes $|\Delta_j| \gg \sqrt{N}\Omega_j, \sqrt{N}(g_j\sqrt{\bar{n}})$; see [27]. When the center-of-mass motion is considered, on the other hand, the coupling strength g_j varies as a function of time. Moreover, atoms with different velocities experience different Doppler shifts, which modify the resonance condition. These effects can be neglected when the corresponding time scales are longer than the typical time scale in which the excited state is occupied, i.e., when $k\bar{p}_j/m_j \ll |\Delta_j|$ (with $\bar{p}_j = \sqrt{\langle p_j^2 \rangle}$), which is satisfied when the atomic gas has previously been Doppler cooled [3,28].

Formally, the effective master equation describing the dynamics of cavity field and atoms' center-of-mass motion is obtained by deriving a closed equation of motion for the reduced density operator $\hat{v}$ when the atoms are all in the internal ground state $|\boldsymbol{g}\rangle = |g_1, g_2, \ldots, g_N\rangle$. The reduced density operator $\hat{v}$ is defined as $\hat{v} = P\hat{\rho}$, where

$$\hat{v} = P\hat{\rho} = |\boldsymbol{g}\rangle\langle\boldsymbol{g}|\langle\boldsymbol{g}|\hat{\rho}|\boldsymbol{g}\rangle, \tag{8}$$

such that $\hat{\rho} = \hat{v} + \hat{w}$ with

$$\hat{w} = Q\hat{\rho}, \tag{9}$$

where P and $Q = 1 - P$ are projectors ($P^2 = P$, $Q^2 = Q$, $P^\dagger = P$, $Q^\dagger = Q$) and $(P + Q)\hat{\rho} = \hat{\rho}$. In order to adiabatically eliminate the excited state, we rewrite the Lindbladian as $\mathcal{L} = (P + Q)\mathcal{L}(P + Q)$ and introduce the decomposition

$$\mathcal{L} = \mathcal{L}^A + \mathcal{L}^F + \mathcal{J} + \mathcal{L}^{\rm int}, \tag{10}$$

where

$$\mathcal{L}^F\hat{\rho} = -\frac{i}{\hbar}\left[\sum_{j=1}^{N}\frac{\hat{p}_j^2}{2m_j} - \hbar\Delta_c\hat{a}^\dagger\hat{a}, \hat{\rho}\right] + \mathcal{L}_\kappa\hat{\rho}, \tag{11}$$

with $\mathcal{L}^F P = P\mathcal{L}^F$. Term

$$\mathcal{L}^A\hat{\rho} = \sum_{j=1}^{N}\left[i\Delta_j[|e\rangle_j\langle e|, \hat{\rho}] - \frac{\gamma_j}{2}(|e\rangle\langle e|_j\hat{\rho} + \hat{\rho}|e\rangle_j\langle e|)\right] \tag{12}$$

is such that $Q\mathcal{L}^A Q = \mathcal{L}^A$ and $\mathcal{L}^A P = P\mathcal{L}^A = 0$, while $\mathcal{J}P = 0$ and $P\mathcal{J} = P\mathcal{J}Q$. Finally, $P\mathcal{L}^{\rm int}P = 0$, with

$$\mathcal{L}^{\rm int}\hat{\rho} = -i\sum_{j=1}^{N}[\{|e\rangle\langle g|_j[\Omega_j + g_j(\hat{x}_j)\hat{a}] + \text{H.c.}\}, \hat{\rho}]. \tag{13}$$

The master equation (1) is thus rewritten in terms of coupled differential equations for the time evolution of $\hat{v}$ and $\hat{w}$ defined in Eqs. (8) and (9). The formal solution for $\hat{w}$ reads

$$\hat{w}(\tau) = \int_0^\tau d\tau' e^{\mathcal{Q}(\mathcal{L}^A+\mathcal{L}^F)(\tau-\tau')}Q\mathcal{L}^{\rm int}\hat{w}(\tau') + \int_0^\tau d\tau' e^{\mathcal{Q}(\mathcal{L}^A+\mathcal{L}^F)(\tau-\tau')}Q\mathcal{L}^{\rm int}\hat{v}(\tau'), \tag{14}$$

where we have assumed $\hat{w}(0) = 0$, namely, all atoms are in the internal ground state at $t = 0$. Using Eq. (14) in the differential equation for $\hat{v}$ leads to an integrodifferential equation of motion,

$$\frac{\partial}{\partial t}\hat{v} = P\mathcal{L}^F\hat{v} + P(\mathcal{J} + \mathcal{L}^{\rm int}) \times \int_0^t d\tau e^{\mathcal{Q}(\mathcal{L}^A+\mathcal{L}^F)(t-\tau)}Q\mathcal{L}^{\rm int}[\hat{v}(\tau) + \hat{V}(\tau)], \tag{15}$$

with

$$\hat{V}(\tau) = \int_0^\tau d\tau' e^{\mathcal{Q}(\mathcal{L}^A+\mathcal{L}^F)(\tau-\tau')}Q\mathcal{L}^{\rm int}[\hat{v}(\tau') + \hat{w}(\tau')].$$

Equation (15) can be brought to the form of an effective Born-Markov master equation by performing a perturbative expansion to the second order in the small parameters $\epsilon_{\rm int} \propto \sqrt{N}\frac{g\sqrt{\bar{n}}}{|\Delta_a|}, \sqrt{N}\frac{\Omega}{|\Delta_a|}$ and $\epsilon_F \propto \frac{|\Delta_c|}{|\Delta_a|}, \frac{\kappa}{|\Delta_a|}$, which consists in neglecting terms such as $(\mathcal{L}^{\rm int})^3$, $(\mathcal{L}^{\rm int})^2\mathcal{L}^F$, $\mathcal{L}^{\rm int}(\mathcal{L}^F)^2$, $(\mathcal{L}^F)^3$, and higher. In this approximation, the master equation for the reduced density matrix $\hat{v}$, given by Eq. (15), is reduced to the form

$$\frac{\partial}{\partial t}\hat{v} = -\frac{i}{\hbar}[\hat{\mathcal{H}}_{\rm eff}, \hat{v}] - \kappa(\hat{a}^\dagger\hat{a}\hat{v} + \hat{v}\hat{a}^\dagger\hat{a} - 2\hat{a}\hat{v}\hat{a}^\dagger) - \sum_{j=1}^{N}\frac{\gamma_j'}{2}\left\{\hat{B}_j^\dagger\hat{B}_j\hat{v} + \hat{v}\hat{B}_j^\dagger\hat{B}_j - 2\int_{-1}^{1}duN_j(u)\hat{B}_j\hat{v}\hat{B}_j^\dagger\right\}, \tag{16}$$

where $\gamma_j' = \gamma_j g_j^2/(\Delta_j^2 + \gamma_j^2/4)$ is the rate of incoherent photon scattering via spontaneous decay, while operator

$$\hat{B}_j = e^{-ik_j u\hat{x}_j}\left[\cos(k\hat{x}_j)\hat{a} + \frac{\Omega_j}{g_j}\right] \tag{17}$$

describes the mechanical effect associated with absorption of a laser or a cavity photon and followed by a spontaneous emission. The effective Hamiltonian $\hat{\mathcal{H}}_{\rm eff}$ reads

$$\hat{\mathcal{H}}_{\rm eff} = \sum_{j=1}^{N}\frac{\hat{p}_j^2}{2m_j} - \hbar\left[\Delta_c - \sum_{j=1}^{N}U_j\cos^2(k\hat{x}_j)\right]\hat{a}^\dagger\hat{a} + \hbar\sum_{j=1}^{N}S_j\cos(k\hat{x}_j)(\hat{a} + \hat{a}^\dagger). \tag{18}$$

It contains the shift of the cavity frequency due to the interaction with the atoms, which scales with the frequency

$$U_j = \frac{\Delta_j g_j^2}{\Delta_j^2 + \gamma_j^2/4}, \tag{19}$$

and the pump on the cavity field due to coherent scattering into the cavity mode, which scales with the amplitude

$$S_j = \Delta_j\frac{g_j\Omega_j}{\Delta_j^2 + \gamma_j^2/4}. \tag{20}$$

The corresponding terms in Eq. (18) depend on the atomic positions and give rise to mechanical forces on the atoms. We remark that the master equation in Eq. (16) has been reported, for instance, in Refs. [17,19], where the internal dynamics is eliminated by setting $\hat{\sigma}_z \approx -1$ and ultimately expressing $\hat{\sigma}_j$ and $\hat{\sigma}_j^\dagger$ in terms of cavity field operators. Here, we have given its detailed derivation using second-order perturbation theory by means of projectors acting on density operators [29].

III. SEMICLASSICAL MODEL

In this section, we analyze the predictions of Eq. (16) under the assumption that the atoms' center-of-mass motion can be treated semiclassically. For this purpose, we first consider the dynamics of the atoms in Wigner representation and denote by $\hat{W}_t(\boldsymbol{x},\boldsymbol{p})$ the operator for the cavity field degrees of freedom, where the subscript t indicates the time. Operator $\hat{W}_t(\boldsymbol{x},\boldsymbol{p})$ is related to the reduced density operator $\hat{v}$ by the equation

$$\hat{W}_t(\boldsymbol{x},\boldsymbol{p}) = \frac{1}{(2\pi\hbar)^N}\int_{-\infty}^{\infty} d\boldsymbol{\xi}\, e^{-\frac{i}{\hbar}\boldsymbol{p}\cdot\boldsymbol{\xi}}\left\langle \boldsymbol{x}+\frac{1}{2}\boldsymbol{\xi}|\hat{v}|\boldsymbol{x}-\frac{1}{2}\boldsymbol{\xi}\right\rangle, \tag{21}$$

with $\boldsymbol{y}=(y_1,\ldots,y_N)$, where $\boldsymbol{y}=\boldsymbol{x},\boldsymbol{p},\boldsymbol{\xi}$. It is a scalar function of the atoms' positions x_j and canonically conjugated momenta p_j of the atoms. Note that $\boldsymbol{p}\cdot\boldsymbol{\xi}=\sum_{j=1}^N p_j\xi_j$ and $\int_{-\infty}^{\infty} d\boldsymbol{\xi}=\prod_{j=1}^N\int_{-\infty}^{\infty} d\xi_j$. The Wigner function for the atoms is denoted by $f(\boldsymbol{x},\boldsymbol{p},t)$ and is defined as

$$f(\boldsymbol{x},\boldsymbol{p},t)=\mathrm{Tr}\{\hat{W}_t(\boldsymbol{x},\boldsymbol{p})\}. \tag{22}$$

From the density operator in Eq. (21), one can find the combined atom-field Wigner function $W(\boldsymbol{x},\boldsymbol{p},\alpha,\alpha^*)$ used in Ref. [19] by means of the relation

$$W_t(\boldsymbol{x},\boldsymbol{p},\alpha,\alpha^*)=\int\frac{d^2\eta}{\pi^2}e^{\eta^*\alpha-\eta\alpha^*}\mathrm{Tr}\{\hat{W}_t(\boldsymbol{x},\boldsymbol{p})\hat{\mathcal{D}}(\eta)\}, \tag{23}$$

where α and α^* are the variables for the cavity field amplitude and $\hat{\mathcal{D}}(\eta)=\exp(\eta\hat{a}^\dagger-\eta^*\hat{a})$ is the displacement operator for the cavity field, with η complex variables.

Let us now discuss the conditions under which the motion can be treated as a semiclassical variable. This is possible when the typical width of the momentum distribution, which we denote by Δp_j for the atom j, is much larger than the photon momentum $\hbar k$,

$$\hbar k \ll \Delta p_j. \tag{24}$$

In this limit, the momentum changes due to emission and the absorption of a photon are very small. In addition, the uncertainty in the atomic position, Δx_j, is larger than the value set by the Heisenberg uncertainty relation, $\Delta x_j > \hbar/\Delta p_j$. These conditions are met when the atoms are at the stationary state of Doppler cooling, such that $\Delta p_j^2/(2m_j)\sim\hbar\gamma_j/4$ when $\gamma_j\gg\omega_r$, with $\omega_r=\frac{\hbar k^2}{2m}$ the recoil frequency [3,28]. In this work, we derive a Fokker-Planck equation starting from this assumption, and then check that the corresponding stationary state fulfills the conditions under which the Fokker-Planck equation is valid.

A. Semiclassical model below the self-organization threshold

We now derive equations of motion for the atomic degrees of freedom by eliminating the cavity degrees of freedom. This is possible provided the cavity degrees of freedom evolve on a faster time scale than the atomic motion, namely, when

$$k\Delta p_j/m_j \ll |\kappa+\mathrm{i}\Delta_c|. \tag{25}$$

As one can easily check, this condition is consistent with Eq. (24), provided that $\omega_r\ll\kappa$. The following treatment extends the method applied in Ref. [20] to the dynamics of atoms coupled to a resonator. We start with the master equation in Eq. (16) in Wigner representation for the atomic degrees of freedom and consider the reference frame moving with the atoms and defined by the relation

$$\hat{\tilde{W}}_t(\boldsymbol{x},\boldsymbol{p})=\hat{W}_t(\boldsymbol{x}+\boldsymbol{v}(t-t_0),\boldsymbol{p}), \tag{26}$$

where $\boldsymbol{v}=(p_1/m_1,\ldots,p_N/m_N)$, $\hat{W}_t(\boldsymbol{x},\boldsymbol{p})$ is defined in Eq. (21), and $\hat{\tilde{W}}_t(\boldsymbol{x},\boldsymbol{p})$ is given in the reference frame moving with the atoms, with t_0 an initial time. Its time evolution reads

$$\begin{aligned}
\frac{\partial}{\partial t}\hat{\tilde{W}}_t\begin{pmatrix}\boldsymbol{x}\\ \boldsymbol{p}\end{pmatrix} &= \mathcal{L}_0'\hat{\tilde{W}}_t\begin{pmatrix}\boldsymbol{x}\\ \boldsymbol{p}\end{pmatrix}+\mathcal{L}^\gamma\hat{\tilde{W}}_t\begin{pmatrix}\boldsymbol{x}\\ \boldsymbol{p}\end{pmatrix}-\frac{i}{2}\sum_j S_j\Bigg\{(\hat{a}+\hat{a}^\dagger)\Bigg[e^{ik(x_j+\frac{p_j}{m_j}\tau)}\hat{\tilde{W}}_t\begin{pmatrix}\boldsymbol{x}+\tau\hbar\boldsymbol{k_j}/(2m_j)\\ \boldsymbol{p}-\hbar\boldsymbol{k_j}/2\end{pmatrix}\\
&+e^{-ik(x_j+\frac{p_j}{m_j}\tau)}\hat{\tilde{W}}_t\begin{pmatrix}\boldsymbol{x}-\tau\hbar\boldsymbol{k_j}/(2m_j)\\ \boldsymbol{p}+\hbar\boldsymbol{k_j}/2\end{pmatrix}\Bigg]-\Bigg[e^{ik(x_j+\frac{p_j}{m_j}\tau)}\hat{\tilde{W}}_t\begin{pmatrix}\boldsymbol{x}-\tau\hbar\boldsymbol{k_j}/(2m_j)\\ \boldsymbol{p}+\hbar\boldsymbol{k_j}/2\end{pmatrix}\\
&+e^{-ik(x_j+\frac{p_j}{m_j}\tau)}\hat{\tilde{W}}_t\begin{pmatrix}\boldsymbol{x}+\tau\hbar\boldsymbol{k_j}/(2m_j)\\ \boldsymbol{p}-\hbar\boldsymbol{k_j}/2\end{pmatrix}\Bigg](\hat{a}+\hat{a}^\dagger)\Bigg\}\\
&-\frac{i}{4}\sum_j U_j\Bigg\{\hat{a}^\dagger\hat{a}\Bigg[e^{2ik(x_j+\frac{p_j}{m_j}\tau)}\hat{\tilde{W}}_t\begin{pmatrix}\boldsymbol{x}+\tau\hbar\boldsymbol{k_j}/m_j\\ \boldsymbol{p}-\hbar\boldsymbol{k_j}\end{pmatrix}+e^{-2ik(x_j+\frac{p_j}{m_j}\tau)}\hat{\tilde{W}}_t\begin{pmatrix}\boldsymbol{x}-\tau\hbar\boldsymbol{k_j}/m_j\\ \boldsymbol{p}+\hbar\boldsymbol{k_j}\end{pmatrix}+2\hat{\tilde{W}}_t\begin{pmatrix}\boldsymbol{x}\\ \boldsymbol{p}\end{pmatrix}\Bigg]\\
&-\Bigg[e^{2ik(x_j+\frac{p_j}{m_j}\tau)}\hat{\tilde{W}}_t\begin{pmatrix}\boldsymbol{x}-\tau\hbar\boldsymbol{k_j}/m_j\\ \boldsymbol{p}+\hbar\boldsymbol{k_j}\end{pmatrix}+e^{-2ik(x_j+\frac{p_j}{m_j}\tau)}\hat{\tilde{W}}_t\begin{pmatrix}\boldsymbol{x}+\tau\hbar\boldsymbol{k_j}/m_j\\ \boldsymbol{p}-\hbar\boldsymbol{k_j}\end{pmatrix}+2\hat{\tilde{W}}_t\begin{pmatrix}\boldsymbol{x}\\ \boldsymbol{p}\end{pmatrix}\Bigg]\hat{a}^\dagger\hat{a}\Bigg\},
\end{aligned} \tag{27}$$

where $\hat{\tilde{W}}_t(\boldsymbol{x},\boldsymbol{p})\equiv\hat{\tilde{W}}_t\left(\begin{smallmatrix}\boldsymbol{x}\\ \boldsymbol{p}\end{smallmatrix}\right)$, $\tau=t-t_0$, and $(\boldsymbol{k_j})_\ell=k\delta_{\ell,j}$, while

$$\mathcal{L}_0'\hat{\tilde{W}}_t\begin{pmatrix}\boldsymbol{x}\\ \boldsymbol{p}\end{pmatrix}=i\Delta_c\left[\hat{a}^\dagger\hat{a},\hat{\tilde{W}}_t\begin{pmatrix}\boldsymbol{x}\\ \boldsymbol{p}\end{pmatrix}\right]+\kappa\left[2\hat{a}\hat{\tilde{W}}_t\begin{pmatrix}\boldsymbol{x}\\ \boldsymbol{p}\end{pmatrix}\hat{a}^\dagger-\hat{a}^\dagger\hat{a}\hat{\tilde{W}}_t\begin{pmatrix}\boldsymbol{x}\\ \boldsymbol{p}\end{pmatrix}-\hat{\tilde{W}}_t\begin{pmatrix}\boldsymbol{x}\\ \boldsymbol{p}\end{pmatrix}\hat{a}^\dagger\hat{a}\right]. \tag{28}$$

The effects of spontaneous emission are included in $\mathcal{L}^{\gamma}\hat{\tilde{W}}_t(\begin{smallmatrix}x\\p\end{smallmatrix})$, whose detailed form is reported in Appendix A. After performing a Taylor expansion up to second order in the parameters $\epsilon_1 = \hbar k/\Delta p$ and $\epsilon_2 = \frac{k\Delta p}{m\kappa}$, Eq. (27) can be cast in the form

$$\frac{\partial}{\partial t}\hat{\tilde{W}}_t(\boldsymbol{x},\boldsymbol{p}) = [\mathcal{L}_0 + \mathcal{L}_1(t) + \mathcal{L}_2(t)]\hat{\tilde{W}}_t(\boldsymbol{x},\boldsymbol{p}), \tag{29}$$

where $\mathcal{L}_j$ is of the jth order in ϵ_1,ϵ_2 and we have assumed $\epsilon_1 \sim \epsilon_2 \sim \epsilon$, which is correct provided that $\omega_r \ll \kappa$. Now, operators $\hat{\tilde{W}}_t(\boldsymbol{x},\boldsymbol{p})$ appear all at the same positions and momenta $\boldsymbol{x},\boldsymbol{p}$, so that we omit writing the argument explicitly. Superoperators $\mathcal{L}_j$ are defined as

$$\mathcal{L}_0\hat{\tilde{W}}_t = \mathcal{L}_0'\hat{\tilde{W}}_t - i\sum_j U_j[\hat{a}^\dagger\hat{a},\cos^2(kx_j)\hat{\tilde{W}}_t] - i\sum_j S_j[(\hat{a}+\hat{a}^\dagger),\cos(kx_j)\hat{\tilde{W}}_t] + \mathcal{L}_0^{\gamma'}\hat{\tilde{W}}_t, \tag{30}$$

$$\mathcal{L}_1\hat{\tilde{W}}_t = +\frac{i}{\hbar}\tau\sum_j\left[\frac{p_j}{m_j}\hat{F}_j,\hat{\tilde{W}}_t\right] - \frac{1}{2}\sum_j\left[\left(\frac{\partial}{\partial p_j} - \frac{\tau}{m_j}\frac{\partial}{\partial x_j}\right)\hat{\tilde{W}}_t,\hat{F}_j\right]_+ + \mathcal{L}_1^{\gamma'}\hat{\tilde{W}}_t, \tag{31}$$

$$\mathcal{L}_2\hat{\tilde{W}} = \frac{i\hbar}{8}\sum_j\left[\frac{\partial^2}{\partial p_j^2}\hat{\tilde{W}}_t,\frac{\partial}{\partial x_j}\hat{F}_j\right] + \mathcal{L}_2^{\gamma'}\hat{\tilde{W}}_t, \tag{32}$$

with $\hat{F}_j$ the force operator on the jth atom [29], which is defined as

$$\hat{F}_j = \hbar k S_j\sin(kx_j)(\hat{a}+\hat{a}^\dagger) + \hbar k U_j\sin(2kx_j)\hat{a}^\dagger\hat{a} - i(\hat{a}^\dagger-\hat{a})\hbar k\frac{\gamma_j'}{2}s_j\sin(kx_j),$$

with $s_j = \Omega_j/g_j$. The terms $\mathcal{L}_0^{\gamma'}\hat{\tilde{W}}$, $\mathcal{L}_1^{\gamma'}\hat{\tilde{W}}$, and $\mathcal{L}_2^{\gamma'}\hat{\tilde{W}}$ are due to spontaneous emission and their explicit form is given in Appendix A. Note that $\mathcal{L}_2$ is evaluated at $\tau = 0$ since this term is already of the second order in ϵ.

We rewrite the operator $\hat{\tilde{W}}_t$ as

$$\tilde{W}_t(\boldsymbol{x},\boldsymbol{p}) = \tilde{f}(\boldsymbol{x},\boldsymbol{p},t)\sigma_s(\boldsymbol{x}) + \tilde{\chi}(\boldsymbol{x},\boldsymbol{p},t), \tag{33}$$

where $\sigma_s(\boldsymbol{x})$ is the density matrix for the field, which solves equation $\mathcal{L}_0\sigma_s(\boldsymbol{x}) = 0$ for N atoms fixed at positions x_j, while $\tilde{f}(\boldsymbol{x},\boldsymbol{p},t)$ is the Wigner function of Eq. (22) in the reference frame moving with the atom. Therefore, $\tilde{f}(\boldsymbol{x},\boldsymbol{p},t)\sigma_s(\boldsymbol{x})$ corresponds to the solution in which the cavity field adiabatically follows the external atomic motion, while the nonadiabatic terms are contained in the (traceless) operator $\tilde{\chi} = \tilde{W} - \mathrm{Tr}\{\tilde{W}\}\sigma_s$. When condition (25) is fulfilled, this contribution is expected to be a small correction and reads

$$\tilde{\chi}(t) = \int_{t_0}^{t} dt' e^{\mathcal{L}_0(t-t')}[\mathcal{L}_1(t')f(\boldsymbol{x},\boldsymbol{p},t')\sigma_s - \mathrm{Tr}\{\mathcal{L}_1(t')f(\boldsymbol{x},\boldsymbol{p},t')\sigma_s\}\sigma_s], \tag{34}$$

where the value at $t = t_0$ is taken to be zero, as is consistent with the assumption that when the transverse laser is switched on, there are no correlations between field and atoms. Under this assumption, we use Eq. (33) in Eq. (29) and consider a coarse-grained dynamics. Applying the Markov approximation after tracing over the cavity degrees of freedom, we obtain the equation governing the time evolution of the Wigner function $\tilde{f}(\boldsymbol{x},\boldsymbol{p},t)$, which is valid up to second order in ϵ:

$$\begin{aligned}\frac{\partial}{\partial t}\tilde{f}(\boldsymbol{x},\boldsymbol{p},t)\Big|_{t=t_0} &= \mathrm{Tr}\{[\mathcal{L}_1(\boldsymbol{x},\boldsymbol{p},t_0) + \mathcal{L}_2(\boldsymbol{x},\boldsymbol{p},t_0)]\cdot\tilde{f}(\boldsymbol{x},\boldsymbol{p},t_0)\sigma_s(\boldsymbol{x})\} \\ &+ \mathrm{Tr}\Big\{\mathcal{L}_1(\boldsymbol{x},\boldsymbol{p},t_0)\int_{-\infty}^{t_0}dt' e^{\mathcal{L}_0(t_0-t')}[\mathcal{L}_1(\boldsymbol{x},\boldsymbol{p},t') \\ &\cdot\tilde{f}(\boldsymbol{x},\boldsymbol{p},t_0)\sigma_s(\boldsymbol{x}) \\ &- \mathrm{Tr}[\mathcal{L}_1(\boldsymbol{x},\boldsymbol{p},t')\cdot\tilde{f}(\boldsymbol{x},\boldsymbol{p},t_0)\sigma_s(\boldsymbol{x})]\sigma_s(\boldsymbol{x})]\Big\}.\end{aligned} \tag{35}$$

The equation in the original reference frame is found by using the relation $\tilde{f}(\boldsymbol{x},\boldsymbol{p},t_0) = f(\boldsymbol{x},\boldsymbol{p},t_0)$ together with equation

$$\frac{\partial}{\partial t}\tilde{f}|_{t=t_0} = \frac{\partial}{\partial t}f|_{t=t_0} + \boldsymbol{v}\cdot\frac{\partial}{\partial\boldsymbol{x}}f|_{t=t_0}.$$

After observing that the trace over the term containing operator $\mathcal{L}_2$ (neglecting $\mathcal{L}_2^{\gamma'}$) vanishes, we cast Eq. (35) in the form

$$\begin{aligned}\frac{\partial}{\partial t}f(\boldsymbol{x},\boldsymbol{p},t)|_t &= -\sum_{j=1}^{N}\frac{\partial}{\partial x_j}\frac{p_j}{m_j}f(\boldsymbol{x},\boldsymbol{p},t) \\ &- \sum_{j=1}^{N}\frac{\partial}{\partial p_j}\left(\Phi_j - \sum_{\ell=1}^{N}\gamma_{j\ell}\,p_\ell\right)f(\boldsymbol{x},\boldsymbol{p},t) \\ &+ \sum_{j,\ell=1}^{N}\frac{\partial^2}{\partial p_j\partial p_\ell}D_{j\ell}f(\boldsymbol{x},\boldsymbol{p},t) \\ &+ \sum_{j,\ell=1}^{N}\frac{\partial}{\partial p_j}\eta_{j\ell}\frac{\partial}{\partial x_\ell}f(\boldsymbol{x},\boldsymbol{p},t),\end{aligned} \tag{36}$$

where the derivatives are now explicitly reported. This equation has the form of a Fokker-Planck equation for the atomic center-of-mass variables, while the field enters in the coefficients through the expectation values of field variables taken over the density matrix $\sigma_s(\boldsymbol{x})$. In particular, $\Phi_j = \mathrm{Tr}\{\sigma_s(\boldsymbol{x})\hat{F}_j\}$ is the mean dipole force over the j atom due to the cavity field, and $\gamma_{j\ell}$ are the friction coefficients which read

$$\gamma_{j\ell} = \gamma_{j\ell}' + \mathrm{Tr}\left\{\hat{F}_j\int_0^\infty d\tau\,\exp(\mathcal{L}_0\tau)\,\frac{i\tau}{\hbar m_\ell}[\hat{F}_\ell,\sigma_s(\boldsymbol{x})]\right\},$$

where $\gamma_{j\ell}'$ is the contribution due to spontaneous emission, while the second term arises from the coupling with the cavity. Coefficients $D_{j\ell}$ are the diffusion matrix coefficients; they include the contribution due to spontaneous decay ($D_{j\ell}'$) and the contribution to diffusion due to the cavity field,

$$D_{j\ell} = D_{j\ell}' + \mathrm{Tr}\left(\hat{F}_j\int_0^\infty d\tau\,\exp(\mathcal{L}_0\tau)\left\{\frac{1}{2}[\sigma_s(\boldsymbol{x}),\hat{F}_\ell]_+ - \mathrm{Tr}[\sigma_s(\boldsymbol{x})\hat{F}_\ell]\sigma_s(\boldsymbol{x})\right\}\right).$$

Finally, the Fokker-Planck equation exhibits cross derivatives between position and momentum of the particles with

coefficients

$$\eta_{j\ell} = \eta'_{j\ell} + \mathrm{Tr}\left(\hat{F}_j \int_0^\infty d\tau \exp(\mathcal{L}_0\tau)\frac{\tau}{m_\ell}\left\{\frac{1}{2}[\sigma_s(\boldsymbol{x}),\hat{F}_\ell]_+ - \mathrm{Tr}[\sigma_s(\boldsymbol{x})\hat{F}_\ell]\sigma_s(\boldsymbol{x})\right\}\right),$$

where the first term $\eta'_{j\ell}$ is due to spontaneous emission. This term can be rewritten as

$$\sum_{j,\ell=1}^{N}\frac{\partial}{\partial p_j}\eta_{j\ell}\frac{\partial}{\partial x_\ell}f = \sum_{j,\ell=1}^{N}\frac{\partial}{\partial p_j}\left[\frac{\partial}{\partial x_\ell}(\eta_{j\ell}f) - \left(\frac{\partial\eta_{j\ell}}{\partial x_\ell}\right)f\right],$$

where the second term in the brackets gives a contribution to the force of higher order in ϵ and can thus be discarded [21,22]. The other term can also be neglected well below the self-organization threshold, when the spatial distribution has a width which largely exceeds the cavity wavelength λ [20]. It must be taken into account, nevertheless, at and above the self-organization threshold, when spatial structures with periodicity λ form.

We note that the explicit form of the coefficients due to spontaneous emission, $\gamma'_{j\ell}, D'_{j\ell}, \eta'_{j\ell}$, is reported in Appendix A. These coefficients characterize the dynamics also in the absence of the resonator. In the limit which we will consider here, where the laser and cavity fields are far detuned from the atomic resonance, they are of higher order and their contribution to the dynamics can often be discarded.

We finally give the form of the field density matrix $\sigma_s(\boldsymbol{x})$. By solving $\mathcal{L}_0\sigma_s(\boldsymbol{x}) = 0$, we find $\sigma_s(\boldsymbol{x}) = |\alpha(\boldsymbol{x})\rangle\langle\alpha(\boldsymbol{x})|$, with $|\alpha(\boldsymbol{x})\rangle$ the coherent state of amplitude

$$\alpha(\boldsymbol{x}) = \frac{\sum_j S_j[1 - \mathrm{i}(\gamma_j/2\Delta_j)]\cos(kx_j)}{[\Delta_c - \sum_j U_j\cos^2(kx_j)] + \mathrm{i}\kappa'}, \tag{37}$$

with

$$\kappa' = \kappa + \sum_j \frac{g_j^2}{(\gamma_j/2)}\left(\frac{\gamma_j}{2\Delta_j}\right)^2\frac{\Delta_j^2}{\Delta_j^2+\gamma_j^2/4}\cos^2(kx_j).$$

Operators of the form $\mathcal{F}(a,a^\dagger)$, which are a function of the field variables, have expectation value

$$\langle\mathcal{F}\rangle = \int d\boldsymbol{x}\,d\boldsymbol{p}\,\mathrm{Tr}\{W_t(\boldsymbol{x},\boldsymbol{p})\mathcal{F}\}, \tag{38}$$

where W_t is found from Eq. (33) using the nonadiabatic term in Eq. (34) after applying the Markov approximation.

B. Comparison with the semiclassical model in Ref. [19]

We now consider the Fokker-Planck equation derived in Ref. [19]. This is based on the assumption that both the atomic motion and cavity field can be treated semiclassically. With respect to the previous treatment, hence, here one also assumes that the mean-field amplitude is large, $\langle\hat{a}\rangle = |\alpha_0| \gg 1$, so that one can perform an expansion in the quantum fluctuations about the mean value α_0. This allows one to discard higher derivatives in the field and atomic variables, thereby obtaining a Fokker-Planck equation.

In this regime, it is convenient to consider the Wigner function for field and atomic motion in Eq. (23), whose time evolution is given by master equation (16) in Wigner representation. The corresponding Fokker-Planck equation in the semiclassical limit is obtained by performing an expansion up to second order in the small parameters $\epsilon_{1,j} = \frac{\hbar k}{(\Delta p)_j}$ and $\epsilon_2 = \frac{1}{|\alpha_0|}$, where it is assumed that $\epsilon_{1,j}$ and ϵ_2 are approximately of the same order. The resulting time evolution reads

$$\begin{aligned}\frac{\partial}{\partial t}W_t =& -\frac{\partial}{\partial\alpha_r}\left[-\Delta'_c\alpha_i - \kappa'\alpha_r - \sum_{j=1}^{N}s_j\Gamma_j\cos(kx_j)\right]W_t\\ &-\frac{\partial}{\partial\alpha_i}\left[\Delta'_c\alpha_r - \kappa'\alpha_i - \sum_{j=1}^{N}s_jU_j\cos(kx_j)\right]W_t\\ &-\sum_{j=1}^{N}\hbar\frac{\partial}{\partial p_j}\nabla_j[-U_j|\alpha|^2\cos^2(kx_j)\\ &-s_jU_j\cos(kx_j)(2\alpha_r) + (2\alpha_i)s_j\Gamma_j\cos(kx_j)]W_t\\ &-\sum_{j=1}^{N}\frac{\partial}{\partial x_j}\left[\frac{p_j}{m_j}\right]W_t + \frac{1}{4}\left(\frac{\partial^2}{\partial\alpha_r^2}+\frac{\partial^2}{\partial\alpha_i^2}\right)\kappa'W_t\\ &+\sum_{j=1}^{N}\frac{\hbar k}{2}\Gamma_j\sin(2kx_j)\frac{\partial}{\partial p_j}\left(\alpha_i\frac{\partial}{\partial\alpha_r}-\alpha_r\frac{\partial}{\partial\alpha_i}\right)W_t\\ &+\sum_{j=1}^{N}(\hbar k)^2\Gamma_j\frac{\partial^2}{\partial p_j^2}\{|\alpha|^2[\sin^2(kx_j)+(\overline{u^2})_j\cos^2(kx_j)]\\ &+s_j(\overline{u^2})_j[2\alpha_r\cos(kx_j)+s_j]\}W_t,\end{aligned} \tag{39}$$

where $\alpha_r = \mathrm{Re}\{\alpha\}$, $\alpha_i = \mathrm{Im}\{\alpha\}$, while $s_j = \Omega_j/g_j$, $\Gamma_j = \gamma'_j/2$, with

$$\gamma'_j = \gamma_j\frac{g_j^2}{\Delta_j^2+\gamma_j^2/4}$$

as the effective rate of spontaneous emission. Moreover, $\kappa' = \kappa + \sum_{j=1}^{N}\Gamma_j\cos^2(kx_j)$ is the rate at which cavity photons are lost (via both cavity decay and spontaneous emission), and

$$\Delta'_c = \Delta_c - \sum_{j=1}^{N}U_j\cos^2(kx_j)$$

is the effective detuning between cavity and laser, which includes the dynamical Stark shift due to the coupling with the atoms.

Equation (39) is a Fokker-Planck equation for the variables $\boldsymbol{x}$, $\boldsymbol{p}$, α_r, and α_i. We note that its derivation does not require one to explicitly assume a time-scale separation between the cavity field and atomic motion. On the other hand, its derivation consists of neglecting derivatives corresponding to orders $\epsilon_{1,j}\epsilon_2^2, \epsilon_{1,j}^2\epsilon_2$, which is motivated under the assumption that the semiclassical limit for the field amplitude applies. Such approximation becomes invalid for small photon numbers and thus, for instance, below and close to the self-organization threshold. Nevertheless, this equation is used in the literature for studying the dynamics of the system below threshold [17,25].

IV. DYNAMICS FOR LOW PUMP INTENSITIES

We now analyze the predictions of Eq. (36) for low pump intensities Ω, such that the cavity field is essentially in the vacuum state. We first solve Eq. (36) at the asymptotics of the dynamics and find an explicit form for the stationary distribution; we then extract numerical predictions based on stochastic differential equations that we will define below. In the following discussion, we will assume, for simplicity, that all atoms are identical and set $m_j = m$, $S_j = S$, $U_j = U$, and $\gamma_j = \gamma$.

A. Fokker-Planck equation for small intracavity photon numbers

We assume that the low effective pumping rate S is small compared with the cavity decay rate κ (more precisely, $\sqrt{N}S \ll \kappa$). Consequently, the mean number of intracavity photons is close to zero, $|\alpha|^2 \ll 1$. In this limit, we can analytically evaluate σ_s by reducing the Hilbert space of the photon field to zero- and one-photon states. The coefficients can be then analytically determined in lowest order in $|\alpha|$, and Eq. (36) can be cast in the form

$$\begin{aligned}\frac{\partial}{\partial t} f(\boldsymbol{x},\boldsymbol{p},t) &= -\sum_{n=1}^{N} \frac{\partial}{\partial x_n}\frac{p_n}{m} f \\ &- 2\hbar k S^2 \sum_{\ell,n=1}^{N} \frac{\partial}{\partial p_n}\frac{\Delta_c'}{\Delta_c'^2+\kappa^2}\sin(kx_n)\cos(kx_\ell) f \\ &- \frac{4\hbar k^2}{m} S^2 \sum_{\ell,n=1}^{N} \frac{\partial}{\partial p_n}\frac{\Delta_c'\kappa}{\left(\Delta_c'^2+\kappa^2\right)^2}\sin(kx_n)\sin(kx_\ell)\, p_\ell f \\ &+ \hbar^2 k^2 S^2 \sum_{\ell,n=1}^{N} \frac{\partial^2}{\partial p_n \partial p_\ell}\frac{\kappa}{\Delta_c'^2+\kappa^2}\sin(kx_n)\sin(kx_\ell) f,\end{aligned} \tag{40}$$

where we have additionally assumed that $s = \Omega/g = S/U \gtrsim 1$.

In Eq. (40), we did not report the cross derivative between position and momentum, since we assume that the atoms' spatial density $n_{\rm at}$ is uniform: In fact, the pump intensity is taken to be well below the self-organization threshold, the mean intracavity photon number is close to zero, and we expect that the intracavity optical lattice does not confine the atoms. We will check the consistency of this hypothesis later on.

We have also neglected spontaneous emission, since we choose $|\Delta| \gg \gamma/2$ and consider large cooperativity, $C = g^2/(\kappa\gamma/2)$ [30]. This can be checked when comparing the contribution to the diffusion coefficient due to spontaneous decay to the one due to the coupling with the cavity field. Their ratio reads

$$\frac{\overline{u^2}}{\langle \sin^2(kx_n)\rangle}\left(\frac{\kappa\gamma}{2g^2}\right)\frac{\Delta_c^2+\kappa^2}{\kappa^2}\frac{\Delta^2+\gamma^2/4}{\Delta^2} \cong 2\overline{u^2}\frac{1}{C}\frac{\Delta_c^2+\kappa^2}{\kappa^2},$$

where we have used that $|\Delta_c| \gg N|U|$ and that $\langle \sin^2(kx_j)\rangle = 1/2$ when the atoms are not spatially localized inside the volume of the cavity mode. Therefore, the effect of spontaneous decay can be neglected when $C \gg 1$ (and Δ_c is of the order of κ), which are the conditions we consider in the following. In the other regime, when the atoms are localized at the points where their coupling with the field is maximum (the self-organized phase), then $\langle \sin^2(kx_j)\rangle \approx 0$ and diffusion is mainly due to spontaneous emission.

1. Stationary state

We first analyze the predictions of the Fokker-Planck equations under plausible assumptions, which we then verify numerically later on. We extract, in particular, the cooling rate and steady-state momentum distribution. In the following, we assume $N|U| \ll |\Delta_c|$, which is consistent with uniform spatial distributions, as shown in the following.

Let us first define the momentum distribution at time t, which is the integral of the Wigner function over the positions:

$$F(\boldsymbol{p},t) = \int d\boldsymbol{x}\, f(\boldsymbol{x},\boldsymbol{p},t).$$

Under the assumption of uniform spatial distribution, $f(\boldsymbol{x},\boldsymbol{p},t) \approx F(\boldsymbol{p},t) n_{\rm at}$, where we denote the spatial density by $n_{\rm at}$. We then integrate Eq. (40) over $\boldsymbol{x}$ and obtain an equation for the momentum distribution of the form

$$\begin{aligned}\frac{\partial}{\partial t}F(\boldsymbol{p},t) \approx -4\omega_r \sum_{n=1}^{N}\frac{\partial}{\partial p_n} S^2 \frac{\Delta_c\kappa\delta_1}{\left(\Delta_c^2+\kappa^2\right)^2} p_n F(\boldsymbol{p},t) \\ + \hbar m\omega_r \sum_{n=1}^{N}\frac{\partial^2}{\partial p_n^2} S^2 \frac{\kappa\delta_2}{\Delta_c^2+\kappa^2} F(\boldsymbol{p},t),\end{aligned} \tag{41}$$

which has been obtained assuming $N|U| \ll |\Delta_c|$, with

$$\delta_1 = 1 + \frac{3\Delta_c^2-\kappa^2}{\Delta_c^2+\kappa^2}\frac{NU/2}{\Delta_c}\frac{2N-1}{2N},$$

$$\delta_2 = 1 + \frac{2\Delta_c^2}{\Delta_c^2+\kappa^2}\frac{NU/2}{\Delta_c}\frac{2N-1}{2N}.$$

We note that the assumption $N|U| \ll |\Delta_c|$ is consistent with uniform spatial distributions. In Eq. (41), there are no terms which mix variables from different atoms: In fact, for uniform spatial distributions, they vanish after integrating over the positions. In this limit, the equations for the momentum of each atom can be decoupled using the ansatz $F(\boldsymbol{p},t) = \prod_{j=1}^{N} F_j(p_j,t)$, which delivers the equation of motion for the momentum distribution $F_j(p_j,t)$ for atom j:

$$\frac{\partial}{\partial t}F_j(p_j,t)|_t = -\frac{\partial}{\partial p_j}A p_j F_j(p_j,t) + \frac{\partial^2}{\partial p_j^2} B F_j(p_j,t), \tag{42}$$

with

$$A = 4\omega_r S^2 \frac{\Delta_c\kappa\delta_1}{\left(\Delta_c^2+\kappa^2\right)^2},$$

$$B = \frac{1}{2}(\hbar k)^2 S^2 \frac{\kappa\delta_2}{\Delta_c^2+\kappa^2}.$$

A stationary solution exists for $A < 0$, which is verified when $\Delta_c < 0$. In this case, one can make the ansatz that the momentum distribution of one atom is a Gaussian of width Δp_j. From Eq. (42), we find that $\Delta p_j = \Delta p(t)$, which is given

by the equation

$$\Delta p(t) = \left\{\Delta p(0)^2 e^{2At} + (1 - e^{2At})\Delta p_\infty^2\right\}^{1/2}, \quad (43)$$

with $\Delta p(0)$ the width at $t = 0$ and $\Delta p_\infty = \sqrt{-B/A}$ the width of the stationary state. Since the momentum distribution is a Maxwell-Boltzmann distribution, we can associate a temperature T to the width, with $k_B T = \Delta p_\infty^2/m$, whereby

$$k_B T = \hbar \frac{\Delta_c^2 + \kappa^2}{-4\Delta_c} \frac{\delta_2}{\delta_1}. \quad (44)$$

The steady state is reached with rate $\Gamma_{\rm cool} = -2A$, which we denote by the cooling rate and reads

$$\Gamma_{\rm cool} = 8\omega_r S^2 \frac{|\Delta_c|\kappa\delta_1}{\left(\Delta_c^2 + \kappa^2\right)^2}.$$

The cooling rate thus scales with the square of the scattering amplitude S and with the recoil frequency ω_r and is independent of the number of atoms. In fact, when the atoms spatial distribution is uniform, superradiant effects are negligible and the atoms can be considered as independent scatterers. Minimum temperature and faster rate are found for $\Delta_c = -\kappa$. For this choice, $k_B T = \hbar\kappa/2$ and $\Gamma_{\rm cool} = 2\omega_r (S/\kappa)^2 \delta_1$. It is interesting to observe that, also in the case when the cavity is driven, the final temperature of the atomic ensemble is determined by the cavity linewidth, and it is minimal for $\Delta_c \approx -\kappa$ [31].

2. Limits of validity

On the basis of the results we just derived, we are now able to identify the parameter regime for which the semiclassical description of the atomic motion we applied is valid at the final stages of the cooling dynamics. It is simple to check using Eq. (44) that both conditions (24) and (25) are verified provided that $|\Delta_c| \sim \kappa$ and $\omega_r \ll \kappa$. In particular, the requirement that the motion evolves more slowly than the cavity field, given by Eq. (25), leads to the restriction that the detuning between the cavity field and pump cannot be either much larger or much smaller than the cavity linewidth.

Let us now consider the assumption that the atoms' spatial distribution is uniform in space. This assumption shall be checked, since the atoms are subject to the dispersive potential due to the mechanical effects of the cavity field on their motion. Using a uniform spatial distribution in Eq. (37), one finds that the mean-field amplitude vanishes. The mean intracavity photon number is found using Eq. (38) for $\mathcal{F} = a^\dagger a$, and reads

$$n_{\rm cav} \approx \frac{NS^2/2}{\Delta_c^2 + \kappa^2}, \quad (45)$$

which discards the higher-order contribution due to nonadiabatic effects. This value is much smaller than unity provided that $\sqrt{N}S \ll |\Delta_c + i\kappa|$. The corresponding potential depth is $U_0 = U n_{\rm cav}$, and it is much smaller than the mean kinetic energy (thus, the atoms are not spatially confined by the potential) when $U_0 \ll \kappa/2$, which corresponds to the condition

$$\sqrt{N}S \ll \kappa\sqrt{\frac{\kappa}{U}}. \quad (46)$$

When S or N are such that this inequality is not fulfilled, the assumption of spatial flat distribution becomes invalid. Correspondingly, the cavity field starts to establish correlations between the atoms which ultimately lead to the formation of ordered structures.

B. Numerical results

In this section, we evaluate the dynamics predicted by the Fokker-Planck equation obtained in the semiclassical limit by adiabatically eliminating the cavity degrees of freedom. Our aim is to get an insight in the dynamics of the system by analyzing the trajectories of the atoms. For this purpose, we use Ito-type stochastic differential equations (SDE) [19,23,24], which we extract from Eq. (36). They read

$$dx_j = \frac{p_j}{m} dt + dX_j, \quad (47)$$

$$dp_j = 2\hbar k S^2 \sum_{i=1}^{N} \frac{\Delta_c'}{\Delta_c'^2 + \kappa^2} \cos(kx_i)\sin(kx_j)dt, + \sum_{i=1}^{N} 8\omega_r S^2 \frac{\Delta_c'\kappa}{\left(\Delta_c'^2 + \kappa^2\right)^2} \sin(kx_i)\sin(kx_j)p_i dt + dP_j, \quad (48)$$

where $j = 1, \ldots, N$ labels the atoms and dP_j denotes the noise term, which is simulated by means of a Wiener process. In particular, $\langle dP_j\rangle = 0$ and $\langle dP_i dP_j\rangle = 2D_{ij}dt$, with

$$D_{ij} = (\hbar k)^2 S^2 \frac{\kappa}{\Delta_c'^2 + \kappa^2} \sin(kx_i)\sin(kx_j) \quad (49)$$

as the element of the diffusion matrix, while $\langle dP_j dX_\ell\rangle = \eta_{j\ell}dt$, with

$$\eta_{j\ell} = 2\hbar\omega_r S^2 \sin(kx_j)\sin(kx_\ell)\frac{\kappa^2 - \Delta_c'^2}{\left(\Delta_c'^2 + \kappa^2\right)^2}. \quad (50)$$

When one includes spontaneous emission, the elements of the diffusion matrix read

$$D_{ij} = (\hbar k)^2 \left\{\frac{S^2\kappa}{\Delta_c'^2 + \kappa^2}\sin(kx_i)\sin(kx_j) + \delta_{ij}\frac{\gamma'}{2}s^2\overline{u^2}\right\}, \quad (51)$$

which reports the dominant contributions [the rescattering of a cavity photon by the atom is neglected here; see Eq. (A6)]. The analytical estimate of the steady-state momentum width for homogeneous spatial distribution increases accordingly,

$$\Delta p_\infty = \sqrt{-B/A}\left\{1 + 2\overline{u^2}\frac{\Delta^2 + \gamma^2/4}{\Delta^2}\frac{\Delta_c^2 + \kappa^2}{\kappa^2 C\delta_2}\right\}^{1/2}. \quad (52)$$

The simulations are performed considering a gas of ^{85}Rb atoms, whose D_2 line, namely, the hyperfine transition $5^2S_{1/2} \leftrightarrow 5^2P_{3/2}$ at wavelength $\lambda = 780$ nm and linewidth $\gamma/2 = 2\pi \times 3$ MHz, couples with the mode of the resonator and with the transverse laser. The laser frequency is assumed to be detuned from the atomic frequency by $\Delta_a = -500\gamma/2$ and from the cavity frequency by Δ_c, with N the number of atoms and $\kappa = 0.5\gamma/2$. The dynamics and steady state of the atoms are studied, assuming that initially the atoms are at a steady state of Doppler cooling with $k_B T = \hbar\gamma/2$. The initial state is

a Gaussian distribution (the initial momentum is generated by means of Gaussian-distributed random numbers) with uniform density (the initial positions of the atoms are given by means of uniformly distributed random numbers in the interval $[0,\lambda]$).

In the calculations, we neglect spontaneous emission, which is plausible under the assumption that the cavity is far-off resonance from the atomic transition. We have checked for a sample of values when this assumption is justified by comparing the simulations including spontaneous emission with the simulations in which spontaneous decay was not included (see Fig. 4 and related discussion). We further discard the cross correlations, setting $\langle dP_j dX_\ell \rangle = 0$, after verifying that this assumption is justified for the considered parameter choice [32]. We first check that the parameters are chosen so that the number of intracavity photons is sufficiently close to zero. We choose $\Delta_c = -\kappa$, for which one expects the minimum value from Eq. (44). Using Eq. (38) and setting $n_{\rm cav} = 0.1$, we obtain $\sqrt{N}\Omega \sim 0.6|\Delta_a|\kappa/g$. For the parameters that we chose and $NU/\Delta_c = 0.05$, $\Omega \sim 45\gamma/2$. We set $\Omega \sim 21\gamma/2$, which corresponds to $n_{\rm cav} \sim 0.02$. In this regime, we evaluate the density matrix of the field in the reduced Hilbert space, where the photon states are truncated up to $n = 2$; see Sec. IV A.

On the basis of this result, we evaluate the time evolution of the width Δp of the momentum distribution for each atom taking $N = 5$ atoms. If we take identical particles with the same initial temperature, the momentum distribution of each atom will be the same at all times. We then focus on the momentum distribution averaged over all the atoms,

$$F_0(p) = \frac{1}{N}\sum_{j=1}^{N}\int_{-\infty}^{\infty} dp_j \delta(p - p_j) F_j(p_j).$$

Figure 2 displays the width of the momentum distribution as a function of time: The points are obtained from 5000 trajectories for an initial momentum distribution corresponding to a Maxwell-Boltzmann distribution with $k_B T = \hbar\gamma/2$ for each atom. The dashed line is the function given in Eq. (43), which has been obtained by assuming that all atoms are independently cooled and show excellent agreement with the numerics. The lower panels show the momentum distribution at given instants of times, $t = (0.1,1,9)$ ms. The dashed line corresponds to the prediction extracted from Eq. (42), which gives a Gaussian at all times.

We now analyze the dependence of the final temperature on the detuning Δ_c. In order to perform a systematic comparison with the predictions of the Fokker-Planck equation in Ref. [25], we express the pumping strength Ω of the laser in units of the self-organization threshold defined as [25]

$$|\Omega_c| = \frac{\kappa^2 + \delta^2}{2|\delta|\sqrt{N}}\frac{|\Delta_a|}{g},$$

with $\delta = \Delta_c - NU/2$. This value scales with the number of atoms and the detuning Δ_c. We fix $\Omega = 0.3\,\Omega_c$, for which the mean photon number, given by Eq. (38), takes the form

$$n_{\rm cav} \approx \left(\frac{\Omega}{\Omega_c}\right)^2 \frac{\Delta_c^2 + \kappa^2}{8\Delta_c^2}.$$

This equation shows that when $|\Delta_c|$ becomes too small, the number of intracavity photons increases like $n_{\rm cav} \propto \frac{1}{\Delta_c^2}$.

Figure 3 displays the momentum distribution at the asymptotics of the dynamics, which is found by integrating the SDE after several ms, for three values of Δ_c. The curves are fitted by Gaussian of width given in Eq. (43): The stationary momentum distribution is thus a Gaussian with width $\Delta p_\infty = \sqrt{mk_B T}$, with T given in Eq. (44).

Figure 4 shows the stationary momentum width as a function of Δ_c, which has been extracted by numerically integrating the SDE (see blue circles). The curve exhibits a minimum at $\Delta_c = -\kappa$ and is in excellent agreement with Eq. (43), evaluated at $t \to \infty$ at the corresponding value of Δ_c (see blue dashed line). We have compared the predictions of the Fokker-Planck equation, given by Eq. (36), with the ones of the Fokker-Planck equation in Eq. (39), based on the assumption that the cavity field can be treated semiclassically. The simulations are performed by integrating the SDE reported in Ref. [19], which for completeness are reported in Appendix B (see red stars). Agreement between the predictions of the two Fokker-Planck equations is found: This is remarkable since the cavity field in this regime is in the vacuum, and thus outside the formal limits of validity of Eq. (39). In order to check the effect of spontaneous emission, we have integrated Eqs. (47) and (48) using Eq. (51). The result is shown by the black circles. The black dashed line corresponds to Δp_∞ in Eq. (52) and fits the numerical data. We observe an increase of Δp_∞ by about 15% with respect to the case in which spontaneous emission is not included.

We finally comment on the type of momentum distribution we find. In [25], by studying the equation of motion of atoms inside a resonator and driven well below threshold,

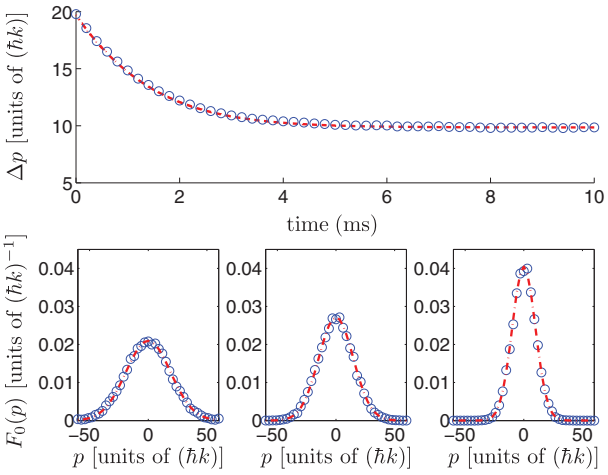

FIG. 2. (Color online) Time evolution of the momentum distribution $F_0(p,t)$ evaluated from 5000 trajectories simulated by integrating Eqs. (47) and (48) for $N = 5$ atoms. The top panel gives $\Delta p(t)$ in units of the momentum recoil $\hbar k$ (circles). The dashed line corresponds to Eq. (43). Lower panels: Momentum distribution at $t = (0.1,1,9)$ ms (circles) compared to a Gaussian of width $\Delta p(t)$ given by Eq. (43) (dashed line). The parameters are $\kappa = 0.5\gamma/2$, $NU/\Delta_c = 0.05$, $\Omega \sim 21\gamma/2$, and $\Delta_c = -\kappa$. The initial momentum distribution is a Gaussian with $k_B T_{\rm in} = \hbar\gamma/2$ for each atom.

it was argued that the steady-state momentum distribution for the atoms far below threshold can obey a q-Gaussian distribution with $q = 1 + \omega_r/|\delta|$, where $\delta = \Delta_c - NU/2$ and $N|U| \ll |\Delta_c|$. This calculation was performed by neglecting spontaneous decay. In our model, we do find Gaussian distributions ($q \approx 1$), whose steady-state temperature, given by Eq. (44), is comparable with the result in [25]. Indeed, our model can only allow for regular Gaussian distribution. In fact, this is consistent with the limits of validity of the Fokker-Planck equation we derive, which requires the separation of the time scales between cavity field and atoms dynamics, namely, $|\Delta_c| \approx \kappa \gg \omega_r$.

V. DISCUSSION AND CONCLUSIONS

In this article, we have derived a Fokker-Planck equation which describes the dynamics of atoms which are cooled by radiative processes, where laser photons are scattered into the mode of a high-finesse resonator. The derivation is based on the assumption that the time scale of the atomic center-of-mass motion dynamics is much larger than the cavity field typical time scales, and thus holds for resonators whose linewidth κ is much larger than the atomic recoil frequency ω_r. It cannot be applied, thus, to the setup in Ref. [33]. In this limit, $\kappa \gg \omega_r$, we eliminate the cavity field from the atomic motion dynamics using a perturbative expansion up to second order in the retardation effects and derive a Fokker-Planck equation for the atomic variables. The equation we derive constitutes an alternative theoretical description for the cavity cooling dynamics of atomic ensembles in high-finesse resonators. In particular, our model provides a description which is not restricted by the value of the laser intensity.

We have analyzed the predictions when the laser intensity is well below the self-organization threshold. In this limit, collective effects can be discarded and there is no spatial localization of the atoms by the light forces: at the steady state of the dynamics, the atoms are uniformly distributed inside the cavity and their momenta obey a Maxwell-Boltzmann distribution, whose width is determined by the cavity linewidth [34]. This result is in agreement with previous studies based on other approaches [17,25]. In future studies, we will apply this formalism to the dynamics of atoms and field when the laser intensity is close to threshold. This will allow us to investigate the onset of self-organization and to predict, among others, the coherence properties of the light emitted by the resonator.

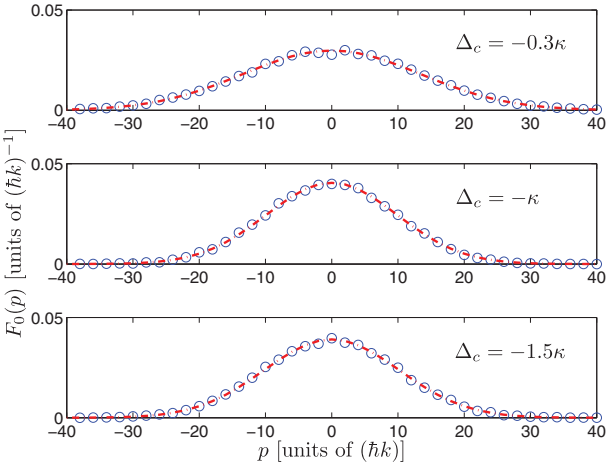

FIG. 3. (Color online) Steady-state momentum distribution (circles) for $\Delta_c = -0.3\kappa$ (top), $\Delta_c = -\kappa$ (middle), and $\Delta_c = -1.5\kappa$ (bottom). The points are extracted from 5000 trajectories evaluated for each value Δ_c by integrating the SDE in Eqs. (47) and (48). The dashed line is a Gaussian whose width is given by Eq. (43). The parameters are $\kappa = 0.5\gamma/2$, $NU/\Delta_c = 0.05$, $\Omega/\Omega_c = 0.3$, and $N = 5$. The initial momentum distribution is a Maxwell Boltzmann with mean kinetic energy $k_B T_{\rm in} = \hbar\gamma/2$ for each atom.

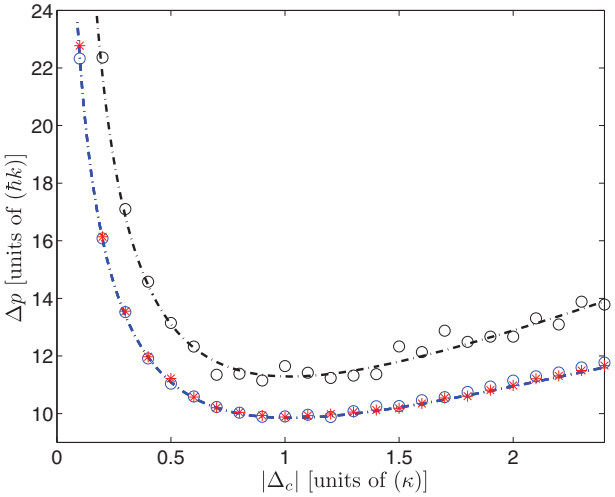

FIG. 4. (Color online) Width of the steady-state momentum distribution as a function of Δ_c. The blue circles correspond to the result of numerically integrating 5000 trajectories using Eqs. (47) and (48) for each value of Δ_c, together with Eq. (49). The blue dashed line plots Eq. (43). The red stars correspond to the result of numerically integrating 5000 trajectories corresponding to the Fokker-Planck equation (39), where the cavity field is treated in the semiclassical limit (details are reported in Appendix B). The results are obtained by neglecting spontaneous emission. Spontaneous emission is included in the results reported by the black circles, which have been obtained by integrating Eqs. (47) and (48) with Eq. (51) for 200 trajectories. The black dashed line gives the corresponding analytical estimate according to Eq. (52). The deviations of the simulation data from the fit originate from statistical noise. The parameters are $\kappa = 0.5\gamma/2$, $NU/\Delta_c = 0.05$, $\Omega/\Omega_c = 0.3$, and $N = 5$.

ACKNOWLEDGMENTS

The authors are grateful to A. Vukics, W. Niedenzu and H. Ritsch for stimulating discussions and helpful comments. This work was supported by the European Commission (IP AQUTE, STREP PICC), the BMBF (QuORep), and the German Research Foundation.

APPENDIX A: SPONTANEOUS EMISSION

In this appendix, we report the Lindbladian in Eq. (27) and the coefficients of Fokker-Planck (36) which are due to spontaneous decay. For simplicity, we assume $k_j = k$.

The Lindbladian in Eq. (27) reads

$$\begin{aligned}
\mathcal{L}^{\gamma}\hat{\tilde{W}}_t\begin{pmatrix}\boldsymbol{x}\\ \boldsymbol{p}\end{pmatrix} &= -\sum_j \frac{\gamma_j'}{2}s_j^2\left[2\hat{\tilde{W}}_t\begin{pmatrix}\boldsymbol{x}\\ \boldsymbol{p}\end{pmatrix} - 2\int_{-1}^{1} du N_j(u)\hat{\tilde{W}}_t\begin{pmatrix}\boldsymbol{x}-\frac{\tau}{m_j}\hbar\boldsymbol{k_j}u\\ \boldsymbol{p}+\hbar\boldsymbol{k_j}u\end{pmatrix}\right]\\
&- \sum_j \frac{\gamma_j'}{8}\left\{\hat{a}^\dagger\hat{a}\left[e^{2ik(x_j+\frac{p_j}{m_j}\tau)}\hat{\tilde{W}}_t\begin{pmatrix}\boldsymbol{x}+\frac{\tau}{m_j}\hbar\boldsymbol{k}_j\\ \boldsymbol{p}-\hbar\boldsymbol{k_j}\end{pmatrix} + e^{-2ik(x_j+\frac{p_j}{m_j}\tau)}\hat{\tilde{W}}_t\begin{pmatrix}\boldsymbol{x}-\frac{\tau}{m_j}\hbar\boldsymbol{k}_j\\ \boldsymbol{p}+\hbar\boldsymbol{k_j}\end{pmatrix}\right]\right.\\
&+ \left[e^{2ik(x_j+\frac{p_j}{m_j}\tau)}\hat{\tilde{W}}_t\begin{pmatrix}\boldsymbol{x}-\frac{\tau}{m_j}\hbar\boldsymbol{k}_j\\ \boldsymbol{p}+\hbar\boldsymbol{k_j}\end{pmatrix} + e^{-2ik(x_j+\frac{p_j}{m_j}\tau)}\hat{\tilde{W}}_t\begin{pmatrix}\boldsymbol{x}+\frac{\tau}{m_j}\hbar\boldsymbol{k}_j\\ \boldsymbol{p}-\hbar\boldsymbol{k_j}\end{pmatrix}\right]\hat{a}^\dagger\hat{a}\\
&+ 2\left[\hat{a}^\dagger\hat{a},\hat{\tilde{W}}_t\begin{pmatrix}\boldsymbol{x}\\ \boldsymbol{p}\end{pmatrix}\right]_+ - 2\int_{-1}^{1} N_j(u)\hat{a}\left[e^{2ik(x_j+\frac{p_j}{m_j}\tau)}\hat{\tilde{W}}_t\begin{pmatrix}\boldsymbol{x}-\frac{\tau}{m_j}\hbar\boldsymbol{k}_j u\\ \boldsymbol{p}+\hbar\boldsymbol{k_j}u\end{pmatrix}\right.\\
&+ \hat{\tilde{W}}_t\begin{pmatrix}\boldsymbol{x}-\frac{\tau}{m_j}\hbar\boldsymbol{k}_j(u-1)\\ \boldsymbol{p}+\hbar\boldsymbol{k_j}(u-1)\end{pmatrix} + \hat{\tilde{W}}_t\begin{pmatrix}\boldsymbol{x}-\frac{\tau}{m_j}\hbar\boldsymbol{k}_j(u+1)\\ \boldsymbol{p}+\hbar\boldsymbol{k_j}(u+1)\end{pmatrix} + e^{-2ik(x_j+\frac{p_j}{m_j}\tau)}\hat{\tilde{W}}_t\left.\left.\begin{pmatrix}\boldsymbol{x}-\frac{\tau}{m_j}\hbar\boldsymbol{k}_j u\\ \boldsymbol{p}+\hbar\boldsymbol{k_j}u\end{pmatrix}\right]\hat{a}^\dagger du\right\}\\
&- \sum_j \frac{\gamma_j'}{2}s_j\left\{(\hat{a}+\hat{a}^\dagger)\frac{1}{2}\left[e^{ik(x_j+\frac{p_j}{m_j}\tau)}\hat{\tilde{W}}_t\begin{pmatrix}\boldsymbol{x}+\frac{\tau}{2m_j}\hbar\boldsymbol{k_j}\\ \boldsymbol{p}-\frac{1}{2}\hbar\boldsymbol{k_j}\end{pmatrix} + e^{-ik(x_j+\frac{p_j}{m_j}\tau)}\hat{\tilde{W}}_t\begin{pmatrix}\boldsymbol{x}-\frac{\tau}{2m_j}\hbar\boldsymbol{k_j}\\ \boldsymbol{p}+\frac{1}{2}\hbar\boldsymbol{k_j}\end{pmatrix}\right]\right.\\
&+ \frac{1}{2}\left[e^{ik(x_j+\frac{p_j}{m_j}\tau)}\hat{\tilde{W}}_t\begin{pmatrix}\boldsymbol{x}-\frac{\tau}{2m_j}\hbar\boldsymbol{k_j}\\ \boldsymbol{p}+\frac{1}{2}\hbar\boldsymbol{k_j}\end{pmatrix} + e^{-ik(x_j+\frac{p_j}{m_j}\tau)}\hat{\tilde{W}}_t\begin{pmatrix}\boldsymbol{x}+\frac{\tau}{2m_j}\hbar\boldsymbol{k_j}\\ \boldsymbol{p}-\frac{1}{2}\hbar\boldsymbol{k_j}\end{pmatrix}\right](\hat{a}+\hat{a}^\dagger)\\
&- \int_{-1}^{1} N_j(u)\left(\hat{a}\left[e^{ik(x_j+\frac{p_j}{m_j}\tau)}\hat{\tilde{W}}_t\begin{pmatrix}\boldsymbol{x}-\frac{\tau}{m_j}\hbar\boldsymbol{k_j}\left(u-\frac{1}{2}\right)\\ \boldsymbol{p}+\hbar\boldsymbol{k_j}\left(u-\frac{1}{2}\right)\end{pmatrix}\right.\right.\\
&+ e^{-ik(x_j+\frac{p_j}{m_j}\tau)}\hat{\tilde{W}}_t\left.\left.\begin{pmatrix}\boldsymbol{x}-\frac{\tau}{m_j}\hbar\boldsymbol{k_j}\left(u+\frac{1}{2}\right)\\ \boldsymbol{p}+\hbar\boldsymbol{k_j}\left(u+\frac{1}{2}\right)\end{pmatrix}\right] + \left[e^{ik(x_j+\frac{p_j}{m_j}\tau)}\hat{\tilde{W}}_t\begin{pmatrix}\boldsymbol{x}-\frac{\tau}{m_j}\hbar\boldsymbol{k_j}\left(u+\frac{1}{2}\right)\\ \boldsymbol{p}+\hbar\boldsymbol{k_j}\left(u+\frac{1}{2}\right)\end{pmatrix}\right.\right.\\
&+ \left.\left.e^{-ik(x_j+\frac{p_j}{m_j}\tau)}\hat{\tilde{W}}_t\begin{pmatrix}\boldsymbol{x}-\frac{\tau}{m_j}\hbar\boldsymbol{k_j}\left(u-\frac{1}{2}\right)\\ \boldsymbol{p}+\hbar\boldsymbol{k_j}\left(u-\frac{1}{2}\right)\end{pmatrix}\right]\hat{a}^\dagger\right)du\Bigg\}. \qquad \text{(A1)}
\end{aligned}$$

This superoperator is expanded in power of ϵ, such that the zeroth-order term in Eq. (30) reads

$$\mathcal{L}_0^{\gamma'}\hat{\tilde{W}} = \sum_j \frac{\gamma_j'}{2}s_j[(\hat{a}-\hat{a}^\dagger),\cos(kx_j)\hat{\tilde{W}}] - \sum_j \frac{\gamma_j'}{2}\cos^2(kx_j)(\hat{a}^\dagger\hat{a}\hat{\tilde{W}} + \hat{\tilde{W}}\hat{a}^\dagger\hat{a} - 2\hat{a}\hat{\tilde{W}}\hat{a}^\dagger), \qquad \text{(A2)}$$

while the first- and second-order terms, given in Eqs. (31) and (32), respectively, take the form

$$\begin{aligned}
\mathcal{L}_1^{\gamma'}\hat{\tilde{W}} &= -\sum_j \frac{\gamma_j'}{2}(\hbar k)\frac{\partial}{\partial p_j}\frac{-i}{2}\sin(2kx_j)[\hat{a}^\dagger\hat{a},\hat{\tilde{W}}] - \sum_j \frac{\gamma_j'}{2}(\hbar k)\frac{1}{2}\frac{\tau i}{m_j}\sin(2kx_j)\left[\hat{a}^\dagger\hat{a},\frac{\partial}{\partial x_j}\hat{\tilde{W}}\right]\\
&+ \sum_j \frac{\gamma_j'}{2}\frac{kp_j}{m_j}\tau\sin(2kx_j)(\hat{a}^\dagger\hat{a}\hat{\tilde{W}} + \hat{\tilde{W}}\hat{a}^\dagger\hat{a} - 2\hat{a}\hat{\tilde{W}}\hat{a}^\dagger), \qquad \text{(A3)}
\end{aligned}$$

$$\begin{aligned}
\mathcal{L}_2^{\gamma'}\hat{\tilde{W}} &= \sum_j \frac{\gamma_j'}{2}s_j^2(\hbar k)^2(\overline{u^2})_j\frac{\partial^2}{\partial p_j^2}\hat{\tilde{W}} - \sum_j \frac{\gamma_j'}{2}\frac{1}{8}(\hbar k)^2\left[2\cos(2kx_j)\left(\hat{a}^\dagger\hat{a}\frac{\partial^2}{\partial p_j^2}\hat{\tilde{W}} + \frac{\partial^2}{\partial p_j^2}\hat{\tilde{W}}\hat{a}^\dagger\hat{a}\right)\right.\\
&\left. - 4\hat{a}\frac{\partial^2}{\partial p_j^2}\hat{\tilde{W}}\hat{a}^\dagger - 2(\overline{u^2})_j[2\cos(2kx_j)+2]\hat{a}\frac{\partial^2}{\partial p_j^2}\hat{\tilde{W}}\hat{a}^\dagger\right] + \sum_j \frac{\gamma_j'}{2}s_j(\hbar k)^2(\overline{u^2})_j\cos(kx_j)\left(\hat{a}\frac{\partial^2}{\partial p_j^2}\hat{\tilde{W}} + \frac{\partial^2}{\partial p_j^2}\hat{\tilde{W}}\hat{a}^\dagger\right). \qquad \text{(A4)}
\end{aligned}$$

Finally, the coefficients appearing in Eq. (36) and due to spontaneous emission are given by the expressions

$$\gamma_{j\ell}' = \frac{\gamma_\ell'}{2}\frac{k}{m_\ell}\sin(2kx_\ell)\mathrm{Tr}\left\{\hat{F}_j\int_0^\infty d\tau\exp(\mathcal{L}_0\tau)\,\tau[\hat{a}^\dagger\hat{a}\sigma_s(\boldsymbol{x}) + \sigma_s(\boldsymbol{x})\hat{a}^\dagger\hat{a} - 2\hat{a}\sigma_s(\boldsymbol{x})\hat{a}^\dagger]\right\}, \qquad \text{(A5)}$$

$$\begin{aligned}
D_{j\ell}' &= -\frac{\gamma_\ell'}{2}(\hbar k)\frac{i}{2}\sin(2kx_\ell)\mathrm{Tr}\left\{\hat{F}_j\int_0^\infty d\tau\exp(\mathcal{L}_0\tau)[\hat{a}^\dagger\hat{a},\sigma_s(\boldsymbol{x})]\right\}\\
&+ \delta_{j\ell}(\hbar k)^2\frac{\gamma_j'}{2}\left\{\langle\hat{a}^\dagger\hat{a}\rangle_{\sigma_s(\boldsymbol{x})}[\sin^2(kx_j) + (\overline{u^2})_j\cos^2(kx_j)] + s_j(\overline{u^2})_j[\langle\hat{a}+\hat{a}^\dagger\rangle_{\sigma_s(\boldsymbol{x})}\cos(kx_j) + s_j]\right\}, \qquad \text{(A6)}
\end{aligned}$$

$$\eta_{j\ell}' = \frac{\gamma_\ell'}{2}\frac{-i\hbar k}{2m_\ell}\sin(2kx_\ell)\mathrm{Tr}\left\{\hat{F}_j\int_0^\infty d\tau\exp(\mathcal{L}_0\tau)\,\tau[\hat{a}^\dagger\hat{a},\sigma_s(\boldsymbol{x})]\right\}. \qquad \text{(A7)}$$

APPENDIX B: FOKKER-PLANCK EQUATION FOR LARGE PHOTON NUMBERS

For the Fokker-Planck equation (39), the SDE take the form [19]

$$dx_j = \frac{p_j}{m_j}dt, \tag{B1}$$

$$dp_j = -\hbar\nabla_j[U_j|\alpha|^2\cos^2(kx_j) + s_jU_j\cos(kx_j)(2\alpha_r) - (2\alpha_i)\Gamma_j s_j\cos(kx_j)]dt + dP_j, \tag{B2}$$

$$d\alpha_r = \left[-\Delta_c'\alpha_i - \kappa'\alpha_r - \sum_j \Gamma_j s_j\cos(kx_j)\right]dt + dA_r, \tag{B3}$$

$$d\alpha_i = \left[\Delta_c'\alpha_r - \kappa'\alpha_i - \sum_j s_jU_j\cos(kx_j)\right]dt + dA_i, \tag{B4}$$

where the noise terms dP_j, dA_r, and dA_i are simulated by means of Wiener processes,

$$\begin{pmatrix} dA_r \\ dA_i \\ dP_1 \\ \cdots \\ dP_N \end{pmatrix} = B\begin{pmatrix} dW_1 \\ dW_2 \\ dW_3 \\ \cdots \\ dW_{N+2} \end{pmatrix}, \tag{B5}$$

where $BB^T = D'$. The diffusion matrix now reads (39)

$$D' = \begin{pmatrix} a & 0 & -b_1\alpha_i & -b_2\alpha_i & \cdots & -b_N\alpha_i \\ 0 & a & b_1\alpha_r & b_2\alpha_r & \cdots & b_N\alpha_r \\ -b_1\alpha_i & b_1\alpha_r & c_1 & 0 & \cdots & 0 \\ -b_2\alpha_i & b_2\alpha_r & 0 & c_2 & \ddots & \vdots \\ \vdots & \vdots & \vdots & \ddots & \ddots & 0 \\ -b_N\alpha_i & b_N\alpha_r & 0 & \cdots & 0 & c_N \end{pmatrix},$$

with $a = \kappa'/2$, $b_j = -(\hbar k/2)\Gamma_j\sin(2kx_j)$, and

$$c_j = 2(\hbar k)^2\Gamma_j\{|\alpha|^2[\sin^2(kx) + (\overline{u^2})_j\cos^2(kx_j)] + s_j(\overline{u^2})_j[2\alpha_r\cos(kx_j) + s_j]\}.$$

When we integrate these stochastic differential equations, we assume that the initial state of the cavity field is a coherent state with $\langle\alpha_r\rangle = 5$ and $\langle\alpha_i\rangle = 0$. This ensures the validity of the semiclassical description for the cavity field at $t = 0$, which has to be verified for all later times.

[1] S. Chu, Rev. Mod. Phys. **70**, 685 (1998); C. N. Cohen-Tannoudji, *ibid.* **70**, 707 (1998); W. D. Phillips, *ibid.* **70**, 721 (1998).
[2] D. J. Wineland and W. M. Itano, Phys. Rev. A **20**, 1521 (1979).
[3] S. Stenholm, Rev. Mod. Phys. **58**, 699 (1986).
[4] P. Horak, G. Hechenblaikner, K. M. Gheri, H. Stecher, and H. Ritsch, Phys. Rev. Lett. **79**, 4974 (1997).
[5] V. Vuletic and S. Chu, Phys. Rev. Lett. **84**, 3787 (2000).
[6] P. Domokos and H. Ritsch, J. Opt. Soc. Am. B **20**, 1098 (2003).
[7] J. McKeever, J. R. Buck, A. D. Boozer, A. Kuzmich, H.-C. Nägerl, D. M. Stamper-Kurn, and H. J. Kimble, Phys. Rev. Lett. **90**, 133602 (2003).
[8] P. Maunz, T. Puppe, I. Schuster, N. Syassen, P. W. H. Pinkse, and G. Rempe, Nature (London) **428**, 50 (2004).
[9] K. Murr, Phys. Rev. Lett. **96**, 253001 (2006).
[10] B. Nagorny, Th. Elsässer, and A. Hemmerich, Phys. Rev. Lett. **91**, 153003 (2003); S. Gupta, K. L. Moore, K. W. Murch, and D. M. Stamper-Kurn, *ibid.* **99**, 213601 (2007); S. Ritter, F. Brennecke, K. Baumann, T. Donner, C. Guerlin, and T. Esslinger, Appl. Phys. B **95**, 213 (2009).
[11] C. von Cube, S. Slama, D. Kruse, C. Zimmermann, Ph. W. Courteille, G. R. M. Robb, N. Piovella, and R. Bonifacio, Phys. Rev. Lett. **93**, 083601 (2004).
[12] R. Bonifacio and L. De Salvo, Nucl. Instrum. Methods Phys. Res., Sect. A **341**, 360 (1994); D. Kruse, C. von Cube, C. Zimmermann, and Ph. W. Courteille, Phys. Rev. Lett. **91**, 183601 (2003).
[13] P. Domokos and H. Ritsch, Phys. Rev. Lett. **89**, 253003 (2002).

[14] A. T. Black, H. W. Chan, and V. Vuletic, Phys. Rev. Lett. **91**, 203001 (2003).
[15] K. Baumann, C. Guerlin, F. Brennecke, and T. Esslinger, Nature (London) **464**, 1301 (2010).
[16] K. J. Arnold, M. P. Baden, and M. D. Barrett, Phys. Rev. Lett. **109**, 153002 (2012).
[17] J. K. Asbóth, P. Domokos, H. Ritsch, and A. Vukics, Phys. Rev. A **72**, 053417 (2005).
[18] H. Ritsch, P. Domokos, F. Brennecke, and T. Esslinger, Rev. Mod. Phys. **85**, 553 (2013).
[19] P. Domokos, P. Horak, and H. Ritsch, J. Phys. B **34**, 187 (2001).
[20] J. Dalibard and C. Cohen-Tannoudji, J. Phys. B **18**, 1661 (1985).
[21] J. Javanainen and S. Stenholm, Appl. Phys. **21**, 283 (1980).
[22] J. Javanainen and S. Stenholm, Appl. Phys. **21**, 35 (1980).
[23] C. W. Gardiner and P. Zoller, *Quantum Noise* (Springer-Verlag, Berlin, 2001).
[24] C. W. Gardiner, *Stochastic Methods* (Springer-Verlag, Berlin Heidelberg, 2009).
[25] W. Niedenzu, T. Grießer, and H. Ritsch, Europhys. Lett. **96**, 43001 (2011).
[26] See, for instance, Y. Castin and J. Dalibard, Europhys. Lett. **14**, 761 (1991).
[27] H. Habibian, S. Zippilli, and G. Morigi, Phys. Rev. A **84**, 033829 (2011).
[28] Y. Castin, H. Wallis, and J. Dalibard, J. Opt. Soc. Am. B **6**, 2046 (1989).
[29] J. I. Cirac, R. Blatt, P. Zoller, and W. D. Phillips, Phys. Rev. A **46**, 2668 (1992).
[30] H. J. Kimble, in *Cavity Quantum Electrodynamics*, edited by P. R. Berman (Academic, New York, 1994), p. 203.
[31] A. Vukics and P. Domokos, Phys. Rev. A **72**, 031401 (2005).
[32] We have performed the numerical simulation with and without Eq. (50) and found no relevant difference in dynamics and asymptotic behavior, both with and without spontaneous decay.
[33] M. Wolke, J. Klinner, H. Keßler, and A. Hemmerich, Science **337**, 75 (2012).
[34] G. Hechenblaikner, M. Gangl, P. Horak, and H. Ritsch, Phys. Rev. A **58**, 3030 (1998).

CHAPTER 2

Prethermalization of Atoms Due to Photon-Mediated Long-Range Interactions

Prethermalization of Atoms Due to Photon-Mediated Long-Range Interactions

PHYSICAL REVIEW LETTERS **113**, 203002 (2014)

DOI: 10.1103/PhysRevLett.113.203002

Authors: Stefan Schütz and Giovanna Morigi

Theoretische Physik, Universität des Saarlandes, D-66123 Saarbrücken, Germany

Author Contributions:
The theoretical model was developed by S. Schütz and G. Morigi. Numerical simulations were designed and performed by S. Schütz. The calculations and results were checked, discussed and analysed by all authors. The article was written by all authors.

Abstract:
Atoms can spontaneously form spatially ordered structures in optical resonators when they are transversally driven by lasers. This occurs when the laser intensity exceeds a threshold value and results from the mechanical forces on the atoms associated with superradiant scattering into the cavity mode. We treat the atomic motion semiclassically and show that, while the onset of spatial ordering depends on the intracavity-photon number, the stationary momentum distribution is a Gaussian function whose width is determined by the rate of photon losses. Above

threshold, the dynamics is characterized by two time scales: after a violent relaxation, the system slowly reaches the stationary state over time scales exceeding the cavity lifetime by several orders of magnitude. In this transient regime the atomic momenta form non-Gaussian metastable distributions, which emerge from the interplay between the long-range dispersive and dissipative mechanical forces of light. We argue that the dynamics of self-organization of atoms in cavities offers a test bed for studying the statistical mechanics of long-range interacting systems.

PRL 113, 203002 (2014) PHYSICAL REVIEW LETTERS week ending 14 NOVEMBER 2014

Prethermalization of Atoms Due to Photon-Mediated Long-Range Interactions

Stefan Schütz and Giovanna Morigi
Theoretische Physik, Universität des Saarlandes, D-66123 Saarbrücken, Germany
(Received 29 July 2014; published 14 November 2014)

Atoms can spontaneously form spatially ordered structures in optical resonators when they are transversally driven by lasers. This occurs when the laser intensity exceeds a threshold value and results from the mechanical forces on the atoms associated with superradiant scattering into the cavity mode. We treat the atomic motion semiclassically and show that, while the onset of spatial ordering depends on the intracavity-photon number, the stationary momentum distribution is a Gaussian function whose width is determined by the rate of photon losses. Above threshold, the dynamics is characterized by two time scales: after a violent relaxation, the system slowly reaches the stationary state over time scales exceeding the cavity lifetime by several orders of magnitude. In this transient regime the atomic momenta form non-Gaussian metastable distributions, which emerge from the interplay between the long-range dispersive and dissipative mechanical forces of light. We argue that the dynamics of self-organization of atoms in cavities offers a test bed for studying the statistical mechanics of long-range interacting systems.

DOI: 10.1103/PhysRevLett.113.203002 PACS numbers: 37.30.+i, 05.65.+b, 05.70.Ln, 42.65.Sf

Long-range interactions characterize the dynamics of systems from microscopic to macroscopic scales, ranging from nuclear to astrophysical distances [1]. In these systems the individual components can interact with a long-range potential that decays with the interparticle distance r slower than r^{-d} in d dimensions. This property leads, to mention some, to ensemble inequivalence and to the existence of quasistationary states, i.e., metastable states with nonthermal distributions [1].

Cold atoms driven by laser light constitute a promising laboratory realization of long-range interacting systems [2–5]. Here, multiple scattering of photons by atoms gives rise to mechanical forces that are infinitely long ranged when the atoms couple to a single-mode high-finesse cavity [6]. In the overdamped regime this long-ranged potential lies at the origin of synchronization [7] and collective atomic recoil lasing [8]. When the cavity mode is a standing wave and the atoms are transversally pumped, as in the setup sketched in Fig. 1, spontaneous ordering in spatially periodic structures occurs [3,9–11]. The phenomenon can be described in terms of formation of atomic gratings that maximize coherent scattering of laser photons into the cavity mode. These "Bragg gratings" are stably trapped by the mechanical effects of the light they scatter, provided that the laser compensates the cavity losses so that the number of intracavity photons is sufficiently large. This takes place when the strength of the laser coupling exceeds a threshold value Ω_c depending, amongst others, on the rate of photon losses and the number of atoms N that couple with the cavity mode [12,13]. This spatial self-organization was first predicted in Refs. [4,9] and then reported in a series of experiments at laser-cooling temperatures [10,14] and in the ultracold regime [11,15].

In this Letter we theoretically analyze the dynamics leading to the formation of spatial structures and their stationary properties in one dimension. For this purpose we resort to a Fokker-Planck equation (FPE) derived when the atoms are classically polarizable particles; their center-of-mass motion is treated semiclassically, while the cavity field is a full quantum variable [16]. This semiclassical limit can be applied when the cavity linewidth κ (which determines the scattering cross section) exceeds the recoil energy $\omega_r = \hbar k^2/(2m)$, scaling the exchange of mechanical energy between an atom of mass m and a photon of wave number k. Our approach complements the one applied in Refs. [9,12,13,17], based on the assumption that the cavity field is a semiclassical variable. By treating the cavity field quantum mechanically, we determine its state for any value of the laser amplitude and, in particular, at threshold, where quantum fluctuations are important. This information is extracted provided that retardation

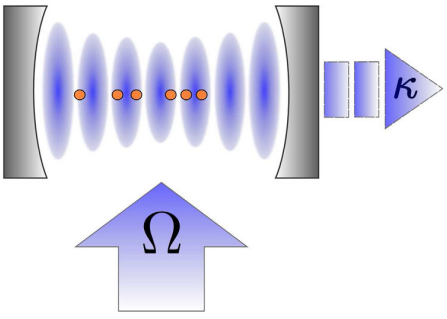

FIG. 1 (color online). Atoms in a standing-wave cavity and driven by a transverse laser can spontaneously form ordered patterns when the laser intensity Ω exceeds the rate of photon losses, here due to cavity decay at rate κ. In this regime the atoms experience a long-range interaction mediated by the cavity photons and their motion becomes strongly correlated.

PRL 113, 203002 (2014) PHYSICAL REVIEW LETTERS week ending 14 NOVEMBER 2014

effects in the scattering processes are perturbations, such that at leading order the field is determined by the instantaneous atomic distribution [18]. Thus, for N identical atoms confined in one dimension along the cavity axis, the total scattering amplitude depends on their positions $x_1, \ldots, x_N$ within the cavity standing wave $\cos(kx)$ and the cavity electric field at time t is $E_c(t) \propto \sqrt{N\bar{n}}\langle\Theta\rangle_t$. Here, $\bar{n}$ is the maximum intracavity-photon number per atom, and is thus controlled by the strength of the external laser pump [19], while the order parameter

$$\Theta = \sum_{j=1}^{N} \cos(kx_j)/N$$

characterizes spatial ordering in the cavity [12]. The field reaches its maximum when $|\Theta| = 1$, namely, when the atoms form a Bragg grating. The corrections to E_c due to the atomic motion are systematically included in the following as perturbation, assuming that the Doppler shifts of the atoms are smaller than the cavity linewidth κ [16].

The averages $\langle\cdot\rangle_t$ are taken over the normalized distribution $f(x_1, p_1; \ldots; x_N, p_N; t)$ at time t, where $p_1, \ldots, p_N$ are the atomic momenta and f obeys the FPE [16]

$$\partial_t f + \{f, H\} \simeq -\bar{n}\Gamma \sum_i \sin(kx_i)\partial_{p_i} \frac{1}{N} \sum_j \sin(kx_j)\left(p_j + \frac{m}{\beta}\partial_{p_j}\right) f. \tag{1}$$

Here, the left-hand side (LHS) contains the Poisson brackets with the Hamiltonian H governing the coherent dynamics, that originate from the conservative mechanical forces of light. The right-hand side (RHS) contains the friction coefficient due to retardation and the diffusion, due to fluctuations of the cavity field because of photon losses [20]: These terms are scaled by $\bar{n}$ and by the rate $\Gamma = 8\omega_r\kappa\Delta_c/(\Delta_c^2 + \kappa^2)$, with $\Delta_c = \omega_L - \omega_c$ the detuning between laser and cavity-mode frequencies, such that $\bar{n}\Gamma$ is the maximum damping rate of a single atom ($N = 1$). In addition, $\hbar\beta = -4\Delta_c/(\Delta_c^2 + \kappa^2)$. The Hamiltonian

$$H = \sum_j \frac{p_j^2}{2m} + \hbar\Delta_c\bar{n}N\Theta^2 + \mathcal{O}(U) \tag{2}$$

contains the cavity-mediated potential, which scales with $\bar{n}$ and is attractive when Δ_c is negative. Hence, this detuning determines whether the formation of Bragg gratings is energetically favored. Equation (2) summarizes in a compact way a property that was observed in several previous works [9,10,12]. It is reported at leading order in $|NU/\Delta_c|$, where U is the dynamical Stark shift due to the coupling with the cavity field [19], and whose effect is systematically included in the numerical simulations.

Remarkably, at leading order in $|NU/\Delta_c|$, Eq. (2) allows one to draw a direct connection with the Hamiltonian Mean Field (HMF) model, the workhorse of the statistical mechanics of systems with long-range interaction, which in a canonical ensemble exhibits a second-order phase transition from a paramagnetic to a ferromagnetic phase controlled by the temperature [1]. This analogy becomes explicit, writing $\Theta^2 = \sum_{i,j}\{\cos[k(x_i + x_j)] + \cos[k(x_i - x_j)]\}/(2N^2)$, which shows that H is extensive as it satisfies the Kac prescription [1], and suggests to identify Θ with the x component of a two-dimensional magnetization.

Differing from the HMF model, the term $\cos[k(x_i + x_j)]$ originates from the underlying cavity standing-wave potential that breaks continuous translational invariance. Moreover, the cavity coupling at higher order in $|NU/\Delta_c|$ gives rise to deviations from the Hamiltonian dynamics due to further terms in the LHS of Eq. (1) (see, e.g., [21]) which are responsible for bistable behavior [22]. Retardation effects and cavity losses, in addition, can establish long-range correlations between the atoms, as visible by inspecting the RHS. In fact, diffusion is here due to global quenches of the cavity potential. Similarly, retardation effects modify the cavity potential [23]. When the density is uniform, the terms in the RHS reduce to the Langevin terms of a FPE, which fulfills detailed balance and the model is analogous to the Brownian mean field model [24]. However, this is valid at all times only well below the self-organization threshold. Indeed, the stationary density is here controlled by $\bar{n}$, and thus by the laser intensity, which scales both the strength of the long-range coherent and incoherent forces. This becomes evident when studying the dynamics at the asymptotics: A solution of $\partial_t f_\infty = 0$ is the thermal distribution $f_\infty = f_0 \exp(-\beta H)$ for $\Delta_c < 0$, with f_0 normalizing factor. The temperature is *independent* of the laser intensity and its minimum $k_B T_{\min} = \hbar\kappa/2$ is achieved for $\Delta_c = -\kappa$, as also found in Refs. [12,13,25] using different approaches. In [13] the self-organization threshold $\bar{n}_c = (1 + \kappa^2/\Delta_c^2)/4$ was estimated by means of a kinetic theory based on treating the cavity field semiclassically. This value is consistent with our results.

We first discuss the predictions of Eq. (1) at the asymptotics. Figure 2(a) displays the stationary distribution of the magnetization, $P(\Theta_0) = \langle\delta(\Theta_0 - \Theta)\rangle_\infty$, for different values of $\bar{n}$. For $\bar{n} < \bar{n}_c$, $P(\Theta_0)$ is approximately a Gaussian centered at zero. At threshold it broadens and becomes increasingly localized at the values ± 1 as $\bar{n}$ grows. The width of this distribution is determined by the fluctuations of the trajectories $\Theta(t)$: the larger $\bar{n}$ is, the more localized are the atoms at a Bragg grating, while the probability of a jump between gratings vanishes accordingly. Typical trajectories $\Theta(t)$ at the asymptotics of the dynamics are shown in Fig. 2(b): They are obtained by integrating the stochastic differential equations (SDE) derived from Eq. (1) [16]. While below threshold $\Theta(t)$ fluctuates about zero

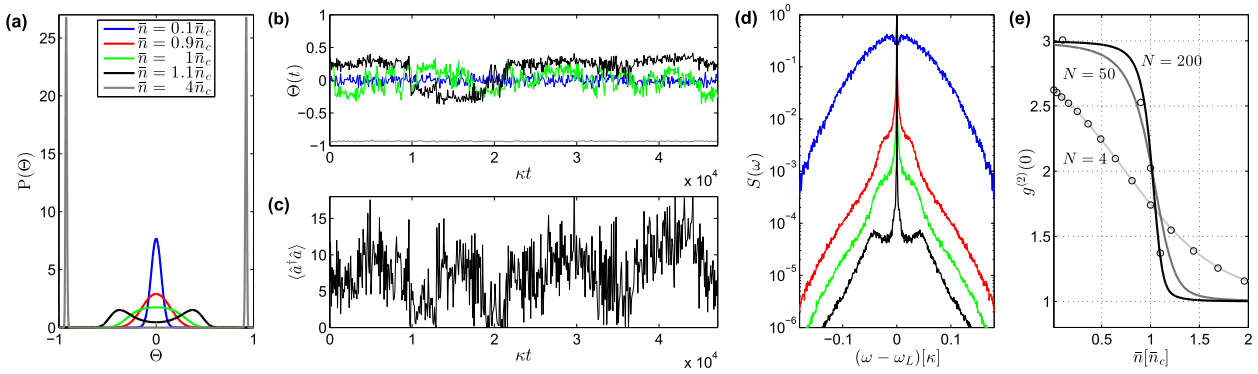

FIG. 2 (color online). (a) Distribution $P(\Theta)$ of the magnetization Θ at steady state for $\bar{n}/\bar{n}_c = 0.1, 0.9, 1, 1.1, 4$ (see box for color code). (b) Typical trajectories at the asymptotics for $N = 200$ atoms are shown in (b) as a function of time (in units of $1/\kappa$) and for $\bar{n}/\bar{n}_c = 0.1, 1, 1.1, 4$. Note that the cavity field amplitude is proportional to Θ. (c) Mean intracavity-photon number as a function of time for the trajectory at $\bar{n} = 1.1\bar{n}_c$. (d) Spectrum $S(\omega)$ of the intensity of the emitted light (arbitrary units) as a function of ω (in units of κ) for $\bar{n}/\bar{n}_c = 0.1, 0.9, 1, 1.1$ (from top to bottom). (e) $g^{(2)}(0)$ as a function of $\bar{n}$ for different atom numbers. The dots correspond to numerical results obtained by integrating the SDE. The cavity parameters are rescaled with N so that $\bar{n}_c$ is independent on N and finite (see [21]). The atomic transition is the D_2 line of ^{85}Rb at half linewidth $\gamma = 2\pi \times 3$ MHz. The laser detuning from the atomic frequency is $\Delta_a = -500\gamma$. Here, $\Delta_c = -\kappa$ with $\kappa = 0.5\gamma$.

(corresponding to a uniform spatial distribution), as $\bar{n}$ is increased above threshold it takes either positive or negative values, in which it remains trapped for time intervals which grow with $\bar{n}$. Jumps between the two values correspond to quenches of the intracavity-photon number following losses, as shown in (c) for $\bar{n} = 1.1\bar{n}_c$, and take place over time intervals approximately scaling with the recoil frequency. Note that these jumps correspond to a simultaneous jump of all atomic trajectories out of the Bragg gratings [9,12]. For $\bar{n} = 4\bar{n}_c$ the residence time is infinite: photon losses give rise to small fluctuations of the potential depth and the atoms remain locked in a Bragg grating. These features determine the light amplitude at the cavity output, the jumps correspond to jumps of the field phase and can be measured by heterodyne detection [10,26]. Additional information is contained in the power spectrum of the light intensity, which is the Fourier transform $S(\omega)$ of the correlation function $g^{(1)}(\tau) = \lim_{t\to\infty}\langle\Theta(\tau + t)\Theta(t)\rangle/\langle|\Theta(t)|\rangle^2$ and is displayed in Fig. 2(d) for different values of $\bar{n}$. $S(\omega)$ exhibits a narrow peak at the laser frequency as the threshold is approached, and is associated with the creation of Bragg gratings coherently scattering light into the resonator. The broad background spectrum is progressively suppressed, corresponding to a suppression of fluctuations of the order parameter as the atoms become localized in Bragg gratings. Moreover, at threshold two broad sidebands appear whose maximum moves away from $\omega = \omega_L$ as $\bar{n}$ increases from $\bar{n}_c$. A qualitative analysis shows that the sidebands width decreases as $\bar{n}$ is increased from $\bar{n}_c$. Similar features have been observed in the ultracold [15,26,27] and have been interpreted in terms of density waves that drive the instability. Figure 2(e) displays the second-order correlation function of the emitted light at zero-time delay $g^{(2)}(0)$ as a function of $\bar{n}$, where $g^{(2)}(\tau) = \lim_{t\to\infty}\langle\Theta(\tau + t)^2\Theta(t)^2\rangle/\langle\Theta(t)^2\rangle^2$. Below threshold $g^{(2)}(0) \to 3$. This value is also found analytically after discarding correlations between the atoms. It monotonically decreases with $\bar{n}$ and reaches unity above threshold, $g^{(2)}(0) \to 1$, corresponding to a coherent state inside the resonator [28]. The crossover between these two regimes narrows as the number of atoms is increased, suggesting a jump at $\bar{n}_c$ in the thermodynamic limit (here consisting of keeping $\bar{n}_c$ constant as $N \to \infty$ [12,21]).

These features are consistent with the conjecture that self-organization is a second-order phase transition controlled by $\bar{n}$. This is also supported by the behavior of the susceptibility $\chi = \langle\Theta(t)^2\rangle - \langle|\Theta(t)|\rangle^2$ as a function of $\bar{n}$, which suggests a divergence at $\bar{n}_c$ for $N \to \infty$. We remark that the typical understanding of spatial domain formation at a second-order phase transition is here meaningless due to the nonadditivity of the energy: mesoscopic Bragg gratings with $\Theta = \pm 1$ cannot stably coexist in space, since the resulting cavity field vanishes and with it the interatomic potential.

We now turn to the dynamics leading to self-organization. We assume that the initial distribution is spatially uniform, while the momentum distribution is Gaussian with $1/\beta = \hbar\kappa/2$. For $\Delta_c = -\kappa$, at $\bar{n} \ll \bar{n}_c$ this distribution is stationary [16]. At $t = 0$ the transverse field is quenched to a value corresponding to $\bar{n}$ above threshold. Figure 3 displays a sample of 500 trajectories of $\Theta(t)$ as a function of time when $\bar{n} = 4\bar{n}_c$ and $N = 200$. The trajectories are bunched and their behavior can be ordered into three regimes, characterized by different time scales. First, a fast relaxation occurs over the time scale of dozens cavity lifetimes $\tau_c = 1/\kappa$, in which the magnetization reaches an intermediate value of about 0.6 [Fig. 3(b)], where it remains

PRL 113, 203002 (2014) PHYSICAL REVIEW LETTERS week ending 14 NOVEMBER 2014

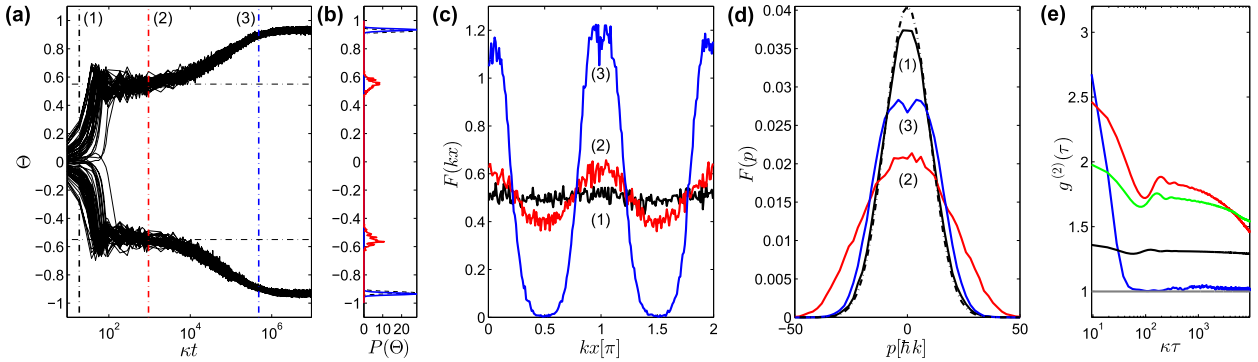

FIG. 3 (color online). Dynamics of the order parameter above threshold: (a) Θ as a function of time (in units of κ^{-1}) for $N = 200$ atoms and 500 trajectories at $\bar{n} = 4\bar{n}_c$ and $\Delta_c = -\kappa$, for an initially spatially uniform distribution at temperature $k_B T = \hbar\kappa/2$. $P(\Theta)$ at the transient and at the asymptotics is shown in panel (b). The position (c) and momentum (d) distributions are displayed at the times indicated by (1), (2), and (3) in panel (a). The dashed lines correspond to the initial distributions [which overlaps to (1) in (c)]. (e) Intensity-intensity correlations of the light at the cavity output, $g^{(2)}(\tau)$ as a function of τ (in units of κ^{-1}) for $\bar{n}/\bar{n}_c = 0.1, 0.9, 1, 1.1, 4$, (same color code as in Fig. 2) evaluated after the system has reached the stationary state.

for a time scale exceeding τ_c by 4 orders of magnitude. During the relaxation the spatial density is almost uniform, therefore cross-correlations due to noise and mechanical forces are almost negligible. After this relaxation, part of the atoms form a Bragg grating [Fig. 3(c)] while the momentum distribution is non-Gaussian [Fig. 3(d)]. We denote this regime by prethermalization. Then, the magnetization slowly grows to the stationary value over time scales which are 6 orders of magnitude of the cavity lifetime. Remarkably, for times of the order of $t \sim 10^5 \tau_c$ the momentum distribution exhibits clear deviations from a Gaussian, and, hence, from a thermal state, even though the spatial distribution is very close to the asymptotic one. This behavior can be understood considering that the diffusion is a function of the spatial distribution: As visible in the RHS of Eq. (1), the strength of noise (and thus the relaxation rate) decreases the more the atoms are localized in the Bragg gratings, and thus at the nodes of the $\sin(kx)$ function. In the prethermalization time scale we verified that spatial diffusion follows a power law according to $\langle x(t)^2 \rangle \propto t^{2\alpha}$, where α is monotonically decreasing as $\bar{n}$ increases. In particular, it is superdiffusive ($\alpha > 1/2$) below $\bar{n}_c$, while above $\bar{n}_c$ it becomes increasingly subdiffusive. In this latter case, in the long tails of relaxation it becomes normal again, $\alpha \to 1/2$. Figure 3(e) displays $g^{(2)}(\tau)$ for different values of $\bar{n}$. Below threshold it rapidly decays from 3 to unity on a time scale of the order of cavity decay; at threshold its relaxation is orders of magnitude slower and exhibits damped oscillations, which can be associated with the density waves that become unstable and determine the Bragg grating [cf. Fig. 2(d)]. Well above threshold, instead, it remains locked to unity, corresponding to coherent light.

The prethermalization behavior, followed by the slow rate at which the steady state is approached, is typical above the self-organization threshold. We argue that it is a manifestation of the long-range correlations mediated by the cavity photons, and is analogous to observations made in studies of nonequilibrium stochastic long-range-interacting systems [29]. We further note that similar prethermalization features have been observed in quantum spin models with spatially correlated noise [30]. Differing from these latter models, here the stationary state exhibits long-range spatial correlations. On the other hand, we do not find signatures of quasistationary states, whose relaxation times increase with N^δ, with $\delta > 1$ and whose existence is intrinsically related to the long-range nature of the interaction [1]. We believe this is due to the effect of the external environment, consistently with studies showing that its action can make these states dynamically unstable [31,32].

In this work we discarded the effect of spontaneous decay, assuming it is negligible as the laser field is far off resonance. Its role is expected to become more important as $\bar{n}$ is increased above threshold, and thus to enforce the dynamical instability of quasistationary states. Our model is also valid for any optically polarizable particles which can be confined within the resonator [33]. It is also valid for $\bar{n} \gg \bar{n}_c$, when the atoms are tightly trapped in the potentials, as long as the effective trap frequency ν of the resulting lattice is smaller than the cavity linewidth [34]. The description breaks down for $\nu \simeq \kappa$, when quantum mechanical coherence between the motional levels can be observed [35,36].

In view of these results, one shall consider the self-organization transition observed in the ultracold regime by quenching the laser intensity [11] in terms of an intrinsically out-of-equilibrium phenomenon. Indeed, our results predict that Hamiltonian solutions that possess the spatial modulation of the Bragg gratings will experience very small noise, even if they do not correspond with the stationary state. This raises the need to develop a kinetic theory for these systems as in Ref. [29]. Preliminary studies in this direction have appeared in [13,25,37,38]. To

conclude, our study shows that photonic systems offer a promising platform to study the statistical mechanics of long-range interacting systems, thus gaining insight into the dynamical properties of non-neutral plasmas and self-gravitating clusters [1].

The authors thank S. Fishman, H. Habibian, G. Manfredi, F. Piazza, H. Ritsch, L. Santen, W. Niedenzu, S. Ruffo, A. Vukics, and especially S. Jäger for fruitful discussions. This work was partially supported by the German Research Foundation (DFG). G. M. acknowledges the Ion Storage Group at NIST for hospitality, where part of this work was done.

[1] A. Campa, T. Dauxois, and S. Ruffo, Phys. Rep. **480**, 57 (2009).
[2] R. Bachelard, T. Manos, P. de Buyl, F. Staniscia, F. S. Cataliotti, G. De Ninno, D. Fanelli, and N. Piovella, J. Stat. Mech. (2010) P06009.
[3] H. Ritsch, P. Domokos, F. Brennecke, and T. Esslinger, Rev. Mod. Phys. **85**, 553 (2013).
[4] D. H. J. O'Dell, S. Giovanazzi, and G. Kurizki, Phys. Rev. Lett. **90**, 110402 (2003).
[5] G. Labeyrie, E. Tesio, P. M. Gomes, G.-L. Oppo, W. J. Firth, G. R. M. Robb, A. S. Arnold, R. Kaiser, and T. Ackemann, Nat. Photonics **8**, 321 (2014).
[6] P. Münstermann, T. Fischer, P. Maunz, P. W. H. Pinkse, and G. Rempe, Phys. Rev. Lett. **84**, 4068 (2000).
[7] M. Xu, D. A. Tieri, E. C. Fine, J. K. Thompson, and M. J. Holland, arXiv:1307.5891.
[8] C. von Cube, S. Slama, D. Kruse, C. Zimmermann, Ph. W. Courteille, G. R. M. Robb, N. Piovella, and R. Bonifacio, Phys. Rev. Lett. **93**, 083601 (2004).
[9] P. Domokos and H. Ritsch, Phys. Rev. Lett. **89**, 253003 (2002).
[10] A. T. Black, H. W. Chan, and V. Vuletic, Phys. Rev. Lett. **91**, 203001 (2003).
[11] K. Baumann, C. Guerlin, F. Brennecke, and T. Esslinger, Nature (London) **464**, 1301 (2010).
[12] J. K. Asbóth, P. Domokos, H. Ritsch, and A. Vukics, Phys. Rev. A **72**, 053417 (2005).
[13] W. Niedenzu, T. Grießer, and H. Ritsch, Europhys. Lett. **96**, 43001 (2011).
[14] K. J. Arnold, M. P. Baden, and M. D. Barrett, Phys. Rev. Lett. **109**, 153002 (2012).
[15] R. Mottl, F. Brennecke, K. Baumann, R. Landig, T. Donner, and T. Esslinger, Science **336**, 1570 (2012).
[16] S. Schütz, H. Habibian, and G. Morigi, Phys. Rev. A **88**, 033427 (2013).
[17] P. Domokos, P. Horak, and H. Ritsch, J. Phys. B **34**, 187 (2001).
[18] J. Dalibard and C. Cohen-Tannoudji, J. Phys. B **18**, 1661 (1985).
[19] The maximum intracavity photon number per atom is $\bar{n} = NS^2/(\Delta_c^2 + \kappa^2)$, where S is the scattering amplitude of a laser photon into the cavity field by one atom. In detail, $S = g\Omega/\Delta_a$, with g the cavity vacuum Rabi frequency, Ω the Rabi frequency of the driving laser, and Δ_a the detuning of the fields from the excited state of the atomic transition. This detuning is the largest parameter of the problem. The dynamical Stark shift U is $U = g^2/\Delta_a$. See [16] for further details.
[20] K. Murr, P. Maunz, P. W. H. Pinkse, T. Puppe, I. Schuster, D. Vitali, and G. Rempe, Phys. Rev. A **74**, 043412 (2006).
[21] S. Fernández-Vidal, G. De Chiara, J. Larson, and G. Morigi, Phys. Rev. A **81**, 043407 (2010).
[22] S. Gupta, K. L. Moore, K. W. Murch, and D. M. Stamper-Kurn, Phys. Rev. Lett. **99**, 213601 (2007)
[23] P. Domokos and H. Ritsch, J. Opt. Soc. Am. B **20**, 1098 (2003).
[24] P. H. Chavanis, J. Vatteville, and F. Bouchet, Eur. Phys. J. B **46**, 61 (2005); P. H. Chavanis, Eur. Phys. J. B **87**, 120 (2014).
[25] F. Piazza and P. Strack, arXiv:1407.5642.
[26] K. Baumann, R. Mottl, F. Brennecke, and T. Esslinger, Phys. Rev. Lett. **107**, 140402 (2011).
[27] F. Brennecke, R. Mottl, K. Baumann, R. Landig, T. Donner, and T. Esslinger, Proc. Natl. Acad. Sci. U.S.A. **110**, 11 763 (2013).
[28] H. Habibian, S. Zippilli, and G. Morigi, Phys. Rev. A **84**, 033829 (2011).
[29] C. Nardini, S. Gupta, S. Ruffo, T. Dauxois, and F. Bouchet, J. Stat. Mech. (2012) P12010.
[30] B. Olmos, I. Lesanovsky, and J. P. Garrahan, Phys. Rev. Lett. **109**, 020403 (2012).
[31] S. Gupta and D. Mukamel, Phys. Rev. Lett. **105**, 040602 (2010).
[32] P.-H. Chavanis, F. Baldovin, and E. Orlandini, Phys. Rev. E **83**, 040101 (2011).
[33] A. Vukics and P. Domokos, Phys. Rev. A **72**, 031401 (2005).
[34] A Fokker-Planck equation for laser-cooled interacting atoms in the Lamb-Dicke regime is, for instance, in G. Morigi and J. Eschner, Phys. Rev. A **64**, 063407 (2001).
[35] M. Wolke, J. Klinner, H. Keßler, and A. Hemmerich, Science **337**, 75 (2012).
[36] R. M. Sandner, W. Niedenzu, and H. Ritsch, Europhys. Lett. **104**, 43001 (2013).
[37] E. G. Dalla Torre, S. Diehl, M. D. Lukin, S. Sachdev, and P. Strack, Phys. Rev. A **87**, 023831 (2013).
[38] T. Grießer, H. Ritsch, M. Hemmerling, and G. R. M. Robb, Eur. Phys. J. D **58**, 349 (2010).

CHAPTER 3

Thermodynamics and dynamics of atomic self-organization in an optical cavity

Thermodynamics and dynamics of atomic self-organization in an optical cavity

PHYSICAL REVIEW A **92**, 063808 (2015)

DOI: 10.1103/PhysRevA.92.063808

Authors: Stefan Schütz, Simon B. Jäger, and Giovanna Morigi

Theoretische Physik, Universität des Saarlandes, D-66123 Saarbrücken, Germany

Author Contributions:
The theoretical model was developed by S. Schütz and G. Morigi. Analytical calculations were performed by S. B. Jäger and S. Schütz. Numerical simulations were designed and performed by S. Schütz. The calculations and results were checked, discussed and analysed by all three authors. The article was written by all three authors.

Abstract:
Pattern formation of atoms in high-finesse optical resonators results from the mechanical forces of light associated with superradiant scattering into the cavity mode. It occurs when the laser intensity exceeds a threshold value such that the pumping processes counteract the losses. We consider atoms driven by a laser and coupling with a mode of a standing-wave cavity and describe their dynamics with a Fokker-Planck equation, in which the atomic motion is semiclassical

but the cavity field is a full quantum variable. The asymptotic state of the atoms is a thermal state, whose temperature is solely controlled by the detuning between the laser and the cavity frequency and by the cavity loss rate. From this result we derive the free energy and show that in the thermodynamic limit self-organization is a second-order phase transition. The order parameter is the field inside the resonator to which one can associate a magnetization in analogy to ferromagnetism, the control field is the laser intensity, but the steady state is intrinsically out of equilibrium. In the symmetry-broken phase, quantum noise induces jumps of the spatial density between two ordered patterns: We characterize the statistical properties of this temporal behavior at steady state and show that the thermodynamic properties of the system can be extracted by detecting the light at the cavity output. The results of our analysis are in full agreement with previous studies; we extend them by deriving a self-consistent theory which is valid also when the cavity field is in the shot-noise limit and elucidate the nature of the self-organization transition.

PHYSICAL REVIEW A **92**, 063808 (2015)

Thermodynamics and dynamics of atomic self-organization in an optical cavity

Stefan Schütz, Simon B. Jäger, and Giovanna Morigi
Theoretische Physik, Universität des Saarlandes, D-66123 Saarbrücken, Germany
(Received 27 August 2015; published 7 December 2015)

Pattern formation of atoms in high-finesse optical resonators results from the mechanical forces of light associated with superradiant scattering into the cavity mode. It occurs when the laser intensity exceeds a threshold value such that the pumping processes counteract the losses. We consider atoms driven by a laser and coupling with a mode of a standing-wave cavity and describe their dynamics with a Fokker-Planck equation, in which the atomic motion is semiclassical but the cavity field is a full quantum variable. The asymptotic state of the atoms is a thermal state, whose temperature is solely controlled by the detuning between the laser and the cavity frequency and by the cavity loss rate. From this result we derive the free energy and show that in the thermodynamic limit self-organization is a second-order phase transition. The order parameter is the field inside the resonator to which one can associate a magnetization in analogy to ferromagnetism, the control field is the laser intensity, but the steady state is intrinsically out of equilibrium. In the symmetry-broken phase, quantum noise induces jumps of the spatial density between two ordered patterns: We characterize the statistical properties of this temporal behavior at steady state and show that the thermodynamic properties of the system can be extracted by detecting the light at the cavity output. The results of our analysis are in full agreement with previous studies; we extend them by deriving a self-consistent theory which is valid also when the cavity field is in the shot-noise limit and elucidate the nature of the self-organization transition.

DOI: 10.1103/PhysRevA.92.063808 PACS number(s): 37.30.+i, 42.65.Sf, 05.65.+b, 05.70.Ln

I. INTRODUCTION

There is ample experimental evidence that electromagnetic fields can cool matter to ultralow temperatures [1–3]. This is achieved by tailoring scattering processes, so that the frequency of the emitted photon is, on average, larger than that of the absorbed one, the energy balance being warranted by the mechanical energy which is exchanged between matter and light [4,5]. When atoms or molecules interact with high-finesse optical resonators, these processes can be tailored using the strong coupling with the cavity field [6–13].

A peculiar aspect of light-matter interaction inside optical cavities consists of the long-range interactions between the atoms, which are mediated by multiple scattering of photons [14,15]. The onset of this behavior is observed when the system is driven by external pumps, whose strength overcomes the loss rate. Some prominent examples are optomechanical bistability [16,17], synchronization [18], and spontaneous spatial ordering [12,19–23]. Among several setups, spontaneous pattern formation in standing-wave and single-mode cavities has been the object of several theoretical and experimental studies [12]. This phenomenon occurs when the atoms are confined within the resonator and are transversally driven by a laser and consists of the formation of atomic gratings that maximize coherent scattering of laser photons into the cavity mode, as sketched in Figs. 1(a) and 1(b). These "Bragg gratings" are stably trapped by the mechanical effects of the light they scatter, provided that the laser compensates the cavity losses so that the number of intracavity photons is sufficiently large. It takes place when the laser intensity, pumping the atoms, exceeds a threshold value depending on, among other things, the rate of photon losses and the number of atoms [12,21]. This behavior was first predicted in Ref. [21] and experimentally demonstrated in several settings, which differ majorly from the initial temperature of the atomic ensemble: In Refs. [22,24] the atoms were cooled by the mechanical effects of the photons scattered into the resonator, while in Refs. [23,25] the atoms initially formed a Bose-Einstein condensate, and the mechanical effects of light were giving rise to conservative forces. As a consequence, matter-wave coherence was preserved during the experiment. In this regime, the transition to self-organization can be cast in terms of the Dicke phase transition [26].

In this work we theoretically analyze the dynamics leading to the formation of spatial structures and their properties at the asymptotics. Our analysis is based on a semiclassical treatment and specifically on a Fokker-Planck equation (FPE) derived when the atoms are classically polarizable particles and their center-of-mass motion is along one dimension [27]. The cavity field, instead, is a full quantum variable, which makes our treatment valid also in the shot-noise limit [27] and describes parameter regimes that are complementary to those of the model in Ref. [28], where the field is a semiclassical variable. Our formalism permits us, in particular, to consistently eliminate the cavity variables from the equations of motion of the atoms, and to analyze the properties of the cavity field across the self-organization threshold, where the intracavity field is characterized by large fluctuations.

This work extends and complements the study presented in Ref. [29]. In particular, we perform a detailed analysis of the stationary state and obtain an analytic expression, which allows us to determine the phase diagram of the transition as a function of the relevant parameters. Drawing from this result, in addition, we show that the onset of self-organization in spatially ordered patterns is a second-order phase transition, associated with a symmetry breaking in the phase of the intracavity field. This allows us to verify conjectures on the nature of the self-organization transition, previously discussed in Refs. [30–32]. We further analyze in detail the effects of the nature of the long-range interactions mediated by the photons and report on several features which are analogously found in the Hamiltonian Mean Field (HMF) model, the workhorse

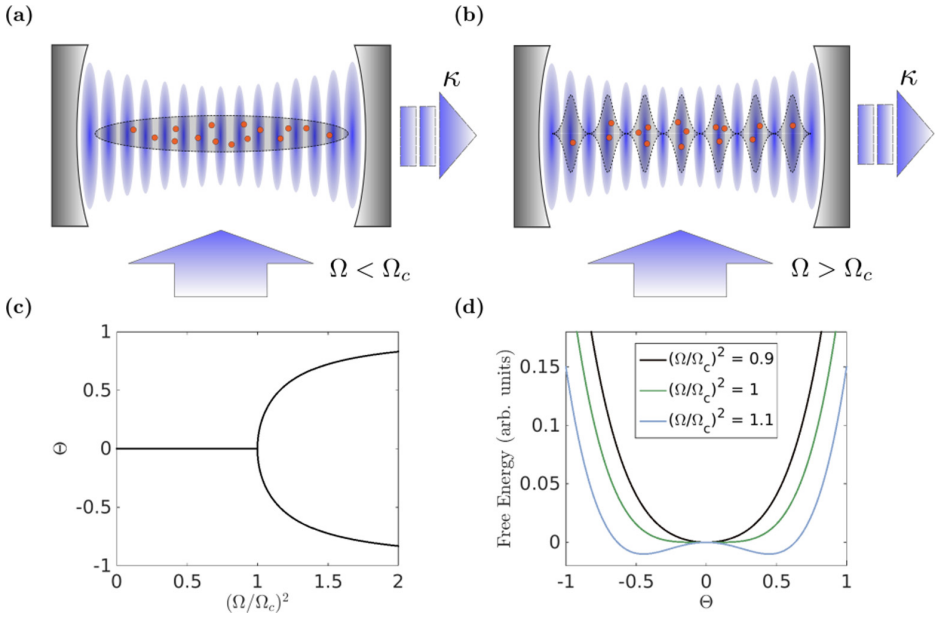

FIG. 1. (Color online) (a) Atoms in a standing-wave cavity and driven by a transverse laser can spontaneously form ordered patterns (b) when the laser intensity Ω exceeds a threshold value Ω_c, which depends on the rate of photon losses, here due to cavity decay at rate κ. In this regime the atoms experience a long-range interaction mediated by the cavity photons and their motion becomes strongly correlated. (c) Spatial ordering of atoms is described by the parameter Θ, which characterizes the localization of the atoms within the standing-wave mode of the cavity and is proportional to the cavity field. This parameter undergoes a bifurcation at $\Omega = \Omega_c$, corresponding to two different stable patterns. The values it takes are the minima of an effective Landau potential, displayed in (d) for some values of Ω, demonstrating that self-organization is a second-order phase transition. See text for details.

of the statistical physics with long-range interactions [33]. This article is the first of a series of works devoted to the semiclassical theory of self-organization.

In the present work we analyze the thermodynamics of self-organization and the dynamics at the asymptotics, while in following articles we investigate the dynamics following sudden quenches across the phase transition [34] and compare our analysis with a mean-field model that discards some relevant effects of the long-range correlations [35]. This paper is organized as follows. In Sec. II the FPE at the basis of our analysis is reported and discussed. In Sec. III the stationary properties of the distribution function are characterized both analytically and numerically. In Sec. IV the correlation functions of the light at the cavity output are determined. The conclusions are drawn in Sec. V, while the Appendixes report details of analytical calculations and of the numerical program that is used to simulate the FPE.

II. MODEL

The dynamics of N atoms or molecules of mass m inside a single-mode standing-wave cavity is analyzed when the particles are transversally illuminated by a laser field, as illustrated in Fig. 1(a). Laser and cavity couple to a dipole transition of the scatterers and are assumed to be sufficiently far-off resonance so that the coupling with the internal degrees of freedom is described by the particles polarizability. From now on we assume that the particles are atoms, but the treatment in this paper can be extended to any ensemble of linearly polarizable particle that can be confined within the optical resonator [36].

In this regime the atoms scatter all coherently and the cavity field E_c is the sum of the fields that each atom scatters. We assume that the atoms' center-of-mass motion is confined along the cavity axis, which coincides with the x axis (we disregard their motion in the transverse plane), and that the atoms are uniformly illuminated by the laser field. Denoting the atomic position by x_j and the cavity-mode function by $\cos(kx)$, with k the wave number, then $E_c \propto N\Theta$, where

$$\Theta = \frac{1}{N}\sum_j \cos(kx_j) \tag{1}$$

measures the ordering of the atoms within the cavity standing wave. For $N \gg 1$, when the atoms are uniformly distributed, $\Theta \sim 0$ and the field within the cavity vanishes. The intracavity intensity is maximal when the positions are such that $\cos(kx_j) = 1$ (even pattern) or $\cos(kx_j) = -1$ (odd pattern), namely, when the atoms form Bragg gratings; see Fig. 1(b). These gratings are the two possible stable configurations the atoms can form when the laser pump is above threshold, as shown in Fig. 1(c).

The formation and stability of the Bragg gratings is determined by the mechanical effects of photon scattering on the atoms. In this section we report the basic equations describing the dynamics of the coupled systems, as well as the assumptions that lead to a FPE governing the semiclassical trajectories of N atoms inside the single-mode resonator [27]. The FPE is derived under the assumption that the atomic

motion is at all times in the semiclassical regime, while the cavity field adjusts quasi-instantaneously to the atomic density distribution. In this limit, using a perturbative treatment, the cavity field can be eliminated by the equations of motion of the atoms' external degrees of freedom [37]. Readers interested in the detailed derivation of the FPE from the full quantum master equation of atoms and cavity are referred to Refs. [27,37]. An alternative FPE, where fluctuations of the intracavity field are treated semiclassically but no time-scale separation between atoms and cavity dynamics is assumed, is derived in Ref. [28].

A. The cavity field

In our treatment the cavity field is a quantum variable. We report its equation of motion in the limit in which the atoms constitute a nonsaturated medium and their internal atomic transitions are described by the polarizability. Our starting point is the Heisenberg-Langevin equation for operator $\hat{a}(t)$, which annihilates a cavity photon at frequency ω_c and wave number k. The equation is reported in the reference frame rotating at the laser frequency ω_L and reads [38]

$$\frac{\partial}{\partial t}\hat{a}(t) = -\{\kappa - i[\Delta_c - NU\hat{\mathcal{B}}(t)]\}\hat{a}(t) - iNS\hat{\Theta}(t) + \hat{\xi}(t), \tag{2}$$

where $\Delta_c = \omega_L - \omega_c$ is the detuning of the laser from the cavity frequency, $\hat{\xi}(t)$ is the Langevin force with $\langle\hat{\xi}(t')\hat{\xi}^{\dagger}(t)\rangle = 2\kappa\delta(t-t')$, and κ is the cavity decay rate. The cavity field is a function of the two operators $\hat{\mathcal{B}}(t)$ and $\hat{\Theta}(t)$, which, in turn, are functions of the atomic positions $\hat{x}_j$ at time t. In detail, U is a frequency, $U = g^2/\Delta_a$, where g is the vacuum Rabi frequency at the antinodes of the cavity mode, $\Delta_a = \omega_L - \omega_a$ is the detuning of the laser frequency from the atomic transition resonance ω_a, and operator $\hat{\mathcal{B}}$ is defined as

$$\hat{\mathcal{B}} = \frac{1}{N}\sum_j \cos^2(k\hat{x}_j) \tag{3}$$

and takes on values between 0 and 1. Its expectation value $B = \langle\hat{\mathcal{B}}\rangle$ is the so-called bunching parameter [12]. Operator $\hat{\Theta}(t)$ is the quantum variable corresponding to the order parameter in Eq. (1). In Eq. (2) it is scaled by the frequency $S = \Omega g/\Delta_a$, which is proportional to the laser Rabi frequency Ω and corresponds to the scattering amplitude of a laser photon into the cavity mode by an atom at an antinode, with $S/U = \Omega/g$. Equation (2) shows that the pump on the cavity is maximum when $\langle\hat{\Theta}\rangle = \pm 1$, corresponding to the situation in which the atoms form Bragg gratings. Self-organization occurs when these gratings are mechanically stable, namely, when the mechanical effects of the scattered light stabilize the atoms in ordered structures, which, in turn, generate the field. In order to determine these dynamics one would need to solve the coupled equations of cavity and atomic motion.

We can further simplify the problem by considering the regime in which the time scale over which the atomic motion evolves is much larger than the time scale determining the evolution of the cavity field. This is typically fulfilled when $k\bar{p}/m \ll |\kappa + i\Delta_c|$, where $\bar{p} = \sqrt{\langle\hat{p}^2\rangle}$ is the variance of the atomic momentum (the mean value vanishes), under the condition that the coupling between cavity and atomic motion is sufficiently weak. This latter condition requires that [39]

$$\sqrt{\omega_r}\sqrt{N}|S| \ll |\Delta_c + i\kappa|^{3/2}, \tag{4}$$

where $\omega_r = \hbar k^2/(2m)$ is the recoil frequency, scaling the exchange of mechanical energy between photons and atoms. At zero order in this expansion the cavity field operator depends on the instantaneous density and reads

$$\hat{a}_{\rm ad}(t) = \frac{NS\hat{\Theta}(t)}{\hat{\Delta}_c'(t) + i\kappa}, \tag{5}$$

where the subscript indicates the adiabatic limit and we omitted to report the noise term. Operator $\hat{\Delta}_c'$ is defined as

$$\hat{\Delta}_c' = \Delta_c - UN\hat{\mathcal{B}}. \tag{6}$$

Its mean value vanishes for certain density distributions, giving rise to resonances. For $|NU| > \kappa$ small changes of Δ_c about the resonance can induce large variations of the field, resulting in the appearance of optomechanical bistable behavior [16,17,40]. In this paper we focus on the regime in which $|NU| \ll \kappa$, and treat this as a small parameter on the same footing as the retardation term. In this limit, the field, including the diabatic corrections, reads

$$\hat{a}(t) = \frac{NS\hat{\Theta}(t)}{\Delta_c + i\kappa}\left[1 + \frac{NU}{\Delta_c + i\kappa}\hat{\mathcal{B}}(t)\right] + \hat{a}_{\rm ret}(t), \tag{7}$$

where

$$\hat{a}_{\rm ret}(t) = \frac{iNS}{(i\Delta_c - \kappa)^2}\dot{\hat{\Theta}} \tag{8}$$

accounts for retardation effects and depends on the time derivative of operator $\hat{\Theta}$, Eq. (1). The derivative, in particular, takes the form

$$\dot{\hat{\Theta}} = -\frac{1}{2N}\sum_j \left\{\sin[k\hat{x}_j(t)]\frac{k\hat{p}_j(t)}{m} + \frac{k\hat{p}_j(t)}{m}\sin[k\hat{x}_j(t)]\right\}$$

and shows that the diabatic correction scales with $(k\bar{p}/m)/|\kappa + i\Delta_c|$. When this parameter is small, then one can perform a coarse graining for the atomic motion, over which the cavity field fast relaxes.

It is also useful to discuss the mean number of photons inside the resonator. In the adiabatic limit it is given by

$$\langle\hat{n}\rangle_{t,\rm ad} = N\bar{n}\langle\hat{\Theta}^2\rangle_t, \tag{9}$$

which is valid in zero order in the delay time. For later convenience, we introduced the dimensionless quantity

$$\bar{n} = \frac{NS^2}{\Delta_c^2 + \kappa^2}, \tag{10}$$

such that $N\bar{n}$ gives the maximum intracavity photon number, corresponding to the value $\langle\Theta^2\rangle_t = 1$, namely, when the atoms form a perfectly ordered Bragg grating. The average photon number can be different from zero also when the field inside the resonator has vanishing mean expectation value, since in this case it is proportional to the fluctuations of the order parameter.

B. Fokker-Planck equation for N atoms

An equation for the motion of the N atoms within the resonator is derived under the assumption that at all times the atomic momentum distribution has width $\Delta p = \bar{p}$, which is much larger than the quantum of linear momentum $\hbar k$ that the atom exchanges with the individual photons (but sufficiently small so that the atoms are within the velocity capture range [11]). This assumption is valid for cavities whose decay rate κ exceeds the recoil frequency ω_r: $\omega_r \ll \kappa$. In fact, we show that κ determines the minimum stationary width of the momentum distribution. This regime is encountered in several existing experiments [17,22,24]. We note that, with this assumption, the requirement of time-scale separation between cavity and motion is fulfilled, since the inequality $k\bar{p}/m \ll \kappa$ is consistent with $\omega_r \ll \kappa$ after using $\bar{p}^2/2m = \hbar\kappa/2$.

Reference [27] reports the detailed steps that lead to the derivation of a FPE for the distribution $f(\boldsymbol{x},\boldsymbol{p},t)$ of the N atoms positions and momenta $\boldsymbol{x} = (x_1, x_2, \ldots, x_N)$ and $\boldsymbol{p} = (p_1, p_2, \ldots, p_N)$. The FPE can be cast in the form

$$\frac{\partial f}{\partial t} = -\sum_i \frac{p_i}{m}\frac{\partial}{\partial x_i} f + S^2 L f, \tag{11}$$

where $f \equiv f(\boldsymbol{x},\boldsymbol{p},t)$. The right-hand side (RHS) separates the ballistic motion from the term proportional to the scattering rate S and describes the dynamics due to the mechanical effects of light. This latter term specifically reads

$$\begin{aligned} L f = &-\sum_i \frac{\partial}{\partial p_i} F_0(\boldsymbol{x}) \sin(kx_i) f \\ &- \sum_{i,j} \frac{\partial}{\partial p_i} \Gamma_0(\boldsymbol{x}) \sin(kx_i)\sin(kx_j) p_j f \\ &+ \sum_{i,j} \frac{\partial^2}{\partial p_i \partial x_j} \eta_0(\boldsymbol{x}) \sin(kx_i)\sin(kx_j) f \\ &+ \sum_{i,j} \frac{\partial^2}{\partial p_i \partial p_j} D_0(\boldsymbol{x}) \sin(kx_i)\sin(kx_j) f \\ &+ \frac{\gamma'}{2} \sum_i \frac{\partial^2}{\partial p_i^2} \mathcal{D}^{\mathrm{sp}}(x_i) f. \end{aligned} \tag{12}$$

Here the first term on the RHS describes the dispersive force associated with scattering of laser photons into the resonator, where

$$F_0(\boldsymbol{x}) = (\hbar k)\frac{2\Delta_c'}{\Delta_c'^2 + \kappa^2}(1+\delta_F) N \Theta. \tag{13}$$

Its amplitude is proportional to the order parameter Θ [Eq. (1)], which is the Wigner representation of operator $\hat{\Theta}$ [27]. Its sign is also determined by the frequency shift of the cavity frequency $\Delta_c'(\boldsymbol{x})$ from the laser, which takes the same form as in Eq. (6), now with the corresponding Wigner form for operator $\hat{\mathcal{B}}$. Coefficient δ_F is a small correction for the parameter regime we consider; its general form is given in Appendix A. The same applies for the coefficients δ_j ($j = \Gamma, \eta, D$) appearing in the other terms we specify below.

The second term on the RHS of Eq. (12) describes the damping force due to retardation between the scattered field and the atomic motion. It depends on the atomic momentum and is scaled by the function

$$\Gamma_0(\boldsymbol{x}) = \omega_r \frac{8\Delta_c'\kappa}{\left(\Delta_c'^2 + \kappa^2\right)^2}(1+\delta_\Gamma). \tag{14}$$

The third summand is due to the anharmonicity of the cavity optical lattice. The function scaling this term has the form

$$\eta_0(\boldsymbol{x}) = 2\hbar\omega_r \frac{\left(-\Delta_c'^2 + \kappa^2\right)}{\left(\Delta_c'^2 + \kappa^2\right)^2}(1+\delta_\eta) \tag{15}$$

and vanishes when $\Delta_c' = \pm\kappa$.

The last two terms describe diffusion. In particular, the one scaled by the function

$$D_0(\boldsymbol{x}) = (\hbar k)^2 \frac{\kappa}{\Delta_c'^2 + \kappa^2}(1+\delta_D) \tag{16}$$

corresponds to the diffusion associated with global fluctuations of the cavity field and is characterized by long-range correlations, while the term with coefficient $\mathcal{D}^{\mathrm{sp}}(x_i)$ is instead due to spontaneous emission of a photon outside the resonator with $\gamma' = \gamma g^2/\Delta_a^2$, where γ is the decay rate of the excited state. It is the sole term which acts locally, and the dynamics it implies does not establish correlations between the atoms. Its explicit form is reported in Appendix A.

C. Dynamics away from the bistable regime

Equation (11) describes the coherent and dissipative dynamics associated with the mechanical effects of light on the atomic motion. In this work we assume that γ' is much smaller than the other rates and discard the effect of spontaneous decay in the dynamics, so that losses are due to cavity decay. As far as it concerns the terms due to the cavity, we note their nonlinear dependence on the bunching parameter, which appears in the denominator of all coefficients and gives rise to bistable behavior. Here we focus on the regime in which $|NU| \ll \kappa$. In this regime the dispersive forces due to the mechanical effects of light in leading order are due to scattering of laser photons into the cavity. In this limit, we choose detunings $|\Delta_c| \sim \kappa$ so that the motion is efficiently cooled, as we show below. Correspondingly, the coefficients of the functional in Eq. (12) are modified so that $\Delta_c' \simeq \Delta_c$ and the functions $\delta_F, \delta_\eta, \delta_\Gamma, \delta_D \approx 0$. More precisely, we perform an expansion in first order in $N|U|/\kappa$. In this limit, the FPE, Eq. (11), can be cast in the form

$$\begin{aligned} &\partial_t f + \{f, H\} + \bar{n}\frac{NU}{\Delta_c} L_1 f \\ &\quad = -\bar{n}\Gamma \sum_i \sin(kx_i)\partial_{p_i}\frac{1}{N} \\ &\qquad \times \sum_j \sin(kx_j)\left(p_j + \frac{m}{\beta}\partial_{p_j} + \frac{\bar{\eta}}{\beta}\partial_{x_j}\right) f, \end{aligned} \tag{17}$$

where all terms due to the coupling with the light scale with $\bar{n}$, given in Eq. (10). In detail, the left-hand side (LHS) collects the Hamiltonian terms, expressed in terms of Poisson brackets

with Hamiltonian

$$H = \sum_j \frac{p_j^2}{2m} + \hbar\Delta_c \bar{n} N \Theta^2, \tag{18}$$

as well as the terms scaling with U, summarized in the functional L_1, whose detailed form is given in Appendix A. The RHS reports terms of different origin, which can be classified as damping, diffusion, and a third term which scales cross derivatives in position and momentum. In the order of this list, they are scaled by the coefficients

$$\Gamma = 8\omega_r \kappa \Delta_c / \left(\Delta_c^2 + \kappa^2\right), \tag{19}$$

$$\beta = -4\Delta_c/\hbar/\left(\Delta_c^2 + \kappa^2\right), \tag{20}$$

$$\bar{\eta} = \frac{\kappa^2 - \Delta_c^2}{\kappa\left(\Delta_c^2 + \kappa^2\right)}. \tag{21}$$

We remark that the term in the FPE scaled by parameter $\bar{\eta}$ was already found in the derivation of Ref. [37]. While its effect is to date not well understood, we checked that for the parameters we consider it gives rise to small corrections in the quantities we evaluate. In the mean-field treatment it can be cast in terms of a correction of the effective mean-field potential the atoms experience. In that limit it induces a shift to the critical value of the pump strength at the self-organization transition [35].

D. Long-range correlations

Let us now make some preliminary remarks on the FPE discussed this far. We first focus on the Hamiltonian term, Eq. (18). In addition to the kinetic energy this contains the cavity-mediated potential, which has been obtained in zero order in the retardation time. Its sign is determined by the sign of the detuning Δ_c: When $\Delta_c < 0$, the formation of Bragg gratings, which maximizes the value of $|\Theta|$, is energetically favored. Thus, Eq. (18) summarizes in a compact way a property which was observed in several previous works [21,22,29,30].

We note that the Hamiltonian in Eq. (18) exhibits several analogies with the HMF model [33], whose Hamiltonian reads

$$H_{\mathrm{MF}} = \sum_j \frac{p_j^2}{2m} + \frac{J}{2N}\sum_{i\neq j}[1 - \cos(\theta_i - \theta_j)], \tag{22}$$

where θ_i are angle variables that in our case would correspond to $\theta_i = kx_i$. The analogy becomes explicit in Eq. (18) by using

$$\Theta^2 = \sum_{i,j}\{\cos[k(x_i + x_j)] + \cos[k(x_i - x_j)]\}/(2N^2).$$

Like Hamiltonian H_{MF}, also Hamiltonian H is extensive as it satisfies the Kac prescription [33] for the thermodynamic limit we choose, which keeps $\bar{n}$ fixed for $N \to \infty$ (see the next section). In a canonical ensemble, for $J > 0$ the HMF exhibits a second-order phase transition from a paramagnetic to a ferromagnetic phase controlled by the temperature, where the order parameter is the magnetization $M = (M_x, M_y)$, with $M_x = \sum_j \cos\theta_j/N$ and $M_y = \sum_j \sin\theta_j/N$. This suggests that Θ identifies with the x component of a two-dimensional magnetization and creates an expectation of a transition to order for negative values of the detunings, $\Delta_c < 0$, for which a nonvanishing interaction potential term tends to minimize the energy (we mention that the dynamics for $\Delta_c > 0$ has been recently studied in Ref. [41]).

Differing from the HMF model, the term $\cos[k(x_i + x_j)]$ in Θ^2 originates from the underlying cavity standing-wave potential that breaks continuous translational invariance. Moreover, the cavity coupling at higher order in $|NU/\Delta_c|$ gives rise to deviations from the Hamiltonian dynamics due to further terms in the LHS of Eq. (17), which for larger values are responsible for bistable behavior [40] and only in certain limits can be cast in the form of conservative forces.

We further highlight that long-range correlations can also be established by the terms on the RHS of the FPE in Eq. (17), which are usually associated with incoherent processes. In fact, retardation effects in the scattering of one atom modify the intracavity potential which traps the whole atomic ensemble. Photon losses, in addition, give rise to sudden quenches of the global potential [11,42]. When the density is uniform, the terms in the RHS can be reduced to a form [27] which is analogous to the Brownian Mean Field model [43]. However, this mapping applies only when the system is deep in the paramagnetic phase. When the atoms form a Bragg grating, instead, damping and diffusion become smaller, the atoms being localized at the points where $\sin(kx_j) \sim 0$. Moreover, when several atoms are trapped in a Bragg grating, also damping and diffusion of atoms which are away from the nodes become smaller. These properties share some analogies with models constructed to simulate correlated damping [44] and suggest that incoherent dynamics can endorse coherent effects for transient but long times [29,34].

III. PROPERTIES AT EQUILIBRIUM

We now discuss the existence and the form of the stationary state, namely, of the solution of Eq. (17) satisfying

$$\partial_t f_{\mathrm{S}} = 0.$$

It is simple to verify that the function of the form

$$f_{\mathrm{S}} = f_0 \exp(-\beta H) \tag{23}$$

is a stationary solution in zero order in the parameter UN/κ and $\bar{\eta}$, where f_0 warrants normalization. Equation (23) describes a thermal state whose temperature T is solely controlled by the detuning Δ_c:

$$k_B T = 1/\beta = \frac{\hbar\left(\Delta_c^2 + \kappa^2\right)}{-4\Delta_c}. \tag{24}$$

We mention that this result has been reported in Ref. [29] and was also found in Refs. [30,31,45] using different theoretical approaches.

In this section, starting from Eq. (23) we analyze the properties of the system at steady state. We show that Eq. (23) makes it possible to identify the transition to self-organization and the corresponding critical value at which it occurs. By deriving the single-particle free energy in an appropriate thermodynamic limit, we demonstrate that the transition to self-organization is a second-order phase transition, whose order parameter is Θ. We point out that the treatment here presented applies concepts of equilibrium thermodynamics

and is strictly valid at the steady state, because it is a thermal distribution.

This section contains analytical results, extracted from Eq. (23), and data of numerical simulations, obtained by integrating the stochastic differential equations (SDEs) which simulate the dynamics of Eq. (17). These equations have been reported in Ref. [27] and for completeness are also detailed in Appendix B . A single trajectory for N atoms corresponds to integrating the set of coupled equations (B1) and (B2) for the variables $\{x_\ell(t); p_\ell(t)\}$ with $\ell = 1, \ldots, N$ and for a given initial condition. From this calculation, for instance, we find

$$\Theta(t) = \sum_{\ell=1}^{N} \cos[k x_\ell(t)]/N.$$

The mean values are numerically computed by taking the average over n such trajectories, which statistically satisfy the initial conditions, and deliver quantities such as $\langle \Theta^2 \rangle_t = \sum_{i=1}^{n} \Theta_i(t)^2/n$, where i now labels the trajectory, $i = 1, \ldots, n$.

In the simulations we assume an ensemble of ^{85}Rb atoms with transition wavelength $\lambda = 780$ nm (D_2 line). This gives the recoil frequency $\omega_r = 2\pi \times 3.86$ kHz. The transition linewidth is $\gamma = 2\pi \times 6$ MHz and the linewidth of the resonator is $\kappa = 2\pi \times 1.5$ MHz. These parameters correspond to the ones of the experiment of Ref. [23]; they warrant the validity of our semiclassical treatment based on a time-scale separation.

A. Self-organization as second-order phase transition

In order to characterize the thermodynamic properties of the self-organization transition, we first determine the free energy per particle. Our starting point is the definition of the free energy $F = -k_B T \ln \mathcal{Z}$, where $\mathcal{Z}$ is the partition function,

$$\mathcal{Z} = \frac{1}{\Delta^N} \int_{\boldsymbol{x}} d\boldsymbol{x} \int_{\boldsymbol{p}} d\boldsymbol{p} \exp(-\beta H), \tag{25}$$

and Δ is the unit phase space volume. For convenience, we have introduced the notation $\int_{\boldsymbol{x}} d\boldsymbol{x} \equiv \int_0^\lambda dx_1 \cdots \int_0^\lambda dx_N$ and $\int_{\boldsymbol{p}} d\boldsymbol{p} \equiv \int_{-\infty}^{\infty} dp_1 \cdots \int_{-\infty}^{\infty} dp_N$. After integrating out the momentum variables, Eq. (25) can be cast in the form

$$\mathcal{Z} = (Z_0 \lambda/\Delta)^N \int_{-1}^{1} d\Theta \Omega(\Theta) \exp(-N\beta\hbar\bar{n}\Delta_c \Theta^2). \tag{26}$$

Here $Z_0 = (2\pi m/\beta)^{1/2}$ is a constant which depends on the temperature. The functional $\Omega(\Theta)$ is the density of states at a given magnetization Θ and is defined as

$$\Omega(\Theta) = \int_{\boldsymbol{x}} \frac{d\boldsymbol{x}}{\lambda^N} \delta\left[\Theta - \frac{1}{N}\sum_{i=1}^{N} \cos(k x_i)\right]. \tag{27}$$

For identifying the transition to order, we consider $N \gg 1$. This requires an adequate thermodynamic limit. We choose a thermodynamic limit for which the amplitude $\bar{n}$ [Eq. (10)] remains constant as N increases and warrants that Hamiltonian in Eq. (18) is extensive. In detail, it corresponds to scale the vacuum Rabi frequency as $g \sim 1/\sqrt{N}$, which is physically equivalent to scale up the cavity mode volume V linearly with N, being the vacuum Rabi frequency $g \propto 1/\sqrt{V}$. It follows that the scattering rates characterizing the dynamics scale as $S \sim 1/\sqrt{N}$ and $U \sim 1/N$ as $N \to \infty$ (moreover, $S^2\eta_0 \sim 1/N$, but this contribution is here neglected). Such scaling has been applied in a series of theoretical works [30,38,40].

With this definition in mind, we determine an explicit form of the free energy as a function of Θ by using the method of the steepest descent. We identify the fixed point Θ^*, which is given by the equation

$$\Theta^* = \frac{I_1(y\Theta^*)}{I_0(y\Theta^*)}, \tag{28}$$

with $y = 2\bar{n}/\bar{n}_c$ and $\bar{n}_c > 0$, while I_1 and I_0 are modified Bessel functions of the first kind [46] (the details of the calculations are reported in Appendix C). Depending on y, and thus on $\bar{n}$, Eq. (28) allows for either one or three solutions, where the two regimes are separated by the value $\bar{n} = \bar{n}_c$, with

$$\bar{n}_c = \frac{\kappa^2 + \Delta_c^2}{4\Delta_c^2}. \tag{29}$$

Using this result, the free energy per particle in the thermodynamic limit takes the form

$$\mathcal{F}(\Theta) \approx \mathcal{F}_0 + \frac{1}{\beta}\left[\left(1 - \frac{\bar{n}}{\bar{n}_c}\right)\Theta^2 + \frac{1}{4}\Theta^4\right], \tag{30}$$

with $\mathcal{F}_0 = -k_B T \ln(Z_0\lambda/\Delta)$. Equation (30) has the form of the Landau free energy [47], and shows that the transition to self-organization is continuous and of second order. Its form close to threshold for different values of the pump strength, and thus of $\bar{n}$, is sketched in Fig. 1(d), where $(\Omega/\Omega_c)^2 = \bar{n}/\bar{n}_c$. For $\bar{n} < \bar{n}_c$, thus, the order parameter vanishes: The atoms are uniformly distributed in space and one can denote this phase as paramagnetic invoking the analogy between Θ and a magnetization. For $\bar{n} > \bar{n}_c$, on the contrary, the order parameter takes a value different from zero, as shown in Fig. 1(c). By setting the first derivative of the free energy [Eq. (30)] to zero we also find an analytic expression for the order parameter above but close to the threshold: $\Theta = \pm\sqrt{2(\bar{n}/\bar{n}_c - 1)}$.

We remark that in Ref. [30] it was conjectured that self-organization in a standing-wave cavity is a second-order phase transition. In this section we have demonstrated that this conjecture is correct by performing an explicit mapping of the free energy into the form of a Landau model [47]. Our theoretical model demonstrates that the steady-state distribution is thermal; it further naturally delivers the steady-state temperature and the value of the critical pump strength, here cast in terms of the quantity $\bar{n}_c$. We observe that the critical value $\bar{n}_c$ is in agreement with the value determined in Ref. [30] by means of a mean-field model based on a phenomenological derivation. [This is visible after considering the definition in Eq. (10), which gives the critical pump strength value Ω_c after using $S_c = g\Omega_c/\Delta_a$ as a function of the critical value $\bar{n}_c$ of Eq. (29).] In Ref. [31] the self-organization threshold was estimated by means of a kinetic theory based on treating the cavity field semiclassically, finding a value consistent with our result.

We remark that the typical concept in second-order phase transition of spatial domains, whose average size increases with a power-law behavior as the critical value is approached,

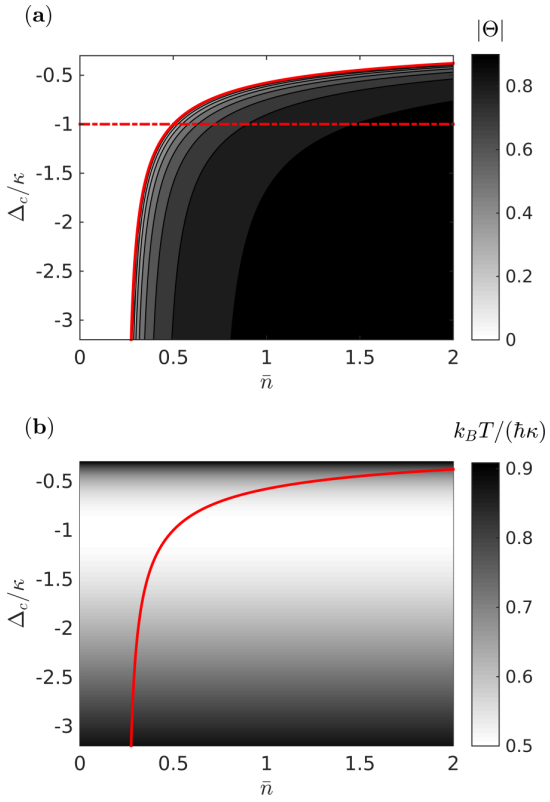

FIG. 2. (Color online) (a) Order parameter $|\Theta|$ and (b) steady-state temperature as a function of $\bar{n}$ and Δ_c (in units of κ). The red line denotes the value $\bar{n}_c$ as a function of Δ_c, as reported in Eq. (29).

becomes now invalid: Their energetic cost scales with the system size due to the long-range cavity-mediated potential. This is simply understood as two domains with $\langle\Theta\rangle = +1$ and $\langle\Theta\rangle = -1$ generate fields which interfere destructively, resulting in a vanishing intracavity photon number. This example illustrates the nonadditivity of long-range interacting systems. We now analyze more in detail the behavior of the magnetization.

B. Phase diagram

The magnetization of our model [Eq. (1)] is intrinsically related to the spatial order of the atoms within the cavity and thus determines the properties of the signal at the cavity output. Its stationary value depends on the various physical quantities, which can be summarized in terms of the single parameter $\bar{n}$ in Eq. (10). The detuning Δ_c, which also enters in the definition of $\bar{n}_c$, determines the temperature of the steady state; see Eq. (24).

Figure 2(a) displays the phase diagram of the magnetization as a function of $\bar{n}$ and Δ_c: The white region is the paramagnetic phase, the dark region the ferromagnetic one, and the scale of gray indicates the value of $|\Theta|$. We note that the lines at constant Δ_c correspond to constant asymptotic temperatures and to a well-defined threshold value of $\bar{n}_c(\Delta_c)$. Following one such line, the value of $|\Theta|$ is zero for $\bar{n} < \bar{n}_c$, while above $\bar{n}_c$ it grows monotonically until unity as $\bar{n} \to \infty$. The magnetization as a function of $\bar{n}$ and at $\Delta_c = -\kappa$ is shown in Fig. 1(c).

Keeping $\bar{n}$ fixed and varying Δ_c instead consists of varying the temperature. However, not for all values of $\bar{n}$ there is a temperature at which the transition to ferromagnetism is observed. In fact, if $\bar{n} < \min(\bar{n}_c) = 1/4$, the phase is paramagnetic for all values of Δ_c. For $\bar{n} > 1/4$, instead, there exists a critical value of $\Delta_c(\bar{n})$ at which the transition to self-organization occurs. In this case, above threshold the magnetization monotonically grows with Δ_c. The temperature of the atoms is shown in Fig. 2(b): Here it is clearly visible that the temperature is independent on $\bar{n}$ and is solely a function of Δ_c. In particular, it reaches a minimum at $\Delta_c = -\kappa$, as one can verify using Eq. (24). The corresponding minimal temperature is $k_B T_{\min} = \hbar\kappa/2$.

C. Dynamics of the magnetization at steady state

The mapping of the free energy to the Landau model allows one to draw an analogy between self-organization and ferromagnetism. Due to the long-range interactions, however, the symmetry-breaking transition does not occur through the spatial formation of magnetized domains of increasing size, rather through the observation of Bragg gratings during long periods of time, whose mean duration increases as the pump strength is increased above threshold. This property was already reported in Refs. [21,30] and is also found in the HMF [33]. The behavior close to threshold is instead to large extent unexplored, as it is characterized by large fluctuations of the cavity field and thus requires a theoretical model that treats the cavity field as a quantum variable, which our model does. Our analysis focuses on the statistical properties of these time intervals and, more generally, of the autocorrelation function of the magnetization across the transition. In this section we discuss this temporal behavior by analyzing trajectories of the magnetization evaluated by means of the SDE as in Appendix B . We set $\Delta_c = -\kappa$ and $N|U|/\kappa = 0.05$.

1. Stationary magnetization for finite N

In order to perform the numerical analysis, we first benchmark the statistical properties for a finite number of trajectories. Typical trajectories at the steady state are shown in Fig. 3 for different values of $\bar{n}$.

They show $\Theta(t)$, obtained by averaging over the instantaneous positions of 50 atoms within the resonator. Fluctuations about the mean value are visible: Their size increases below threshold as $\bar{n}$ is increased and depends on the number of atoms, as one can see in Fig. 4 (see below). In order to extract the order parameter from the numerical data, we thus need to estimate the size of the fluctuations about the mean value as a function of N. For this purpose we determine the probability distribution $P_N(\Theta_0)$ of finding $\Theta = \Theta_0$ at the stationary state, which we define as

$$P_N(\Theta_0) = \mathcal{P}_0 \int_{-1}^{1} d\Theta \delta(\Theta - \Theta_0) \Omega(\Theta) \exp(-\beta\hbar\Delta_c \bar{n} N \Theta^2), \tag{31}$$

where $\Omega(\Theta)$ is given in Eq. (27) and the parameter $\mathcal{P}_0 = (Z_0\lambda/\Delta)^N/\mathcal{Z}$ warrants normalization: $\int_{-1}^{1} d\Theta_0 P_N(\Theta_0) = 1$.

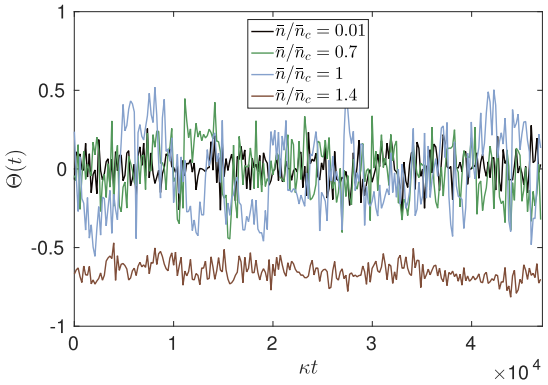

FIG. 3. (Color online) Order parameter as a function of time (in units of κ^{-1}) at the asymptotics of the dynamics and for different values of $\bar{n}$ (see inset). Each trajectory corresponds to a numerical simulation with $N = 50$ atoms.

For a given detuning Δ_c this probability distribution depends on $\bar{n}$ and on the atom number N. We determine $P_N(\Theta_0)$ using our analytical model and performing the integral by means of the Metropolis algorithm [48].

The results are displayed in Fig. 4 for different atom numbers N and pumping strengths $\bar{n}$. The curves clearly show that the size of the fluctuations about the mean value decrease with N. We also observe that, for N fixed, the fluctuations about the mean value increase with $\bar{n}$ as it approaches the threshold value from below. For atom numbers of the order of 50 and larger we verified that $P_N(\Theta_0)$ converges to the form $\exp(-N\,\Theta_0^4/4)$ for $\bar{n} = \bar{n}_c$, in agreement with the result found in the thermodynamic limit. Above threshold, on the contrary, the distribution exhibits two peaks whose centers converge towards the asymptotic values of Eq. (28) for large N and whose widths decrease as $\bar{n}$ is increased. We compare these results with the data obtained after integrating the SDE (circles) and verify the convergence of the numerical results with increasing N to the predictions at the thermodynamic limit.

Figure 5(a) displays $\Theta(t)$ as a function of time obtained by integrating the SDE for $N = 20$ atoms and $\bar{n} = 0.01\,\bar{n}_c$, thus well below threshold. The distribution $P_N(\Theta_0)$ that we extract after averaging over the time and over 100 trajectories of this sort is given by the circles in Fig. 5(b). The curve is in excellent agreement with a Gaussian distribution centered at $\Theta_0 = 0$ (dashed curve) whose explicit derivation is reported in Appendix D and which reads

$$P_N^{\text{theo}}(\Theta_0) = \frac{1}{\sqrt{2\pi\sigma_N^2}} \exp\left(-\frac{\Theta_0^2}{2\sigma_N^2}\right), \tag{32}$$

with

$$\sigma_N = 1/\sqrt{2N}. \tag{33}$$

From this result we identify the width σ_N with the statistical uncertainty in determining the value of Θ_0. Figure 5(c) displays a trajectory $\Theta(t)$ for $\bar{n} = 1.4\,\bar{n}_c$, thus above threshold; the corresponding distribution $P_N(\Theta_0)$ is given by the circles in Fig. 5(d). The trajectory exhibits jumps between the two values of the Bragg gratings, the duration of the time intervals during which the atoms are trapped in a Bragg grating determines the size of the fluctuations about the two peaks of the probability distribution, and the finite rate at which these jumps occur is the reason for the nonvanishing value of the probability at $\Theta_0 \sim 0$.

2. *Autocorrelation function*

We now analyze the autocorrelation function for the magnetization,

$$C(\tau) = \lim_{t\to\infty} \langle \Theta(t)\Theta(t+\tau)\rangle, \tag{34}$$

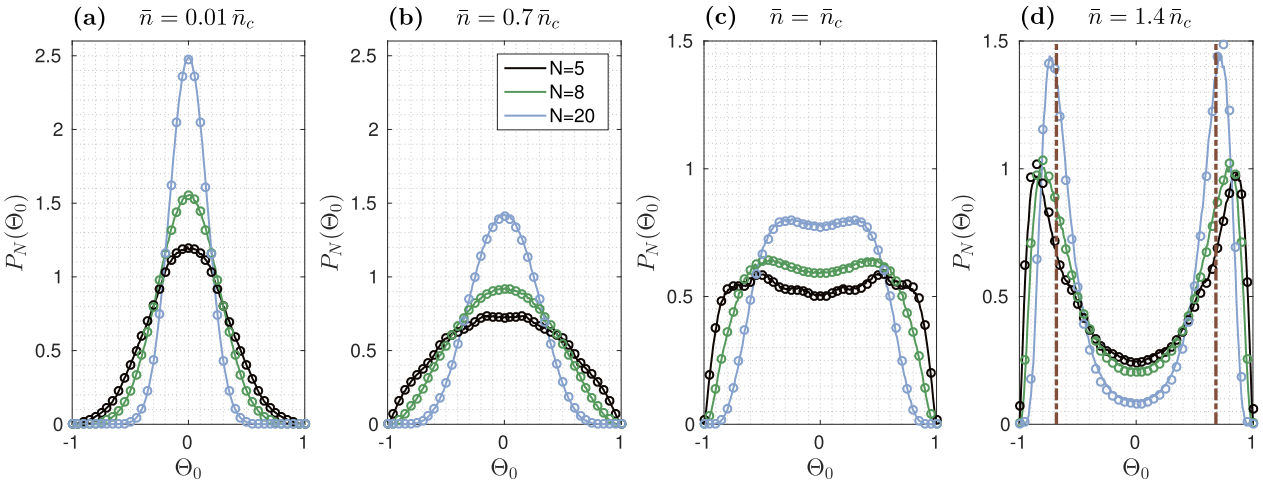

FIG. 4. (Color online) Probability distribution for the order parameter at steady state, $P_N(\Theta_0)$ as in Eq. (31), for $N = 5,8,20$ atoms with $\Delta_c = -\kappa$ and $\bar{n}/\bar{n}_c = 0.01, 0.7, 1, 1.4$ (from left to right). The dots correspond to the probability distribution $P_N(\Theta_0)$ extracted from numerical simulations at steady state, performed by means of the SDE. The dashed vertical lines in (d) indicate the asymptotic value $\Theta_0 = \pm\Theta^*$ [Eq. (28)] for $\bar{n} = 1.4\,\bar{n}_c$.

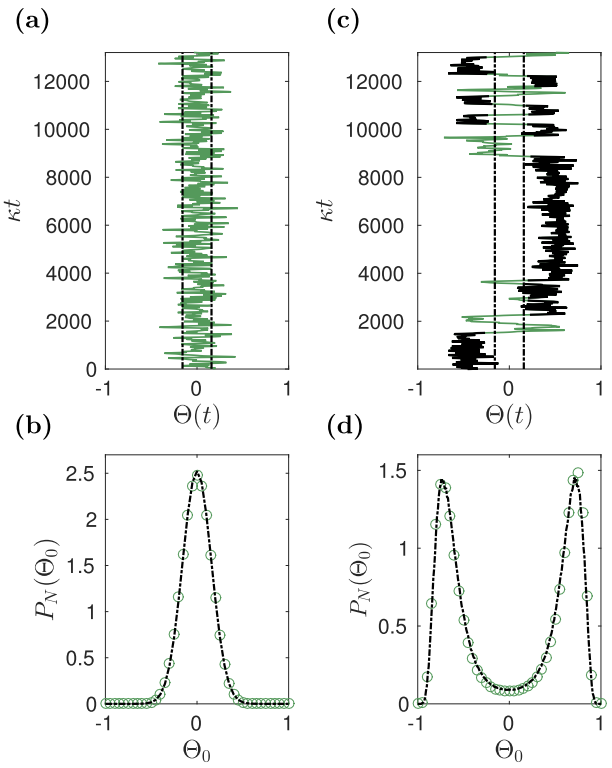

FIG. 5. (Color online) (Top panels) Magnetization Θ as a function of time (in units of κ^{-1}), obtained from a simulation of the SDE for $N = 20$, $\Delta_c = -\kappa$, and $\bar{n} = 0.01\,\bar{n}_c$ (a) and $\bar{n} = 1.4\,\bar{n}_c$ (c). The black dashed lines are located at $\pm\sigma_N = \pm\sqrt{1/(2N)}$ and indicate the statistical uncertainty in the determination of the value of Θ_0. Subplots (b) and (d) display the corresponding probability distribution $P_N(\Theta_0)$ obtained after averaging over time and over 100 trajectories $\Theta(t)$ (circles). The dashed line in (b) is the theoretical prediction in Eq. (32). The dashed line in (d) corresponds to the distribution obtained by numerically integrating Eq. (31) using a Metropolis algorithm [48].

which we extract from the trajectories evaluated using the SDE. Figure 6 displays $C(\tau)$ for different values of $\bar{n}$. For all values of the pump strength a fast decaying component is always present whose temporal width seems to be independent of $\bar{n}$. One also notices the contribution of a slowly decaying component whose decay rate decreases as $\bar{n}$ increases.

In order to gain insight, we first analyze the autocorrelation function below threshold for $\bar{n} = 0.01\,\bar{n}_c$. For this case we can reproduce the numerical result by means of an analytical model, reported in Appendix D . This model assumes that the atoms are homogeneously distributed in space and form a thermal distribution at the temperature determined by Eq. (20), which corresponds to the stationary solution of the FPE in Eq. (17) well below threshold [27]. Starting from this state, their motion is assumed to be ballistic and is thus calculated after setting $\bar{n} = 0$ in Eq. (17). The resulting autocorrelation function reads

$$C_{\text{free}}(\tau) = \sigma_N^2 \exp\left[-\left(\tau/\tau_c^{\text{free}}\right)^2\right], \tag{35}$$

where the correlation time is

$$\tau_c^{\text{free}} = \sqrt{\hbar\beta/\omega_r}. \tag{36}$$

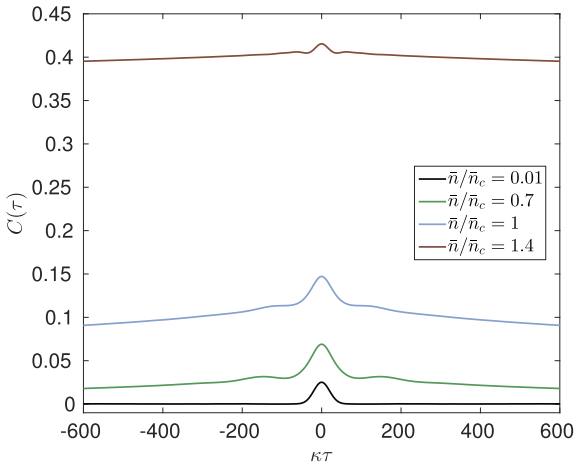

FIG. 6. (Color online) Autocorrelation function $C(\tau) = \lim_{t\to\infty}\langle\Theta(t)\Theta(t+\tau)\rangle$ [Eq. (34)] as a function of the time τ (in units of κ^{-1}) for $N = 20$ atoms, $\Delta_c = -\kappa$, and various values of $\bar{n}$ (see inset). The curves are obtained by determining $\Theta(t)$ with the numerical data (SDE).

Its excellent agreement with the numerics is visible in Fig. 7. This result shows that below threshold the fluctuations are mostly due to thermal motion, while the effect of the cavity forces, which tend to localize the atoms, is negligible. By considering the analogy between the different curves in Fig. 6, we conjecture that thermal fluctuations are responsible for the short-time behavior of the autocorrelation function.

We now turn to the long-time behavior of the autocorrelation function for increasing values of $\bar{n}$. Inspection of typical trajectories close and above threshold, shown in Figs. 3 and 5(c), shows that this is related to the time scales over which the atomic ensemble forms a Bragg grating. The system can take on values for the collective parameter Θ clearly exceeding the value of σ_N for times which are orders of magnitude larger than

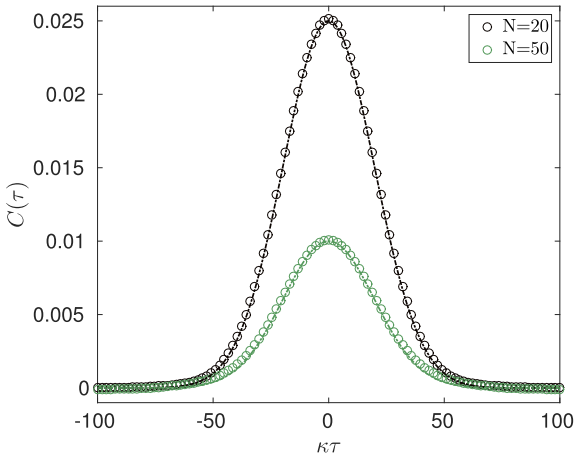

FIG. 7. (Color online) Autocorrelation function $C(\tau) = \lim_{t\to\infty}\langle\Theta(t)\Theta(t+\tau)\rangle$ as a function of the time τ (in units of κ^{-1}) for $N = 20$ and $N = 50$ atoms (see inset). The circles correspond to numerical simulations performed with $\bar{n} = 0.01\,\bar{n}_c$ and $\Delta_c = -\kappa$. The line shows the analytical estimate using Eq. (35).

the correlation time τ_c characteristic of thermal fluctuations, as visible in Fig. 5(c). We call these finite time intervals *trapping times*, corresponding to configurations in which (part of) the atoms are trapped in Bragg gratings.

In order to analyze the statistics of the trapping times, we first introduce the following criterion: the atoms are forming a Bragg grating when $|\Theta(t)| > \sigma_N$. This criterion alone, however, also includes fluctuations that can also happen well below threshold, as visible in Fig. 5(a). For this reason we set an infrared cutoff for the trapping times, such that they shall exceed $\tau_c^{\rm free}$. Herewith, we thus find a trapping time of length $\tau_{\rm trap}$ with starting point t and end point $t+\tau_{\rm trap}$ if $|\Theta(t+t')| > \sigma_N$ for $t' \in [0,\tau_{\rm trap}]$ and $\tau_{\rm trap} > 10\,\tau_c^{\rm free}$. It is important to note that this sets a rather strict criterion on the trapping times as we explain now. In Fig. 5(c), one can see that even if the atoms seem to be trapped in a grating, the order parameter can take on values $|\Theta(t)| < \sigma_N$ for times of the order of $\tau_c^{\rm free}$. We choose to ignore these events when they are not associated with a sign change of Θ. We perform the statistics of the trapping times by evaluating the probability density $P_{\rm trap}(\tau)$ of finding a trapping time of length τ, and then using this quantity to determine the cumulative distribution $F(\tau_{\rm trap})$, defined as

$$F(\tau_{\rm trap}) = \int_{\tau_{\rm trap}}^{\infty} d\tau' P_{\rm trap}(\tau'). \tag{37}$$

Distribution $F(\tau_{\rm trap})$ thus gives the probability that the trapping time is larger than $\tau_{\rm trap}$. Figure 8 displays $F(\tau_{\rm trap})$, as we extracted it for $N = 20$ atoms and different values of $\bar{n}$: It is clearly visible that the trapping times are shifted towards higher values as $\bar{n}$ increases. The distribution exhibits long tails, which suggests that this dynamics is characterized by the existence of rare events with very long trapping times. In order to better understand this behavior, we determine the mean trapping time $\langle\tau_{\rm trap}\rangle_n$. This is numerically found for a given interval of time $t_{\rm tot}$, in which n trapping intervals of length $\tau_{\rm trap}^{(i)}$ are counted ($i = 1,\ldots,n$), and reads

$$\langle\tau_{\rm trap}\rangle_n = \sum_{i=1}^{n} \tau_{\rm trap}^{(i)}/n. \tag{38}$$

In Fig. 8(b) we plot $\langle\tau_{\rm trap}\rangle_n$ as a function of the number of counts for $N = 20$ and various values of $\bar{n}$ above threshold. The mean trapping time $\langle\tau_{\rm trap}\rangle_n$, in particular, seems to converge to a finite value for sufficiently long integration times. We argue, however, that this can be an artifact of the finite integration time $t_{\rm tot}$, which we choose to be $t_{\rm tot} \approx 10^6\kappa^{-1}$: This conjecture is supported by the rather steep decay of the cumulative distribution at $t > 10^5\kappa^{-1}$ visible in Fig. 8(a). Hence, our results do not exclude the existence of a power-law decay of the distribution $F(\tau)$. This discussion clearly shows, nevertheless, that the trapping times are responsible for the long tails of the autocorrelation function.

We now study the statistics of the events which lead to jumps between two Bragg gratings. These events are visible, for instance, in Fig. 5(c) and are characterized by a time scale which we now analyze. We denote these finite times by *jumping times*. More precisely, we define a jump of time length $\tau_{\rm jump}$ as the interval of time $[0,\tau_{\rm jump}]$ within which $|\Theta(t+t')| < \sigma_N$ for $t' \in [0,\tau_{\rm jump}]$. We further impose that

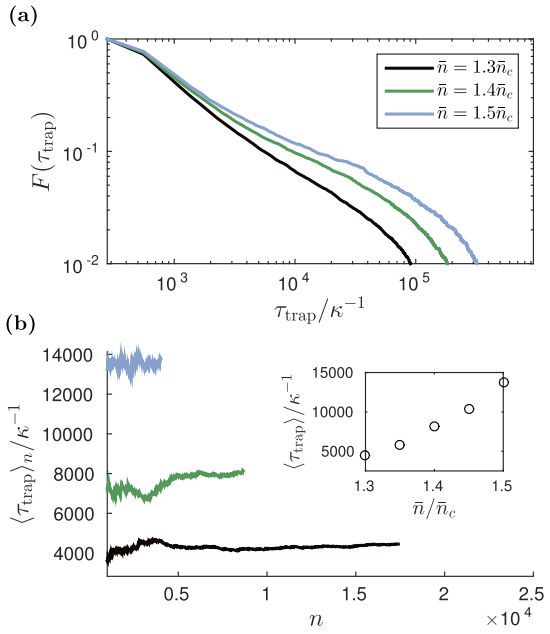

FIG. 8. (Color online) Statistics of the trapping times, evaluated numerically by averaging over 100 trajectories of $N = 20$, $\Delta_c = -\kappa$, and total evolution time $t_{\rm tot} \approx 10^6\kappa^{-1}$. The curves correspond to different values of $\bar{n}$ above threshold (see inset). (a) Cumulative distribution $F(\tau_{\rm trap})$ for the trapping times [Eq. (37)]. Higher pumping strengths lead to longer trapping times. Subplot (b) displays the mean trapping time $\langle\tau_{\rm trap}\rangle_n$ [Eq. (38)] as a function of the number of counts n. The inset shows the values of $\langle\tau_{\rm trap}\rangle$ as a function of $\bar{n}$, which we extrapolate from the curves, like the ones shown in the onset.

at the starting and the end points of the jumps the order parameter Θ has a different sign, such that the configuration has switched, for instance, from an even pattern ($\Theta > \sigma_N$) to an odd one ($\Theta < -\sigma_N$). We identify jump events in Fig. 5(c) with the green segments. An exception is the event at $\kappa t \sim 3000$, which does not fulfill the criteria we impose and thus does not qualify. We numerically determine the probability distribution $P_{\rm jump}(\tau_{\rm jump})$ for the jumping times at a given value of $\bar{n} > \bar{n}_c$. Figure 9(a) displays the probability distribution $P_{\rm jump}(\tau_{\rm jump})$ for $\bar{n} = 1.4\,\bar{n}_c$. We observe that it exhibits the features of exponential decay with time. Further information is extracted from the mean jumping time $\langle\tau_{\rm jump}\rangle_n$, which we evaluate as

$$\langle\tau_{\rm jump}\rangle_n = \sum_{i=1}^{n} \tau_{\rm jump}^{(i)}/n, \tag{39}$$

with $\tau_{\rm jump}^{(i)}$ the jumping time for the ith jump and $i = 1,\ldots n$. Figure 9(b) displays $\langle\tau_{\rm jump}\rangle_n$ for different pumping strengths. The mean values $\langle\tau_{\rm jump}\rangle_n$ do not differ much for different pumping strengths, in agreement with the conjecture that thermal fluctuations are responsible for the short-time behavior of the autocorrelation function. Nevertheless, we see indications that the mean jumping time decreases as $\bar{n}$ increases; thus, at large pump strengths the atoms reorganize in Bragg gratings over shorter time scales.

Insight into the dynamics underlying a jump in the order parameter can be gained by considering the corresponding

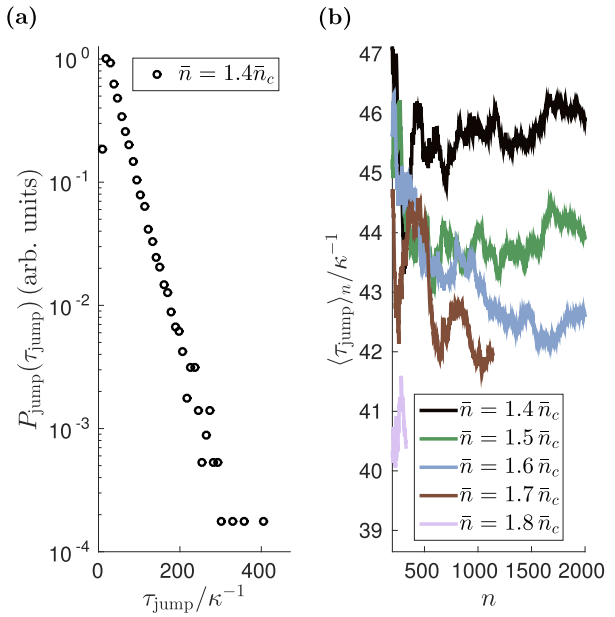

FIG. 9. (Color online) Statistics of the jumping times, evaluated numerically by averaging over 100 trajectories of $N = 20$, $\Delta_c = -\kappa$, total evolution time $t_{\rm tot} \approx 10^6\kappa^{-1}$. (a) Probability distribution $P_{\rm jump}(\tau_{\rm jump})$ for $\bar{n} = 1.4\,\bar{n}_c$. (b) Mean jumping time $\langle\tau_{\rm jump}\rangle_n$ [Eq. (39)] as a function of the number of counts n and for several values of $\bar{n}$ above threshold (see inset).

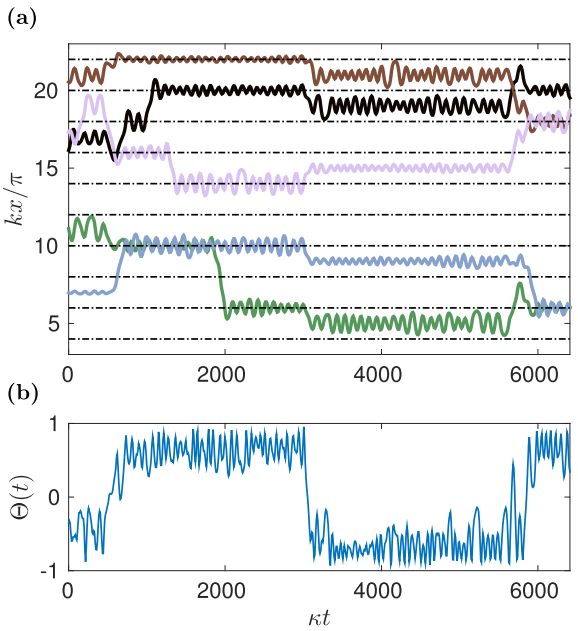

FIG. 10. (Color online) (a) Individual atomic trajectories and (b) corresponding order parameter as a function of time (in units of κ^{-1}) for $N = 5$ atoms, $\Delta_c = -\kappa$, and $\bar{n} = 1.4\,\bar{n}_c$. The black dashed horizontal lines in (a) indicate the position of the even sites of the cavity spatial mode function. The trajectories have been numerically evaluated taking the stationary state as the initial distribution.

individual atomic trajectories. A simulation for $N = 5$ atoms is shown in Fig. 10(a) for the choice of a pump strength above threshold $\bar{n} = 1.4\,\bar{n}_c$. At a given instant of time, the atomic positions are, in general, at distances which are integer multiples of the cavity wavelength, thus localized either at the even or the odd sites of the spatial mode function, thus forming one of the two possible Bragg gratings. When this occurs, the atoms perform oscillations about these positions. The amplitude of these oscillations does not remain constant, and one can observe an effective exchange of mechanical energy among the atoms. This can lead to a change of the potential that can untrap atoms. The onset of this behavior seems to be the precursor of the instability of the whole grating, as one can observe by comparing these dynamics with the one of the corresponding order parameter in subplot (b). The oscillations about the grating minima, moreover, are responsible for the damped oscillation observed in the autocorrelation function in Fig. 6 for values of $\bar{n}$ above threshold.

3. *Power spectrum*

Complementary information to the temporal behavior of the autocorrelation function can be gained by studying its Fourier transform. We thus numerically compute the power spectrum of $\Theta(t)$, which we define as

$$\tilde{S}(\omega) = \langle|\Theta(\omega)|^2\rangle, \tag{40}$$

where

$$\Theta(\omega) = \int_0^t d\tau \exp(-i\omega\tau)\Theta(\tau) \tag{41}$$

is the Fourier transform of the order parameter. Figure 11 displays the spectrum of the autocorrelation function for different values of $\bar{n}$ (a) below and (b) above threshold.

One clearly observes two different kinds of behavior, depending on whether $\bar{n}$ is below or above threshold: For $\bar{n} < \bar{n}_c$ we observe a rather broad spectrum about $\omega = 0$, whose breadth increases as $\bar{n}$ approaches the critical value from below. The emergence of a flat broad structure can be associated with the creation of (unstable) Bragg gratings and is related to the broadening of the distribution $P_N(\Theta_0)$ visible in Figs. 4(b) and 4(c). Above threshold, for $\bar{n} > \bar{n}_c$, the width of the component centered at zero frequency becomes dramatically narrower and narrows further with $\bar{n}$, indicating that the atoms become increasingly localized in a Bragg pattern. The width of this frequency component is determined by the inverse of the mean trapping time, namely, the rate at which jumps between different Bragg gratings occur.

Above threshold sidebands of the central peak appear, which correspond to the damped oscillations of the autocorrelation function. The central frequency of these sidebands increases for higher pumping strength, while their width decreases. We understand these features as the onset of oscillations about the minima of the Bragg grating, which one can also observe in the trajectories of Fig. 10(a). This conjecture is supported by a simple calculation of the oscillation frequency as a function of $\bar{n}$, assuming that the potential about their minima is approximated by harmonic oscillators. Even though the estimated frequency is higher, this estimate qualitatively reproduces the dependence of the sidebands' central frequency

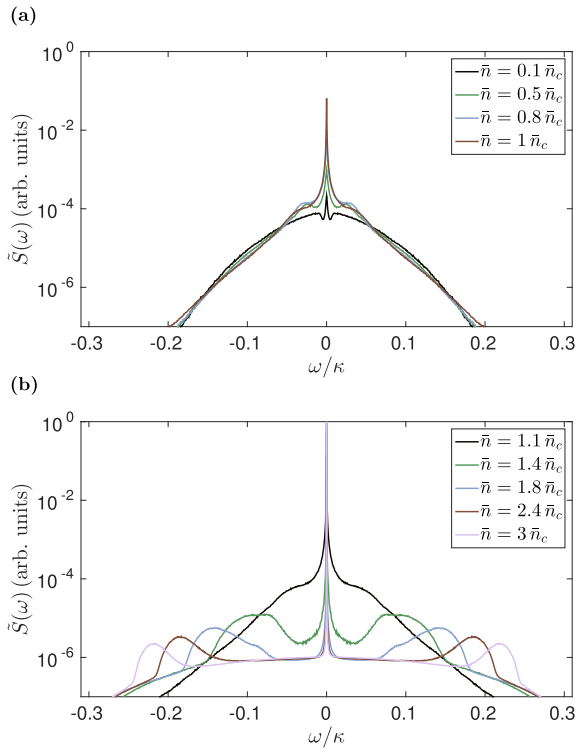

FIG. 11. (Color online) Spectrum of the autocorrelation function $\tilde{S}(\omega)$ [Eq. (40)] and in arbitrary units, as a function of the frequency (in units of κ) for different $\bar{n}$, and evaluated from the numerical data of $\Theta(t)$ for 100 trajectories of $N = 50$ atoms, $\Delta_c = -\kappa$, and evolution time $t_{\rm tot} = 10^4\kappa^{-1}$. The subplots show the spectrum for $\bar{n}$ below (a) and above (b) threshold (see insets).

with $\bar{n}$ above threshold, as visible in Fig. 12. This plot further shows that the behavior between the two parameter regions, below and above threshold, are qualitatively very different. The results of our simulations suggest that the transition in Fig. 12 at $\bar{n}_c$ becomes sharper as the atom number is increased.

IV. PHOTON STATISTICS AND COHERENCE OF THE FIELD AT THE CAVITY OUTPUT

Since the photons scattered by the atoms into the resonator carry the information about the density of the atoms within the cavity spatial mode function, then detection of the light at the cavity output allows to monitor the state of the atoms during the dynamics. This is an established method in experiments with atoms and ions in cavities [22,49–52], and it is at the basis of proposals for detecting nondestructively the quantum phase of ultracold atoms [53,54].

Formally, the field at the cavity output $\hat{a}_{\rm out}(t)$ is directly proportional to the intracavity field $\hat{a}$ via the relation $\hat{a}_{\rm out}(t) = \sqrt{2\kappa}\hat{a} - \hat{a}_{\rm in}(t)$, where $\hat{a}_{\rm in}(t)$ is the input field, with zero mean value and $[\hat{a}_{\rm in}(t),\hat{a}_{\rm in}(t')^\dagger] = \delta(t-t')$ [55]. The intracavity field is, in turn, given by the solution of the coupled atoms-field dynamics, and under the assumption of time-scales separation it can be cast in the form given in Eq. (7), which expresses an effective operator resulting from the coarse-grained dynamics. Equation (7) shows that in leading order the intracavity field is

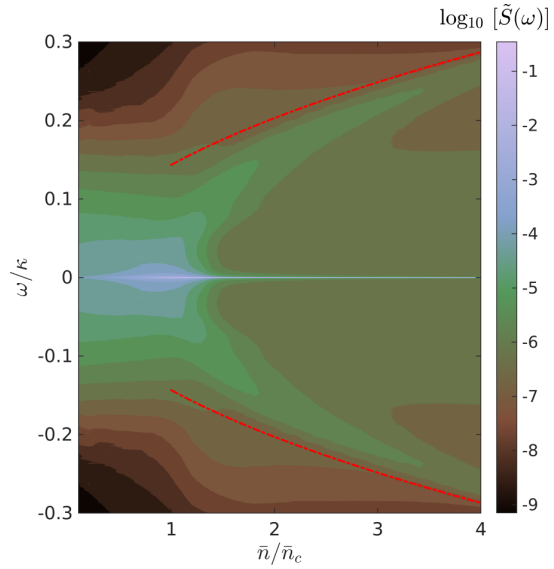

FIG. 12. (Color online) Contour plot of the spectrum of the autocorrelation function $\tilde{S}(\omega)$ [Eq. (40)] as a function of $\bar{n}$ and of the frequency (in units of κ). The other parameters are the same as in Fig. 11. The red dashed line corresponds to an estimate deep in the organized regime assuming the atoms are trapped in a harmonic potential with frequency $\tilde{\omega} = \sqrt{2\omega_r\kappa\bar{n}/\bar{n}_c}$.

proportional to the magnetization $\Theta(t)$; therefore, the features of the magnetization we identified thus far shall be visible also in the photon statistics at the cavity output. In addition, there is a retardation component, which gives rise to cooling and that in our parameter regime is a small correction. We now report the analysis of the intracavity photon number, and of the first- and second-order correlation functions as a function of the pump strength $\bar{n}$. Throughout this analysis we consider that the system has reached the stationary state at $\Delta_c = -\kappa$, corresponding to the minimum temperature of the atoms. Analytically, all averages are taken assuming the atomic distribution is stationary. Numerically, this consists of assuming that the trajectories are evolved starting from the stationary distribution.

A. Intracavity photon number

The intensity of the emitted light is proportional to the mean intracavity photon number

$$n_{\rm cav} = \lim_{t\to\infty} \langle \hat{a}^\dagger(t)\hat{a}(t)\rangle. \tag{42}$$

Figure 13(a) displays $n_{\rm cav}$ as a function of $\bar{n}$ for different atom numbers. The circles correspond to the mean photon number evaluated by numerical simulations using Eq. (7), whereas the dot-dashed lines show the adiabatic solution, Eq. (9), evaluated with the steady-state solution of Eq. (23). For $\bar{n} < \bar{n}_c$ the mean photon number is below unity: Therefore, in this regime shot noise is dominant. Above threshold, $n_{\rm cav}$ rapidly increases with N and $\bar{n}$. For the parameters we choose its value is essentially determined by the adiabatic component of the cavity field, while the contribution due to retardation is negligible (it is less than 0.1%). Thus, the intracavity photon number provides

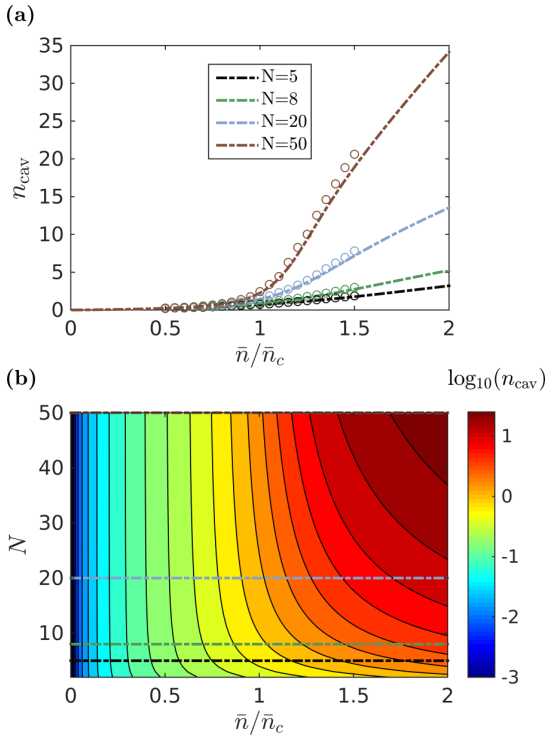

FIG. 13. (Color online) (a) The mean intracavity photon number n_{cav} at steady state is displayed as a function of the pump strength $\bar{n}$ (in units of $\bar{n}_c$) and for different atom numbers (see inset). The circles correspond to the numerical data obtained by using Eq. (7) and integrating the SDE. The dot-dashed lines correspond to the adiabatic limit $n_{cav}|_{ad} = N\bar{n}\lim_{t\to\infty}\langle\Theta(t)^2\rangle$, where the average is performed over the stationary state in Eq. (23). (b) Contour plot of $n_{cav}|_{ad}$ as a function of N and $\bar{n}$. The color code is in logarithmic scale. The horizontal lines correspond to the dot-dashed curves shown in subplot (a).

direct access to the autocorrelation function at zero-time delay, $\langle\Theta^2\rangle$. The numerical data, represented by the circles, follow very closely the curves corresponding to the adiabatic solution $n_{cav}|_{ad} = N\bar{n}\lim_{t\to\infty}\langle\Theta(t)^2\rangle$. The difference between the two curves is indeed small and due to the effect of the dynamical Stark shift scaling with the parameter U, which in the numerics is systematically taken into account. This nonlinear shift of the cavity frequency is maximum when the atoms are localized in a grating and for the chosen sign ($U < 0$) it tends to increase the value of n_{cav}.

Figure 13(b) displays the contour plot of n_{cav} as a function of $\bar{n}$ and N using the adiabatic solution [Eq. (9)] and the steady-state solution in Eq. (23). We observe that well below threshold n_{cav} depends solely on $\bar{n}$ and is independent of N. In this regime, in fact, the atoms are homogeneously distributed; there is no collective effect in photon scattering and thus no superradiance. Using the assumption of a homogeneous spatial distribution and $\bar{n} \ll \bar{n}_c$ we can derive an analytical estimate of n_{cav} which is independent of N (see Appendix D):

$$n_{cav}|_{\bar{n}\ll\bar{n}_c} \approx \bar{n}/2.$$

As $\bar{n}$ approaches and then exceeds the threshold value, instead, the dependence of the mean intracavity photon number on N becomes evident.

B. Spectrum of the emitted light

We now turn to the first-order correlation function at steady state, $g^{(1)}(\tau) = \lim_{t\to\infty}\langle\hat{a}^\dagger(t+\tau)\hat{a}(t)\rangle$. At zero-time delay, $\tau = 0$, it corresponds to the intracavity photon number. For finite delays τ it is proportional to the power spectrum of the autocorrelation function. In addition, it contains the nonlinear contribution of the cavity frequency shift and the retarded component of the cavity field. We discuss here the spectrum of $g^{(1)}(\tau)$,

$$S(\omega) = \lim_{t\to\infty}\frac{1}{2\pi}\int_{-\infty}^{\infty} d\tau e^{-i\omega\tau}\langle\hat{a}^\dagger(t+\tau)\hat{a}(t)\rangle, \qquad (43)$$

which we then compare with the result obtained for the power spectrum of the magnetization. The spectrum $S(\omega)$ is displayed in Fig. 14 for $N = 50$ atoms and different values of the pumping strength.

The behavior is very similar to the spectrum of the autocorrelation function of the magnetization in Fig. 11. Below threshold [Fig. 14(a)] we observe a broad frequency spectrum, while above threshold [Fig. 14(b)] we notice the emergence of sidebands whose frequency increases with $\bar{n}$. In general, the spectrum of the emitted light has the same form as the power spectrum of the magnetization and thus allows to extract information about the thermodynamics of self-organization. The contour plot is very similar to the corresponding one of the autocorrelation function, Fig. 12. A distinct feature is found in a small asymmetry between the red ($\omega < \omega_L$) and the blue ($\omega > \omega_L$) sidebands in Fig. 14(b). The asymmetry seems to be due to the contribution of the diabatic component of the cavity field, given in Eq. (8). Remarkably, the spectrum qualitatively agrees with the one observed in experiments analyzing self-organization of ultracold atoms in single-mode standing-wave resonators [52], thus outside the regime of validity of the semiclassical treatment. In particular, sideband asymmetry above threshold was also reported in Ref. [52].

C. Intensity-intensity correlations

The intracavity photon number below and close to threshold is smaller than unity, and is thus characterized by large photon fluctuations. We now study the properties of these fluctuations by determining the intensity-intensity correlation function,

$$g^{(2)}(\tau) = \lim_{t\to\infty}\frac{\langle\hat{a}^\dagger(t)\hat{a}^\dagger(t+\tau)\hat{a}(t+\tau)\hat{a}(t)\rangle}{\langle\hat{a}^\dagger(t)\hat{a}(t)\rangle^2}. \qquad (44)$$

with $t \to \infty$ indicating the steady-state, and focus on its value at zero-time delay, $g^{(2)}(0)$, as a function of $\bar{n}$ for gaining insight in the photon statistics. Figure 15(a) displays the correlation function $g^{(2)}(0)$ as a function of $\bar{n}$ and for different atom numbers. The circles show $g^{(2)}(0)$ extracted from numerical simulations using Eq. (7), while the dot-dashed lines correspond to the adiabatic solution $g^{(2)}(0)|_{ad} = \langle\Theta^4\rangle/\langle\Theta^2\rangle^2$ using the steady-state solution in Eq. (23). Both curves are in good agreement. We observe a crossover from $g^{(2)}(0) \approx 3$ to $g^{(2)}(0) \approx 1$ when tuning the pumping strength from below to

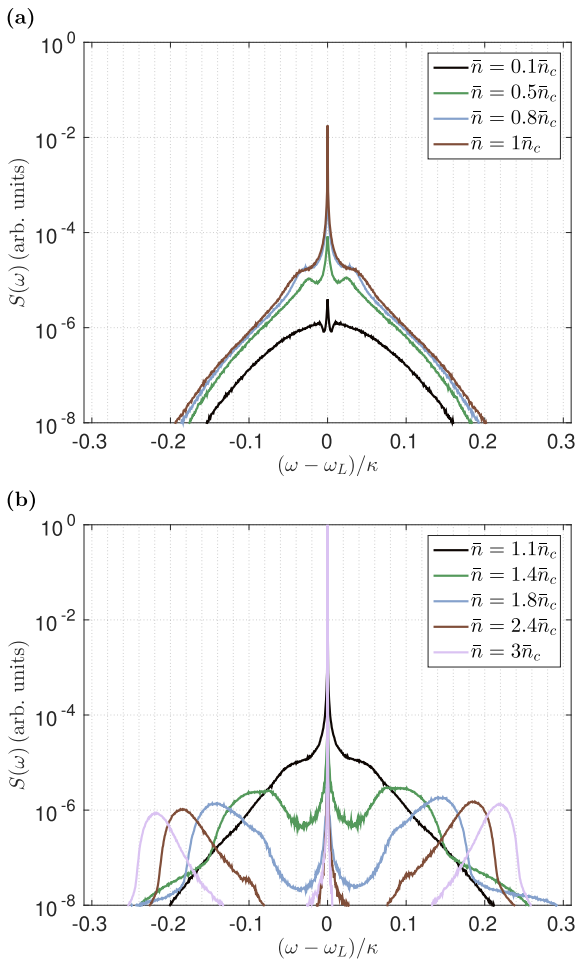

FIG. 14. (Color online) Spectrum of the intracavity field intensity $S(\omega)$ [Eq. (43)] and in arbitrary units at steady state. In (a) the curves correspond to values of $\bar{n} \leqslant \bar{n}_c$ and in (b) they correspond to values of $\bar{n} > \bar{n}_c$. The data have been numerically evaluated for $N = 50$ atoms and over the interval of time $(-10^4 : 1 : 10^4)\kappa^{-1}$.

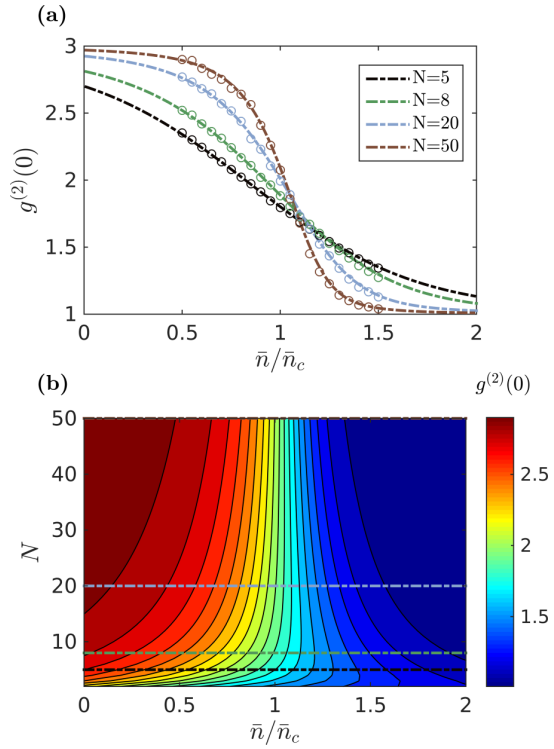

FIG. 15. (Color online) (a) The intensity-intensity correlation at zero-time delay $g^{(2)}(0)$ [Eq. (44)] is shown as a function of the pump strength $\bar{n}$ (in units of $\bar{n}_c$) and for different atom numbers N (see inset). The circles correspond to the data extracted from numerical simulations, the dot-dashed lines are evaluated using the steady state in Eq. (23) and the adiabatic solution, where the field is proportional to the instantaneous value of the magnetization: $g^{(2)}(0)|_{\rm ad} = \langle\Theta^4\rangle/\langle\Theta^2\rangle^2$. (b) Contour plot of the adiabatic component of the intensity-intensity correlation function at zero-time delay $g^{(2)}(0)|_{\rm ad}$ vs $\bar{n}$ and N. The horizontal cuts correspond to the dot-dashed lines in subplot (a).

above the threshold, which sharpens as N grows. The value above threshold is associated with coherent radiation, which is what one expects when the atoms are locked in a Bragg grating. The behavior below threshold can be reproduced by means of an analytical model valid for $\bar{n} \ll \bar{n}_c$, in the limit in which the atoms form a homogeneous distribution. In Appendix D we show that in this limit we can write

$$g^{(2)}(0) = 3 - 3/(2N), \tag{45}$$

which asymptotically tends to 3 as N increases. This result qualitatively agrees with experimental measurements with ultracold atoms performed below threshold [52]. While this value is also found for squeezed states, in our case we could not find any squeezing in the field quadratures and thus attribute the behavior of $g^{(2)}(0)$ below threshold to thermal fluctuations.

Figure 15(b) displays $g^{(2)}(0)$ for different pumping strengths and number of atoms, evaluated using the adiabatic solution $g^{(2)}(0) = \langle\Theta^4\rangle/\langle\Theta^2\rangle^2$ and the steady state in Eq. (23). The dashed horizontal cuts correspond to the dot-dashed curves shown in subplot (a). One clearly observes the crossover from $g^{(2)}(0) \approx 3$ to $g^{(2)}(0) \approx 1$ when $\bar{n}$ exceeds $\bar{n}_c$, while the transition sharpens for increasing atom numbers.

V. CONCLUSIONS

Atoms can spontaneously form spatially ordered structures in optical resonators when they are transversally driven by lasers. In this paper we have characterized the stationary solution, which emerges from the interplay between the coherent dynamics due to scattering of laser photons into the resonator and the incoherent effects associated with photon losses due to cavity decay. We assumed that these dynamics are characterized by a time-scale separation, such that the cavity field relaxes on a faster time scale to a local steady state depending on the atomic density. This assumption is valid when the cavity loss rate κ exceeds the recoil energy ω_r scaling the mechanical effects of light, and it is fulfilled in several existing experiments [17,22,24]. Retardation effects are small, but important in order to establish the stationary state.

Starting from a FPE, which has been derived by means of an *ab initio* theoretical treatment [27], we have shown that the stationary state is thermal, with a temperature that is solely determined by the detuning between cavity and laser. From this result, we could determine the free energy and thus show that atomic self-organization in a standing-wave cavity mode is a second-order transition of Landau type. Our model allows us to determine the phase diagram for the self-organization transition and delivers the critical value of the pump strength in a self-consistent way. This value is in agreement with previous estimates [30,31]. An interesting further step is to connect this theory with quantum-field theoretical models which analyze self-organization in the ultracold regime [32,45,56], thus extending the validity of our model to the regime in which quantum fluctuations in the atomic motion cannot be treated within a semiclassical model.

We further remark that, while our analysis focuses on a one-dimensional model, we expect that from our predictions we can extrapolate the stationary behavior in two spatial dimensions. This can be calculated by means of a straightforward extension of the treatment in Ref. [27] to two dimensions. Differing from one dimension, in the symmetry-broken phase the atoms will form a checkerboard pattern as found in Ref. [23], as long as the atomic gas is uniformly illuminated by the laser and the coupling with the resonator can be treated in the paraxial approximation. The effect of the dimensionality can modify the specific form of friction and diffusion. Moreover, in two dimensions the effect of correlations is expected to be more relevant, so that the statistical properties will be modified.

Photodetection of the emitted light allows one to reveal the thermodynamic properties of the atoms. Our results show that they exhibit several remarkable analogies with experimental results obtained with ultracold atomic ensembles inside of resonators [52]. While our theory is not generally applicable to these systems, it is not surprising that the field at the cavity output does not depend on the presence (or absence) of matter-wave coherence, as it solely depends on the atomic density. Nevertheless, it would be interesting to identify observables for the cavity field output, if possible, that provide information about quantum coherent properties of matter, in the spirit of matter-wave homodyne detection discussed in Ref. [57]. This could be possible when the cavity spectroscopically resolves the many-body excitations, as is verified in the parameter regime of the experimental setup reported in Ref. [58].

This work is the first of a series analyzing the effect of the long-range cavity-mediated interaction. Here we focused on the dynamics at steady state. In Ref. [35] we will compare the results here reported with a mean-field solution, which is systematically derived from this treatment after making a mean-field ansatz, and discuss its validity in the perspective of developing a BBGKY hierarchy for self-organization in optical resonators [33]. In Ref. [34] we will analyze the dynamics of the full distribution after quenches across the phase transition, expanding on the results presented in Ref. [29].

ACKNOWLEDGMENTS

The authors are grateful to R. Landig, G. Manfredi, C. Nardini, F. Piazza, and R. Shaebani for stimulating discussions and helpful comments. This work was supported by the German Research Foundation (DFG, DACH project "Quantum crystals of matter and light") and by the German Ministry of Education and Research (BMBF "Q.com").

APPENDIX A: PARAMETERS OF THE FOKKER-PLANCK EQUATION

In this Appendix we give the explicit form of the parameters appearing in the coefficients of Eq. (12):

$$\delta_F = \frac{NU\Theta}{\Delta_c'}\cos(kx_i), \tag{A1}$$

$$\delta_\Gamma = \cos(kx_j)\frac{NU\Theta}{\Delta_c'}\frac{3\Delta_c'^2-\kappa^2}{\Delta_c'^2+\kappa^2} + \cos(kx_i)\frac{NU\Theta}{\Delta_c'} + 4\cos(kx_i)\cos(kx_j)\frac{(NU\Theta)^2}{\Delta_c'^2+\kappa^2}, \tag{A2}$$

$$\delta_\eta = \frac{(2NU\Theta)^2}{\Delta_c'^2+\kappa^2}\cos(kx_i)\cos(kx_j) + \frac{2NU\Theta\Delta_c'}{-\Delta_c'^2+\kappa^2}\left\{\frac{3\kappa^2-\Delta_c'^2}{\Delta_c'^2+\kappa^2}\cos(kx_j)-\cos(kx_i)\right\}, \tag{A3}$$

$$\delta_D = \frac{4NU\Theta}{\Delta_c'^2+\kappa^2}\cos(kx_j)[\Delta_c' + \cos(kx_i)NU\Theta]. \tag{A4}$$

The diffusion coefficient for the spontaneous decay term reads

$$\mathcal{D}^{\rm sp}(x_i) = (\hbar k)^2\left\{\frac{N^2S^2\Theta^2}{\Delta_c'^2+\kappa^2}[\sin^2(kx_i)+\overline{u^2}\cos^2(kx_i)] + s\overline{u^2}\left[\frac{2NS\Theta\Delta_c'}{\Delta_c'^2+\kappa^2}\cos(kx_i)+s\right]\right\},$$

where $s=\Omega/g$ and $\overline{u^2}$ determines the momentum diffusion due to spontaneous emission recoils projected on the cavity axis (dipole pattern of radiation).

Finally, the correction scaling with NU/κ in Eq. (17) reads

$$L_1 f = 2\hbar k\Delta_c\Theta\sum_i \sin(kx_i)\left[\frac{\Delta_c^2-\kappa^2}{\Delta_c^2+\kappa^2}\mathcal{B}+\Theta\cos(kx_i)\right]\partial_{p_i} f \tag{A5}$$

and is systematically taken into account in our calculations.

APPENDIX B: STOCHASTIC DIFFERENTIAL EQUATIONS

The FPE given in Eq. (17) for $|NU| \ll |\Delta_c|$ can be simulated by SDEs, which in our case read

$$dx_j = \frac{p_j}{m}dt + dX_j, \tag{B1}$$

$$dp_j = \hbar k\frac{2S^2\Delta_c}{\Delta_c^2+\kappa^2}\sin(kx_j)\left[\sum_{i=1}^N\cos(kx_i)\right]\delta_U dt + \frac{8\omega_r S^2\Delta_c\kappa}{\left(\Delta_c^2+\kappa^2\right)^2}\sin(kx_j)\left[\sum_{i=1}^N\sin(kx_i)p_i\right]dt + dP_j, \tag{B2}$$

with

$$\delta_U = 1 + \frac{NU}{\Delta_c}\left[\frac{\Delta_c^2-\kappa^2}{\Delta_c^2+\kappa^2}\mathcal{B} + \Theta\cos(kx_j)\right], \tag{B3}$$

where $j = 1,\ldots,N$ labels the atoms and dP_j denote the momentum noise terms, which are simulated by means of Wiener processes. In particular, $\langle dP_j\rangle = 0$ and $\langle dP_i dP_j\rangle = 2D_{ij}dt$, with

$$D_{ij} = (\hbar k)^2 S^2 \frac{\kappa}{\Delta_c^2+\kappa^2}\sin(kx_i)\sin(kx_j) \tag{B4}$$

the element of the diffusion matrix when spontaneous emission is neglected.

For $\Delta_c \neq -\kappa$, we additionally take into account position noise dX_i, which shows cross-correlations with momentum diffusion $\langle dP_j dX_\ell\rangle = \eta_{j\ell}dt$, with

$$\eta_{j\ell} = 2\hbar\omega_r S^2 \sin(kx_j)\sin(kx_\ell)\frac{\kappa^2-\Delta_c^2}{\left(\Delta_c^2+\kappa^2\right)^2}. \tag{B5}$$

These terms can only be simulated when adding terms as $\langle dX_i dX_j\rangle \neq 0$ to the FPE.

For the numerical simulations, we use the Heun method [59], which is a second-order Runge-Kutta scheme with a Euler predictor.

APPENDIX C: DETERMINATION OF THE FREE ENERGY

The equilibrium state reads

$$f(\boldsymbol{x},\boldsymbol{p}) = \frac{1}{\mathcal{Z}\Delta^N}\exp(-\beta H), \tag{C1}$$

where $\mathcal{Z}$ is the partition function, Δ is the unit phase space volume, and Hamiltonian H is given in Eq. (18). The canonical partition function $\mathcal{Z}$ takes the form

$$\begin{aligned}\mathcal{Z} &= \left(\frac{\lambda}{\Delta}\right)^N \int_{-1}^{1} d\Theta\Omega(\Theta)\int_{-\infty}^{\infty} dp_1\cdots\int_{-\infty}^{\infty} dp_N \exp(-\beta H)\\ &= \left(\frac{Z_0\lambda}{\Delta}\right)^N \int_{-1}^{1} d\Theta\Omega(\Theta)\exp(-\beta\hbar\Delta_c\bar{n}N\Theta^2),\end{aligned} \tag{C2}$$

with $Z_0 = \sqrt{2m\pi/\beta}$ and

$$\Omega(\Theta) = \frac{N}{2\pi}\int_{-\infty}^{\infty} d\omega \exp\left(i\omega N\Theta\right)J_0(\omega)^N, \tag{C3}$$

where $J_n(w) = 1/(i^n\lambda)\int_0^\lambda dx\cos(nkx)\exp[i\omega\cos(kx)]$ is the nth-order Bessel function [46]. In order to compute Eq. (C3), we rewrite it as

$$\Omega(\Theta) = \frac{N}{2\pi}\int_{-\infty}^{\infty} d\omega \exp\left[Nh(\omega)\right], \tag{C4}$$

where we introduced the function

$$h(\omega) = i\omega\Theta + \ln\left[J_0(\omega)\right]. \tag{C5}$$

We can now compute the integral in Eq. (C4) using the method of steepest descent. For this purpose, we derive the stationary condition for Eq. (C5). This reads

$$i\Theta - \frac{J_1(\omega_0)}{J_0(\omega_0)} = 0,$$

which we can rewrite as

$$\Theta = q(\gamma_0) = \frac{I_1(\gamma_0)}{I_0(\gamma_0)} \tag{C6}$$

after defining $\omega_0 = i\gamma_0$ and using that $\frac{J_1(\omega_0)}{J_0(\omega_0)} = i\frac{I_1(\gamma_0)}{I_0(\gamma_0)}$. The function $q:\mathbb{R}\to(-1,1)$ with $y\mapsto\frac{I_1(y)}{I_0(y)}$ is bijective, such that there is a unique solution satisfying the equation

$$\gamma_0 = q^{-1}(\Theta). \tag{C7}$$

With the method of steepest descent, we get

$$\begin{aligned}\Omega(\Theta) &\sim \frac{N}{2\pi}\sqrt{\frac{2\pi}{N|h''(\omega_0)|}}\exp[Nh(\omega_0)]\\ &= \sqrt{\frac{N}{2\pi}}C(\Theta)\exp(N\{\ln[I_0(q^{-1}(\Theta))]-q^{-1}(\Theta)\Theta\}),\end{aligned} \tag{C8}$$

with

$$C(\Theta) = \left|\Theta^2 - \frac{I_0(q^{-1}(\Theta)) + I_2(q^{-1}(\Theta))}{2I_0(q^{-1}(\Theta))}\right|^{-\frac{1}{2}}.$$

Using Eq. (C8) in Eq. (C2), at leading order in N we can cast the canonical partition function into the form

$$\mathcal{Z} = \left(\frac{Z_0\lambda}{\Delta}\right)^N \int_{-1}^{1} d\Theta\sqrt{\frac{N}{2\pi}}C(\Theta)\exp[-\beta N\mathcal{F}(\Theta)],$$

where $\mathcal{F}(\Theta)$ is the free energy per particle,

$$\beta[\mathcal{F}(\Theta)-\mathcal{F}_0] = \beta\hbar\Delta_c\bar{n}\Theta^2 + q^{-1}(\Theta)\Theta - \ln[I_0(q^{-1}(\Theta))], \tag{C9}$$

and $-\beta N\mathcal{F}_0 = N\ln(Z_0\lambda/\Delta)$. After performing a Taylor expansion of Eq. (C9) for small values of the order parameter, close to $\Theta = 0$, we obtain

$$\beta[\mathcal{F}(\Theta)-\mathcal{F}_0] \approx (1-\bar{n}/\bar{n}_c)\Theta^2 + \tfrac{1}{4}\Theta^4, \tag{C10}$$

which shows that close to the instability the free energy can be cast into the form of a Landau potential [47]. This shows that the system undergoes, in the considered limit, a second-order phase transition at the critical value $\bar{n} = \bar{n}_c$ with

$$\bar{n}_c = \frac{\kappa^2+\Delta_c^2}{4\Delta_c^2}. \tag{C11}$$

We use the method of steepest descent to minimize $\mathcal{F}(\Theta)$ in Eq. (C9) and find that the free energy is stationary if the order parameter solves the equation

$$\Theta = q\left(2\frac{\bar{n}}{\bar{n}_c}\Theta\right). \tag{C12}$$

APPENDIX D: ANALYTICAL ESTIMATES

Several quantities of relevance can be analytically determined in the limit of small pumping strength, specifically when $\bar{n} \ll \bar{n}_c$. In this limit we assume that the atoms move ballistically and their spatial distribution is homogeneous. The

steady state then reads

$$f_s(\boldsymbol{x},\boldsymbol{p}) = \frac{1}{\lambda^N}\left(\frac{\beta}{2\pi m}\right)^{N/2} \exp\left(-\beta\sum_i \frac{p_i^2}{2m}\right),$$

which is a homogeneous distribution for the atoms, while the momentum distribution is thermal with β defined in Eq. (20). The mean value of the order parameter for this distribution vanishes $\langle\Theta\rangle = 0$, while fluctuations scale as

$$\langle\Theta^2\rangle = \int d\boldsymbol{x}\int d\boldsymbol{p}\, f_s(\boldsymbol{x},\boldsymbol{p})\Theta^2 = \frac{1}{2N}. \tag{D1}$$

Here we used that the cross terms in $\Theta^2 = \sum_{i,j}\cos(kx_i)\cos(kx_j)/(N^2)$ vanish for a homogeneous distribution. For the standard deviation $\Delta\Theta = (\langle\Theta^2\rangle - \langle\Theta\rangle^2)^{1/2}$ we thus find

$$\Delta\Theta = \sqrt{\frac{1}{2N}}, \tag{D2}$$

which shows that the width $\Delta\Theta_0$ for the distribution function $P_N(\Theta_0)$ in Eq. (31) decreases with $N^{-1/2}$ for very low pumping strengths. We checked that for $\bar{n} \ll \bar{n}_c$ the Gaussian assumption is a good approximation for low values of $|\Theta_0|$ and sufficiently large atom number. This result is reported in Eq. (32).

In Sec. IV cavity field properties such as mean photon number $\langle\hat{a}^\dagger\hat{a}\rangle$ and intensity-intensity correlations at zero-time delay $g^{(2)}(0)$ are discussed. By adiabatically eliminating the cavity field, i.e., using Eq. (9), and neglecting the dynamical Stark shift, we can give the following estimate for the mean photon number

$$\langle\hat{a}^\dagger\hat{a}\rangle = N\bar{n}\langle\Theta^2\rangle = \bar{n}/2 = \frac{\bar{n}_c}{2}\frac{\bar{n}}{\bar{n}_c} \tag{D3}$$

under the assumption of a homogeneous spatial distribution. As long as the spatial distribution remains homogeneous, the mean photon number thus scales with the ratio $\bar{n}/\bar{n}_c$ independent on the atom number N. This result is discussed in Sec. IV A and gets evident in Fig. 13(b). Under the same conditions, far below threshold, we get

$$\begin{aligned}\langle\Theta^4\rangle &= \int d\boldsymbol{x}\int d\boldsymbol{p}\, f_s(\boldsymbol{x},\boldsymbol{p})\left[\sum_i \cos(kx_i)/N\right]^4 \\ &= \frac{1}{N^4}\left[N\frac{I_{(4)}}{2\pi} + 3N(N-1)\frac{I_{(2)}^2}{(2\pi)^2}\right] = \frac{3(N-1)}{8N^3},\end{aligned} \tag{D4}$$

with $I_{(2)} = \int_0^{2\pi} d\tilde{x}\cos^2(\tilde{x})$ and $I_{(4)} = \int_0^{2\pi} d\tilde{x}\cos^4(\tilde{x})$. For the intensity-intensity correlations at zero-time delay

$$g^{(2)}(0) = \langle\Theta^4\rangle/\langle\Theta^2\rangle^2, \tag{D5}$$

using Eqs. (D1) and (D4), we thus find

$$\lim_{\bar{n}\to 0} g^{(2)}(0) = 3 - \frac{3}{2N}. \tag{D6}$$

This function tends towards the value of 3 for increasing atom numbers, as can be seen in Fig. 15.

When assuming ballistic expansion, which is justified whenever the forces on the atoms due to cavity backaction are small, i.e., far below threshold, we can also derive an analytical estimate for the correlation function $C(\tau) = \langle\Theta(t)\Theta(t+\tau)\rangle$ at steady state,

$$\begin{aligned}&\lim_{\bar{n}\to 0}\langle\Theta(t)\Theta(t+\tau)\rangle \\ &= \langle\Theta^2\rangle_t\left(\frac{\beta}{2\pi m}\right)^{1/2}\int dp\exp\left(-\beta\frac{p^2}{2m}\right)\cos\left(k\frac{p}{m}\tau\right) \\ &= \langle\Theta^2\rangle_t\exp\left(-\frac{\omega_r}{\hbar\beta}\tau^2\right) = \langle\Theta^2\rangle_t\exp\left[-\left(\tau/\tau_c^{\text{free}}\right)^2\right],\end{aligned} \tag{D7}$$

with $\tau_c^{\text{free}} = \sqrt{(\hbar\beta/\omega_r)}$, where β is the inverse temperature defined in Eq. (20) and $\langle\Theta^2\rangle_t = \frac{1}{2N}$ according to Eq. (D1). The result is reported in Eq. (35).

[1] S. Chu, Rev. Mod. Phys. **70**, 685 (1998); C. N. Cohen-Tannoudji, *ibid.* **70**, 707 (1998); W. D. Phillips, *ibid.* **70**, 721 (1998).
[2] R. Kaiser, A. Kastberg, and G. Morigi, J. Opt. Soc. Am. B **20**, 883 (2003).
[3] M. Aspelmeyer, T. J. Kippenberg, and F. Marquardt, Rev. Mod. Phys. **86**, 1391 (2014).
[4] D. J. Wineland and W. M. Itano, Phys. Rev. A **20**, 1521 (1979).
[5] S. Stenholm, Rev. Mod. Phys. **58**, 699 (1986).
[6] P. Horak, G. Hechenblaikner, K. M. Gheri, H. Stecher, and H. Ritsch, Phys. Rev. Lett. **79**, 4974 (1997).
[7] P. W. H. Pinkse, T. Fischer, P. Maunz, and G. Rempe, Nature (London) **404**, 365 (2000).
[8] C. J. Hood, T. W. Lynn, A. C. Doherty, A. S. Parkins, and H. J. Kimble, Science **287**, 1447 (2000).
[9] V. Vuletić and S. Chu, Phys. Rev. Lett. **84**, 3787 (2000).
[10] P. Maunz, T. Puppe, I. Schuster, N. Syassen, P. W. H. Pinkse, and G. Rempe, Nature (London) **428**, 50 (2004).
[11] P. Domokos and H. Ritsch, J. Opt. Soc. Am. B **20**, 1098 (2003).
[12] H. Ritsch, P. Domokos, F. Brennecke, and T. Esslinger, Rev. Mod. Phys. **85**, 553 (2013).
[13] T. Kampschulte, W. Alt, S. Manz, M. Martinez-Dorantes, R. Reimann, S. Yoon, D. Meschede, M. Bienert, and G. Morigi, Phys. Rev. A **89**, 033404 (2014).
[14] D. H. J. O'Dell, S. Giovanazzi, and G. Kurizki, Phys. Rev. Lett. **90**, 110402 (2003).
[15] P. Münstermann, T. Fischer, P. Maunz, P. W. H. Pinkse, and G. Rempe, Phys. Rev. Lett. **84**, 4068 (2000).
[16] B. Nagorny, Th. Elsässer, and A. Hemmerich, Phys. Rev. Lett. **91**, 153003 (2003); S. Gupta, K. L. Moore, K. W. Murch, and D. M. Stamper-Kurn, *ibid.* **99**, 213601 (2007).
[17] S. Ritter, F. Brennecke, K. Baumann, T. Donner, C. Guerlin, and T. Esslinger, Appl. Phys. B **95**, 213 (2009).

[18] C. von Cube, S. Slama, D. Kruse, C. Zimmermann, Ph. W. Courteille, G. R. M. Robb, N. Piovella, and R. Bonifacio, Phys. Rev. Lett. **93**, 083601 (2004).
[19] G. Labeyrie, E. Tesio, P. M. Gomes, G.-L. Oppo, W. J. Firth, G. R. M. Robb, A. S. Arnold, R. Kaiser, and T. Ackemann, Nat. Photonics **8**, 321 (2014); G. R. M. Robb, E. Tesio, G.-L. Oppo, W. J. Firth, T. Ackemann, and R. Bonifacio, Phys. Rev. Lett. **114**, 173903 (2015).
[20] D. E. Chang, J. I. Cirac, and H. J. Kimble, Phys. Rev. Lett. **110**, 113606 (2013).
[21] P. Domokos and H. Ritsch, Phys. Rev. Lett. **89**, 253003 (2002).
[22] A. T. Black, H. W. Chan, and V. Vuletić, Phys. Rev. Lett. **91**, 203001 (2003).
[23] K. Baumann, C. Guerlin, F. Brennecke, and T. Esslinger, Nature (London) **464**, 1301 (2010).
[24] K. J. Arnold, M. P. Baden, and M. D. Barrett, Phys. Rev. Lett. **109**, 153002 (2012).
[25] R. Mottl, F. Brennecke, K. Baumann, R. Landig, T. Donner, and T. Esslinger, Science **336**, 1570 (2012).
[26] D. Nagy, G. Kónya, G. Szirmai, and P. Domokos, Phys. Rev. Lett. **104**, 130401 (2010).
[27] S. Schütz, H. Habibian, and G. Morigi, Phys. Rev. A **88**, 033427 (2013).
[28] P. Domokos, P. Horak, and H. Ritsch, J. Phys. B **34**, 187 (2001).
[29] S. Schütz and G. Morigi, Phys. Rev. Lett. **113**, 203002 (2014).
[30] J. K. Asbóth, P. Domokos, H. Ritsch, and A. Vukics, Phys. Rev. A **72**, 053417 (2005).
[31] W. Niedenzu, T. Grießer, and H. Ritsch, Europhys. Lett. **96**, 43001 (2011).
[32] Emanuele G. Dalla Torre, S. Diehl, M. D. Lukin, S. Sachdev, and P. Strack, Phys. Rev. A **87**, 023831 (2013).
[33] A. Campa, T. Dauxois, and S. Ruffo, Phys. Rep. **480**, 57 (2009).
[34] S. Schütz, S. B. Jäger, and G. Morigi (unpublished).
[35] S. B. Jäger, master's thesis, Saarland University, 2015; S. B. Jäger, S. Schütz, and G. Morigi (unpublished).
[36] A. Vukics and P. Domokos, Phys. Rev. A **72**, 031401(R) (2005).
[37] J. Dalibard and C. Cohen-Tannoudji, J. Phys. B **18**, 1661 (1985).
[38] S. Fernández-Vidal, G. De Chiara, J. Larson, and G. Morigi, Phys. Rev. A **81**, 043407 (2010).
[39] More specifically, the condition reads $\omega_r N S^2 \ll (\kappa^2 + \Delta_c^2)^2/(4|\Delta_c|)$ and reduces to the form in Eq. (4) when $|\Delta_c| \sim \kappa$.
[40] J. Larson, B. Damski, G. Morigi, and M. Lewenstein, Phys. Rev. Lett. **100**, 050401 (2008); J. Larson, S. Fernández-Vidal, G. Morigi, and M. Lewenstein, New J. Phys. **10**, 045002 (2008).
[41] F. Piazza and H. Ritsch, Phys. Rev. Lett. **115**, 163601 (2015).
[42] K. Murr, P. Maunz, P. W. H. Pinkse, T. Puppe, I. Schuster, D. Vitali, and G. Rempe, Phys. Rev. A **74**, 043412 (2006).
[43] P. H. Chavanis, J. Vatteville, and F. Bouchet, Eur. Phys. J. B **46**, 61 (2005); P. H. Chavanis, *ibid.* **87**, 120 (2014).
[44] B. Olmos, I. Lesanovsky, and J. P. Garrahan, Phys. Rev. Lett. **109**, 020403 (2012).
[45] F. Piazza and P. Strack, Phys. Rev. A **90**, 043823 (2014).
[46] M. Abramowitz and I. Stegun (editors), *Handbook of Mathematical Functions* (Dover, New York, 1968).
[47] L. D. Landau and E. M. Lifshitz, *Statistical Physics* (Pergamon, Oxford, U.K., 1958).
[48] N. Metropolis, A. W. Rosenbluth, M. N. Rosenbluth, A. H. Teller, and E. Teller, J. Chem. Phys. **21**, 1087 (1953).
[49] K. Baumann, R. Mottl, F. Brennecke, and T. Esslinger, Phys. Rev. Lett. **107**, 140402 (2011).
[50] N. Brahms, T. Botter, S. Schreppler, D. W. C. Brooks, and D. M. Stamper-Kurn, Phys. Rev. Lett. **108**, 133601 (2012).
[51] A. Dantan, J. P. Marler, M. Albert, D. Guénot, and M. Drewsen, Phys. Rev. Lett. **105**, 103001 (2010).
[52] F. Brennecke, R. Mottl, K. Baumann, R. Landig, T. Donner, and T. Esslinger, Proc. Natl. Acad. Sci. USA **110**, 11763 (2013); R. Landig, F. Brennecke, R. Mottl, T. Donner, and T. Esslinger, Nat. Commun. **6**, 7046 (2015).
[53] I. B. Mekhov, C. Maschler, and H. Ritsch, Nat. Phys. **3**, 319 (2007); I. B. Mekhov and H. Ritsch, Phys. Rev. Lett. **102**, 020403 (2009).
[54] S. Rist, C. Menotti, and G. Morigi, Phys. Rev. A **81**, 013404 (2010).
[55] C. W. Gardiner and M. J. Collett, Phys. Rev. A **31**, 3761 (1985).
[56] M. Buchhold, P. Strack, S. Sachdev, and S. Diehl, Phys. Rev. A **87**, 063622 (2013).
[57] S. Rist and G. Morigi, Phys. Rev. A **85**, 053635 (2012).
[58] M. Wolke, J. Klinner, H. Keßler, and A. Hemmerich, Science **337**, 75 (2012).
[59] W. Rümelin, SIAM J. Numer. Anal. **19**, 604 (1982).

CHAPTER 4

Seeding patterns for self-organization of photons and atoms

Seeding patterns for self-organization of photons and atoms

PHYSICAL REVIEW A **88**, 033830 (2013)

DOI: 10.1103/PhysRevA.88.033830

Authors: Wolfgang Niedenzu,[1,2] Stefan Schütz,[2] Hessam Habibian,[2,3] Giovanna Morigi,[2] and Helmut Ritsch[1,*]

[1]*Institut für Theoretische Physik, Universität Innsbruck, Technikerstraße 25, A-6020 Innsbruck, Austria*
[2]*Theoretische Physik, Universität des Saarlandes, Campus E2.6, D-66123 Saarbrücken, Germany*
[3]*ICFO – Institut de Ciències Fotòniques, Mediterranean Technology Park, E-08860 Castelldefels (Barcelona), Spain*
[*]*Helmut.Ritsch@uibk.ac.at*

Author Contributions:
The theoretical model was developed by W. Niedenzu, H. Ritsch, H. Habibian and G. Morigi. Numerical simulations were designed and performed by W. Niedenzu. The calculations and results were checked, discussed and analysed by all authors. The article was majorly written by W. Niedenzu, G. Morigi, and H. Ritsch.

Abstract:
When atoms scatter photons from a transverse laser into a high-finesse optical

cavity, they form crystalline structures which maximize the intracavity light field and trap the atoms in the ordered array. Stable organization occurs when the laser field amplitude exceeds a certain threshold. For planar single-mode cavities there exist two equivalent possible atomic patterns, which determine the phase of the intracavity light field. Under these premises, we show that the effect of an additional laser pumping the cavity makes one pattern more favorable than the other and that it can dynamically force the system into a predetermined configuration. This is an instance of pattern formation and seeding in a nonlinear quantum-optical system.

PHYSICAL REVIEW A **88**, 033830 (2013)

Seeding patterns for self-organization of photons and atoms

Wolfgang Niedenzu,[1,2] Stefan Schütz,[2] Hessam Habibian,[2,3] Giovanna Morigi,[2] and Helmut Ritsch[1,*]
[1]*Institut für Theoretische Physik, Universität Innsbruck, Technikerstraße 25, A-6020 Innsbruck, Austria*
[2]*Theoretische Physik, Universität des Saarlandes, Campus E2.6, D-66123 Saarbrücken, Germany*
[3]*ICFO – Institut de Ciències Fotòniques, Mediterranean Technology Park, E-08860 Castelldefels (Barcelona), Spain*
(Received 26 July 2013; published 18 September 2013)

When atoms scatter photons from a transverse laser into a high-finesse optical cavity, they form crystalline structures which maximize the intracavity light field and trap the atoms in the ordered array. Stable organization occurs when the laser field amplitude exceeds a certain threshold. For planar single-mode cavities there exist two equivalent possible atomic patterns, which determine the phase of the intracavity light field. Under these premises, we show that the effect of an additional laser pumping the cavity makes one pattern more favorable than the other and that it can dynamically force the system into a predetermined configuration. This is an instance of pattern formation and seeding in a nonlinear quantum-optical system.

DOI: 10.1103/PhysRevA.88.033830 PACS number(s): 37.30.+i, 37.10.Vz, 42.50.Wk

I. INTRODUCTION

Pattern formation is a remarkable phenomenon of nonlinear dynamics, which characterizes the physical behavior of complex systems [1]. Among several realizations encountered in the quantum world, one interesting example, on which we will focus in this work, is the formation of self-organized Bragg gratings by particles scattering photons in a high-finesse optical resonator [2,3]. This behavior is due to the mechanical effects of atom–photon interactions and emerges from coherent light scattering by an atomic gas into a single mode of the electromagnetic field inside the cavity. The light scattered by a spatially homogeneous particle distribution cannot significantly excite the cavity mode due to destructive interference of the electric fields stemming from different atoms since they have random phases. Above a certain critical intensity of the transverse pump laser, however, the atomic density undergoes a transition to a periodic distribution for which the intracavity light field is maximized. Vice versa, the field gives rise to a mechanical potential, which confines the atoms in the very same pattern. In a single-mode standing-wave cavity there exist two equivalent such configurations, each corresponding to an intracavity field of the same amplitude but of opposite phase. This behavior was first predicted in Ref. [2] and experimentally confirmed shortly afterwards [4]. Several theoretical [5–9] and experimental studies [10–14] have analyzed various aspects of the self-organization phenomenon, including extensions to multimode resonators [15–19].

Studies of dynamics of pattern formation in other systems have shown that these dynamics can be significantly modified in the presence of further pumping fields [20], which can impose an auxiliary phase favoring a certain pattern. In this work we theoretically study the interplay between longitudinal and transverse laser pump fields in determining spatial ordering inside a single-mode standing-wave resonator. We consider a setup as in Fig. 1 and show that, when the two lasers driving the cavity and the atoms are resonant, the laser pumping the cavity can act as a seed for the dynamics of pattern formation. We identify the conditions on the longitudinal laser for which the phase of Bragg gratings can be predetermined, and for which one can even dynamically force a Bragg grating of atoms to jump into another pattern.

This paper is organized as follows. In Sec. II the theoretical model is introduced, from which semiclassical stochastic differential equations are derived. These equations are the basis of the numerical simulations presented in Sec. III, where the dynamics of self-organization are studied in the presence of a laser pumping the cavity and as a function of its relative phase and amplitude. Finally, in Sec. IV the conclusions are drawn.

II. THEORETICAL MODEL

We consider a cloud of N cold atoms of mass m whose motion is confined along the axis of a linear standing-wave cavity as sketched in Fig. 1. The atoms are directly illuminated by a transverse laser beam whose frequency ω_p is far detuned from any internal atomic transition, but close to a single cavity resonance such that the particles can scatter photons from the driving laser into this resonator mode. A second laser at the same frequency ω_p directly drives the resonator mode through one of the cavity mirrors. In this limit the external and cavity degrees of freedom undergo a coupled dynamics. We denote by x_j and p_j the canonically conjugated position and momentum of the jth atom, while a and $a^\dagger$ are the bosonic annihilation and creation operators of a cavity photon. The coherent dynamics are then described by the Hamiltonian [5]

$$H = \sum_{j=1}^{N}\left[\frac{p_j^2}{2m} + \hbar U_0 a^\dagger a\,\sin^2(kx_j)\right] - \hbar\Delta_\mathrm{c} a^\dagger a + \sum_{j=1}^{N}\hbar\eta(a+a^\dagger)\sin(kx_j) - i\hbar(\eta_\mathrm{p}^* a - \eta_\mathrm{p} a^\dagger), \qquad (1)$$

where k denotes the cavity wave number. The parameter $U_0 < 0$ is the light shift per photon and $\eta \in \mathbb{R}$ is the effective cavity pump strength stemming from the light scattered from the transverse laser into the mode by the atom cloud. In addition, we also consider a longitudinal cavity pump of strength $\eta_\mathrm{p} \in \mathbb{C}$, including the possibility of a different phase with respect to the transverse laser. The Hamiltonian is reported in the reference frame rotating at the transverse frequency ω_p, which

*Helmut.Ritsch@uibk.ac.at

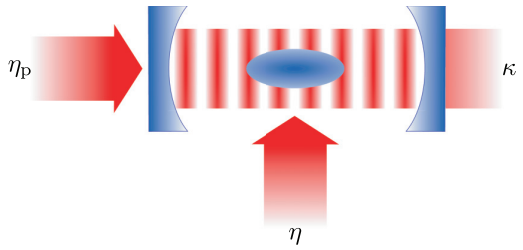

FIG. 1. (Color online) Sketch of the system. Atoms are confined inside a cavity with decay rate κ and illuminated by a transverse laser beam of strength η. When $|\eta|$ exceeds a certain threshold value the atoms self-organize in stable Bragg gratings which maximize scattering into the cavity mode. Here, we study how these dynamics are modified when the cavity mode is additionally driven by a longitudinal laser of strength η_p.

is assumed to be resonant with the laser pumping the cavity. In particular, $\Delta_c := \omega_p - \omega_c$ is the detuning between the pump lasers and the bare cavity resonance frequency.

Owing to the nonperfect mirrors photons leak out of the resonator. These processes are taken into account in the master equation for the joint atom–field density matrix ρ,

$$\dot{\rho} = \frac{1}{i\hbar}[H,\rho] + \mathcal{L}\rho, \tag{2}$$

where the Liouvillean

$$\mathcal{L}\rho = \kappa(2a\rho a^\dagger - a^\dagger a\rho - \rho a^\dagger a) \tag{3}$$

describes cavity decay at rate κ [21]. Dissipation effects due to atomic spontaneous emission are here neglected under the assumption that the atomic transition is driven far-off resonance. Note that the effective model in Eq. (1) is generally valid for any kind of linearly polarizable particles which can be confined within an optical resonator [3].

When the thermal energy $k_B T$ of the atoms is much larger than the recoil energy $E_R \equiv \hbar\omega_R := \hbar^2 k^2/2m$, i.e., $k_B T \gg E_R$, the system dynamics can be described within a semiclassical approximation and the master equation (2) can be mapped onto the following set of coupled Itō stochastic differential equations (SDEs) [5,21,22],

$$dx_j = \frac{p_j}{m}dt, \tag{4a}$$

$$dp_j = -\frac{\partial U(x_j,\alpha)}{\partial x_j}dt, \tag{4b}$$

$$d\alpha = \left[i\left(\Delta_c - U_0\sum_{j=1}^{N}\sin^2(kx_j)\right) - \kappa\right]\alpha\, dt + \eta_p\, dt - i\eta\sum_{j=1}^{N}\sin(kx_j)dt + \sqrt{\frac{\kappa}{2}}(dW_1 + i\, dW_2), \tag{4c}$$

with the single-particle potential

$$U(x,\alpha) = \hbar U_0|\alpha|^2\sin^2(kx) + \hbar\eta(\alpha+\alpha^*)\sin(kx). \tag{5}$$

The term $(dW_1 + i\, dW_2)/\sqrt{2}$ describes a complex Wiener process [23] accounting for cavity input noise. In this work we numerically investigate the dynamics and steady state of this coupled system as a function of the cavity drive η_p.

III. PATTERN FORMATION AND SEEDING

The coupled system of atoms and cavity photons is known to exhibit self-organized patterns in the absence of any longitudinal laser ($\eta_p = 0$) when the transverse laser intensity exceeds a certain threshold value [2–5]. The intracavity field is maximized when the atoms order in one of two equivalent (nonhomogeneous) configurations. The phase of the former, however, depends on the specific pattern realized, i.e., the particles either gather at lattice sites where $\sin(kx) = 1$ or where $\sin(kx) = -1$ (denoted by "even" and "odd" sites, respectively).

It has been argued that the occurrence of self-organization is a symmetry-breaking process, where the symmetry between the two configurations is spontaneously broken by initial particle fluctuations and cavity input noise [5]. Microscopically, one pattern is chosen for each trajectory, to which one can associate an order parameter, here identified with the quantity [5]

$$\Theta := \frac{1}{N}\sum_{j=1}^{N}\sin(kx_j). \tag{6}$$

Below threshold, where the atoms are homogeneously distributed, $\Theta = 0$, while in the perfectly self-organized phase the order parameter adopts values $\Theta = +1$ ($\Theta = -1$) for even (odd) patterns. At this point we have to distinguish between the *instantaneous* temperature-dependent critical pump strength η_{crit} [5], i.e., the minimal laser power required for triggering the self-organization process of a thermal gas of temperature $k_B T$, and the temperature-independent *self-consistent* threshold η_c, above which the phase transition sets in on a long-time scale as a result of dissipation (cooling) [7].

The process of self-organization is exemplified in Fig. 2. Figure 2(a) displays the initial average particle distribution when the transverse laser is switched on. The distribution after a sufficiently long time has elapsed such that the system has reached its steady state is shown in Fig. 2(b); one observes localization at the even and odd sites; for each trajectory only one of the two configurations is reached. Finally, Fig. 2(c) shows Θ as a function of time.

In summary, organization of the atoms in spatially ordered patterns corresponds to the light-induced formation of Bragg gratings. The atoms elastically scatter photons into the cavity and the intracavity field is maximized when all atoms scatter in phase, which here corresponds to arrays with interparticle distance equal to the cavity mode wavelength $\lambda = 2\pi/k$. The intracavity light field gives rise to a potential which has minima at either the even or odd sites, which form from initial fluctuations with equal probability. If the cavity is directly pumped as well, the scenario drastically changes. In this case, in fact, the cavity field is the coherent superposition of the scattered and of the directly injected field as seen in Eq. (4c). Clearly, the phase of the injected field plays a role by favoring one pattern over the other, depending on which one maximizes the depth of the intracavity potential. This allows one to "seed" the emergence of a specific spatial pattern above threshold, provided that the cavity drive $|\eta_p|$ is sufficiently strong.

The effect of a "seeding" field on the atomic spatial distribution is shown in Fig. 3. We choose the dipole potential associated with the cavity pump to be sufficiently shallow so

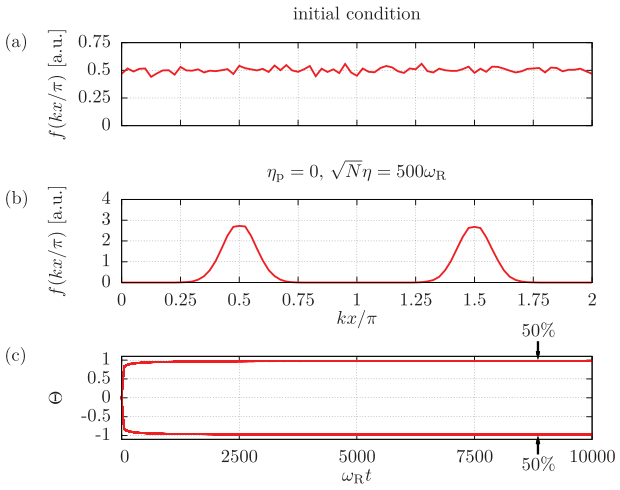

FIG. 2. (Color online) Simulation of self-organization of atoms driven by a laser and coupled to a high-finesse cavity for $\eta_p = 0$, i.e., without additional longitudinal pump. (a) Spatial distribution at $t = 0$ and (b) after reaching the steady state at $t = 10^4\omega_R^{-1}$. The time evolution of the order parameter Θ is displayed in (c). The curves have been obtained by numerically integrating the SDEs (4). Parameters: $N = 1000$, $\sqrt{N}\eta = 500\omega_R$, $NU_0 = -100\omega_R$, $\kappa = 100\omega_R$, and $\Delta_c = NU_0/2 - \kappa$. Ensemble average over 50×10 trajectories, i.e., 50 initial conditions and 10 realizations of the white noise process. The critical pump strength for the considered parameters and initial gas temperature $k_B T = 2\hbar\kappa$ is $\sqrt{N}\eta_{crit} = 200\omega_R$.

that the atoms remain spatially uniformly distributed when the transverse laser is off; cf. Fig. 3(a). Starting from this situation, a transverse laser (atom pump) is switched on at time $t = 0$.

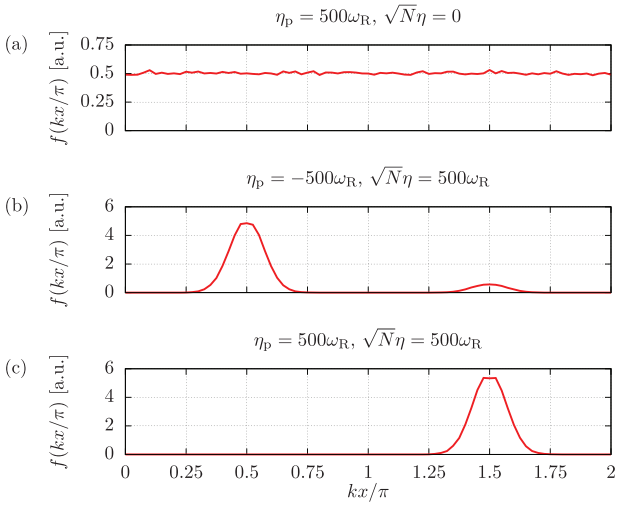

FIG. 3. (Color online) Spatial distribution of the atoms after reaching the steady state at $t = 10^4\omega_R^{-1}$ (a) when the transverse laser is switched off ($\eta = 0$) and the cavity is pumped by a laser of intensity $\eta_p = 500\omega_R$, corresponding to a potential depth $V_0 \sim 2E_R$. Subplots (b) and (c) show the spatial distribution in the presence of both longitudinal and transverse pump, with $\eta_p = -500\omega_R$ and $\eta_p = 500\omega_R$, respectively. Ensemble average over 20×10 trajectories. The other parameters are the same as in Fig. 2.

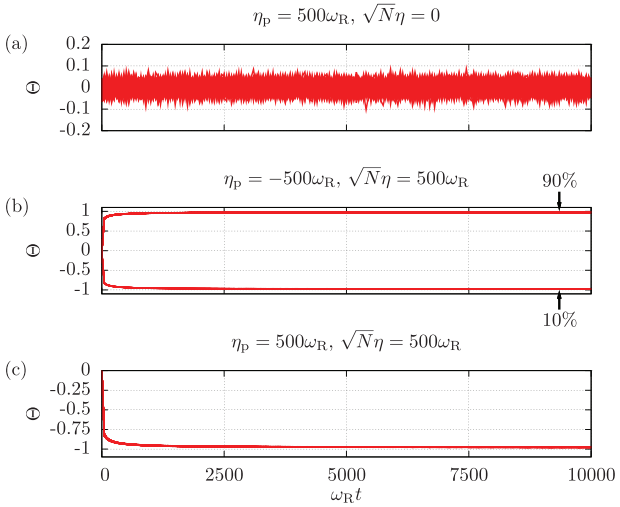

FIG. 4. (Color online) Order parameter Θ (for all trajectories) as a function of time for the parameters corresponding to the three subplots of Fig. 3, respectively.

Figures 3(b) and 3(c) display the two configurations which are obtained after a transient time when the relative phase between the two lasers is set either equal to 0 or π. We observe that the symmetry between the two patterns is broken compared to Fig. 2(b); cf. also the corresponding order parameter in Fig. 4. The atoms are with a high probability either localized in the even or in the odd sites, respectively, depending on the phase difference between the two driving lasers. We see though in Figs. 3(b) and 4(b) that the second pattern is only strongly suppressed and not impossible; there roughly 10% of the trajectories ended up in the "wrong" configuration. This specific number is an artifact of the relatively small ensemble considered, just like the fact that all trajectories ended up in an odd pattern for positive η_p in Figs. 3(c) and 4(c). These two cases thus already suggest a large statistical error of the seeding efficiency and the necessity of averaging over much larger ensembles. As can be seen in Fig. 5 for a large ensemble the probability that a certain configuration is dynamically realized

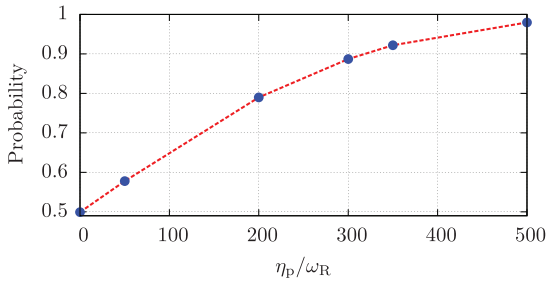

FIG. 5. (Color online) Probability that the atoms organize in an odd pattern as a function of the longitudinal pump strength $\eta_p \geqslant 0$. The second pattern occurs with a small, but finite probability which decreases as η_p is increased. This figure was obtained by integrating the SDEs (4) for a short time ($t = 1\omega_R^{-1}$) and computing the ratio of the number of trajectories for which $\Theta < 0$ and the ensemble size. Ensemble average over 5000×5 trajectories. The other parameters are the same as in Fig. 2.

approaches 100% for sufficiently large values of the cavity drive $|\eta_p|$.

A. Stationary patterns

Pattern seeding by means of a longitudinal field can be understood in terms of interference between the electric fields scattered by the atoms and directly injected by the cavity pump. This determines the intracavity field amplitude and therefore the depth of the $\sin(kx)$ component of the potential (5), which is proportional to the field's real part. Neglecting noise, the steady-state solution of Eq. (4c) for the intracavity field reads

$$\alpha_{ss} = \frac{-i\eta N\Theta + \eta_p}{\kappa - i\Delta}, \tag{7}$$

with the effective detuning $\Delta := \Delta_c - NU_0\mathcal{B} < 0$ and the bunching parameter $\mathcal{B} := \frac{1}{N}\sum_j \sin^2(kx_j)$ [5]. This result is valid for $kv_T \ll \kappa$, where $v_T := \sqrt{2k_BT/m}$ is the thermal velocity. Let us assume for simplicity that also $\eta_p \in \mathbb{R}$. Then, for a given sign of Θ—i.e., whether the atoms form an even or odd pattern—the sign of η_p determines whether $|\mathrm{Re}\alpha|$ becomes larger and hence the potential deeper. For instance, for $\eta_p > 0$ we expect that odd patterns ($\Theta < 0$) will be energetically favored and therefore occur with larger probability as visible from Fig. 5.

We now analyze the steady-state order parameter Θ as a function of the atom pump amplitude η for a chosen value of the phase and magnitude of the cavity pump η_p. Figure 6 displays this quantity for $\eta_p \leqslant 0$ as obtained by numerically integrating Eqs. (4) for long times. For completeness we also report the analytical predictions of [7] valid at $\eta_p = 0$ in the weak-coupling regime ($N|U_0| \ll |\Delta_c|$). Indeed, whilst we observe the expected bifurcation at the self-consistent threshold without cavity drive, only one branch is selected when the latter is sufficiently strong. For larger ensembles, however, the behavior suggested by Fig. 5 is expected to become visible, i.e., a finite number of trajectories ending up in the opposite pattern. In particular, finite probabilities of finding odd patterns are expected at larger values of η. At the same time the sharp transition is smeared out to a smooth crossover—the value of Θ increases monotonously to unity. This behavior becomes more enhanced as $|\eta_p|$ is increased by one order of magnitude.

A special case is realized when the longitudinal pump is sufficiently strong to give rise to a deep intracavity lattice even in the absence of the transverse laser. This is found, for instance, when $\eta_p = -5000\omega_R$. In this regime, at $\eta = 0$ the atoms are localized at the minima of the $\sin^2(kx)$ part of the cavity optical lattice (5) which is reflected by a high value of the bunching parameter $\mathcal{B}$, as visible in the inset of Fig. 6. A small value of η then already gives rise to a finite probability of finding the atoms in the even pattern. We have checked that the observed steady-state value of Θ is mainly due to the mechanical potential associated with the longitudinal laser. For $\eta_p = -500\omega_R$, on the other hand, collective photon scattering plays a crucial role in the formation of even patterns.

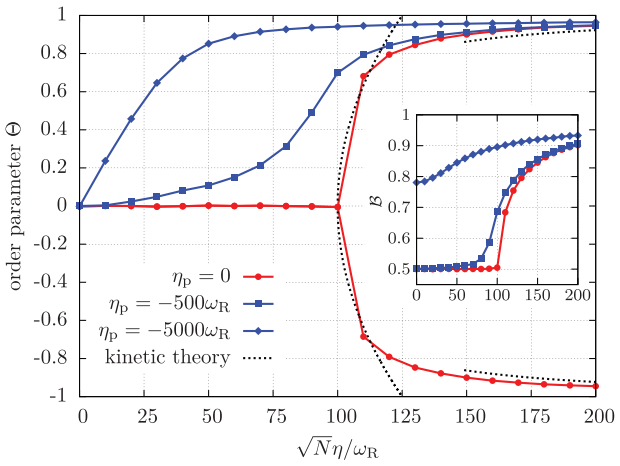

FIG. 6. (Color online) Order parameter Θ evaluated in steady state (at $t = 20N\omega_R^{-1}$) for $\eta_p = 0$ (red dots), $\eta_p = -500\omega_R$ (blue squares), and $\eta_p = -5000\omega_R$ (blue diamonds). For $\eta_p < 0$ the order parameter is always positive when driving the cavity. The black-dotted lines are the asymptotic steady-state predictions from kinetic theory in the weak-coupling limit [7]. Inset: corresponding bunching parameter $\mathcal{B}$. Ensemble average of 5×5 trajectories. The other parameters are the same as in Fig. 2.

B. Dynamical buildup of the organized phase

We now analyze the formation of a seeded pattern (e.g., the even one) considering two situations. First, when the atoms' initial spatial distribution is uniform, and second when the initial distribution corresponds to the opposite pattern. Figure 7 shows the onset of a seeded pattern for an initially uniform distribution, i.e., how the order parameter in Fig. 6 is dynamically established. We observe that the time scale over which the pattern forms decreases as the amplitude of the seeding field is increased. This behavior is particularly pronounced below threshold.

Let us now assume that $\eta_p = 0$ and that the atoms are pumped by a transverse laser with $\eta > 0$ above the

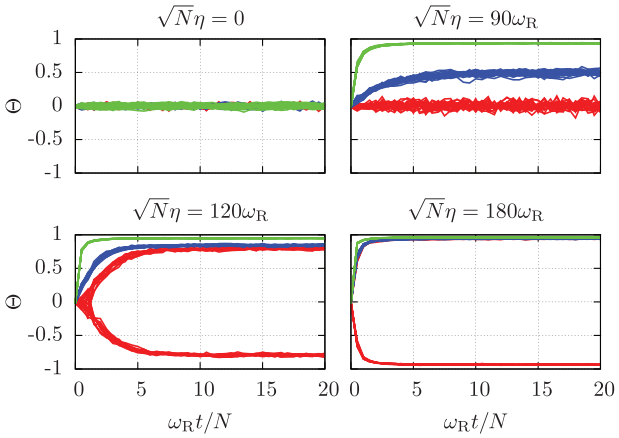

FIG. 7. (Color online) Order parameter Θ for 5×5 trajectories simulated using Eqs. (4) as a function of time for $\eta_p = 0$ (red), $\eta_p = -500\omega_R$ (blue), and $\eta_p = -5000\omega_R$ (green). From top to bottom (left to right) the value of η is $\sqrt{N}\eta = (0, 90, 120, 180)\omega_R$. The other parameters are the same as in Fig. 2.

(instantaneous) threshold. After some time the system reaches a stationary configuration which can be, for instance, an even pattern. An intense longitudinal pump field is then switched on. If its amplitude η_p is chosen to be real, the particles remain in the even pattern since, according to Eq. (7), the number of intracavity photons—and hence the potential depth—increases. Instead, when for instance the relative phase of the longitudinal pump differs from the transverse laser field by $\pi/2$, then the scattered and the injected field can interfere. This situation can lead to a pattern flip in the case that the phase of the scattered field gives rise to destructive interference. We expect that the scattered field vanishes and thus the atoms reorganize in the pattern for which the two field contributions add up coherently. We thus choose the relative phase $\pi/2$ and $|\eta_p|$ about 40 times larger than the maximum scattering rate into the resonator by the atoms ($\sqrt{N}\eta$).

Figure 8 shows the order parameter, mean number of intracavity photons, and the real and imaginary part of the intracavity field amplitude as a function of time for a single trajectory. When the strong longitudinal pump is switched on, one observes that the system readjusts in an odd pattern which augments the intracavity photon number. The order parameter, however, remains smaller than unity, representing a situation in which several defects, namely atoms trapped at even sites, are present. This can be understood through the SDE (4c) for the field and its approximate steady-state value (7): the intracavity field is overcompensated by the external driving such that its real part becomes positive, i.e., the odd sites become deeper than the even ones according to Eq. (5). Due to the external pump the latter, however, remain sufficiently deep to confine a considerable fraction of the particles on the considered short time scale. Afterwards, the longitudinal laser intensity is reduced to $\eta_p = 500\omega_R$, for which the intracavity optical lattice is shallow, and the particles are now again trapped by their own scattered light, i.e., after a transient time, in which the atoms first form a uniform distribution, the order parameter becomes again close to unity. Its sign, however, is the opposite of the initial one prior to the pulse sequence. Alternatively, one could also envisage a scheme where the longitudinal pump power is continuously reduced after the flip. This behavior is exemplary for understanding how the system reacts to external perturbations.

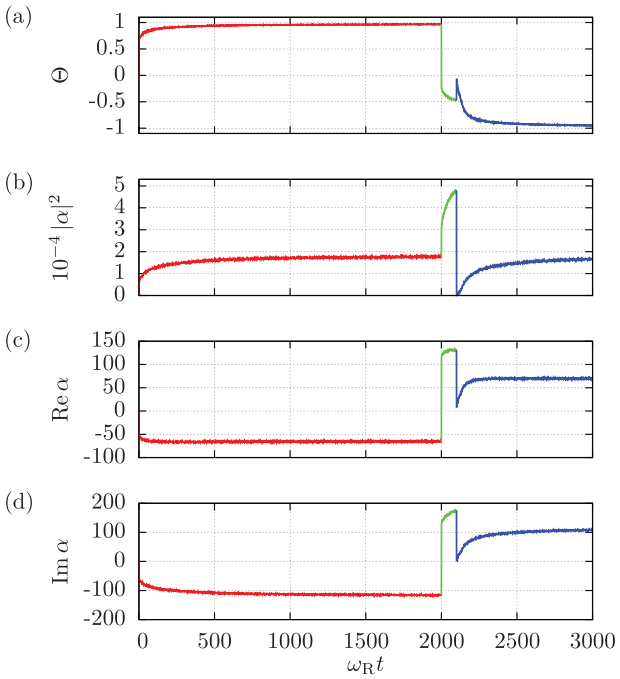

FIG. 8. (Color online) Example of dynamically flipping patterns with a longitudinal pump. The system behavior is shown as a function of time for a sequential change of the cavity drive by plotting (a) the order parameter, (b) the intracavity photon number, and the real (c) and imaginary (d) part of the field amplitude. First, $\eta_p = 0$ and $\sqrt{N}\eta = 500\omega_R$. At $t = 2000\omega_R^{-1}$ the longitudinal laser is switched on with $\eta_p = 2i \times 10^4\omega_R$ in order to compensate for the scattered field for a short time. Finally, at $t = 2100\omega_R^{-1}$ the external laser is reduced to $\eta_p = 500\omega_R$. The other parameters are the same as in Fig. 2.

IV. CONCLUSIONS AND OUTLOOK

In this work we presented a model and a numerical study of the effect of a longitudinal pump on self-organization of cold atoms in an optical resonator. We have focused on the situation in which both the transverse laser, pumping the atoms, and the longitudinal laser, driving the cavity mode, are resonant. The system exhibits a stationary state which can be an ordered pattern even below the self-organization threshold, provided that the longitudinal pump is sufficiently strong. The phase of the pump is crucial in determining the pattern which self-organizes. The longitudinal field, hence, acts as a seed, breaking the symmetry between the even and odd patterns, which are otherwise equivalent. The relative phase between longitudinal and transverse pump is thus a control handle for determining the configuration in which the atoms self-organize, to the point that it can be used to force the atoms to flip patterns.

Our analysis has so far focused on resonant external fields, which allow one to reduce the dynamics to a time-independent problem by moving to the reference frame rotating at the laser frequency. The situation is going to be dramatically modified when the two lasers are detuned one from the other. In this case the equations of motion are explicitly time dependent and exhibit an intrinsic period determined by the frequency mismatch between the two lasers. Chaotic behavior could here emerge at sufficiently low levels of noise.

An extension to the multimode case, e.g., ring cavities—where a continuous symmetry is broken—might also be interesting.

ACKNOWLEDGMENTS

The authors acknowledge discussions with Tobias Donner and András Vukics. W.N. thanks the Universität des Saarlandes, where parts of this work were performed, for hospitality. This work has been supported by the Austrian Science Fund FWF through project F4013, the EU (IP AQUTE, STREP PICC), the German BMBF (QuORep), and the German Research Foundation (DFG).

[1] M. C. Cross and P. C. Hohenberg, Rev. Mod. Phys. **65**, 851 (1993).
[2] P. Domokos and H. Ritsch, Phys. Rev. Lett. **89**, 253003 (2002).
[3] H. Ritsch, P. Domokos, F. Brennecke, and T. Esslinger, Rev. Mod. Phys. **85**, 553 (2013).
[4] A. T. Black, H. W. Chan, and V. Vuletić, Phys. Rev. Lett. **91**, 203001 (2003).
[5] J. K. Asbóth, P. Domokos, H. Ritsch, and A. Vukics, Phys. Rev. A **72**, 053417 (2005).
[6] A. Vukics, C. Maschler, and H. Ritsch, New J. Phys. **9**, 255 (2007).
[7] W. Niedenzu, T. Grießer, and H. Ritsch, Eur. Phys. Lett. **96**, 43001 (2011).
[8] B. Öztop, M. Bordyuh, Ö. E. Müstecaplıoğlu, and H. E. Türeci, New J. Phys. **14**, 085011 (2012).
[9] F. Piazza, P. Strack, and W. Zwerger, arXiv:1305.2928.
[10] A. T. Black, J. K. Thompson, and V. Vuletić, J. Phys. B **38**, S605 (2005).
[11] K. Baumann, C. Guerlin, F. Brennecke, and T. Esslinger, Nature (London) **464**, 1301 (2010).
[12] K. Baumann, R. Mottl, F. Brennecke, and T. Esslinger, Phys. Rev. Lett. **107**, 140402 (2011).
[13] K. J. Arnold, M. P. Baden, and M. D. Barrett, Phys. Rev. Lett. **109**, 153002 (2012).
[14] F. Brennecke, R. Mottl, K. Baumann, R. Landig, T. Donner, and T. Esslinger, Proc. Natl. Acad. Sci. USA **110**, 11763 (2013).
[15] S. Gopalakrishnan, B. L. Lev, and P. M. Goldbart, Nature Phys. **5**, 845 (2009).
[16] S. Gopalakrishnan, B. L. Lev, and P. M. Goldbart, Phys. Rev. A **82**, 043612 (2010).
[17] S. Gopalakrishnan, B. L. Lev, and P. M. Goldbart, Phys. Rev. Lett. **107**, 277201 (2011).
[18] P. Strack and S. Sachdev, Phys. Rev. Lett. **107**, 277202 (2011).
[19] H. Habibian, A. Winter, S. Paganelli, H. Rieger, and G. Morigi, Phys. Rev. Lett. **110**, 075304 (2013).
[20] S. Yang, M. Al-Amri, J. Evers, and M. S. Zubairy, Phys. Rev. A **83**, 053821 (2011).
[21] C. W. Gardiner and P. Zoller, *Quantum Noise*, 2nd ed. (Springer-Verlag, Berlin, 2000).
[22] P. Domokos, P. Horak, and H. Ritsch, J. Phys. B **34**, 187 (2001).
[23] P. E. Kloeden and E. Platen, *Numerical Solution of Stochastic Differential Equations*, 1st ed. (Springer-Verlag, Berlin, 1992).

CHAPTER 5

Mean-field theory of atomic self-organization in optical cavities

Mean-field theory of atomic self-organization in optical cavities

Authors: Simon B. Jäger, Stefan Schütz, and Giovanna Morigi

Theoretische Physik, Universität des Saarlandes, D-66123 Saarbrücken, Germany

Accepted for publication in Physical Review A - with kind permission of the American Physical Society.

see also PREPRINT, arXiv:1603.05148

Author Contributions:
The theoretical model was developed by S. B. Jäger, S. Schütz and G. Morigi. Analytical calculations were performed by S. B. Jäger. Numerical simulations were performed by S. B. Jäger and S. Schütz. The calculations and results were checked, discussed and analysed by all three authors. The article was written by all authors.

Abstract:
Photons mediate long-range optomechanical forces between atoms in high finesse resonators, which can induce the formation of ordered spatial patterns. When a transverse laser drives the atoms, the system undergoes a second order phase transition, that separates a uniform spatial density from a Bragg grating maximizing scattering into the cavity and is controlled by the laser intensity. Starting from a Fokker-Planck equation describing the semiclassical dynamics of the N-atom distribution function, we systematically develop a mean-field model and analyse its predictions for the equilibrium and out-of-equilibrium dynamics. The validity

of the mean-field model is tested by comparison with the numerical simulations of the N-body Fokker-Planck equation and by means of a BBGKY hierarchy. The mean-field theory predictions well reproduce several results of the N-body Fokker-Planck equation for sufficiently short times, and are in good agreement with existing theoretical approaches based on field-theoretical models. Mean-field, on the other hand, predicts thermalization time scales which are at least one order of magnitude shorter than the ones predicted by the N-body dynamics. We attribute this discrepancy to the fact that the mean-field ansatz discards the effects of the long-range incoherent forces due to cavity losses.

Mean-field theory of atomic self-organization in optical cavities

Simon B. Jäger, Stefan Schütz, and Giovanna Morigi
Theoretische Physik, Universität des Saarlandes, D-66123 Saarbrücken, Germany
(Dated: July 3, 2016)

Photons mediate long-range optomechanical forces between atoms in high finesse resonators, which can induce the formation of ordered spatial patterns. When a transverse laser drives the atoms, the system undergoes a second order phase transition, that separates a uniform spatial density from a Bragg grating maximizing scattering into the cavity and is controlled by the laser intensity. Starting from a Fokker-Planck equation describing the semiclassical dynamics of the N-atom distribution function, we systematically develop a mean-field model and analyse its predictions for the equilibrium and out-of-equilibrium dynamics. The validity of the mean-field model is tested by comparison with the numerical simulations of the N-body Fokker-Planck equation and by means of a BBGKY hierarchy. The mean-field theory predictions well reproduce several results of the N-body Fokker-Planck equation for sufficiently short times, and are in good agreement with existing theoretical approaches based on field-theoretical models. Mean-field, on the other hand, predicts thermalization time scales which are at least one order of magnitude shorter than the ones predicted by the N-body dynamics. We attribute this discrepancy to the fact that the mean-field ansatz discards the effects of the long-range incoherent forces due to cavity losses.

PACS numbers: 37.30.+i, 42.65.Sf, 05.65.+b, 05.70.Ln

I. INTRODUCTION

Optically-dense atomic ensembles offer a formidable framework to study collective effects induced by atom-photon interactions [1–3]. Correlations are established by multiple photon scattering [4, 5], which can give rise to phenomena such as synchronization [6, 7], optomechanical bistability [8, 9], and spontaneous spatial ordering [2, 3, 10–12]. Envisaged applications for these systems range from sensors [13], to quantum-enhanced metrology [14] and quantum simulators [12, 15].

Single-mode cavities, furthermore, mediate strong long-range interactions between the atoms [16–18], similarly to gravitational and Coulomb potential in two or more dimensions [19]. In view of this analogy, it is relevant to study the dynamics of these systems at and out-of-equilibrium so to test in a laboratory conjectures and predictions, such as ensemble inequivalence and the existence of quasi-stationary states [16]. The realization in quantum optical setups, like the one sketched in Fig. 1(a), brings additional peculiar features. In fact, these systems are intrinsically lossy, so that non-trivial dynamics can be observed only in presence of a pump. On the one hand, the conservative potential mediated by the cavity photons shares several analogies with the one of the Hamiltonian-Mean-Field model [17, 19–21], of which several features are well reproduced by a mean-field description [19, 20]. On the other hand, cavity losses give rise to damping and diffusion, which are characterized by a spatial structure, thus establishing long-range correlations between the atoms [17, 22]. These correlations, in turn, cannot be captured by a mean-field description.

In this work we systematically develop a mean-field model for cold atoms in a standing-wave resonator, in the setup illustrated in Fig. 1(a), and test its validity by comparing its predictions with the ones of the Fokker-Planck equation for the full atoms distribution [22]. This work completes a series of papers, which analyse the equilibrium and out-of-equilibrium dynamics of spatial self-organization of atomic ensembles in a single-mode resonator. Our analysis is based on a semiclassical treatment, and specifically on a Fokker-Planck equation (FPE) for the N-atom distribution, derived when the atoms are classically polarizable particles and their center-of-mass motion is confined to one dimension [22]. The cavity field, instead, is a full quantum variable. This makes our treatment applicable also in the shot-noise limit [22] and gives access to regimes that are complementary to those based on the model in Ref. [23], where the field is a semiclassical variable.

Our formalism permits us to consistently eliminate the cavity variables from the equations of motion of the atoms and to investigate the properties of the cavity field across the self-organization threshold, where the intracavity field is characterized by large fluctuations. Starting from this model in Ref. [21] we analysed the stationary state of the N-body FPE, and showed that (i) this is a thermal state whose temperature is determined by the linewidth of the resonator, and (ii) that the transition to self-organization is a Landau-type second-order phase transition, as illustrated in Fig. 1(b)-(c). In Ref. [21] we also determined the corresponding phase diagram as a function of the physical parameters and predicted the corresponding features in the light emitted by the resonator. In Ref. [24] we investigated the dynamics following sudden quenches across the phase transition, and found that the interplay between long-range conservative and dissipative forces gives rise to prethermalization dynamics, where the long-range nature of dissipation plays an essential role.

In this work we derive a mean-field treatment from our N-atom FPE. We then benchmark the limits of valid-

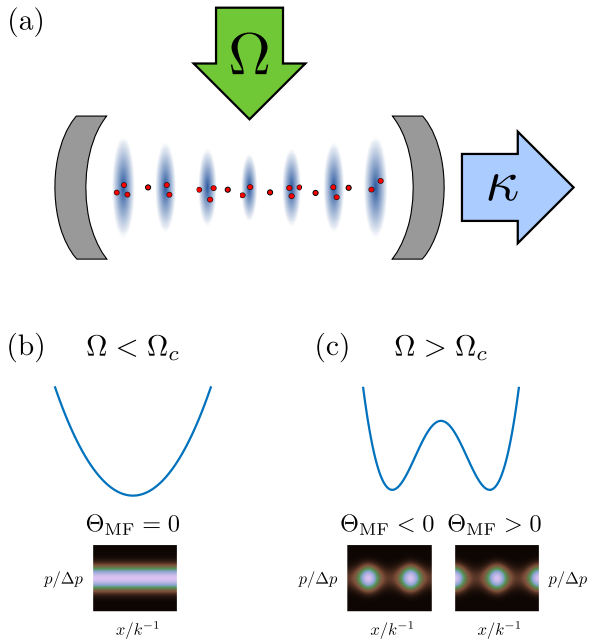

FIG. 1: (Color online) (a) Atoms in a standing-wave cavity and driven by a transverse laser can spontaneously form ordered patterns when the amplitude of the laser coupling Ω, exceeds a threshold value Ω_c, which depends on the rate of photon losses, here due to cavity decay at rate κ. In this regime the system undergoes a second-order phase transition which is characterised by the parameter Θ, indicating spatial ordering of the atoms in Bragg gratings and defined in Eq. (4). Its expectation value in the mean-field description is denoted as $\Theta_{\rm MF}$, see subplots (b) and (c), which display the thermodynamic potential below and above threshold. The lower panels are schematic pictures of the single-particle density distribution $f_1(x,p)$ in phase space with x in units of the inverse wavenumber k^{-1} and p in units of the width Δp of the momentum distribution. In (b) the atomic density is uniform, in (c) it is localized at the even or odd sites of the cavity standing wave, ($\cos(kx) = 1$ or -1, respectively). In this work we derive and discuss a mean-field theory for the dynamics of $f_1(x,p)$.

ity of the mean-field ansatz by means of numerical simulations using the full N-body FPE and by means of a BBGKY hierarchy. The results we obtain are compared with existing literature on spatial self-organization in single-mode cavities, both for the semiclassical treatment [25–28], as well as for the case in which the atomic quantum statistics is assumed to be relevant [15, 28–33].

This work is organized as follows. In Sec. II the Fokker-Planck Equation at the basis of our analysis is reported and the corresponding mean-field equation is derived. In Sec. III the stationary properties of the mean-field FPE distribution function are analytically determined. The mean-field predictions are compared with the ones of the N-body FPE and with further existing theoretical works. In Sec. IV the Vlasov equation, which describes the short time dynamics of the mean-field FPE, is derived. Its predictions are then determined by means of a stability analysis and the analytical results are compared with the numerical simulations of the mean-field FPE. Section V reports a critical analysis of the limits of validity of the mean-field treatment. In Sec. VI the conclusions are drawn, while in the Appendix A calculations are reported that complement the material presented in Sec. III.

II. DERIVATION OF THE MEAN-FIELD MODEL

In this section we derive the mean-field model starting from the Fokker-Planck equation (FPE) describing the dynamics of an atomic ensemble in the optical potential of a high-finesse resonator of Ref. [22]. The atoms are N, have mass m, their motion is assumed to be confined along the x-axis, which also coincides with the axis of a high-finesse cavity and within whose mirrors the atoms are spatially trapped. In the following we denote their canonically-conjugated positions and momenta by x_j and p_j ($j = 1, \ldots, N$). The atomic dipole strongly couples to one cavity mode and is transversally driven by a laser, as sketched in Fig. 1(a). The parameter regime is such that the atoms coherently scatter photons into the cavity mode and their external motion is determined by the light forces associated with these processes. The light forces are periodic, and their period is determined by the cavity mode standing wave, whose spatial mode function is $\cos(kx)$, with k the cavity-mode wave number.

A. Basic assumptions

Before reporting the FPE which governs the dynamics of the N-body distribution function, we summarize the main approximations behind its derivation and the corresponding physical parameters.

One basic assumption of our model is that the only relevant scattering processes are coherent. This regime can be reached when the cavity mode and laser frequencies are tuned far off resonance from the atomic transition [34, 35]. We denote by $\Delta_a = \omega_L - \omega_0$ the detuning between laser (ω_L) and atomic frequency (ω_0), and assume that this is the largest parameter of the problem. It is thus larger than the coupling strengths for the interaction between dipole and fields. It is also larger than the detuning $\Delta_c = \omega_L - \omega_c$ between laser and cavity mode frequency, whose wave numbers are to good approximation denoted by the same parameter k. This allows us to eliminate the internal degrees of freedom of the atoms by a perturbative expansion in the lowest order of the small parameter $1/|\Delta_a|$.

The cavity field is treated as a quantum mechanical variable and the dynamics can be cast as an optomechanical coupling between atomic motion and cavity

field [10, 23]. The parameter regime we assume gives rise to a time-scale separation, such that the cavity degrees of freedom evolve on a faster time-scale than the motion. This is warranted when the cavity line width κ, which determines the relaxation rate of the resonator state, is much larger than the recoil frequency $\omega_r = \hbar k^2/(2m)$, which scales the exchange of mechanical energy between light and atoms. In this limit the cavity field is eliminated from the equations of motion of the atomic external degrees of freedom in a perturbative expansion to first order in the small parameter $1/\kappa$, implementing a procedure first applied in Ref. [36]. The hierarchy of time scales is set by the inequalities $|\Delta_a| \gg \kappa \gg \omega_r$. This is also consistent with a semiclassical treatment, since the kinetic energy of the atoms at steady state scales with $\hbar\kappa$ thus warranting that the width Δp of the single-atom momentum distribution is large in comparison to the linear momentum $\hbar k$ carried by each photon [10, 17, 21].

B. Collective motion of N atoms in a cavity field

The approximations above discussed are at the basis of the theoretical procedure which connects the master equation of atoms in a quantized cavity field with the FPE for the Wigner function $f_N = f_N(x_1, \ldots, x_N; p_1, \ldots, p_N; t)$, describing the positions and momenta of the N atoms at time t. The derivation is detailed in Ref. [22] and the resulting FPE reads

$$\frac{\partial f_N}{\partial t} = -\sum_{i=1}^{N} \frac{\partial}{\partial x_i}\frac{p_i}{m} f_N + S^2 L[f_N]\,, \tag{1}$$

where the second summand on the right-hand side (RHS) is due to mechanical effects of the cavity field on the atoms and scales like S^2. Here $S = \Omega g/\Delta_a$ is the scattering amplitude between laser and cavity mode, it is proportional to the laser strength Ω and to the cavity vacuum Rabi frequency g, which scale the interaction between dipole and laser and between dipole and cavity, respectively. Operator $L[f_N]$ takes the form

$$\begin{aligned} S^2 L[f_N] =& \frac{\partial f_N}{\partial p_i}\frac{\partial V(x_1,\ldots,x_N)}{\partial x_i} && \text{(2a)}\\ &- S^2 \sum_{i,j} \frac{\partial}{\partial p_i}\Gamma_0 \sin(kx_i)\sin(kx_j) p_j f_N && \text{(2b)}\\ &+ S^2 \sum_{i,j} \frac{\partial^2}{\partial p_i \partial p_j} D_0 \sin(kx_i)\sin(kx_j) f_N && \text{(2c)}\\ &+ S^2 \sum_{i,j} \frac{\partial^2}{\partial p_j \partial x_i} \eta_0 \sin(kx_i)\sin(kx_j) f_N\,. && \text{(2d)} \end{aligned}$$

Each line on the RHS of Eq. (2) has a physical meaning. The first term describes the dynamics due to the conservative potential

$$V(x_1,\ldots,x_N) = \frac{\hbar\Delta_c}{\kappa^2+\Delta_c^2} S^2 N^2 \Theta(x_1,\ldots,x_N)^2\,, \tag{3}$$

where

$$\Theta(x_1,\ldots,x_N) = \frac{1}{N}\sum_{j=1}^{N}\cos(kx_j)\,, \tag{4}$$

so that the potential mediates long-range interactions between the atoms. Parameter $\langle|\Theta|\rangle_N$ is the order parameter of self-organization, where $\langle\cdot\rangle_N$ denotes the expectation value taken over the normalized distribution f_N. Specifically, when the atoms form Bragg grating, then $\langle|\Theta|\rangle_N \to 1$ and the potential depth is maximal. When the atoms are instead uniformly distributed in space, then $\langle|\Theta|\rangle_N \simeq 0$ and the potential vanishes. We note that the Bragg gratings minimize the potential when $\Delta_c < 0$, otherwise the uniform distribution is energetically favoured. We will here denote $\langle|\Theta|\rangle_N$ by magnetization, due to the mapping of the self-organization transition to a ferromagnetic model [21].
For later convenience, we define the parameter

$$F_0 = (\hbar k)\frac{2\Delta_c}{\kappa^2+\Delta_c^2}\,, \tag{5}$$

such that $V = F_0(NS\Theta)^2/(2k)$.

The second term on the RHS, Eq. (2b), describes a dissipative force and is scaled by the coefficient Γ_0:

$$\Gamma_0 = \omega_r \frac{8\Delta_c\kappa}{(\kappa^2+\Delta_c^2)^2}\,. \tag{6}$$

This term is due to non-adiabatic corrections in the dynamics of the cavity field.

Term in the line (2c) corresponds to diffusion due to fluctuations of the cavity field associated with losses. The diffusion matrix is the dyadic product of the vector $(\sin(kx_1), ..., \sin(kx_N))$ with itself and scales with the coefficient

$$D_0 = (\hbar k)^2 \frac{\kappa}{\kappa^2+\Delta_c^2}\,. \tag{7}$$

Therefore, beside the diffusion due to the diagonal elements, which is a single-particle effect, we also expect that term (2c) establishes long-range correlations.

The last line (2d) contains cross-derivatives and scales with the coefficient

$$\eta_0 = 2\hbar\omega_r \frac{\kappa^2-\Delta_c^2}{(\kappa^2+\Delta_c^2)^2}\,, \tag{8}$$

whose sign depends on whether the ratio $|\Delta_c/\kappa|$ is smaller or larger than unity, while it vanishes for $|\Delta_c/\kappa| = 1$. An analogous term has also been reported in the semiclassical description of cold atoms in optical lattices [36], where it has been then neglected under the assumption of uniform spatial densities. Such assumption cannot be applied in the self-organized regime, nevertheless we will show that this term can be consistently discarded in the thermodynamic limit we apply, which warrants Kac's scaling [19].

C. Mean-field ansatz

To derive a mean-field FPE we assume that the Wigner function is factorized into single-particle distribution functions according to the prescription

$$f_N(x_1,\dots,x_N;p_1,\dots,p_N;t)=\prod_{i=1}^{N} f_1(x_i,p_i;t)\,, \tag{9}$$

where $f_1(x_i,p_i;t)$ denotes the distribution for the particle i at time t and is thus defined on the phase space of this particle. We use then Eq. (9) in the FPE (1) and integrate out all particles' variables but one. In this way we derive the mean-field FPE, which reads

$$\frac{\partial f_1}{\partial t}=-\frac{\partial}{\partial x}\frac{p}{m}f_1+S^2\mathfrak{L}[f_1]\,, \tag{10}$$

and has same structure as the FPE in Eq. (1). Operator $\mathfrak{L}$ describes, as L, the mechanical effects of light. However, it is now a nonlinear operator of f_1 and takes the form

$$\mathfrak{L}[f_1]=-\frac{\partial}{\partial p}F_0\left(\cos(kx)+(N-1)\Theta_{\rm MF}[f_1]\right)\sin(kx)f_1 \tag{11a}$$

$$-\frac{\partial}{\partial p}\Gamma_0\left(\sin(kx)p+(N-1)\Xi_{\rm MF}[f_1]\right)\sin(kx)f_1 \tag{11b}$$

$$+\frac{\partial^2}{\partial^2 p}D_0\sin^2(kx)f_1 \tag{11c}$$

$$+\frac{\partial^2}{\partial p\partial x}\eta_0\sin^2(kx)f_1\,, \tag{11d}$$

where we have introduced the functionals

$$\Theta_{\rm MF}[f_1]=\frac{1}{\lambda}\int_0^{\lambda}dx\int_{-\infty}^{\infty}dp\cos(kx)f_1\,, \tag{12}$$

$$\Xi_{\rm MF}[f_1]=\frac{1}{\lambda}\int_0^{\lambda}dx\int_{-\infty}^{\infty}dp\sin(kx)pf_1\,. \tag{13}$$

The mean-field order parameter $\Theta_{\rm MF}$ is the expectation value $\langle\cos(kx)\rangle$, where $\langle.\rangle$ indicates the average taken over the single-particle distribution function $f_1(x,p)$. The terms on the RHS contained in lines (11a) and (11b) have a different origin but a similar structure, which can be recognized by analysing the form of the two summands within the respective inner brackets. The first summand in each line describes the interaction of the atom with itself, mediated by the cavity field. The second summand in each line emerges from the interaction between the atom and all other $N-1$ atoms.

We further notice that the term in line (11a) can be cast in terms of a conservative force originated from the potential

$$V_1[f_1](x)=\frac{F_0}{2k}S^2\left(\cos^2(kx)+2(N-1)\Theta_{\rm MF}[f_1]\cos(kx)\right)+\frac{\Gamma_0}{k}(N-1)S^2\Xi_{\rm MF}[f_1]\cos(kx)\,, \tag{14}$$

and contains a term, whose corresponding term in Eq. (1) has dissipative nature (see line (2b)). Using this result, we can rewrite Eq. (11) in the compact form

$$\mathfrak{L}[f_1]=\frac{\partial V_1}{\partial x}\frac{\partial f_1}{\partial p}-\frac{\partial}{\partial p}\left(\Gamma_0 p-\frac{\partial}{\partial p}D_0-\frac{\partial}{\partial x}\eta_0\right)\sin^2(kx)f_1\,,$$

which allows us to simply read out the physical meaning of the other terms, they are in fact the diagonal component of friction, diffusion, and cross-derivative term in Eq. (1).

III. STATIONARY STATE OF THE MEAN-FIELD EQUATION

The stationary properties of the mean-field distribution are analysed by means of the single-particle distribution $f_{\rm st}(x,p)$ that solves Eq. (10) with

$$\partial_t f_{\rm st}(x,p)=0\,. \tag{15}$$

In the following we determine $f_{\rm st}(x,p)$ and then analyse its predictions for relevant physical quantities.

A. Derivation of the steady state solution

In order to solve Eq. (15) we consider the ansatz

$$f_{\rm st}(x,p)=f_0\exp(a(x)+b(p))\,,$$

where $a(x)$ and $b(p)$ are functions which only depend on position and momentum, respectively, and f_0 is the normalization constant. Using this ansatz in Eq. (10) we obtain differential equations for $a(x)$ and $b(p)$, whose solutions read $b(p)=-\beta p^2/(2m)$ and

$$a(x)=(Y/2-1)\ln(1+Z\sin^2(kx))-(N-1)Y\Theta_{\rm MF}[f_{\rm st}]\sqrt{\frac{Z}{1+Z}}\,\mathrm{arctanh}\left(\sqrt{\frac{Z}{1+Z}}\cos(kx)\right)\,, \tag{16}$$

with $Y=F_0/(k\eta_0)$, $Z=\beta\eta_0 S^2$, and

$$\beta=-\frac{\Gamma_0 m}{D_0}=\frac{-4\Delta_c}{\hbar\left(\kappa^2+\Delta_c^2\right)}\,. \tag{17}$$

Therefore,

$$f_{\rm st}(x,p)=\mathcal{F}(\cos kx)\exp\left(-\beta\frac{p^2}{2m}\right)\,, \tag{18}$$

with $\mathcal{F}(\cos kx)=f_0\exp(a(x))$. Equation (18) describes a thermal distribution provided that $\Delta_c<0$: In this limit parameter β, Eq. (17), plays the role of an inverse temperature at steady state. This temperature coincides with the value found by solving the steady state of the N-body FPE, Eq. (1), as shown in Refs. [17, 21].

We note that the function $\mathcal{F}(\cos kx)$ depends on $\Theta_{\rm MF}[f_{\rm st}]$, which leads to the fixed-point equation

$$\Theta_{\rm MF} \equiv \langle \cos(kx) \rangle = \sqrt{\frac{2\pi m}{\beta}} \frac{1}{\lambda} \int_0^\lambda {\rm d}x \cos(kx) \mathcal{F}(\cos kx) \,. \tag{19}$$

Its solution is in general not transparent, but it gets simpler in an appropriately defined thermodynamic limit. This consists in scaling the coupling strength $g \sim 1/\sqrt{N}$ as the number of atoms is increased, leading to the scaling relation $S \propto 1/\sqrt{N}$ [37, 38]. In this limit function $a(x)$, Eq. (16), can be cast into the form

$$a(x) = 2 \frac{\bar{n}}{\bar{n}_c} \Theta_{\rm MF} \cos(kx) \tag{20}$$

with

$$\bar{n} = \frac{NS^2}{\kappa^2 + \Delta_c^2} \,, \tag{21}$$

and

$$\bar{n}_c = \frac{\kappa^2 + \Delta_c^2}{4\Delta_c^2} \,. \tag{22}$$

This leads to a compact form of the stationary distribution in the mean-field limit:

$$f_{\rm st}(x,p) = f_0 \exp\left(-\beta \left(\frac{p^2}{2m} + \hbar \Delta_c \bar{n} \Theta_{\rm MF} \cos(kx) \right) \right) \,, \tag{23}$$

with

$$f_0^{-1} = \sqrt{\frac{2m\pi}{\beta}} I_0 \left(2 \frac{\bar{n}}{\bar{n}_c} \Theta_{\rm MF} \right) \,,$$

and I_j is the modified Bessel function of j-th order [39].

We thus see that in the thermodynamic limit the effect of the cross derivatives vanishes. For finite N, parameter η_0 is small but finite and in the stationary state it gives rise to a correction to the effective potential term, as visible in Eq. (16).

B. Stationary properties in the thermodynamic limit

The mean-field distribution, Eq. (23), allows one to analytically determine several properties of the steady state. First, functional $\Theta_{\rm MF}$ in the exponent has to be determined self-consistently. Using Eq. (20) in Eq. (19) gives the relation

$$\Theta_{\rm MF} = q \left(2 \frac{\bar{n}}{\bar{n}_c} \Theta_{\rm MF} \right) \,, \tag{24}$$

where q is the function of the form

$$q \left(2 \frac{\bar{n}}{\bar{n}_c} \zeta \right) = \frac{I_1 \left(2 \frac{\bar{n}}{\bar{n}_c} \zeta \right)}{I_0 \left(2 \frac{\bar{n}}{\bar{n}_c} \zeta \right)} \,, \tag{25}$$

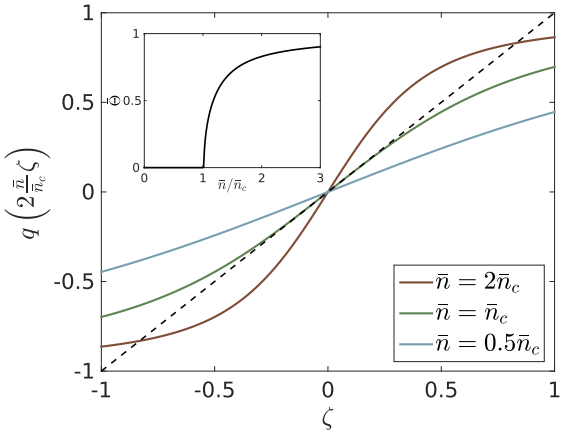

FIG. 2: (Color online) Onset: Plot of $q(2\bar{n}\zeta/\bar{n}_c)$, Eq. (25), as a function of ζ and for different values of $\bar{n}$. The intersection points with the curve $y = \zeta$ (dashed line) give the solutions of Eq. (24). Stable points are at the crossing where $q' < \bar{n}_c/(2\bar{n})$ and are the equilibrium values of the order parameter $\Theta_{\rm MF}$. Inset: The resulting stable solution $\bar{\Theta} \geq 0$ as a function of $\bar{n}$ (in units of $\bar{n}_c$).

and is plotted in Fig. 2 for values of $\bar{n}$ below, at, and above $\bar{n}_c$. The solutions of Eq. (24) are the crossing between the curve $y = \zeta$ and $y = q\,(2\bar{n}\zeta/\bar{n}_c)$, see Eq. (25). For $\bar{n} < \bar{n}_c$ this equation allows for one solution, corresponding to $\Theta_{\rm MF} = 0$. For $\bar{n} > \bar{n}_c$, the solutions are three, of which two are stable and one is unstable. The stable solutions give $\Theta_{\rm MF} = \pm\bar{\Theta}$, with $0 \leq \bar{\Theta} < 1$, and correspond to the self-organized state. Close, but above, the critical point the value $\bar{\Theta}$ can be analytically determined and reads

$$\bar{\Theta} = \sqrt{2(\bar{n}/\bar{n}_c - 1)} \,. \tag{26}$$

The value $\bar{n} = \bar{n}_c$, with $\bar{n}_c$ defined in Eq. (22), determines hence a critical point, at which the transition to self-organization occurs, and is controlled by the detuning from the cavity field and the cavity loss rate, for the thermodynamic limit we chose. The results we obtained so far for the stationary mean-field distribution are in full agreement with the ones found for the stationary distribution of Eq. (1), see Ref. [21]. The stationary mean-field distribution in Eq. (23) corresponds to the one that is found from the stationary N-particle distribution after integrating out the other $N-1$ position and momentum variables, and then taking the thermodynamic limit. The equation for the order parameter, Eq. (24), agrees with the one obtained for the N-particle case and obtained by means of a saddle-point approximation. This agreement is found also for the critical value of Eq. (22) and for the temperature of Eq. (17). Hence, the mean-field model predicts the same phase diagram as the N-body FPE.

It is also instructive to consider the value of the bunch-

ing parameter $\mathcal{B}$ as a function of $\bar{n}$. This is defined as

$$\mathcal{B} = \left\langle \cos^2(kx) \right\rangle , \tag{27}$$

and gives a measure of localization of the particles at the minima of the mechanical potential [21, 25]. Using Eq. (20) we obtain

$$\mathcal{B} = \begin{cases} 1/2 \,, & \bar{n} \leq \bar{n}_c, \\ 1 - \bar{n}_c/(2\bar{n}) \,, & \bar{n} > \bar{n}_c \,, \end{cases} \tag{28}$$

in the stationary state. Therefore, below threshold the atoms are uniformly distributed, while above threshold they increasingly localize at the minima of the Bragg potential. In particular, when the atoms are tightly-bound at the minima, the above-threshold expression in Eq. (28) delivers the amplitude of the fluctuations, namely,

$$k^2 \langle x^2 \rangle \approx \frac{\bar{n}_c}{2\bar{n}} \,, \tag{29}$$

showing that these are inversely proportional to the laser intensity.

C. Comparison with existing literature

The results obtained so far by means of the mean-field model show a remarkable agreement with the predictions of the stationary solution of the N-particle FPE, Eq. (1). It is further worthwhile to compare the results here derived with the results obtained in the literature by means of different approaches.

We first discuss Ref. [25], where, amongst other studies, a mean-field approach is developed based on plausible conjectures. Here, the mean-field potential is calculated and the threshold of self-organization is determined by (i) assuming that the stationary state is thermal, with temperature given by the linewidth of the cavity, and (ii) performing a stability analysis of the uniform density distribution. By means of this study a threshold value for self-organization is identified, which agrees with the prediction in Eq. (22), as it becomes evident after defining the threshold amplitude S_c such that

$$\frac{N S_c^2}{\Delta_c^2 + \kappa^2} \equiv \bar{n}_c \,.$$

In particular, the quantity η^* in [25] is in our notations $S_c \Delta_a / g$ calculated for the case $\Delta_c = -\kappa$.

The stationary state of self-organization has been first derived in the following works [26, 27] by means of a FPE as a function of the atomic and field variables. This description assumes that the field fluctuations are small, and thus cannot reliably reproduce the field correlation functions below and at threshold. It predicts, nevertheless, that the atoms steady state is thermal and its temperature coincides with the inverse of Eq. (17), apart for corrections of the order ω_r/κ, that are systematically neglected in our approach because they are of higher order. It further predicts the same behaviour of the order parameter as in Eq. (26) above, but close, to threshold.

It is also interesting to compare our results with a series of other theoretical studies, which focus on self-organization of ultracold atomic ensembles in cavities but discard retardation effects: In these works only the conservative part of the cavity potential is considered, while the temperature at steady state is due to the coupling to an external heat bath [15, 28–33]. Even though the conditions seem quite different from our case, remarkable agreement is found in the appropriate limits. References [15, 29] analyse the self-organization transition of an ultracold gas of bosonic atoms and derive the mapping to the Dicke model. Here, the recoil energy plays an analogous role as the temperature, and the threshold which is derived agrees with the threshold in Eq. (22) after setting

$$N S_c^2 = \frac{1}{\beta} \frac{\kappa^2 + \Delta_c^2}{-\Delta_c} \,, \tag{30}$$

with $\beta = 4/\hbar\omega_r$. By means of this prescription, the threshold also agrees with the one calculated in Ref. [28]. Furthermore, it also coincides with the one evaluated in Ref. [33] when using the Boltzmann distribution for the atoms statistics.

Another quantity which has been determined in these works is the photon flux, which corresponds to the intracavity photon number in our treatment. In Refs. [28–31] the photon flux scales as $1/|\bar{n} - \bar{n}_c|$ below threshold, while at threshold it diverges as $\sqrt{N}$. These predictions are in perfect agreement with the results we find taking the stationary distribution of Eq. (1), see Appendix A, Eqs. (A4) and (A5). In particular, the intracavity photon number at threshold, Eq. (A5), coincides with the one calculated in Ref. [28] after substituting in their equation $\omega_z = (\omega_0^2 + \kappa^2)/\omega_0$ for the temperature, with $\omega_0 = -\Delta_c$. The result for the intensity-intensity correlations at zero-time delay and below threshold, Eq. (A11), further agrees with the result derived in Ref. [30, 31].

IV. MEAN-FIELD DYNAMICS

We now study the dynamics predicted by the mean-field FPE. We focus on the Vlasov equation, which we derive from Eq. (10) by taking the thermodynamic limit, according to our prescription. The Vlasov equation for our problem reads

$$\frac{\partial f_1}{\partial t} + \frac{p}{m} \frac{\partial f_1}{\partial x_1} - \frac{\partial V_0[f_1](x)}{\partial x} \frac{\partial f_1}{\partial p} = 0 \tag{31}$$

with

$$\begin{aligned} V_0[f_1](x) =& 2\hbar\Delta_c \bar{n} \cos(kx) \Theta_{\mathrm{MF}}[f_1] \\ & - \frac{\hbar^2 k}{m} \bar{n} \beta \kappa \cos(kx) \Xi_{\mathrm{MF}}[f_1] \,, \end{aligned} \tag{32}$$

and it corresponds to the potential in Eq. (14) after neglecting the self-reaction term, which is of order $1/N$. Therefore, the validity of the predictions we will extract are limited to sufficiently short time scales for which the corrections can be discarded. We will quantify this statement in the next section.

A. Preliminary considerations: energy conservation

We first analyse whether Eq. (31) warrants energy conservation. We consider a class of functions for which $\Xi_{\rm MF}[f_1] = 0$. This includes the stationary solution of Eq. (23). For these solutions, the energy of one particle takes the form

$$\epsilon(t) = \frac{\langle p^2 \rangle}{2m} + \hbar \Delta_c \bar{n} \Theta_{\rm MF}^2 \,. \tag{33}$$

In order to determine $\dot{\epsilon}(t)$ we thus calculate $\dot{\Theta}_{\rm MF}$ and $\langle \dot{p^2} \rangle$. This gives

$$\begin{aligned} \dot{\Theta}_{\rm MF} &= -\frac{k}{m} \Xi_{\rm MF} \,, \\ \frac{\langle \dot{p^2} \rangle}{2m} &= 2 \frac{\hbar}{m} \bar{n} \left(k \Delta_c \Theta_{\rm MF} - \omega_r \kappa \beta \Xi_{\rm MF} \right) \Xi_{\rm MF} \,, \end{aligned}$$

and therefore we get for the derivative of the energy

$$\dot{\epsilon} = -2 \frac{\hbar}{m} \bar{n} \omega_r \kappa \beta \Xi_{\rm MF}^2 \,.$$

These derivatives hence vanish when $\Xi_{\rm MF} = 0$, and thus for the class of distribution fulfilling this condition, energy, with the potential term given in Eq. (33), is conserved. Fluctuations, on the other hand, can give rise to finite values of $\Xi_{\rm MF}$. The purpose of the next section is to analyse the stability and short-time dynamics of solutions of the Vlasov equation, Eq. (31), after quenches of the laser parameters.

B. Stability analysis of spatially homogeneous distributions

We now analyse the short-time dynamics described by Eq. (31), assuming that at $t = 0$ the distribution is thermal and with uniform spatial density, thus $f_1(x, p, 0) = f_1(p, 0)$ and $\Theta_{\rm MF}|_{t=0^-} = 0$, with

$$f_1(p, 0) = \left(\frac{2m\pi}{\beta_0} \right)^{-\frac{1}{2}} \exp\left(-\beta_0 \frac{p^2}{2m} \right) , \tag{34}$$

where β_0 is the inverse temperature. This distribution is a stable solution of the Vlasov equation after setting $\bar{n} = 0$. At $t = 0$ the laser strength is quenched above threshold so that parameter $\bar{n}$ takes a finite value larger than $\bar{n}_c$. We then let evolve the distribution of Eq. (34) by taking this value $\bar{n}$ in Eq. (31). Figure 3 shows the results of the numerical integration of Eq. (31) for different value of $\bar{n}$. We analyse these results, keeping in mind that they are strictly valid for short times since the Vlasov equation discards effects, such as diffusion, which are crucial in determining the stationary state. In (a) the order parameter evolves from 0 to a finite value, about which it oscillates. This value is smaller than the one predicted by the stationary solution of the mean-field FPE. It is reached after an initial dynamics characterized by an exponential increase, whose slope is steeper the larger is $\bar{n}$. Subplots (b) and (c) display the corresponding evolution of the quantities $\Xi_{\rm MF}^2$, see Eq. (13). This quantity emerges from the retardation effects of the dynamics, it is thus a signature of memory effects, and mathematically corresponds to the build up correlations between momentum and position that cannot be factorized. The initial distribution, Eq. (34), is chosen so that $\Xi_{\rm MF} = 0$, and we observe that the dynamics give rise to a build up of a finite value of $\Xi_{\rm MF}^2$, with an exponential increase that leads to a maximum where the curve for $\Theta_{\rm MF}$ reaches the plateau. Then, it oscillates like $\Theta_{\rm MF}$ (one can well understand the behaviour of these oscillations observing that $\Xi_{\rm MF}$ is proportional to the time derivative of $\Theta_{\rm MF}$) and is exponentially damped to zero. In the initial phase, the exponential growth of $\Xi_{\rm MF}^2$ increases with $\bar{n}$, similarly in the second phase of the dynamics, where $\Theta_{\rm MF}$ oscillates about a finite mean value, the amplitude of the oscillations of $\Xi_{\rm MF}^2$ are also larger the larger is $\bar{n}$.

We now analyse the initial exponential increase, which is in the regime where the Vlasov equation is a reliable approximation to the full dynamics, as we also verified in Ref. [24]. In order to do so, we use a standard procedure, which is also detailed in Ref. [19, 40]. For short times t after the quench, we write the distribution as

$$f_1(x, p, t) = f_1(p, 0) + \delta f_1(x, p, t) \,, \tag{35}$$

where δf_1 describes small fluctuations which can be due to the finite size of the system, and thus scale with $1/\sqrt{N}$. Using Eq. (35) into the Vlasov equation (31) and neglecting the terms of order $1/N$ we obtain the linearized Vlasov

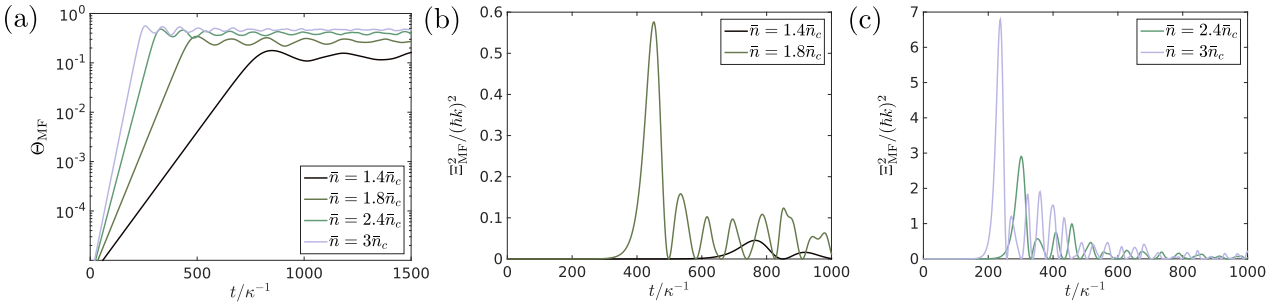

FIG. 3: (Color online) Time evolution of (a) the order parameter $\Theta_{\rm MF}$, Eq. (12), and (b)-(c) parameter $\Xi^2_{\rm MF}$, Eq. (13), calculated by numerical integration of the Vlasov equation (31) for different values of $\bar{n}$ and for $\Delta_c = -\kappa$. The initial distribution is given in Eq. (34) with $\beta_0 = 2/(\hbar\kappa)$.

equation

$$\frac{\partial \delta f_1}{\partial t} + \frac{p}{m}\frac{\partial \delta f_1}{\partial x} - \frac{\partial \delta V}{\partial x}\frac{\partial f_1(p,0)}{\partial p} = 0\,, \tag{36}$$

where $\delta V = V[\delta f_1(x,p,t)]$ and we dropped the argument of function δf_1. We seek for solutions of Eq. (36) by means of the ansatz of Fourier waves with frequency ω and wave number k:

$$\delta f_1 = g_1(p)\mathrm{e}^{i(\omega t - kx)} + g_{-1}(p)\mathrm{e}^{i(\omega t + kx)}, \tag{37}$$

$$\delta V = 2A\cos(kx)\mathrm{e}^{i\omega t}\,, \tag{38}$$

where $A \propto 1/\sqrt{N}$ is some constant and the amplitudes $g_1(p)$ and $g_{-1}(p)$ are sole functions of the momentum p. The dispersion relation $\omega = \omega(k)$ can be derived after using Eqs. (37) and (38) in the linearized Vlasov equation, Eq. (36). By equating the coefficients of $\exp(ikx)$ and $\exp(-ikx)$ we get expressions for the functions $g_1(p)$ and $g_{-1}(p)$. With those expressions one finds the dispersion relation by using the definition $\delta V = V[\delta f_1]$ and Eqs. (32) and (38):

$$0 = 1 + \left(\hbar\Delta_c + i\frac{\hbar\kappa}{2}\hbar\omega\beta\right)\bar{n}\frac{1}{2}\int_{-\infty}^{\infty} dp\left(\frac{-k}{\frac{pk}{m}+\omega} + \frac{-k}{\frac{pk}{m}-\omega}\right)\partial_p f_1(p,0)\,. \tag{39}$$

This relation holds for any initial distribution that describes a uniform spatial density. We now use the Gaussian distribution in Eq. (34) and obtain

$$0 = 1 + \left(\hbar\Delta_c + i\frac{\hbar\kappa}{2}\hbar\omega\beta\right)\bar{n}\beta_0\left(1 - \bar{a}\exp(-\bar{a}^2)\left(i\sqrt{\pi} - 2\int_0^{\bar{a}} du\exp(u^2)\right)\right)\,, \tag{40}$$

where we defined $\bar{a} = \sqrt{\beta_0/(2m)}(m\omega/k)$. We then introduce $\bar{b} = i\bar{a}$ and

$$\gamma = i\omega\,,$$

and cast Eq. (40) into the form:

$$0 = 1 + \left(\hbar\Delta_c + \frac{\hbar\kappa}{2}\hbar\gamma\beta\right)\bar{n}\beta_0\left(1 - \bar{b}\exp\left(\bar{b}^2\right)\left(\sqrt{\pi} - \int_{-\bar{b}}^{\bar{b}} du\exp(-u^2)\right)\right)\,, \tag{41}$$

where $\bar{b} \propto \gamma$. It can be shown that parameter γ, which solves Eq. (41), is a real number. Therefore, ω is an imaginary number. In particular, if $\gamma < 0$ both Eqs. (37) and (38) describe fluctuations which are exponentially damped and therefore $f_1(x,p,t)$ will tend to the initial distribution, which is stable. If instead the solution of Eq. (40) gives $\gamma > 0$, the initial distribution is unstable against fluctuations. The value $\gamma = 0$ separates the two regimes. After setting $\gamma = 0$ in Eq. (41) we thus get the

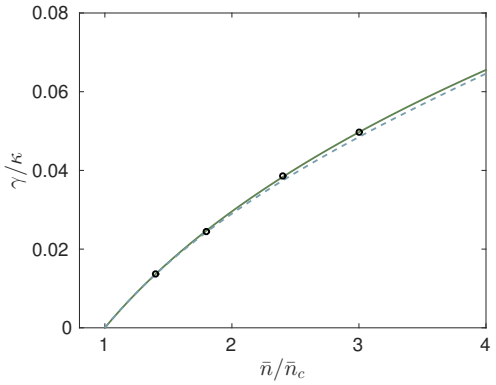

FIG. 4: (Color online) Slope γ of the initial increase of $\Theta_{\rm MF}$. The dots are extracted by fitting the curve obtained from the numerical simulations in Fig. 3, the dashed line is the value predicted by Eq. (43), which well agrees with Eq. (41) (solid line). For these parameters the threshold for the Vlasov stability, Eq. (42), reads $1 = \bar{n}/\bar{n}_c$.

critical condition

$$1 = -\hbar\Delta_c\bar{n}\beta_0\,, \tag{42}$$

which connects Δ_c, $\bar{n}$, and the initial temperature $1/\beta_0$, which is an external parameter. If β_0 coincides with the value in Eq. (17), then Eq. (42) corresponds to the same relation as in Eq. (22), which defines the critical value of $\bar{n}$ for self-organization. For the values of the parameters, for which $\gamma > 0$, the uniform distribution is unstable and tends to form a grating at the wave vector k of the resonator with exponential increase, giving rise to a violent relaxation. Parameter γ gives the rate at which the amplitude of this density modulation grows.

Figure 4 compares the value of γ extracted by fitting the exponential increase of $\Theta_{\rm MF}$ in the first phase of the dynamics of Fig. 3 and for different values of $\bar{n}$, with the one determined by Eq. (41), showing very good agreement. In particular, we note that in the limit $|\Delta_c| \gg |\gamma|$ Eq. (41) can be reduced to the form [41]

$$\gamma = \omega_0\,(1-p\chi)\,\frac{\ln\left(\frac{\chi}{1.135}\right) - \ln\left(1-p\chi\right)}{1.4\,(1-p\chi) + \hbar\kappa\beta\omega_0/(2|\Delta_c|)}\,, \tag{43}$$

with $\chi = \hbar|\Delta_c|\bar{n}\beta_0 = (\bar{n}/\bar{n}_c)(\beta_0/\beta)$, $\omega_0 = \sqrt{2\omega_r/(\hbar\beta_0)}$ and $p = 27/227$.

V. VALIDITY OF THE MEAN-FIELD ANSATZ

The mean-field treatment is based on the assumption that the distribution function for the N particle can be approximated by the product of the single-particle distribution. This ansatz thus discards interparticle correlations which emerge from the photon-mediated interactions: the factorized ansatz is very different from the form of the distributions one obtains from the full N-particle FPE [17, 21]. Nevertheless, the assumption still captures essential features of the short-time dynamics of distributions, which have initially the form of Eq. (9). We will follow the procedure illustrated in Ref. [19, 42] and study the validity of the mean-field ansatz within a BBGKY hierarchy, which we derive from the N-particle FPE, Eq. (1). We will particularly focus on the dynamics of two-particle correlations and determine the characteristic time scale of their dynamics.
For convenience, we introduce the vectors $\mathbf{x} = (x_1, ..., x_N)^T$ and $\mathbf{p} = (p_1, ..., p_N)^T$, and define $f_N(\mathbf{x};\mathbf{p};t) \equiv f_N(x_1, ..., x_N; p_1, ..., p_N; t)$.

A. BBGKY hierarchy of the photon-mediated Fokker-Planck equation

For the derivation of the BBGKY hierarchy we assume that the energy of the system is finite. This corresponds to assume that the limit holds:

$$\lim_{|\mathbf{p}|\to\infty} f_N(\mathbf{x};\mathbf{p};t) = 0, \tag{44}$$

where $|\mathbf{p}| = \sqrt{\sum_{i=1}^N p_i^2}$, and that expectation values of all moments exist. Furthermore f_N is periodic with wavelength λ in every x_i, which implies

$$f_N(\mathbf{x} + \lambda\mathbf{z};\mathbf{p};t) = f_N(\mathbf{x};\mathbf{p};t), \tag{45}$$

for every $\mathbf{z} \in \mathbb{Z}^N$. Distribution function f_N is invariant under particle exchange, which we can express by means of the permutation matrix $\mathbf{P}$, such that:

$$f_N(\mathbf{P}\mathbf{x};\mathbf{P}\mathbf{p};t) = f_N(\mathbf{x};\mathbf{p};t), \tag{46}$$

where each row and column of $\mathbf{P}$ contain only one entry different from zero and equal to 1.
In order to derive the BBGKY hierarchy of the FPE in Eq. (1) we first define the l-particle distribution function:

$$f_l = \int_0^\lambda \frac{\mathrm{d}x_{l+1}}{\lambda} \int_{-\infty}^{\infty} \mathrm{d}p_{l+1} \ldots \int_0^\lambda \frac{\mathrm{d}x_N}{\lambda} \int_{-\infty}^{\infty} \mathrm{d}p_N f_N\,, \tag{47}$$

where f_l inherits the three properties in Eqs. (44), (45) and (46) from f_N. Index l takes the value $l = 1, \ldots, N$, such that for $l = 1$ the distribution f_l is the single-particle phase-space function, and for $l = N$ it describes the N particle state. The evolution of f_l is found from Eq. (1) after integrating out the other $N - l$ particle variables, and can be cast in the form

$$\frac{\partial f_l}{\partial t} = \sum_{j=1}^{l} \left(\mathcal{L}_j^{(l)} f_l + \mathcal{G}_j^{(l)}[f_{l+1}]\right)\,, \tag{48}$$

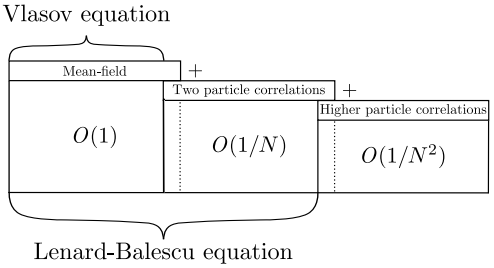

FIG. 5: Illustration of the order of magnitude of the corrections of the Vlasov and of the Lenard-Balescu equations, and of which type of correlations they include.

where the first operator on the RHS solely depends on the variables of the l particles and reads

$$\mathcal{L}_j^{(l)} f_l = -\frac{\partial}{\partial x_j}\frac{p_j}{m} f_l \tag{49}$$
$$-S^2\frac{\partial}{\partial p_j}\sum_{i=1}^{l}\left(F_0\cos(kx_i)+\Gamma_0\sin(kx_i)p_i\right)\sin(kx_j)f_l$$
$$+S^2\frac{\partial}{\partial p_j}\sum_{i=1}^{l}\left(D_0\frac{\partial}{\partial p_i}+\eta_0\frac{\partial}{\partial x_i}\right)\sin(kx_i)\sin(kx_j)f_l\,.$$

The second operator, instead, depends nonlinearly on the $(l+1)$-particle distribution function. This term vanishes when $l = N$, while for $l < N$ it describes the dynamics of correlations, which are established by the interparticle potential. It reads

$$\mathcal{G}_j^{(l)}[f_{l+1}] = -S^2(N-l)\frac{\partial}{\partial p_j}\sin(kx_j) \times\left(F_0\Theta_l[f_{l+1}]+\Gamma_0\Xi_l[f_{l+1}]\right)\,, \tag{50}$$

where

$$\Theta_l[f_{l+1}] = \int_0^\lambda \frac{\mathrm{d}x_{l+1}}{\lambda}\int_{-\infty}^{\infty}\mathrm{d}p_{l+1}\cos(kx_{l+1})f_{l+1} \tag{51}$$
$$\Xi_l[f_{l+1}] = \int_0^\lambda \frac{\mathrm{d}x_{l+1}}{\lambda}\int_{-\infty}^{\infty}\mathrm{d}p_{l+1}\sin(kx_{l+1})p_{l+1}f_{l+1}\,, \tag{52}$$

while $\Theta_0[f_1] = \Theta_{\mathrm{MF}}$ and $\Xi_0[f_1] = \Xi_{\mathrm{MF}}$. Note that when the factorization ansatz of Eq. (9) holds, then $\Theta_1[f_2] = \Theta_{\mathrm{MF}}f_1$ and $\Xi_1[f_2] = \Xi_{\mathrm{MF}}f_1$. A closed set of equations for f_l can be thus strictly obtained for $l = N$, giving Eq. (1), or for $S = 0$, hence in absence of the cavity field.

B. The Lenard-Balescu equation

For $l = 2$ we can generally decompose the distribution function into two terms:

$$f_2(x_1,x_2,p_1,p_2) = f_1(x_1,p_1)f_1(x_2,p_2) + g_2(x_1,x_2,p_1,p_2)\,, \tag{53}$$

where the first term on the RHS is the mean-field term and the second term describes all corrections beyond mean field. When at $t = 0$ the distribution function is factorized in a form like Eq. (9), the dynamics beyond mean field will tend to build correlations which are described by g_2. We obtain the mean-field FPE, Eq. (10) by performing the approximation $\mathcal{G}_1^{(1)}[f_2] \to \mathcal{G}_1^{(0)}[f_1]f_1$. In the following we analyse the regime in which this approximation is justified by studying the equation describing the evolution of the function g_2 under some approximation, which permits us to truncate the BBGKY hierarchy till second order. This equation is known in the literature as Lenard-Balescu equation [19], and it will allow us to identify a time-scale where the mean-field treatment provides reliable predictions.

In order to derive the Lenard-Balescu equation we first consider the distribution function for $l = 3$. Using the same type of decomposition as in Eq. (53), this can be written as

$$f_3(x_1,x_2,x_3,p_1,p_2,p_3) = f_1(x_1,p_1)f_1(x_2,p_2)f_1(x_3,p_3) + \sum_{i,j,k=1}^{3}|\epsilon_{ijk}|f_1(x_i,p_i)g_2(x_j,p_j,x_k,p_k) + g_3(x_1,x_2,x_3,p_1,p_2,p_3),$$

where ϵ_{ijk} is the Levi-Civita tensor and g_3 describes all three-body correlations which cannot be written as a function of f_1 and/or f_2. We assume now that g_3 is of higher order (from the treatment below we will see that $g_3 \propto 1/N^2$) and drop g_3 in the equation describing the dynamics of f_2, Eq. (48). By means of this assumption we obtain two

coupled equations for f_1 and f_2, which can be then cast into the Lenard-Balescu equations for f_1 and g_2 using Eq. (53) and which read

$$\frac{\partial f_1}{\partial t} = \mathcal{L}^{(1)} f_1 + \mathcal{G}^{(1)}[f_1] f_1 + \mathcal{G}^{(1)}[g_2] \tag{54a}$$

$$\begin{aligned}\frac{\partial g_2}{\partial t} =& -\frac{\partial}{\partial x_1}\frac{p_2}{m} g_2 - \frac{\partial}{\partial x_2}\frac{p_1}{m} g_2 \\ & - S^2 \sum_{j=1}^{2}\sum_{i\neq j} \frac{\partial}{\partial p_j} F_0 \sin(k x_j)\left(\cos(k x_i) - \Theta_{\mathrm{MF}}[f_1]\right) f_1 f_1 \\ & - S^2 \sum_{j=1}^{2}\sum_{i\neq j} \frac{\partial}{\partial p_j} \Gamma_0 \sin(k x_j)\left(\sin(k x_i) p_i - \Xi_{\mathrm{MF}}[f_1]\right) f_1 f_1 \\ & + S^2 \sum_{j=1}^{2}\sum_{i\neq j} \frac{\partial}{\partial p_j} \sin(k x_j)\left(D_0 \frac{\partial}{\partial p_i} + \eta_0 \frac{\partial}{\partial x_i}\right) \sin(k x_i) f_1 f_1 \\ & - N S^2 F_0 \sum_{j=1}^{2}\sum_{i\neq j} \frac{\partial}{\partial p_j} \sin(k x_j)\left(\Theta_1[g_2]_i f_1(x_j,p_j) + \Theta_{\mathrm{MF}}[f_1] g_2\right) \\ & - N S^2 \Gamma_0 \sum_{j=1}^{2}\sum_{i\neq j} \frac{\partial}{\partial p_j} \sin(k x_j)\left(\Xi_1[g_2]_i f_1(x_j,p_j) + \Xi_{\mathrm{MF}}[f_1] g_2\right) ,\end{aligned} \tag{54b}$$

where we specified the arguments when necessary, and introduced the notation $\Theta_1[g_2]_i$ and $\Xi_1[g_2]_i$ to indicate that these are functions of (x_i, p_i).

The validity of the mean-field FPE, Eq. (10), relies on whether one can discard term $\mathcal{G}^{(1)}[g_2]$ in the RHS of Eq. (54a). Let us recall the thermodynamic limit for which $S^2 \sim 1/N$. If we now assume that g_2 is of order $1/N$ with respect to f_1, then the term $\mathcal{G}^{(1)}[g_2]$ is of order $1/N$ with respect to $\mathcal{G}^{(1)}[f_1] f_1$. A detailed analysis of Eq. (54b) shows that, if $g_2 \sim 1/N$ at $t = 0$, this scaling is preserved by the dynamics. In fact, (i) the first line on the RHS of Eq. (54b) gives a scaling with $1/N$ because it is proportional to g_2, while all other quantities are independent of N, (ii) the second, third, and fourth lines are all proportional to $S^2 \sim 1/N$, (iii) the last two lines scale with $NS^2 g_2 \sim 1/N$. Therefore, for sufficiently short times the contribution of g_2 to the dynamics in the mean-field equation can be neglected.

We note that in Eq. (54a) the term $\mathcal{L}^{(1)} f_1$ has also components which scale with $1/N$. If one consistently neglects all terms scaling with $1/N$, then Eq. (54a) reduces to the Vlasov equation, Eq. (31), and therefore also neglects the diffusion processes leading to equilibrium. Figure 5 illustrates the order of magnitude of the corrections to the Vlasov and Lenard-Balescu equations, as well as the type of correlations that these describe.

C. Mean-Field versus full N-atom dynamics

In order to complete our analysis of the limits of validity of the mean-field ansatz, we now compare its predictions with the ones obtained by numerical simulations of the N-particle FPE of Eq. (1). The latter are performed by means of stochastic differential equations (see Refs. [21, 22] for details). We focus now on the evolution of the expectation value of Θ^2, which explicitly depends on two-particle correlations and scales the strength of the conservative many-body potential. We recall the definition $\langle . \rangle_N$ in order to indicate the mean value of a N-particle observable taken over the N-particle distribution f_N.

Figure 6 compares the N-particle description where the evolution of f_N is governed by FPE (1) (solid line) and the mean-field description, where $f_N(\mathbf{x};\mathbf{p};t) = f_1(x_1,p_1;t)...f_1(x_N,p_N;t)$ and the evolution of f_1 is governed by the mean-field FPE (10) (dashed-dotted line). The curves are plotted as a function of time and for different particle numbers, $N = 20, 50, 200$, where the parameter S^2 has been rescaled according to our thermodynamic limit so to warrant a threshold $\bar{n}_c$ which is independent on N. The parameters have been fixed so that initially the distribution is spatially uniform, while the momentum distribution is a Gaussian whose width coincides with the asymptotic temperature of the dynamics, Eq. (17). The strength of the field is such that $\bar{n} = 2\bar{n}_c$, therefore the asymptotic spatial distribution is a Bragg grating with $|\Theta_{\mathrm{MF}}| \sim 0.83$. The dynamics we observe is the one which leads to the formation of the Bragg gratings starting from a uniform spatial distribution, and exhibit three stages, which have been extensively discussed in Ref. [24]: a violent relaxation, a prethermalized phase, and a slow approach to equilibrium. The solid lines are simulations of the full FPE, the dashed-dotted lines the corresponding mean-field prediction, which indeed qualitatively reproduces the three-stage dynamics.

The violent relaxation is a stage of the dynamics where

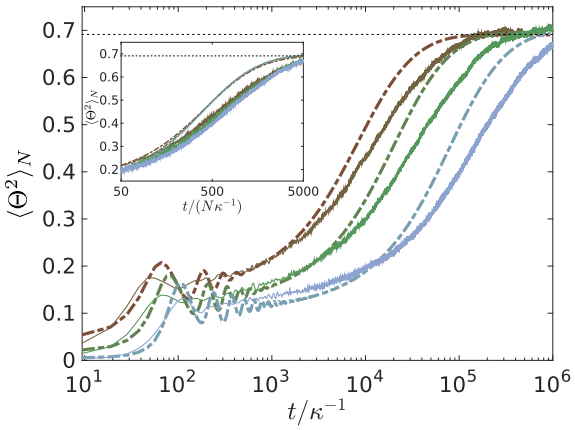

FIG. 6: (Color online) Time evolution of the squared order parameter evaluated by numerically simulating (dashed-dotted lines) the mean-field FPE, Eq. (10) and (solid lines) the N-particle FPE of Eq. (1). The curves correspond to different particle numbers $N = 20$ (brown, upper two curves), $N = 50$ (green, middle two curves) and $N = 200$ (blue, lower two curves) and are calculated taking $\Delta_c = -\kappa$ and $\bar{n} = 2\bar{n}_c$. The number $\mathcal{T}$ of trajectories taken for the N-body FPE is $\mathcal{T} = 1000$ for $N = 20$, $\mathcal{T} = 500$ for $N = 50$, $\mathcal{T} = 100$ for $N = 200$ (see Ref. [21, 22] for details on the simulations). The horizontal dotted line indicates the asymptotic value of the squared order parameter. The inset shows the curves of the onset with the time axis rescaled by N. Note that the initial distribution of the full N-body FPE is the one which statistically corresponds to a spatially uniform distribution with the same temperature as the asymptotic one. Therefore, the value of $\langle\Theta^2\rangle_N$ at $t = 0$ does not vanish due to finite size effects. In order to compare these dynamics with the mean-field FPE, we have taken into account these finite-size effects in the initial mean-field distribution given by $\tilde{f}_0(x,p) = (1+\delta_N \cos(kx)) f_1(p,0)$ where f_1 is given in Eq. (34) and δ_N is a spatial modulation depending on N.

there is a good agreement between mean-field and N-body FPE. This is the short-time regime where the Vlasov equation, Eq. (31), is valid, and the behaviour of the N-body FPE is reproduced by the one observed numerically integrating the Vlasov equation, see Fig. 3(a). This has been also verified in Ref. [24]. The prethermalized regime is also predicted by the Vlasov equation, see Fig. 3(a). The mean-field FPE, however, provides a more accurate description and qualitatively reproduces the N-body FPE. Nevertheless, a clear difference between mean-field and N-body dynamics is found at the onset of the prethermalized stage: In fact, the oscillations are damped at a faster rate in the N-body FPE. Apart from this difference, there is a qualitative agreement between mean-field and N-body FPE also for this stage.

While both mean-field and N-body FPE agree in the asymptotic value, we observe a striking difference between the two results in the relaxation to equilibrium after prethermalization. This is the stage where the role of dissipation and diffusion becomes relevant, as shown in Ref. [24] by comparing this behaviour with the one, where the dynamics is only due to the Hamiltonian term. In particular, the relaxation time scale predicted by the full simulation is about one-order of magnitude longer than the corresponding mean-field prediction. This becomes even more evident by plotting the curves rescaling the time axis with N, as visible in the inset. The curves of the mean-field FPE collapse to one curve, whereby the ones of the N-body FPE collapse to a significantly different curve.

Let us now summarize these results. First, the short time behaviour of the fluctuations of the order parameter are well described by the mean-field equation, and in particular by the Vlasov equation. This is well understood in terms of the typical contributions to the dynamics: For short times the dominant contributions are indeed the terms of Eq. (31) and interparticle correlations are small, as we argued in the previous section. Discrepancies are due to finite size effects. The prethermalized regime, moreover, exhibits a good agreement between mean-field and full dynamics. This regime is dominated by the Hamiltonian dynamics, and the results show that Hamiltonian dynamics with long-range interactions is well reproduced by the mean-field description. Big deviations instead appear for long times, where the mean field ansatz is expected to fail and at the time scales dominated by relaxation to the stationary state.

VI. CONCLUSIONS

In this work we have systematically developed a mean-field description of the self-organization dynamics of atoms in a high-finesse cavity. The predictions of the mean-field model have been explored at equilibrium and out-of-equilibrium, its limits of validity have been tested by comparing them with the ones of the N-body FPE. We have found that the mean-field equation provides an excellent description of the dynamics when this is prevailingly Hamiltonian. It further describes the equilibrium properties of single-particle observables, including the asymptotic temperature and the order parameter. It fails, however, to reproduce the long-time out-of-equilibrium dynamics.

Despite these differences, this analysis shows that from the mean-field model one can analytically extract several predictions on the system dynamics. It is indeed remarkable that several predictions reproduce in the corresponding limits the ones obtained by means of other theoretical treatments, some of which start from a fully quantum mechanical treatment for the atoms. This on the one hand leads us to conjecture that quantum fluctuations play a marginal role in determining the steady state properties of the cavity field. It further urges one to develop a full quantum kinetic theory, analogous to the full N-body semiclassical theory, which shall overcome

all limitations of simplifying theoretical assumptions performed so far. Only such a model, in fact, can give full access to the dynamical interplay between matter waves and cavity photons.

Acknowledgments

The authors are grateful to G. Manfredi and C. Nardini for insightful discussions. This work was supported by the German Research Foundation (DACH project: "Quantum crystals of matter and light").

Appendix A: Cavity field correlation function at steady state

Experimentally accessible quantities are the correlation functions of the field at the cavity output, which allows one to monitor the atoms state and is proportional to the intracavity field. In our formalism, the intracavity field is closely connected to the atomic state by the relation $E_{\rm cav} \propto \sqrt{N\bar{n}}\Theta$, therefore the correlation functions of the cavity field are proportional to the correlation functions of the magnetization Θ [21, 22]. In the following we determine the autocorrelation function of the magnetization, which can be detected by means of the first-order correlation function of the field, and the fourth-moment of the magnetization $\langle\Theta^4\rangle_N$. As we showed in Ref. [21], in fact, $\langle\Theta^4\rangle_N$ delivers the value of the intensity-intensity correlation of the field at zero-time delay and at zero order in the retardation effects.

1. Field intensity across the transition

We first determine the intracavity photon number $n_{\rm cav}$ at steady state for $\bar{n}$ below, at, and above threshold. For this purpose we use the relation [21, 22]

$$n_{\rm cav} = N\bar{n}\langle\Theta^2\rangle_N\,, \tag{A1}$$

which, by introducing $\alpha = \bar{n}/\bar{n}_c$, can be cast in the form (see also the Appendix A 3)

$$n_{\rm cav} = \frac{1}{2}\bar{n}_c + \bar{n}\frac{\partial}{\partial\alpha}\mathcal{G}(\alpha)\,, \tag{A2}$$

where

$$\mathcal{G}(\alpha) = \ln\left(\int_{-\infty}^{\infty} dy \exp\left[-N\left(\alpha y^2 - \ln(I_0(2\alpha y))\right)\right]\right)\,. \tag{A3}$$

We then analyse the prediction of this expression close to threshold, for $\bar{n} \sim \bar{n}_c$ and thus $\alpha \sim 1$. For this purpose we expand the exponent of $\mathcal{G}(\alpha)$ about the value $y = 0$ and consider the behaviour of $n_{\rm cav}$ for $\alpha \to 1^-$, hence for $\bar{n} < \bar{n}_c$ but sufficiently close to the transition point, so that the truncation of the expansion is valid. In this limit we find

$$n_{\rm cav} \approx \frac{\bar{n}_c^2/2}{\bar{n}_c - \bar{n}}\,, \tag{A4}$$

where the details of the derivation are reported in the Appendix A 3. The value at the transition point is reported at leading order in N and reads (see Appendix A 3):

$$n_{\rm cav} \approx 2\sqrt{N}\bar{n}_c\frac{\Gamma\left[\frac{3}{4}\right]}{\Gamma\left[\frac{1}{4}\right]}\,, \tag{A5}$$

where $\Gamma[x]$ denotes the Gamma function [39].

The value of the intracavity photon number above threshold is found after observing that the exponent of function $\mathcal{G}(\alpha)$ has two minima that are given by the non vanishing solutions of the fixed-point equation (24), which we denote by $\Theta_{\rm MF} = \pm\bar{\Theta}$, with $\bar{\Theta}$ given in Eq. (26). Therefore it holds

$$n_{\rm cav} = N\bar{n}\bar{\Theta}^2 \approx 2N(\bar{n} - \bar{n}_c)\,,$$

sufficiently close to the critical point. In particular, the mean number of photons increases linearly with $\bar{n}$. We analyse now some properties of the first order correlation function of the intracavity field, $g^{(1)}(\tau) = \lim_{t\to\infty}{\rm Re}\langle E_{\rm cav}(t+\tau)E_{\rm cav}(t)\rangle_N$. This function has been extensively studied in Ref. [21] by numerically solving the N-particle FPE. Here, we will use the mean-field ansatz in order to better understand the two sidebands of its Fourier transform, at which it exhibits maxima above threshold. For this purpose we first notice that the correlation function is proportional to the autocorrelation function $C(\tau)$ of the magnetization by the relation $g^{(1)}(\tau) = N\bar{n}C(\tau)$, and

$$C(\tau) \;=\; \lim_{t\to\infty}\langle\Theta(t)\Theta(t+\tau)\rangle_N\,. \tag{A6}$$

We want to derive $C(\tau)$ in mean-field and hence the mean value has now to be taken over the factorized distribution as in Eq. (9) with the stationary mean-field distribution given in Eq. (23). We calculate $C(\tau)$ by solving the equations of the mathematical pendulum

$$\begin{aligned}\dot{x} &= \frac{p}{m}\\ \dot{p} &= 2\hbar k\Delta_c\bar{n}\bar{\Theta}\sin(kx)\,,\end{aligned} \tag{A7}$$

with initial conditions $x(0) = x_0$ and $p(0) = p_0$. The value $\bar{\Theta}$ is here the positive stable solution of Eq. (24). In the limit of small oscillations, these equations describe harmonic motion at the frequency

$$\omega_0 = \sqrt{-4\omega_r\Delta_c\bar{n}\bar{\Theta}}\,. \tag{A8}$$

The mean frequency, however, is the result of the possible trajectories of the mathematical pendulum weighted by the probability density function $f_{\rm st}(x_0, p_0)$. For $x_0 \neq 0$ and $p_0 \neq 0$ the oscillation period results to be larger than $2\pi/\omega_0$ and this prediction fits quite well the maximum found numerically by integrating the coupled equations of N particles, as shown in Fig. 7.

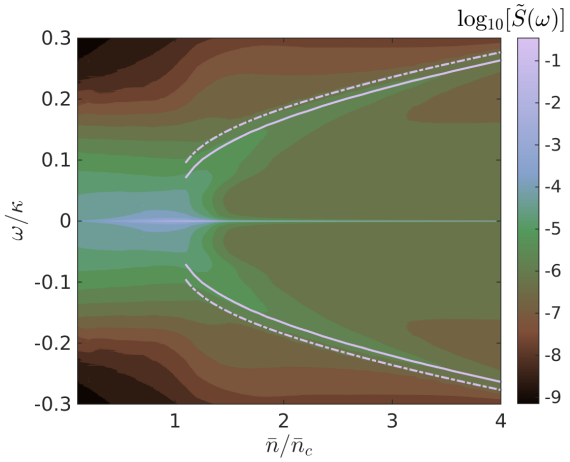

FIG. 7: (Color online) Contour plot of the spectrum of the autocorrelation function $\tilde{S}(\omega)$ as a function of $\bar{n}$ and of the frequency (in units of κ) evaluated from the numerical data of $\Theta(x_1,\ldots,x_N)$, Eq. (4), by integrating the N-particle FPE, Eq. (1), for 100 trajectories of $N = 50$ atoms, $\Delta_c = -\kappa$, and evolution time $t_{\rm tot} = 10^4\kappa^{-1}$, see Ref. [21]. The lines are analytical estimates of the spectrum maximum for $\bar{n} > \bar{n}_c$. The dashed line corresponds to the frequency of the corresponding harmonic oscillator in Eq. (A8). The solid line is at the frequency extracted by solving Eqs. (A7) for a mathematical pendulum and in good agreement with the peaks position of the numerically evaluated spectra.

2. Intensity-intensity correlations at zero-time delay

The intensity-intensity correlation function at zero time delay, $g^{(2)}(0)$, provides a direct measurement of the fourth moment of the magnetization when retardation effects are sufficiently small [21]:

$$g^{(2)}(0) = \langle\Theta^4\rangle_N / \langle\Theta^2\rangle_N^2 \,. \tag{A9}$$

Above threshold $\langle\Theta^n\rangle_N = \bar{\Theta}^n + O(1/N)$, with $\bar{\Theta}$ the solution of Eq. (24). Therefore, for $\bar{n} > \bar{n}_c$ we obtain

$$g^{(2)}(0)_{\bar{n}>\bar{n}_c} = 1\,, \tag{A10}$$

which corresponds to coherent light and is valid at leading order, with an error that scales with $1/N$. In mean-field for the factorized distribution, Eq. (9), we get

$$\langle\Theta^2\rangle_N = \frac{1}{N}\mathcal{B} + \frac{N-1}{N}\bar{\Theta}^2$$

and

$$\begin{aligned}\langle\Theta^4\rangle_N =& \frac{N(N-1)(N-2)(N-3)}{N^4}\bar{\Theta}^4 \\ &+ \frac{6N(N-1)(N-2)}{N^4}\bar{\Theta}^2\mathcal{B} + \frac{3N(N-1)}{N^4}\mathcal{B}^2 \\ &+ \frac{4N(N-1)}{N^4}\bar{\Theta}\langle\cos^3(x)\rangle + \frac{N}{N^4}\langle\cos^4(x)\rangle.\end{aligned}$$

Notice that above threshold for $\bar{\Theta} \neq 0$ we can again write $\langle\Theta^4\rangle_N = \bar{\Theta}^4 + O(1/N)$. Hence we get the same value for $g^{(2)}(0) = 1$ (above threshold) in the thermodynamic limit $N \to \infty$. Below threshold, in Appendix A 3 we show that the expression takes the value

$$g^{(2)}(0)_{\bar{n}<\bar{n}_c} = 3\,, \tag{A11}$$

which corresponds to super-Poissonian light. Corrections scale with $1/N$. The same holds for the calculation with the factorized ansatz. Below threshold we get

$$\langle\Theta^2\rangle_N = \frac{1}{N}\mathcal{B}$$

and

$$\langle\Theta^4\rangle_N = \frac{3}{N^2}\mathcal{B}^2 + O\left(\frac{1}{N}\right)$$

and therefore the same value of $g^{(2)}(0) = 3$ (below threshold) as for the N-particle description. Finally, at threshold we obtain

$$g^{(2)}(0)_{\bar{n}=\bar{n}_c} \approx \frac{1}{4}\left(\frac{\Gamma\left[\frac{1}{4}\right]}{\Gamma\left[\frac{3}{4}\right]}\right)^2\,, \tag{A12}$$

with corrections scaling with $1/\sqrt{N}$, thus giving a slower convergence than the one found for the values above and below threshold. We want to mention here that the mean-field description cannot reproduce the value in Eq. (A12). Figure 8 displays the mean-field predictions for the $g^{(2)}(0)$ at the thermodynamic limit and as a function of $\bar{n}$. These curves are compared with the mean-field calculation at finite N and with the corresponding one of the N-particle FPE. Even though the mean-field curve at finite N is tendentially closer to the thermodynamic limit than the N-particle FPE prediction, they both converge to the values of Eqs. (A10), (A12) (A11), depending on whether $\bar{n} <, =, > \bar{n}_c$, for $N \to \infty$.

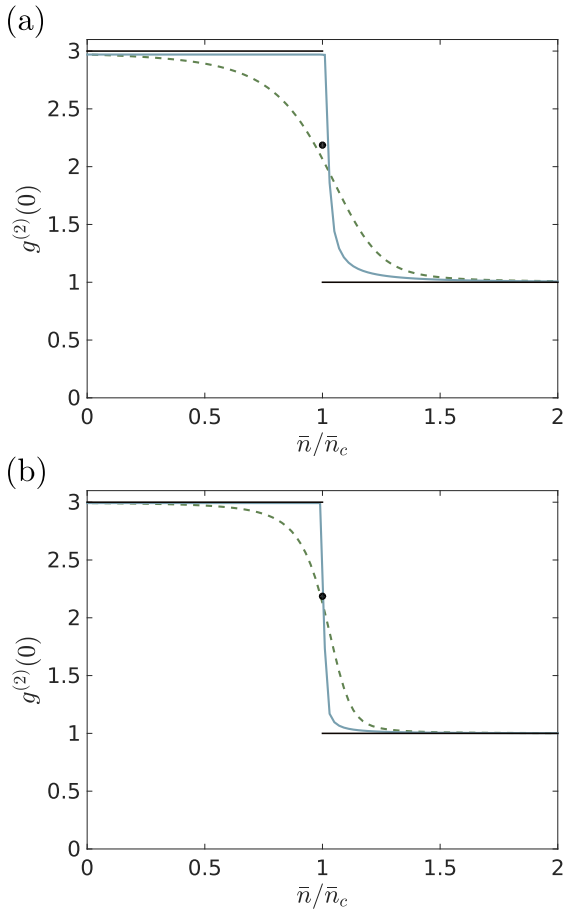

FIG. 8: (Color online) Intensity-intensity correlation function at zero time delay $g^{(2)}(0)$, Eq. (A9), as a function of $\bar{n}$ for (a) $N = 50$ atoms and (b) $N = 200$ atoms. The solid blue (light gray) lines are the curves evaluated using in Eq. (A9) the mean-field steady state (23). The dashed lines are calculated for the corresponding full N-particle distribution given in [17]. The horizontal black solid lines are the values at the thermodynamic limit given at $\bar{n} < \bar{n}_c$ by Eq. (A11) and at $\bar{n} > \bar{n}_c$ by Eq. (A10). The point at $\bar{n} = \bar{n}_c$ is at the value of Eq. (A12). The discrepancy between the mean-field curve and the full N-particle predictions decreases as $N \to \infty$, where they both converge to the value given by the thermodynamic limit.

3. Useful relations

In order to demonstrate Eq. (A2) we first consider the relation

$$\int_{-\infty}^{\infty} dy \exp\left(-\alpha N\left(y - \frac{1}{N}\sum_{i=1}^{N}\cos(kx_i)\right)^2\right) = \sqrt{\frac{\pi}{\alpha N}}\,,$$

and cast it into the form

$$\int_{-\infty}^{\infty} dy e^{-\alpha N y^2} \exp\left(2\alpha N y \frac{1}{N}\sum_{i=1}^{N}\cos(kx_i)\right) = \sqrt{\frac{\pi}{\alpha N}} \exp\left(\alpha N \Theta(\mathbf{x})^2\right)\,.$$

From these relations, it follows

$$\ln\left(\frac{1}{\lambda^N}\int d\mathbf{x}\exp\left(\alpha N\Theta(\mathbf{x})^2\right)\right)=\frac{1}{2}\ln\left(\frac{N}{\pi}\alpha\right)+\ln\left(\int_{-\infty}^{\infty}dy\exp\left[-N\left(\alpha y^2-\ln(I_0(2\alpha y))\right)\right]\right).$$

We use it for evaluating expression (A1) and obtain

$$n_{\rm cav}=\bar{n}\frac{\partial}{\partial\alpha}\ln\left(\frac{1}{\lambda^N}\int d\mathbf{x}\exp\left(\alpha N\Theta(\mathbf{x})^2\right)\right)=\bar{n}\left(\frac{1}{2\alpha}+\frac{\frac{\partial}{\partial\alpha}\int_{-\infty}^{\infty}dy\exp\left[-N\left(\alpha y^2-\ln(I_0(2\alpha y))\right)\right]}{\int_{-\infty}^{\infty}dy\exp\left[-N\left(\alpha y^2-\ln(I_0(2\alpha y))\right)\right]}\right), \tag{A13}$$

that leads to Eq. (A2) by using definition (A3).

In order to determine the intracavity photon number close to threshold, we expand the exponent of Eq. (A3) about $y=0$ till fourth order:

$$\alpha y^2-\ln(I_0(2\alpha y))=\alpha(1-\alpha)y^2+\frac{\alpha^4}{4}y^4+\mathrm{O}(y^6).$$

For $\bar{n}<\bar{n}_c$, the coefficient of the quadratic term is positive and we thus discard the fourth order term. Expression (A2) takes the form

$$\begin{aligned}n_{\rm cav}\approx&\bar{n}\left(\frac{1}{2\alpha}+\frac{\frac{\partial}{\partial\alpha}\int_{-\infty}^{\infty}dy\exp\left[-N\alpha(1-\alpha)y^2\right]}{\int_{-\infty}^{\infty}dy\exp\left[-N\alpha(1-\alpha)y^2\right]}\right)\\=&\bar{n}\left(\frac{1}{2\alpha}+\frac{2\alpha-1}{2\alpha(1-\alpha)}\right)=\frac{\bar{n}}{2(1-\alpha)}.\end{aligned}$$

Using the explicit value of α, then

$$n_{\rm cav}=\frac{\bar{n}\bar{n}_c}{2(\bar{n}_c-\bar{n})}\approx\frac{\bar{n}_c^2/2}{\bar{n}_c-\bar{n}}, \tag{A14}$$

which thus gives Eq. (A4).

At the transition point $\bar{n}=\bar{n}_c$ the integral in Eq. (A2) diverges in the limit $N\to\infty$. We determine its value for finite N, and keep the leading order. Moreover, since the coefficient of the quadratic term in the expansion in y vanishes, we include the fourth order and evaluate the integral at $\alpha=1$, obtaining:

$$n_{\rm cav}\approx\bar{n}_c\left(\frac{1}{2}+\frac{\int_{-\infty}^{\infty}dy\left(Ny^2-Ny^4\right)\exp\left[-\frac{N}{4}y^4\right]}{\int_{-\infty}^{\infty}dy\exp\left[-\frac{N}{4}y^4\right]}\right)\approx\bar{n}_c\frac{2\sqrt{N}\Gamma\left[\frac{3}{4}\right]}{\Gamma\left[\frac{1}{4}\right]},$$

which is the expression in Eq. (A5).

To calculate $g^{(2)}(0)$ below and at threshold we notice that

$$N^2\left\langle\Theta^4\right\rangle_N-N^2\left\langle\Theta^2\right\rangle_N^2=\frac{\partial^2}{\partial\alpha^2}\ln\left(\frac{1}{\lambda^N}\int d\mathbf{x}\exp\left(\alpha N\Theta(\mathbf{x})^2\right)\right)=N\frac{\partial}{\partial\alpha}\left\langle\Theta^2\right\rangle_N$$

holds. Below threshold for $\alpha<1$ we calculated in leading order that

$$\frac{\partial}{\partial\alpha}\frac{1}{2(1-\alpha)}=\frac{1}{2(1-\alpha)^2},$$

which then delivers expression

$$g^{(2)}(0)_{\bar{n}<\bar{n}_c}=\frac{\frac{1}{2(1-\alpha)^2}+\frac{1}{4(1-\alpha)^2}}{\frac{1}{4(1-\alpha)^2}}=3,$$

and thus Eq. (A11). In order to calculate the value at threshold we use

$$N^2\langle\Theta^4\rangle_N-N^2\left\langle\Theta^2\right\rangle_N^2\approx N-4N\left(\frac{\Gamma\left[\frac{3}{4}\right]}{\Gamma\left[\frac{1}{4}\right]}\right)^2, \tag{A15}$$

which is valid in leading order and which gives Eq. (A12).

[1] H. Ritsch, P. Domokos, F. Brennecke, and T. Esslinger, Rev. Mod. Phys. **85**, 553 (2013).

[2] G. Labeyrie, E. Tesio, P. M. Gomes, G.-L. Oppo, W. J.

Firth, G. R. M. Robb, A. S. Arnold, R. Kaiser, and T. Ackemann, Nat. Photonics **8**, 321 (2014); G. R. M. Robb, E. Tesio, G.-L. Oppo, W. J. Firth, T. Ackemann, and R. Bonifacio, Phys. Rev. Lett. **114**, 173903 (2015).
[3] D. E. Chang, J. I. Cirac, and H. J. Kimble, Phys. Rev. Lett. **110**, 113606 (2013).
[4] D. H. J. O'Dell, S. Giovanazzi, and G. Kurizki, Phys. Rev. Lett. **90**, 110402 (2003).
[5] P. Münstermann, T. Fischer, P. Maunz, P. W. H. Pinkse, and G. Rempe, Phys. Rev. Lett. **84**, 4068 (2000).
[6] C. von Cube, S. Slama, D. Kruse, C. Zimmermann, Ph. W. Courteille, G. R. M. Robb, N. Piovella, and R. Bonifacio, Phys. Rev. Lett. **93**, 083601 (2004).
[7] B. Zhu, J. Schachenmayer, M. Xu, F. Herrera, J. G. Restrepo, M. J. Holland, and A. M. Rey, New J. Phys. **17**, 083063 (2015). J. M. Weiner, K. C. Cox, J. G. Bohnet, and J. K. Thompson, arXiv:1503.06464.
[8] B. Nagorny, Th. Elsässer, and A. Hemmerich, Phys. Rev. Lett. **91**, 153003 (2003); S. Gupta, K. L. Moore, K. W. Murch, and D. M. Stamper-Kurn, Phys. Rev. Lett. **99**, 213601 (2007).
[9] S. Ritter, F. Brennecke, K. Baumann, T. Donner, C. Guerlin, and T. Esslinger, Appl. Phys. B **95**, 213 (2009).
[10] P. Domokos and H. Ritsch, Phys. Rev. Lett. **89**, 253003 (2002).
[11] A. T. Black, H. W. Chan, and V. Vuletić, Phys. Rev. Lett. **91**, 203001 (2003).
[12] K. Baumann, C. Guerlin, F. Brennecke, and T. Esslinger, Nature (London) **464**, 1301 (2010).
[13] S. Schreppler, N. Spethmann, N. Brahms, T. Botter, M. Barrios, and D. M. Stamper-Kurn, Science **344**, 1486 (2014).
[14] F. Haas, J. Volz, R. Gehr, J. Reichel, and J. Estève, Science **344**, 180 (2014).
[15] D. Nagy, G. Kónya, G. Szirmai, and P. Domokos, Phys. Rev. Lett. **104**, 130401 (2010).
[16] R. Bachelard, T. Manos, P. de Buyl, F. Staniscia, F. S. Cataliotti, G. De Ninno, D. Fanelli, and N. Piovella, J. Stat. Mech. (2010) P06009.
[17] S. Schütz and G. Morigi, Phys. Rev. Lett. **113**, 203002 (2014).
[18] E. Tesio, G. R. M. Robb, G.-L. Oppo, P. M. Gomes, T. Ackemann, G. Labeyrie, R. Kaiser, and W. J. Firth, Phil. Trans. R. Soc. A **372**, 20140002 (2014).
[19] A. Campa, T. Dauxois, and S. Ruffo, Phys. Rep. **480**, 57 (2009).
[20] M. Antoni and S. Ruffo, Phys. Rev. E **52**, 2361 (1995).
[21] S. Schütz, S. B. Jäger, and G. Morigi, Phys. Rev. A **92**, 063808 (2015).
[22] S. Schütz, H. Habibian, and G. Morigi, Phys. Rev. A **88**, 033427 (2013).
[23] P. Domokos, P. Horak, and H. Ritsch, J. Phys. B **34**, 187 (2001).
[24] S. Schütz, S. B. Jäger, and G. Morigi, arXiv:1512.05243.
[25] J. K. Asbóth, P. Domokos, H. Ritsch, and A. Vukics, Phys. Rev. A **72**, 053417 (2005).
[26] W. Niedenzu, T. Grießer, and H. Ritsch, Europhys. Lett. **96**, 43001 (2011).
[27] T. Grießer, W. Niedenzu, and H. Ritsch, New J. Phys. **14**, 053031 (2012).
[28] E. G. Dalla Torre, S. Diehl, M. D. Lukin, S. Sachdev, and P. Strack, Phys. Rev. A **87**, 023831 (2013).
[29] D. Nagy, G. Szirmai, and P. Domokos, Phys. Rev. A **84**, 043637 (2011).
[30] B. Öztop, M. Bordyuh, Ö. E. Müstecaplıoğlu, and H. E. Türeci, New J. Phys. **14**, 085011 (2012).
[31] M. Kulkarni, B. Öztop, and H. E. Türeci, Phys. Rev. Lett. **111**, 220408 (2013).
[32] F. Piazza, P. Strack, and W. Zwerger, Ann. Phys. (Amsterdam) **339**, 135 (2013).
[33] F. Piazza and P. Strack, Phys. Rev. A **90**, 043823 (2014).
[34] P. Horak, G. Hechenblaikner, K. M. Gheri, H. Stecher, and H. Ritsch, Phys. Rev. Lett. **79**, 4974 (1997).
[35] V. Vuletic and S. Chu, Phys. Rev. Lett. **84**, 3787 (2000).
[36] J. Dalibard and C. Cohen-Tannoudji, J. Phys. B **18**, 1661 (1985).
[37] J. Larson, B. Damski, G. Morigi, and M. Lewenstein, Phys. Rev. Lett. **100**, 050401 (2008); J. Larson, S. Fernández-Vidal, G. Morigi, and M. Lewenstein, New J. Phys. **10**, 045002 (2008).
[38] S. Fernández-Vidal, G. De Chiara, J. Larson, and G. Morigi, Phys. Rev. A **81**, 043407 (2010).
[39] M. Abramowitz and I. Stegun, *Handbook of Mathematical Functions* (Dover, New York, 1968).
[40] T. Grießer, H. Ritsch, M. Hemmerling, and G. R. M. Robb, Eur. Phys. J. D **58**, 349 (2010).
[41] G. K. Karagiannidis and A. S. Lioumpas, IEEE Commun. Lett. **11**, 664 (2007).
[42] C. Nardini, *Energy landscapes, equilibrium and out of equilibrium physics of long and short range interacting systems*, PHD Thesis, École normale supérieure de Lyon and Università degli Studi di Firenze, NNT : 2013ENSL0804 (2013).

CHAPTER 6

Dissipation-assisted prethermalization in long-range interacting atomic ensembles

Dissipation-assisted prethermalization in long-range interacting atomic ensembles

Authors: Stefan Schütz, Simon B. Jäger, and Giovanna Morigi

Theoretische Physik, Universität des Saarlandes, D-66123 Saarbrücken, Germany

Sumitted to Physical Review Letters - with kind permission of the American Physical Society.

see also PREPRINT arXiv:1512.05243
"Relaxation after quenches in systems with photon-mediated long-range interactions" (The manuscript has been substantially revised during the review process.)

Author Contributions:
The theoretical model was developed by S. Schütz and G. Morigi. Analytical and numerical calculations were performed by S. B. Jäger and S. Schütz. The calculations and results were checked, discussed and analysed by all three authors. The article was written by all authors.

Abstract:
We theoretically characterize the semiclassical dynamics of an ensemble of atoms after a sudden quench across a driven-dissipative second-order phase transition. The atoms are driven by a laser and interact via conservative and dissipative long-range forces mediated by the photons of a single-mode cavity. These forces can cool the motion and, above a threshold value of the laser intensity, induce spatial ordering. We show that the relaxation dynamics following the quench

exhibits a long prethermalizing behaviour which is first dominated by coherent long-range forces, and then by their interplay with dissipation. Remarkably, dissipation-assisted prethermalization is orders of magnitude longer than prethermalization due to the coherent dynamics. We show that it is associated with the creation of momentum-position correlations, which remain nonzero for even longer times than mean-field predicts. This implies that cavity cooling of an atomic ensemble into the selforganized phase can require longer time scales than the typical experimental duration. In general, these results demonstrate that noise and dissipation can substantially slow down the onset of thermalization in long-range interacting many-body systems.

Dissipation-assisted prethermalization in long-range interacting atomic ensembles

Stefan Schütz, Simon B. Jäger, and Giovanna Morigi
Theoretische Physik, Universität des Saarlandes, D-66123 Saarbrücken, Germany
(Dated: July 3, 2016)

We theoretically characterize the semiclassical dynamics of an ensemble of atoms after a sudden quench across a driven-dissipative second-order phase transition. The atoms are driven by a laser and interact via conservative and dissipative long-range forces mediated by the photons of a single-mode cavity. These forces can cool the motion and, above a threshold value of the laser intensity, induce spatial ordering. We show that the relaxation dynamics following the quench exhibits a long prethermalizing behaviour which is first dominated by coherent long-range forces, and then by their interplay with dissipation. Remarkably, dissipation-assisted prethermalization is orders of magnitude longer than prethermalization due to the coherent dynamics. We show that it is associated with the creation of momentum-position correlations, which remain nonzero for even longer times than mean-field predicts. This implies that cavity cooling of an atomic ensemble into the selforganized phase can require longer time scales than the typical experimental duration. In general, these results demonstrate that noise and dissipation can substantially slow down the onset of thermalization in long-range interacting many-body systems.

PACS numbers: 37.30.+i, 42.65.Sf, 05.65.+b, 05.70.Ln

The quest for a systematic understanding of non-equilibrium phenomena is an open problem in theoretical physics for its importance in the description of dynamics from the microscopic up to astrophysical scales [1–3]. Aspects of these dynamics are studied in the relaxation of systems undergoing temporal changes (quenches) of the control field across a critical point [4–6]. Quenches across a non-equilibrium phase transition provide further insight into the interplay between noise and external drives on criticality and thermalization [7, 8]. In this context photonic systems play a prominent role, thanks to their versatility [9–15].

Polarizable particles in a high-finesse cavity, like in the setup illustrated in Fig. 1(a), offer a unique system to study relaxation in long-range interacting systems. Here, multiple photon scattering mediates particle-particle interactions whose range scales with the system size in a single-mode cavity [15–18]. In this limit, atomic ensembles in cavities are expected to share several features with other long-range interacting systems such as gravitational clusters and non-neutral plasmas in two or more dimensions [3, 16, 19]. The equilibrium thermodynamics of these systems can exhibit ensemble inequivalence [3, 20], while quasi-stationary states (QSS) typically characterise the out-of-equilibrium dynamics [3, 21–23]. QSS are metastable states in which the system is expected to remain trapped in the thermodynamic limit, they are Vlasov-stable solutions and thus depend on the initial state. So far, however, evidence of QSS has been elusive. It has been conjectured that noise and dissipation can set a time scale that limits the QSS lifetime [24–27], and possibly gives rise to dynamical phase transitions [25]. In Ref. [28] it was shown that, in presence of dissipation due to viscous damping or local inelastic collisions, the relaxation dynamics of long-range interacting systems can be cast in terms of so-called scaling QSS, which are solutions of the kinetic mean-field equation and asymptotically tend to a unique QSS [28]. Accordingly, one would expect to observe QSS in cavity systems [19]. In Ref. [16], however, we found no evidence of the typical superlinear dependence on N of the QSS time scale [3], which we attributed to the effect of noise and dissipative processes. Nonetheless, the dissipative dynamics is here due to retardation effects in the coupling between the atoms and a global variable, the cavity field, and can also establish long-range correlations [29, 30] whose influence on the relaxation dynamics is still unexplored.

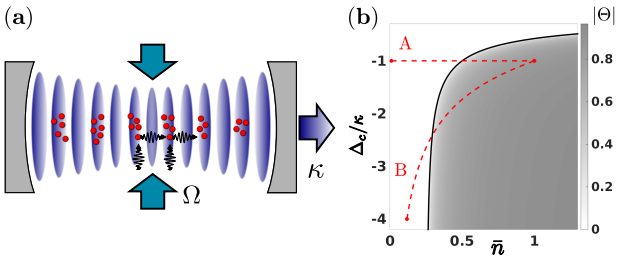

FIG. 1. (Color online) (a) Atoms interact with the standing-wave mode of a cavity and are transversally driven by a laser. The laser amplitude (Ω) and/or frequency (Δ_c) are suddenly quenched across the threshold, above which the atoms organize in regular spatial patterns at steady state. The coherent scattering amplitude per atom, S, is tuned by the laser, $S \propto \Omega$, the resonator dissipates photons at rate κ. (b) Phase diagram of the second-order self-organization transition as a function of $\bar{n}$ (proportional to S^2) and Δ_c/κ (that determines the asymptotic temperature). The black line separates the homogeneous phase (with order parameter $\Theta = 0$) from the self-organized one (with $\Theta \to \pm 1$). The red dashed lines A and B illustrate the initial and final values of the sudden quenches we analyse.

In this work we characterise the interplay between dissipative and conservative long-range forces in the semiclassical dynamics of N polarizable particles (atoms) confined within a high-finesse single-mode cavity and transversally driven by a laser [16, 31–33] (see Fig. 1(a)). The particles motion is along the cavity axis (x-axis), and the dynamics results from their opto-mechanical coupling with the cavity mode at wave number k and spatial mode function $\cos(kx)$. We focus on the regime where the laser frequency ω_L is smaller than the cavity frequency ω_c, such that $\Delta_c = \omega_L - \omega_c < 0$. Here, the dynamics is characterised by a thermal stationary state, which can exhibit a second-order driven-dissipative phase transition (spatial selforganization) as a function of the laser intensity and of Δ_c [31]. This transition is due to the interplay between the dispersive and the dissipative forces: The dispersive forces tend to order the atoms in gratings for which the order parameter $\Theta = \sum_{j=1}^{N} \cos(kx_j)/N \to \pm 1$, with x_j the particles positions, and the intracavity photon number is maximum. The dissipative forces, instead, are due to retardation effects in the dynamics of atoms and field: For $\Delta_c < 0$ they cool the atoms into a thermal state whose effective temperature $T_{\rm eff}$ is determined by Δ_c and by the cavity loss rate κ: $k_B T_{\rm eff} = \hbar(\Delta_c^2 + \kappa^2)/(-4\Delta_c)$, with k_B Boltzmann constant [30–32, 34–37]. $T_{\rm eff}$ determines the threshold S_c of the coherent laser scattering amplitude S per atom at which spatial self-organization occurs, such that $\sqrt{N} S_c = 2k_B T_{\rm eff}/\hbar$ [31, 34, 38] and separates the regime where the spatial distribution is uniform and $\Theta \simeq 0$ from the symmetry broken phase in which the atoms form Bragg gratings, as shown in Fig. 1(b).

We analyse the semiclassical dynamics of the atoms after a quench across the transition using a Fokker-Planck equation (FPE) for the phase space distribution $f(x_1, \ldots, x_N; p_1, \ldots, p_N; t)$ at time t and as a function of the atoms positions x_j and the momenta p_j. The FPE is valid when the cavity linewidth κ exceeds the recoil frequency $\omega_r = \hbar k^2/(2m)$ and the width of the momentum distribution Δp is larger than the photon linear momentum $\hbar k$ [30]. It reads [31, 39]

$$\partial_t f = \{H, f\} + \bar{n}\mathcal{L}_\beta f + \mathrm{O}(U_0), \tag{1}$$

where Hamiltonian $H = \sum_{j=1}^{N} p_j^2/(2m) + \hbar\Delta_c \bar{n} N \Theta^2$ determines the coherent dynamics and is a realization of the anisotropic Hamiltonian Mean Field model (HMF) [16, 21, 40]. The dimensionless parameter $\bar{n} = NS^2/(\kappa^2 + \Delta_c^2)$ scales the depth of the conservative potential. It also scales the dissipator $\mathcal{L}_\beta$, describing the effective long-ranged friction and diffusion [30, 31]:

$$\mathcal{L}_\beta f = \sum_i^N \frac{\Gamma}{N} \sum_j^N \sin(kx_i)\partial_{p_i} \sin(kx_j) \left(p_j + \frac{m}{\beta}\partial_{p_j} \right) f\,, \tag{2}$$

with $\Gamma = 2\omega_r \hbar\kappa\beta$ and $\beta = (k_B T_{\rm eff})^{-1}$. For $\Delta_c < 0$ the incoherent dynamics drives the system into the stationary state $f_S(\beta, \bar{n}) = f_0 \exp(-\beta H)$, where f_0 warrants normalization. This state is well defined in the thermodynamic limit we choose, according to which as N is increased, the quantity NS^2 (and thus $\bar{n}$) is kept constant. This choice warrants that the Hamiltonian satisfies Kac's scaling [3].

The relaxation dynamics following a sudden quench at $t = 0$ is numerically evaluated by means of stochastic differential equations (SDE). Averages are taken over several trajectories, sampling the dynamics of N atoms according to the given initial distribution [30, 41]. Before the quench is performed ($t < 0$), we assume that the system has reached the equilibrium solution $f_S(\beta, \bar{n}_i)$ of the FPE at a given value of $\bar{n} = \bar{n}_i$ and Δ_c. At $t = 0$ the value of $\bar{n}$ is quenched from $\bar{n}_i < \bar{n}_c$, deep in the disordered phase, to $\bar{n}_f > \bar{n}_c$, well inside the ordered phase. This corresponds to the horizontal path A of Fig. 1(b), keeping Δ_c, and hence the asymptotic temperature, constant. We evolve the initial state setting $\bar{n} = \bar{n}_f$ in Eq. (1). In what follows we focus on quenches from the disordered to the ordered phase along path A, nevertheless the essential features of the dynamics we will report on characterize also the quenches in the opposite direction as well as along paths of type B, which connects points with different asymptotic temperatures (see Supplemental Material, SM, [42]).

The time evolution of the modulus of the order parameter $\langle|\Theta|\rangle$ is displayed in Fig. 2(a) for different values of $\bar{n}_f$: $\langle|\Theta|\rangle$ tends towards an asymptotic value, that is closer to unity the larger is $\bar{n}_f$. Before reaching the steady state the dynamics go through different stages, which we classify as: (i) a fast relaxation towards an intermediate value of the magnetization with time scale $t \lesssim 10^2\kappa^{-1}$; this time scale decreases with $\bar{n}_f$. (ii) A transient regime where $\langle|\Theta|\rangle$ seems to grow logarithmically with time. (iii) Finally, the dissipation becomes dominant and brings the system to the asymptotic value, which is exponentially approached over time scales of the order of $10^6\kappa^{-1}$. These time scales are illustrated in Fig. 2(a) and here reported for $N = 50$ particles but generally depend on N, as we discuss later on.

We first observe that, being Δ_c negative, the growth of $\langle|\Theta|\rangle$, Fig. 2(a), corresponds to a monotonic decrease of the potential energy, $V = \hbar\Delta_c \bar{n} N \Theta^2$. In the fast relaxation stage (i), this decrease is well-fitted by an exponential, and is associated with a corresponding decrease of the relative fluctuations (see inset), indicating that the cavity field exponentially grows and creates a mechanical potential, which increasingly localizes the atoms at its minima. The exponential potential depth growth is due to this nonlinearity: the more the atoms become localized in the Bragg grating the larger is the scattering amplitude, and thus the potential depth. The increasing localization correspondingly augments the ki-

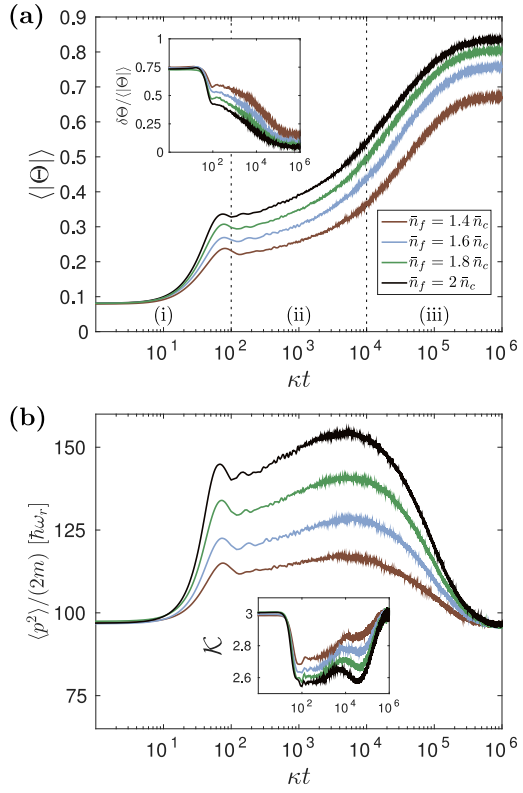

FIG. 2. (Color online) Numerical simulation of the dynamics following a sudden quench along path A using the SDE [31]. At $t = 0$ the atoms are in the stationary state of Eq. (1) for $\bar{n}_i = 0.01\bar{n}_c$ with $\Delta_c = -\kappa$ and $\bar{n}$ is quenched to the value $\bar{n}_f > \bar{n}_c$ (see legenda in (a)). (a) The modulus of the order parameter $\langle|\Theta|\rangle$ and (b) the single-particle kinetic energy $\langle p^2/(2m)\rangle$ (in units of $\hbar\omega_r$) as a function of time (in units of κ^{-1}) for $N = 50$. The corresponding insets display the time evolution of the relative localization $\delta\Theta/\langle|\Theta|\rangle$, where $\delta\Theta = \sqrt{\langle\Theta^2\rangle - \langle|\Theta|\rangle^2}$, and of the Kurtosis $\mathcal{K}$. The initial values $\langle|\Theta|\rangle_{t=0} \simeq 1/\sqrt{\pi N} \approx 0.08$ in (a) are due to finite N [31]. Here, $\kappa \approx 390\,\omega_r$ and $N|U_0| = 0.05\,\kappa$. The three relaxation stages are indicated by the labels (i),(ii),(iii).

netic energy, as visible in Fig. 2(b). In this regime, thus, the total energy is conserved, the dynamics is coherent and consists in a transfer of energy from spatial into momentum fluctuations. Correspondingly, the single-particle momentum distribution becomes increasingly non-thermal, as visible by inspecting the time-evolution of the Kurtosis, $\mathcal{K} = \langle p^4\rangle/\langle p^2\rangle^2$, shown in the inset of Fig. 2(b): $\mathcal{K}$ exponentially deviates from the value of the initial Gaussian ("thermal") state, for which $\mathcal{K}_{\rm gauss} = 3$. We have verified that this dynamics is well described by a Vlasov equation for the single-particle distribution $f_1(x, p; t)$, which we derive assuming $f(x_1, \ldots, x_N; p_1, \ldots, p_N; t) = \prod_{j=1}^{N} f_1(x_j, p_j; t)$, integrating out the $N - 1$ variables from Eq. (1) for the initial uniform distribution and taking the thermodynamic limit (see SM [42] and [43]). Figure 3(a) compares the result of the FPE with the predictions of the Vlasov equation (red curve), showing an excellent agreement in the fast relaxation regime. Numerical and analytical results show that the time scale of this dynamics depends on N only through the parameter $\bar{n}$ (and is thus constant when Kac's scaling applies), see also SM [42].

After this fast relaxation, the growth in the order parameter and in the kinetic energy seems logarithmic in time. This transient regime (ii) is of Hamiltonian origin: It exhibits damped oscillations, which can be understood as oscillations of the atoms at the minima. Energy is periodically transferred from the kinetic to the potential energy. Since the potential energy depends on a global variable, energy is exchanged between the particles by means of elastic collisions, hence damping the oscillations. Correspondingly, the Kurtosis starts to increase towards the Gaussian value, showing that the sample starts to equilibrate. In order to verify this hypothesis, in Fig. 3(a) we compare the predictions of the full simulation (black curves) for order parameter and Kurtosis with the ones obtained after setting $\Gamma = 0$ in Eq. (1) (blue curves): in the transient regime the curves nearly overlap for $t \lesssim 10^4\kappa^{-1}$. Noise and dissipation, however, lead to a discrepancy between the predictions of the Hamiltonian and of the full FPE. This discrepancy becomes increasingly evident at longer time scales: When the dynamics is solely Hamiltonian, in fact, the Kurtosis increases monotonically towards the Gaussian value. Due to the analogy with the Hamiltonian dynamics, some of the features of the transient regime are reminiscent of the HMF, where for a similar quench a violent relaxation is observed, then followed by prethermalization in a QSS [21, 40]. In our case, for $\Gamma \neq 0$, as in Ref. [16], we do not find evidence of a superlinear scaling with N of the QSS lifetime. The QSS lifetime, in fact, is limited by the dissipative effects, which have the same physical origin as the long-range conservative forces and whose characteristic time scale is linear in N (see SM, [42], and Ref. [43]). Note that at the end of this stage the atoms are localised, but their temperature is hotter than $T_{\rm eff}$.

In stage (iii), when the effect of dissipation becomes relevant, the atoms are cooled and further localised at the minima. The Kurtosis, however, further decreases till reaching a minimum, before increasing again towards the Gaussian value. We first compare this behaviour with the predictions of a mean-field (MF) model, which we extract from Eq. (1) by means of the factorization ansatz, see SM [42]. The grey lines in Fig. 3(a) and its inset show the MF predictions as a function of time and indicate that, even though MF reproduces qualitatively the dynamical features, it fails to give the correct time scale by at least one order of magnitude. Further insight is provided by

the observable for QSS [28], which we here define as:

$$\phi_{11} = \frac{\langle |\sin(kx)p| \rangle}{\langle |\sin(kx)| \rangle \langle |p| \rangle} - 1 \,. \tag{3}$$

When $\phi_{11} \neq 0$, the distribution is not factorizable into a kinetic and a potential term. Figure 3(b) displays the time evolution of ϕ_{11} for the Hamiltonian, mean-field, and full dynamics. In stages (i) and (ii) the three models predict approximately the same behaviour. Instead, in stage (iii), ϕ_{11} evolves differently: For both MF and full FPE it exhibits a minimum, however reached at different times, which possesses features typical of a scaling QSS, namely, a sequence of QSS with identical correlations [28]. Its nature could be understood in terms of the onset of collective oscillations which are (almost) decoupled from noise and dissipation. Analogous behaviours have been reported for the case of atomic arrays in a cavity [29, 44]. Since the trajectories of ϕ_{11} are different for the three types of simulations, the corresponding QSS are expected to not be the same. In particular, the discrepancy between full FPE and MF in stage (iii) remains of the same order when scaling up the system, while instead Hamiltonian prethermalization tends towards the corresponding mean-field prediction. Figure 4 displays the relaxation time scales for the MF and the full FPE: the two curves suggest a linear increase with N for both cases, nevertheless they run parallel thus showing that the discrepancy is a scalable effect. We deduce that this discrepancy is due to the momentum-position correlations due to noise, which are otherwise discarded in the MF treatment.

This prethermalization is not related to the critical slowing down observed in Ref. [45], but is due to the creation of correlations between momentum and position, and is reminiscent of kinetic-stop dynamics [46]. It implies that cavity-cooling of a large sample of atoms into the self-organized phase, corresponding to a sudden quench along path B, can be very slow and thus inefficient (see also Ref. [34]). Our analysis sets the stage for the development of a kinetic equation that is valid in the full quantum regime [47–51].

We acknowledge discussions with Ralf Betzholz, Cesare Nardini, and Stefano Ruffo, and support by the German Research Foundation (DFG, DACH project "Quantum crystals of matter and light") and by the German Ministry of Education and Research (BMBF "Q.com").

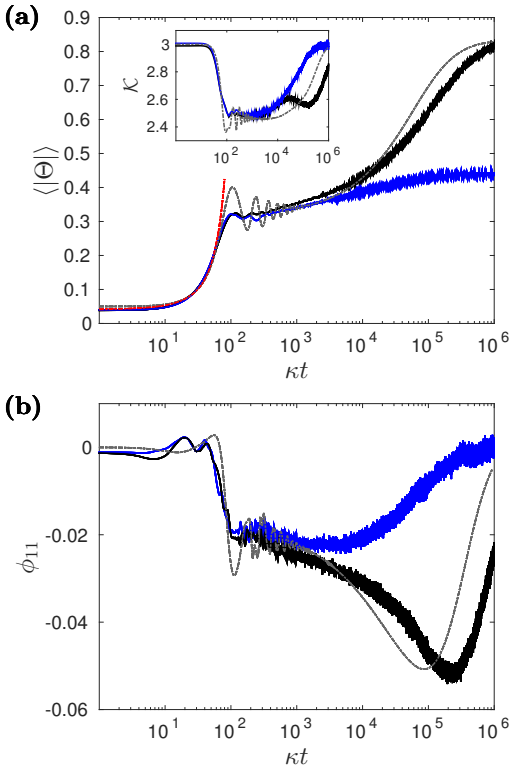

FIG. 3. (Color online) Dynamics following a sudden quench along path A with $\bar{n}_f = 2\bar{n}_c$ and $N = 200$. At $t = 0$ the atoms are in the stationary state of Eq. (1) for $\bar{n}_i = 0.01\bar{n}_c$ and $\Delta_c = -\kappa$. Subplot (a) compares the evolution of $\langle|\Theta|\rangle$ and $\mathcal{K}$ (inset) obtained by integrating Eq. (1) (black line), with the one found after setting $\Gamma = U_0 = 0$ (blue line). Onset: The red line is the fit obtained by a stability analysis of the homogeneous Vlasov solution, the dashed-dotted line by a mean-field model (see SM [42]). (b) Time evolution of the QSS observable ϕ_{11}, Eq. (3), corresponding to the curves in (a).

[1] T. Chou, K. Mallick, and R. K. P. Zia, Rep. Prog. Phys. **74**, 116601 (2011).
[2] Y. Levin, R. Pakter, F. B. Rizzato, T. N. Teles, and F. P. C. Benetti, Phys. Rep. **535**, 1 (2014).
[3] A. Campa, T. Dauxois, and S. Ruffo, Phys. Rep. **480**, 57 (2009).
[4] P. Calabrese and J. Cardy, J. Stat. Mech. P06008 (2007).
[5] L. Foini, L. F. Cugliandolo, and A. Gambassi, Phys. Rev. B **84**, 212404 (2011); F. Iglói and H. Rieger, Phys. Rev. Lett. **106**, 035701 (2011).
[6] A. Polkovnikov, K. Sengupta, A. Silva, and M. Vengalattore, Rev. Mod. Phys. **83**, 863 (2011).
[7] P. C. Hohenberg and B. I. Halperin, Rev. Mod. Phys. **49**, 435 (1977); M. C. Cross and P. C. Hohenberg, Rev. Mod. Phys. **65**, 851 (1993).
[8] L. M. Sieberer, M. Buchhold, and S. Diehl, preprint arXiv:1512.00637 (2015).
[9] A. Tomadin and R. Fazio, J. Opt. Soc. Am. B **27**, A130 (2010).
[10] A. Aspuru-Guzik and P. Walther, Nature Physics **8**, 285 (2012).
[11] P. Kirton and J. Keeling, Phys. Rev. Lett. **111**, 100404 (2013).
[12] L. J. Zou, D. Marcos, S. Diehl, S. Putz, J. Schmiedmayer, J. Majer, and P. Rabl, Phys. Rev. Lett. **113**, 023603 (2014).

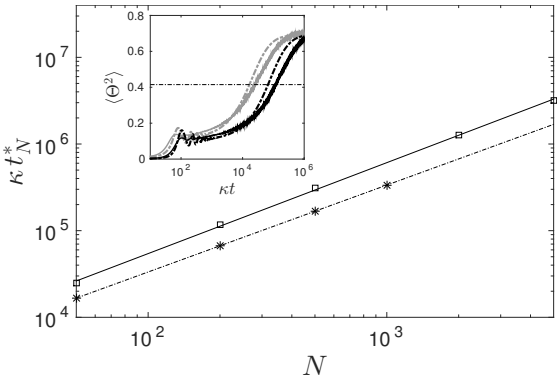

FIG. 4. Relaxation after a sudden quench along path A for the parameters of Fig 3 ($\bar{n}_f = 2\bar{n}_c$) and for different N. Inset: Time evolution of $\langle\Theta^2\rangle$ for $N = 50$ (gray) and $N = 200$ (black). The dashed lines are the prediction of the MF model (see SM, [42]). The horizontal dashed line indicates where $\langle\Theta^2\rangle$ has reached 60% of its stationary value and identifies the corresponding time t_N^*. Onset: time t_N^* (in units of κ^{-1}) as a function of N for the full FPE (squares) and MF (stars). The lines are the corresponding linear fits in the log-log plot.

[13] I. Carusotto and C. Ciuti, Rev. Mod. Phys. **85**, 299 (2013).
[14] V. Peano, C. Brendel, M. Schmidt, and F. Marquardt, Phys. Rev. X **5**, 031011 (2015).
[15] H. Ritsch, P. Domokos, F. Brennecke, and T. Esslinger, Rev. Mod. Phys. **85**, 553 (2013).
[16] S. Schütz and G. Morigi, Phys. Rev. Lett. **113**, 203002 (2014).
[17] F. Piazza and H. Ritsch, Phys. Rev. Lett. **115**, 163601 (2015).
[18] E. Tesio, G. R. M. Robb, G.-L. Oppo, P. M. Gomes, T. Ackemann, G. Labeyrie, R. Kaiser, and W. J. Firth, Phil. Trans. R. Soc. A **372**, 20140002 (2014).
[19] R. Bachelard, T. Manos, P. de Buyl, F. Staniscia, F. S. Cataliotti, G. De Ninno, D. Fanelli, and N. Piovella, J. Stat. Mech. (2010) P06009.
[20] I. Latella, A. Pérez-Madrid, A. Campa, L. Casetti, and S. Ruffo, Phys. Rev. Lett. **114**, 230601 (2015).
[21] M. Antoni and S. Ruffo, Phys. Rev. E **52**, 2361 (1995).
[22] A. Gabrielli, M. Joyce, and B. Marcos, Phys. Rev. Lett. **105**, 210602 (2010).
[23] T. M. Rocha Filho, A. E. Santana, M. A. Amato, and A. Figueiredo, Phys. Rev. E **90**, 032133 (2014).
[24] S. Gupta and D. Mukamel, Phys. Rev. Lett. **105**, 040602 (2010).
[25] P.-H. Chavanis, F. Baldovin, and E. Orlandini, Phys. Rev. E **83**, 040101 (2011).
[26] C. Nardini, S. Gupta, S. Ruffo, T. Dauxois, and F. Bouchet, J. Stat. Mech. (2012) P12010.
[27] P. H. Chavanis, Eur. Phys. J. B **87**, 120 (2014).
[28] M. Joyce and T. Worrakitpoonpon Phys. Rev. E **84**, 011139 (2011); M. Joyce, J. Morand, F. Sicard, and P. Viot, Phys. Rev. Lett. **112**, 070602 (2014); M. Joyce, J. Morand, and P. Viot, Phys. Rev. E **93**, 052129 (2016).
[29] J. K. Asbóth, P. Domokos, and H. Ritsch, Phys. Rev. A **70**, 013414 (2004).
[30] S. Schütz, H. Habibian, and G. Morigi, Phys. Rev. A **88**, 033427 (2013).
[31] S. Schütz, S. B. Jäger, and G. Morigi, Phys. Rev. A **92**, 063808 (2015).
[32] P. Domokos and H. Ritsch, Phys. Rev. Lett. **89**, 253003 (2002).
[33] A. T. Black, H. W. Chan, and V. Vuletić, Phys. Rev. Lett. **91**, 203001 (2003).
[34] W. Niedenzu, T. Grießer, and H. Ritsch, Europhys. Lett. **96**, 43001 (2011).
[35] P. Horak, G. Hechenblaikner, K. M. Gheri, H. Stecher, and H. Ritsch, Phys. Rev. Lett. **79**, 4974 (1997).
[36] V. Vuletić and S. Chu, Phys. Rev. Lett. **84**, 3787 (2000).
[37] A. Vukics and P. Domokos, Phys. Rev. A **72**, 031401(R) (2005).
[38] J. K. Asbóth, P. Domokos, H. Ritsch, and A. Vukics, Phys. Rev. A **72**, 053417 (2005).
[39] Equation (1) contains also the processes scaling with the dynamical Stark shift $U_0 = g^2/\Delta_a$, where g is the cavity vacuum Rabi frequency and $\Delta_a = \omega_L - \omega_a$ the detuning between laser and atomic transition frequency. These processes are here small but accounted for in the numerical simulations [31].
[40] K. Jain, F. Bouchet, and D. Mukamel, J. Stat. Mech. P11008 (2007).
[41] P. Domokos, P. Horak, and H. Ritsch, J. Phys. B **34**, 187 (2001).
[42] See Supplemental Material for the Quenches along path B in Fig. 1 and the derivation of the mean-field FPE and the Vlasov equation.
[43] S. B. Jäger, S. Schütz, and G. Morigi, preprint arXiv:1603.05148 (2016).
[44] O. S. Mishina, New J. Phys. **16**, 033021 (2014).
[45] M. J. Bhaseen, J. Mayoh, B. D. Simons, and J. Keeling, Phys. Rev. A **85**, 013817 (2012).
[46] B. Olmos, I. Lesanovsky, and J. P. Garrahan, Phys. Rev. Lett. **109**, 020403 (2012).
[47] D. Nagy and P. Domokos, Phys. Rev. Lett. **115**, 043601 (2015).
[48] M. Kulkarni, B. Öztop, and H. E. Türeci, Phys. Rev. Lett. **111**, 220408 (2013).
[49] F. Piazza and P. Strack, Phys. Rev. A **90**, 043823 (2014).
[50] K. Baumann, C. Guerlin, F. Brennecke, and T. Esslinger, Nature (London) **464**, 1301 (2010); F. Brennecke, R. Mottl, K. Baumann, R. Landig, T. Donner, and T. Esslinger, PNAS **110**, 11763 (2013).
[51] M. Wolke, J. Klinner, H. Keßler, and A. Hemmerich, Science **337**, 75 (2012); J. Klinder, H. Keßler, M. Wolke, L. Mathey, and A. Hemmerich, PNAS **112**, 3290 (2015).

Supplemental Material for Dissipation-assisted prethermalization in long-range interacting atomic ensembles

Mean-Field equation and Vlasov limit

The mean-field equation is derived from Eq. (1) in the main text by assuming $f(x_1,\dots,x_N;p_1,\dots,p_N;t)=\prod_{j=1}^{N} f_1(x_j,p_j;t)$, and integrating out the $N-1$ variables. It reads

$$\partial_t f_1 = \{H_{\mathrm{MF}}[f_1], f_1\} + \bar{n}\mathcal{L}_{\beta,\mathrm{MF}} f_1 \tag{S1}$$

where the mean-field Hamiltonian $H_{\mathrm{MF}}[f_1]$ is given by

$$H_{\mathrm{MF}}[f_1] = \frac{p^2}{2m} + \frac{2\hbar\Delta_c\bar{n}}{N}\left(\frac{1}{2}\cos(kx) + (N-1)\langle\cos(kx')\rangle_{f_1} - \frac{\hbar k\beta\kappa}{2m\Delta_c}(N-1)\langle p'\sin(kx')\rangle_{f_1}\right)\cos(kx)\,,$$

with $\langle\mathcal{A}(x',p')\rangle_{f_1} = \int_0^{\lambda}\mathrm{d}x'\int_{-\infty}^{\infty}\mathrm{d}p'\mathcal{A}(x',p')f_1(x',p')$ and $\mathcal{A}$ a phase space function. Furthermore the mean-field dissipator $\mathcal{L}_{\beta,\mathrm{MF}}$ is defined as

$$\mathcal{L}_{\beta,\mathrm{MF}} f_1 = \frac{\Gamma}{N}\sin^2(kx)\partial_p\left(p + \frac{m}{\beta}\partial_p\right) f_1\,.$$

The dissipator $\mathcal{L}_{\beta,\mathrm{MF}}$ is responsible for the relaxation of the system to the thermal stationary state with temperature $\beta^{-1} = k_B T_{\mathrm{eff}} = \hbar(\Delta_c^2+\kappa^2)/(-4\Delta_c)$ [S1–S3]. Since the dissipator decreases with N^{-1} (for increasing N), the mean-field predicts a relaxation timescale that extends linearly with N. Although the relaxation for the full FPE, Eq. (1) in the main text, is orders of magnitudes slower (see Fig. 4 in the paper), the corresponding growth of the timescale with N is almost indistinguishable from a linear one.

In order to make some statements for the short time dynamics we derive the Vlasov equation. This equation is derived from Eq. (S1) after performing the limit $N\to\infty$ with NS^2 =const. and reads

$$\partial_t f_1 + \frac{p}{m}\partial_x f_1 - \partial_x V[f_1]\partial_p f_1 = 0\,, \tag{S2}$$

where the Vlasov potential $V[f_1]$ is

$$V[f_1] = 2\hbar\Delta_c\bar{n}\left(\langle\cos(kx')\rangle_{f_1} - \frac{\hbar k\beta\kappa}{2m\Delta_c}\langle p'\sin(kx')\rangle_{f_1}\right)\cos(kx)\,.$$

The stability analysis of Eq. (S2) shows that a spatially homogeneous distribution is unstable against small fluctuations δf when $\bar{n}_f > \bar{n}_c$. The fluctuations exhibit exponential growth at rate γ, which monotonously increases with $\bar{n}_f$ and is a solution of the equation

$$[1 - 2\kappa\gamma/(\Delta_c^2+\kappa^2)]F(\gamma)\bar{n}_f/\bar{n}_c = 1\,, \tag{S3}$$

with $F(\gamma) = 1 - \sqrt{\pi}b\exp(b^2)\mathrm{erfc}(b)$, $b^2 = \hbar\gamma^2\beta/(4\omega_r)$ and erfc is the complementary error function. The solution (red line in Fig. 3(a) in the main text for a fixed value of $\bar{n}_f$) well fits the numerical result in the fast relaxation regime. Thus, this initial behaviour is analogous to the violent relaxation observed in the HMF and has mainly Hamiltonian origin.

Quenches along path B

Figure S1 displays a sudden quench in the detuning Δ_c while keeping Ω, hence the laser amplitude, constant. This quench corresponds to path B of Fig. 1(b) in the paper and alters both $\bar{n}$ and β in Eq. (1), namely both the asymptotic order and temperature. We consider quenches from the disordered (with $\Delta_c=-4\kappa$) to the ordered phase (with $\Delta_c=-\kappa$), and vice versa, assuming that the initial state is the asymptotic state of the parameter choice before the quench. Also in this case the three regimes can be identified. Remarkably, for the quench from the ordered to the disordered phase, the system remains for long times trapped in an ordered pattern. The pattern stays stable due to the long-range forces. This transient is further accompanied by a momentum distribution that is narrower than the initial and the asymptotic value, as visible in the inset of subplot (b). On

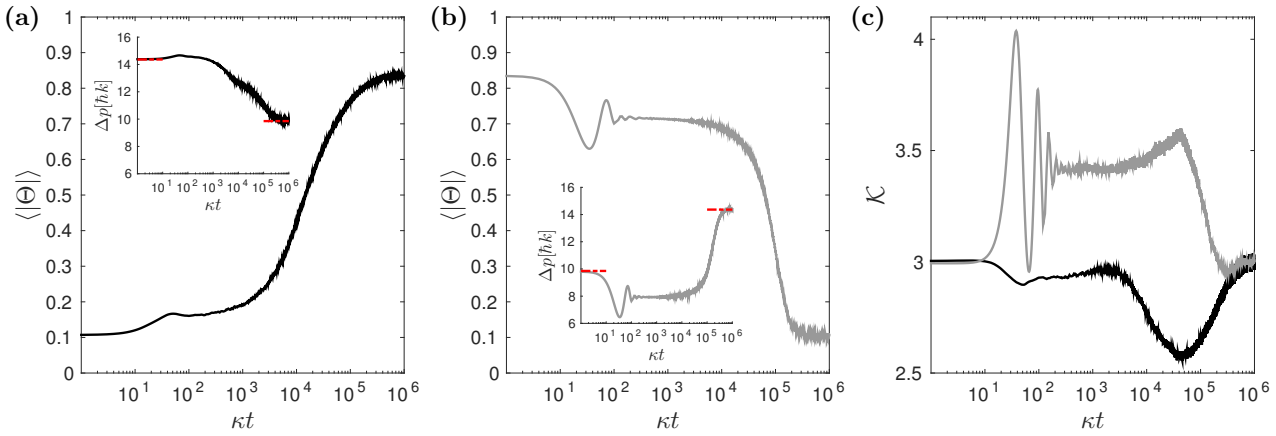

FIG. S1: Numerical simulation of the dynamics for $N = 50$ atoms following a sudden quench along path B, where Δ_c is varied but the laser intensity is kept fixed. The black line corresponds to the results for the evolution when the value of the detuning is suddenly quenched from $\Delta_c = -4\kappa$ with $\bar{n}_i \approx 0.44\,\bar{n}_c$ to $\Delta_c = -\kappa$ with $\bar{n}_f = 2\,\bar{n}_c$. The grey line displays the case where initial and final points are swapped. (a) and (b): Time evolution of $\langle|\Theta|\rangle$ and Δp (inset) as a function of time (in units of κ^{-1}). Subplot (c) displays the behaviour of the kurtosis $\mathcal{K}$.

the other hand, the momentum distribution is markedly non-Gaussian, as visible in (c). This behaviour shows that, even if the final value of the parameter $\bar{n}$ is well below threshold and the asymptotic number of intracavity photons $\langle\hat{a}^\dagger\hat{a}\rangle \approx N\bar{n}\langle\Theta^2\rangle$ is small, yet there is a metastable regime in which the number of intracavity photons is significantly larger, due to the metastable atomic patterns which support superradiant scattering of photons into the resonator until they decay.

[S1] S. Schütz and G. Morigi, Phys. Rev. Lett. **113**, 203002 (2014).
[S2] S. Schütz, S. B. Jäger, and G. Morigi, Phys. Rev. A **92**, 063808 (2015).
[S3] S. B. Jäger, S. Schütz, and G. Morigi, preprint arXiv:1603.05148 (2016).

CHAPTER 7

Supercooling of Atoms in an Optical Resonator

PHYSICAL REVIEW LETTERS **116**, 153002 (2016)

DOI: 10.1103/PhysRevLett.116.153002

Authors: Minghui Xu,[1,2] Simon B. Jäger,[3] S. Schütz,[3] J. Cooper,[1] Giovanna Morigi,[3] and M. J. Holland[1,2]

[1] *JILA, National Institute of Standards and Technology and Department of Physics, University of Colorado, Boulder, Colorado 80309-0440, USA*
[2] *Center for Theory of Quantum Matter, University of Colorado, Boulder, Colorado 80309, USA*
[3] *Theoretische Physik, Universität des Saarlandes, D-66123 Saarbrücken, Germany*

Author Contributions:
The theoretical model was developed by M. Xu, S. Schütz, M. J. Holland and G. Morigi. The numerical simulations were designed and performed by M. Xu. Analytical calculations were performed by M. Xu, J. Cooper and S. B. Jäger. The calculations and results were checked, discussed and analysed by all authors. The article was majorly written by M. Xu and M. J. Holland.

Abstract:
We investigate laser cooling of an ensemble of atoms in an optical cavity. We demonstrate that when atomic dipoles are synchronized in the regime of steady-state superradiance, the motion of the atoms may be subject to a giant frictional

force leading to potentially very low temperatures. The ultimate temperature limits are determined by a modified atomic linewidth, which can be orders of magnitude smaller than the cavity linewidth. The cooling rate is enhanced by the superradiant emission into the cavity mode allowing reasonable cooling rates even for dipolar transitions with ultranarrow linewidth.

PRL 116, 153002 (2016) PHYSICAL REVIEW LETTERS week ending 15 APRIL 2016

Supercooling of Atoms in an Optical Resonator

Minghui Xu,[1,2] Simon B. Jäger,[3] S. Schütz,[3] J. Cooper,[1] Giovanna Morigi,[3] and M. J. Holland[1,2]
[1]JILA, National Institute of Standards and Technology and Department of Physics, University of Colorado, Boulder, Colorado 80309-0440, USA
[2]Center for Theory of Quantum Matter, University of Colorado, Boulder, Colorado 80309, USA
[3]Theoretische Physik, Universität des Saarlandes, D-66123 Saarbrücken, Germany
(Received 11 December 2015; published 15 April 2016)

We investigate laser cooling of an ensemble of atoms in an optical cavity. We demonstrate that when atomic dipoles are synchronized in the regime of steady-state superradiance, the motion of the atoms may be subject to a giant frictional force leading to potentially very low temperatures. The ultimate temperature limits are determined by a modified atomic linewidth, which can be orders of magnitude smaller than the cavity linewidth. The cooling rate is enhanced by the superradiant emission into the cavity mode allowing reasonable cooling rates even for dipolar transitions with ultranarrow linewidth.

DOI: 10.1103/PhysRevLett.116.153002

The discovery of laser cooling [1] has enabled new areas of quantum gas physics and quantum state engineering [2]. Laser cooling is an essential technology in many fields, including precision measurements, quantum optics, and quantum information processing [3–5]. Doppler laser cooling [6,7] relies on repeated cycles of electronic excitation by lasers followed by spontaneous relaxation, reaching temperature limits determined by the atomic linewidth. Only specific atomic species can be Doppler cooled because they should possess an internal level structure that allows for closed cycling transitions.

Cavity-assisted laser cooling [8,9] utilizes the decay of an optical resonator instead of atomic spontaneous emission for energy dissipation. It is based on the preferential coherent scattering of laser photons into an optical cavity [10,11]. Temperatures that can be achieved in this way are limited by the cavity linewidth. Since the particle properties enter only through the coherent scattering amplitude, cavity-assisted cooling promises to be applicable to any polarizable object [12–20], including molecules [17,18] and even mesoscopic systems such as nanoparticles [19,20].

The many-atom effects of cavity-assisted cooling were theoretically discussed by Ritsch and collaborators [21] and experimentally reported [22,23]. The cavity-mediated atom-atom coupling typically leads to a cooling rate that is faster for an atomic ensemble than for a single atom. Self-organization may occur and is observed as patterns in the atomic distribution that maximize the cooperative scattering. Recently, it has been shown that the long-range nature of the cavity-mediated interaction between atoms gives rise to interesting prethermalization behavior [24]. In spite of the intrinsic many-body nature, the underlying cooling mechanism shares much with the single-atom case, and indeed the final temperature observed in these systems is limited by the cavity linewidth.

In this Letter, we demonstrate that the mechanical action of the atom-cavity coupling takes on a dramatically new character for atoms in the regime of steady-state superradiance [25–30]. Specifically, the frictional force on a single atom is significantly enhanced, and the final temperature is much lower than the temperature that can be achieved in cavity-assisted cooling [10,11]. Furthermore, as the atom number increases, the cooling may become faster due to the increasing rate of superradiant collective emission. We show that ability to achieve much lower temperatures than for single-atom cavity-assisted cooling derives from the emergence of atom-atom dipole correlations in the many-body atomic ensemble.

Steady-state superradiant lasers were proposed in Ref. [25] as possible systems for generating milliHertz linewidth light, and demonstrated in a recent experiment using a two-photon Raman transition [27]. In steady-state superradiance, the cavity decay is much faster than all other processes and plays the role of a dissipative collective coupling for the atoms that leads to the synchronization of atomic dipoles [29,30]. The emergence of a macroscopic collective dipole induces an extremely narrow linewidth for the generated light [25,30]. The optimal parameters are in the weak-coupling regime of cavity QED [31], which is opposite to the strong-coupling situation usually considered in cavity-assisted cooling [8,9]. Superradiant lasers require weak-dipole atoms (e.g., using intercombination lines or other forbidden transitions) confined in a high-finesse optical cavity.

We consider an ensemble of N pointlike two-level atoms with transition frequency ω_a and natural linewidth γ, interacting with a single-mode cavity with resonance frequency ω_c and linewidth κ, as shown in Fig. 1. The atoms are restricted to move freely along the direction of the cavity axis (x axis) and are tightly confined in the other two directions. The atom-cavity coupling is given by $g\cos(kx)$, where g is the vacuum Rabi frequency at the

PRL 116, 153002 (2016) PHYSICAL REVIEW LETTERS week ending 15 APRIL 2016

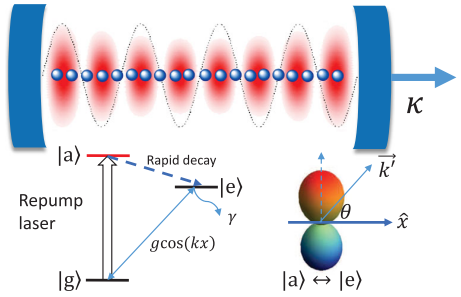

FIG. 1. Atoms with ultranarrow transition $|g\rangle \leftrightarrow |e\rangle$ are confined to the axis of a standing-wave mode of an optical cavity. Different implementations of pumping may be considered [25,27]. In the simplest scenario shown, a transition is driven from the ground state $|g\rangle$ to an auxiliary state $|a\rangle$ that rapidly decays to the excited state $|e\rangle$. In this way $|a\rangle$ can be adiabatically eliminated and a two-state pseudospin description in the $\{|g\rangle, |e\rangle\}$ subspace used, with repumping corresponding to an effective rate w from $|g\rangle$ to $|e\rangle$. If the repumping laser is directed normal to the cavity axis, the absorption does not modify the momentum. Momentum recoil is induced by the on-axis component of the wave vector $\vec{k}'$ of the dipole radiation pattern for the $|a\rangle \leftrightarrow |e\rangle$ transition.

field maximum, and $\cos(kx)$ describes the one-dimensional cavity mode function [32]. The atoms are incoherently repumped at rate w, providing the photon source.

The Hamiltonian in the rotating frame of the atomic transition frequency is given by

$$\hat{H} = \hbar\Delta\hat{a}^\dagger\hat{a} + \sum_{j=1}^{N}\frac{\hat{p}_j^2}{2m} + \hbar\frac{g}{2}\sum_{j=1}^{N}(\hat{a}^\dagger\hat{\sigma}_j^- + \hat{\sigma}_j^+\hat{a})\cos(k\hat{x}_j), \tag{1}$$

where $\Delta = \omega_c - \omega_a$. We have introduced the bosonic annihilation and creation operators, $\hat{a}$ and $\hat{a}^\dagger$, for cavity photons. The jth atom is represented by Pauli pseudospin operators, $\hat{\sigma}_j^z$ and $\hat{\sigma}_j^- = (\hat{\sigma}_j^+)^\dagger$, and position and momentum $\hat{x}_j$ and $\hat{p}_j$, respectively.

In the presence of dissipation, the evolution of the system is described by the Born-Markov quantum master equation for the density matrix $\hat{\rho}$ for the cavity and atoms,

$$\frac{d}{dt}\hat{\rho} = \frac{1}{i\hbar}[\hat{H},\hat{\rho}] + \kappa\mathcal{L}[\hat{a}]\rho + w\sum_{j=1}^{N}\int_{-1}^{1} duN(u)\mathcal{L}[\hat{\sigma}_j^+ e^{iuk'\hat{x}_j}]\rho, \tag{2}$$

where $\mathcal{L}[\hat{\mathcal{O}}]\hat{\rho} = (2\hat{\mathcal{O}}\hat{\rho}\hat{\mathcal{O}}^\dagger - \hat{\mathcal{O}}^\dagger\hat{\mathcal{O}}\hat{\rho} - \hat{\rho}\hat{\mathcal{O}}^\dagger\hat{\mathcal{O}})/2$ is the Linbladian superoperator describing the incoherent processes. The term proportional to κ describes the cavity decay. The repumping is the term proportional to w and is modeled by spontaneous absorption with recoil [33]. The recoil is parametrized by the normalized emission pattern $N(u)$ and wave vector k'. We neglect free-space spontaneous emission, since the natural linewidth γ is assumed to be extremely small for atoms with an ultraweak-dipole transition.

In the regime of interest, the cavity linewidth is much larger than other system frequencies, and the cavity field can be adiabatically eliminated, resulting in phase locking of the cavity field to the collective atomic dipole [26,29,30]. In order to correctly encapsulate the cavity cooling mechanism, the adiabatic elimination of the cavity field must be expanded beyond leading order. This includes retardation effects between the cavity field and atomic variables. As shown in the Supplemental Material [34], in the large κ limit [35],

$$\hat{a}(t) \approx \frac{-i\frac{g}{2}\hat{J}^-}{\kappa/2 + i\Delta} + \frac{\frac{d}{dt}(i\frac{g}{2}\hat{J}^-)}{(\kappa/2 + i\Delta)^2} - \frac{2i\sqrt{\Gamma_C}}{g}\hat{\xi}(t) + \mathcal{O}[\kappa^{-3}], \tag{3}$$

where $\hat{J}^- = \sum_{j=1}^{N}\hat{\sigma}_j^-\cos(k\hat{x}_j)$ is the collective dipole operator, $\Gamma_C = g^2\kappa/4(\kappa^2/4 + \Delta^2)$ is the spontaneous emission rate through the cavity, and $\hat{\xi}(t)$ is the quantum noise originating from the vacuum field entering through the cavity output.

The dipole force on the jth atom is given by the gradient of the potential energy, which takes the form

$$F_j = \frac{d}{dt}\hat{p}_j = -\nabla_j\hat{H} = \frac{1}{2}\hbar kg\sin(k\hat{x}_j)(\hat{\sigma}_j^+\hat{a} + \hat{a}^\dagger\hat{\sigma}_j^-). \tag{4}$$

We maximize the single-atom dissipative force by working at the detuning $\Delta = \kappa/2$ [34], and in that case by substituting Eq. (3) into Eq. (4), we find

$$\begin{aligned}\frac{d}{dt}\hat{p}_j \approx & -\frac{1}{2}\hbar k\Gamma_C\sin(k\hat{x}_j)((1+i)\hat{\sigma}_j^+\hat{J}^- + (1-i)\hat{J}^+\hat{\sigma}_j^-) \\ & -\frac{1}{2}\eta\Gamma_C\sin(k\hat{x}_j)\sum_{l=1}^{N}(\hat{\sigma}_j^+\hat{\sigma}_l^- + \hat{\sigma}_l^+\hat{\sigma}_j^-)\frac{1}{2}[\sin(k\hat{x}_l), \hat{p}_l]_+ \\ & + \hat{\mathcal{N}}_j. \end{aligned} \tag{5}$$

Here the anticommutator is $[\hat{A},\hat{B}]_+ = \hat{A}\hat{B} + \hat{B}\hat{A}$. We have defined $\eta = 4\omega_r/\kappa$, which characterizes the likelihood that a photon emission into the cavity mode will be in the same direction as the motion, in terms of the recoil frequency $\omega_r = \hbar k^2/2m$. The three terms on the right-hand side of Eq. (5) can be interpreted as the conservative force, the friction, and the noise-induced momentum fluctuations, respectively.

For temperatures above the recoil temperature, the motion is well described by a semiclassical treatment. A systematic semiclassical approximation, to make the mapping $\langle\hat{x}_j\rangle \to x_j$ and $\langle\hat{p}_j\rangle \to p_j$, where x_j and p_j are classical variables, is based on the symmetric ordering of operator expectation values. In order to accurately incorporate the effects of quantum noise, we match the equations of motion for the second-order moments of momenta between the quantum and semiclassical theories so that

we obtain the correct momentum diffusion [34]. This procedure yields Ito stochastic equations,

$$\frac{d}{dt}p_j \approx \hbar k\Gamma_C \sin(kx_j)(\mathrm{Im}[\langle\hat{\sigma}_j^+\hat{J}^-\rangle] - \mathrm{Re}[\langle\hat{\sigma}_j^+\hat{J}^-\rangle]) - \eta\Gamma_C \sin(kx_j)\sum_{l=1}^{N}\mathrm{Re}[\langle\hat{\sigma}_j^+\hat{\sigma}_l^-\rangle]\sin(kx_l)p_l + \xi_j^p, \tag{6}$$

where ξ_j^p is the classical noise and $\langle\xi_j^p(t)\xi_l^p(t')\rangle = D^{jl}\delta(t-t')$ with diffusion matrix

$$D^{jl} = \hbar^2k^2\Gamma_C \sin(kx_j)\sin(kx_l)\mathrm{Re}[\langle\hat{\sigma}_l^+\hat{\sigma}_j^-\rangle] + \hbar^2k'^2w\bar{u^2}\langle\hat{\sigma}_j^-\hat{\sigma}_l^+\rangle\delta_{jl}, \tag{7}$$

involving the geometrical average $\bar{u^2} \equiv \int_{-1}^{1} u^2N(u)du$ and Kronecker delta δ_{jl}. The momentum evolution is paired with the usual equation for x_j,

$$\frac{d}{dt}x_j = \frac{p_j}{m}. \tag{8}$$

We first consider the case in which the effect of recoil associated with the repumping is neglected; i.e., we set $k' = 0$. This determines the ultimate temperature limit imposed by the vacuum noise due to the cavity output. For the one-atom case, we can then find the friction (α) and diffusion (D) coefficient from Eq. (6) and Eq. (7). The steady-state temperature T for the single atom (labeled by 1) is

$$k_BT = \frac{\langle p_1^2\rangle}{m} = \frac{D}{2m\alpha} = \frac{\hbar\kappa}{4}, \tag{9}$$

since

$$D = \hbar^2k^2\Gamma_C\sin^2(kx_1)\langle\hat{\sigma}_1^+\hat{\sigma}_1^-\rangle, \quad \alpha = \eta\Gamma_C\sin^2(kx_1)\langle\hat{\sigma}_1^+\hat{\sigma}_1^-\rangle. \tag{10}$$

Note that this is precisely the same temperature limit previously found in the cavity-assisted cooling case where the system is operating in the strong coupling cavity-QED region. Here the rate of the decay into the cavity mode is proportional to $\Gamma_C\langle\hat{\sigma}_1^+\hat{\sigma}_1^-\rangle$, which is applicable to the weak coupling regime of cavity QED [31]. In Fig. 2(a), we show a numerical simulation of the cooling trajectory of a single atom as a function of time. As expected, the final temperature k_BT asymptotes to $\hbar\kappa/4$ and the cooling rate is well approximated by $R_S = \eta\Gamma_C\langle\hat{\sigma}_1^+\hat{\sigma}_1^-\rangle$.

The cooling in the many-atom case exhibits a distinctly different character. A feature of this model is the pseudospin-to-motion coupling of the atoms. In order to close the evolution equations of the atomic motion as described by Eq. (6) and Eq. (8), it is necessary to solve the pseudospin dynamics. For this purpose, we derive in the Supplemental Material [34] the quantum master equation for the pseudospins,

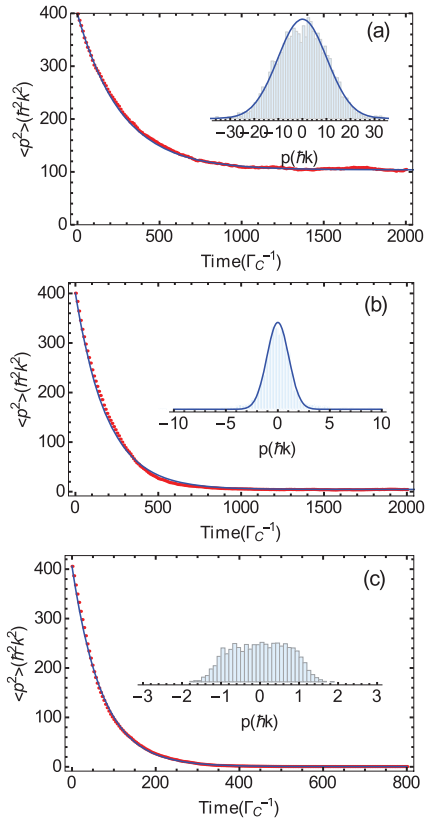

FIG. 2. Time evolution of the average momentum square (red dots) evaluated from 4000 trajectories simulated by integrating Eqs. (6) and (8) for 1 (a), 20 (b), and 60 atoms (c). The blue solid line is a fit to an exponential decay. The parameters are $\Delta = \kappa/2 = 100$, $\Gamma_C = 0.1$, and $\omega_r = 0.25$. The repumping rates are chosen such that the average atomic population inversion in all cases is the same [$w = 0.15$ (a), 0.28 (b), 1.3 (c)]. Insets show the momentum statistics. The blue solid line is a fit to a Gaussian distribution.

$$\frac{d}{dt}\hat{\rho} = \frac{1}{i\hbar}[\hat{H}_{\mathrm{eff}},\hat{\rho}] + \Gamma_C\mathcal{L}[\hat{J}^-]\hat{\rho} + w\sum_{j=1}^{N}\int_{-1}^{1}duN(u)\mathcal{L}[\hat{\sigma}_j^+e^{iuk'\hat{x}_j}]\rho, \tag{11}$$

where the effective Hamiltonian $\hat{H}_{\mathrm{eff}} = -\hbar\Gamma_C\hat{J}^+\hat{J}^-/2$ describes the coherent coupling between atoms, and the collective decay [term proportional to Γ_C in Eq. (11)] leads to dissipative coupling. It is the dissipative coupling that gives rise to dipole synchronization and steady-state superradiance [25–30]. The full pseudospin Hilbert space dimension scales exponentially with the atom number. To solve Eq. (11), we employ a cumulant approximation that is applicable to many atoms [26,29,30]. All nonzero observables are expanded in terms of $\langle\hat{\sigma}_j^+\hat{\sigma}_j^-\rangle$ and $\langle\hat{\sigma}_j^+\hat{\sigma}_l^-\rangle$ ($j \neq l$), describing the population inversion and spin-spin

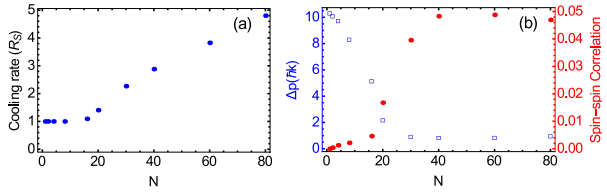

FIG. 3. (a) Cooling rate (in units of the single atom cooling rate R_S) as a function of atom number. (b) Final momentum width ($\Delta p = \sqrt{\langle p^2 \rangle}$, blue squares) and spin-spin correlation (red dots) as a function of atom number. The parameters are the same as those in Fig. 2.

correlations, respectively. Their equations of motion are derived in the Supplemental Material [34].

Simulations of the cooling dynamics for many atoms are shown in Figs. 2(b) and 2(c). Remarkably, we find the collective atomic effects lead to a more rapid cooling rate, and, simultaneously, to a lower final temperature. Figure 3 shows the cooling rate (a) and the final momentum width (b) as a function of the atom number. We note that the cooling rate exhibits two kinds of behavior, hinting towards the existence of an N-dependent threshold; see Fig. 3(a). For $N \lesssim 20$, the cooling rate is independent of N, while for $N \gtrsim 20$, it increases monotonically. Correspondingly, in this regime, the momentum width reaches a minimum independent of N; see Fig. 3(b). When the final temperature gets closer to the recoil temperature, the momentum distribution is no longer Gaussian, rendering the notion of temperature invalid. The semiclassical treatment predicts a uniform distribution in the momentum interval $[-\hbar k, \hbar k]$ corresponding to the recoil limit, as shown in the inset of Fig. 2(c). We note that sub-Doppler temperatures for a similar setup have been reported in Refs. [36–38], where spontaneous decay was assumed to be the fastest incoherent process. Differing from that regime, the recoil limit is here reached thanks to the small spontaneous decay rate. When the temperature approaches the recoil temperature, however, the validity of the semiclassical treatment of atomic motion is questionable and a full quantum model is necessary in order to determine the asymptotic energy. These results demonstrate that not only is the cooling more efficient due to the rapid rate of superradiant light emission, but also the final temperature is determined by the relaxation rate Γ_C of the atomic dipole, and not by the cavity linewidth.

The principal new feature is that spin-spin correlations between atoms develop due to the cavity-mediated coupling. In order to measure the extent of this effect, we introduce $\langle \hat{\sigma}^+ \hat{\sigma}^- \rangle_E$ defined as averaged spin-spin correlations,

$$\langle \hat{\sigma}^+ \hat{\sigma}^- \rangle_E = \left(\langle \hat{J}^+ \hat{J}^- \rangle - \sum_{j=1}^{N} \langle \hat{\sigma}_j^+ \hat{\sigma}_j^- \rangle \cos^2(k x_j) \right) / [N(N-1)]. \tag{12}$$

Figure 3(b) shows $\langle \hat{\sigma}^+ \hat{\sigma}^- \rangle_E$ as a function of the atom number. The equilibrium temperature decreases as the collective spin-spin correlation emerges. This is reminiscent of the linewidth of the superradiant laser, where the synchronization of spins leads to a significant reduction of the linewidth to the order of Γ_C [25,30]. The establishment of spin-spin correlations is a competition between dephasing due to both cavity output noise and repumping, and the dissipative coupling between atoms which tends to synchronize the dipoles [30]. Since the coupling strength scales with N, a sufficient atom number is required to establish strong spin-spin correlations [30].

Further characterizing the ultimate temperature limits, Fig. 4(a) shows the final momentum width as a function of Γ_C. We see that as Γ_C is decreased, the final temperature reduces in proportion to Γ_C until it hits the recoil limit. This effect is consistent with a significantly increased friction coefficient providing a reduction of the order of the final temperature from the one to many atom case from κ to Γ_C.

So far our discussion has neglected the recoil associated with repumping. We have done that because its effect on the final temperature will depend crucially on specifics of its implementation, including factors such as the polarizations and directions of repump lasers, the atomic system, and the transitions used. However, in the specific repumping model shown in Fig. 1, the magnitude of k' controls the recoil effect of the repumping on the momentum diffusion. Figure 4(b) shows the final momentum width as a function of repumping for $k' = 0$ and $k' = k$. Again, in the region of small and large repumping, where spin-spin correlations are very small, the final temperature is high. When the recoil due to repumping is included, the final temperature becomes higher and is eventually determined by $w\bar{u^2}$. However, for weak repumping, with w not significantly larger then Γ_C it is still possible to achieve temperatures not much higher than that predicted when pump recoil was neglected. This is especially promising for the implementation of supercooling in realistic experimental systems. Note that $k = k'$ is more or less a worst case scenario, since by using a dipole allowed transition for the relaxation from the auxiliary state to the excited state, one could, in

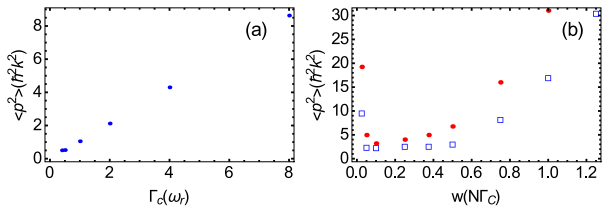

FIG. 4. (a) Final momentum width as a function of Γ_C for 40 atoms. The parameters are $\Delta = \kappa/2 = 200$, $w = N\Gamma_C/4$, and $\omega_r = 0.25$. (b) Final momentum width as a function of repumping strength for 40 atoms without ($k' = 0$, blue squares) and with recoil associated with repumping ($k' = k$, red dots). The parameters are $\Delta = \kappa/2 = 200$, $\Gamma_C = 0.5$, and $\omega_r = 0.25$.

principle, use a much reduced frequency with correspondingly small recoil.

In conclusion, we have proposed supercooling of the atomic motion along the axis of an optical cavity. The superradiant emission was observed to lead to an enhanced cooling rate and extremely low final temperature. The ultimate temperatures were constrained by the relaxation of the atomic dipole, and may be orders of magnitude lower than for single atom cooling where temperatures are limited by the cavity linewidth. From a broader viewpoint, we have demonstrated an example of many-body laser cooling in which all motional degrees of freedom of a collective system are simultaneously cooled, and in which macroscopic spin-spin correlations are essential and must develop for the cooling mechanism to work.

We acknowledge helpful discussions with A. M. Rey, J. Ye, and J. K. Thompson. This work has been supported by the DARPA QuASAR program, the NSF (Grants No. AMO-1404263, No. PFC-1125844, and No. QIS-1521080), NIST, the German Research Foundation (DACH project "Quantum crystals of matter and light"), and the German Ministry of Education and Research BMBF (Q.Com).

[1] C. E. Wieman, D. E. Pritchard, and D. J. Wineland, Rev. Mod. Phys. **71**, S253 (1999).
[2] I. Bloch, J. Dalibard, and W. Zwerger, Rev. Mod. Phys. **80**, 885 (2008).
[3] A. D. Ludlow, M. M. Boyd, J. Ye, E. Peik, and P. O. Schmidt, Rev. Mod. Phys. **87**, 637 (2015).
[4] I. A. Walmsley, Science **348**, 525 (2015).
[5] D. J. Wineland, Rev. Mod. Phys. **85**, 1103 (2013).
[6] T. W. Hänsch and A. L. Schawlow, Opt. Commun. **13**, 68 (1975).
[7] D. J. Wineland and W. M. Itano, Phys. Rev. A **20**, 1521 (1979).
[8] P. Domokos and H. Ritsch, J. Opt. Soc. Am. B **20**, 1098 (2003).
[9] H. Ritsch, P. Domokos, F. Brennecke, and T. Esslinger, Rev. Mod. Phys. **85**, 553 (2013).
[10] P. Horak, G. Hechenblaikner, K. M. Gheri, H. Stecher, and H. Ritsch, Phys. Rev. Lett. **79**, 4974 (1997).
[11] V. Vuletić and S. Chu, Phys. Rev. Lett. **84**, 3787 (2000).
[12] J. McKeever, J. R. Buck, A. D. Boozer, A. Kuzmich, H.-C. Nägerl, D. M. Stamper-Kurn, and H. J. Kimble, Phys. Rev. Lett. **90**, 133602 (2003).
[13] P. Maunz, T. Puppe, I. Schuster, N. Syassen, P. W. H. Pinkse, and G. Rempe, Nature (London) **428**, 50 (2004).
[14] D. R. Leibrandt, J. Labaziewicz, V. Vuletić, and I. L. Chuang, Phys. Rev. Lett. **103**, 103001 (2009).
[15] M. H. Schleier-Smith, I. D. Leroux, H. Zhang, M. A. Van Camp, and V. Vuletić, Phys. Rev. Lett. **107**, 143005 (2011).
[16] M. Wolke, J. Klinner, H. Kessler, and A. Hemmerich, Science **337**, 75 (2012).
[17] G. Morigi, P. W. H. Pinkse, M. Kowalewski, and R. deVivie-Riedle, Phys. Rev. Lett. **99**, 073001 (2007).
[18] B. L. Lev, A. Vukics, E. R. Hudson, B. C. Sawyer, P. Domokos, H. Ritsch, and J. Ye, Phys. Rev. A **77**, 023402 (2008).
[19] N. Kiesel, F. Blaser, U. Delic, D. Grass, R. Kaltenbaek, and M. Aspelmeyer, Proc. Natl. Acad. Sci. U.S.A. **110**, 14180 (2013).
[20] J. Millen, P. Z. G. Fonseca, T. Mavrogordatos, T. S. Monteiro, and P. F. Barker, Phys. Rev. Lett. **114**, 123602 (2015).
[21] P. Domokos and H. Ritsch, Phys. Rev. Lett. **89**, 253003 (2002).
[22] H. W. Chan, A. T. Black, and V. Vuletić, Phys. Rev. Lett. **90**, 063003 (2003).
[23] K. J. Arnold, M. P. Baden, and M. D. Barrett, Phys. Rev. Lett. **109**, 153002 (2012).
[24] S. Schütz and G. Morigi, Phys. Rev. Lett. **113**, 203002 (2014).
[25] D. Meiser, J. Ye, D. R. Carlson, and M. J. Holland, Phys. Rev. Lett. **102**, 163601 (2009).
[26] D. Meiser and M. J. Holland, Phys. Rev. A **81**, 033847 (2010); **81**, 063827 (2010).
[27] J. G. Bohnet, Z. Chen, J. M. Weiner, D. Meiser, M. J. Holland, and J. K. Thompson, Nature (London) **484**, 78 (2012).
[28] J. G. Bohnet, Z. Chen, J. M. Weiner, K. C. Cox, and J. K. Thompson, Phys. Rev. Lett. **109**, 253602 (2012).
[29] Minghui Xu, D. A. Tieri, E. C. Fine, J. K. Thompson, and M. J. Holland, Phys. Rev. Lett. **113**, 154101 (2014).
[30] Minghui Xu and M. J. Holland, Phys. Rev. Lett. **114**, 103601 (2015).
[31] P. Meystre and M. Sargent III, *Elements of Quantum Optics* (Springer, New York, 1998).
[32] The finite spatial mode of the cavity causes a spread in g. This leads to a reduced effective atom number, which has no significant impact on the cooling mechanisms discussed in this Letter.
[33] H. Haken, *Laser Theory* (Springer, Berlin, 1984).
[34] See Supplemental Material at http://link.aps.org/supplemental/10.1103/PhysRevLett.116.153002, which includes Refs. [26,29], for the derivation of the equations for the adiabatic elimination of the cavity mode, for the external motion of atoms, and for the internal dynamics of atoms.
[35] This requires $\kappa \gg \sqrt{N\bar{n}}g, w$, and $k\sqrt{\langle p^2 \rangle}/m$, where $\bar{n}$ is the mean photon number in the cavity.
[36] T. Salzburger and H. Ritsch, Phys. Rev. Lett. **93**, 063002 (2004).
[37] T. Salzburger, P. Domokos, and H. Ritsch, Phys. Rev. A **72**, 033805 (2005).
[38] T. Salzburger and H. Ritsch, Phys. Rev. A **74**, 033806 (2006).

Supplemental Material for Supercooling of Atoms in an Optical Resonator

I. ADIABATIC ELIMINATION OF THE CAVITY MODE

The regime of steady-state superradiance is defined by a timescale separation between the single cavity mode and the atomic degrees of freedom. The typical relaxation time of the cavity mode is of the order of $T_C \sim |\kappa + i\Delta|^{-1}$, while the one of the atoms is given by $T_A \sim \left(\max\left\{\sqrt{N\bar{n}}g, w, k\sqrt{\langle p^2\rangle}/m\right\}\right)^{-1}$, where $\bar{n}$ is the mean photon number in the cavity. In order to eliminate the cavity field quasiadiabatically we need the relaxation time of the cavity to be much shorter than the timescale on which the atoms are evolving, namely $T_A \gg T_C$. To this end, we start with the quantum Langevin equation for the cavity field according to the quantum master equation [Eq. (2) in the paper],

$$\frac{d}{dt}\hat{a} = -\frac{\kappa}{2}\hat{a} - i\Delta\hat{a} - i\frac{g}{2}\hat{J}^- + \sqrt{\kappa}\hat{\xi}(t)\,, \tag{S1}$$

where $\hat{\xi}(t)$ is the quantum white noise and $\langle\hat{\xi}(t)\hat{\xi}^\dagger(t')\rangle = \delta(t-t')$. The formal solution to Eq. (S1) is

$$\hat{a}(t) = e^{-(\kappa/2+i\Delta)\Delta t}\hat{a}(t_0) - i\frac{g}{2}\int_0^{\Delta t} ds e^{-(\kappa/2+i\Delta)s}\hat{J}^-(t-s) + \hat{\mathcal{F}}(t)\,, \tag{S2}$$

where $\hat{\mathcal{F}}(t) = \sqrt{\kappa}\int_0^{\Delta t} ds e^{-(\kappa/2+i\Delta)s}\hat{\xi}(t-s)$ is the noise term and $\Delta t = t - t_0$. Under the approximation of coarse graining ($T_A \gg \Delta t \gg T_C$), the first term on the right-hand side (RHS) of Eq. (S2) vanishes, and it can be shown that

$$\langle\hat{\mathcal{F}}(t)\hat{\mathcal{F}}^\dagger(t')\rangle \approx e^{-\kappa|t'-t|/2 - i\Delta(t-t')} \approx \frac{\kappa}{\kappa^2/4+\Delta^2}\delta(t-t')\,. \tag{S3}$$

It would be convenient to choose $\hat{\mathcal{F}}(t) = -i\frac{\sqrt{\Gamma_C}}{g/2}\hat{\xi}(t)$, with

$$\Gamma_C = \frac{g^2\kappa/4}{\kappa^2/4+\Delta^2}. \tag{S4}$$

Furthermore, the integral in Eq. (S2) can be expanded in powers of $1/(\kappa/2+i\Delta)$. As a result we obtain

$$\hat{a}(t) \approx \frac{-i\frac{g}{2}\hat{J}^-}{\kappa/2+i\Delta} - \frac{\frac{d}{dt}(-i\frac{g}{2}\hat{J}^-)}{(\kappa/2+i\Delta)^2} + \hat{\mathcal{F}}(t) + O[(\kappa/2+i\Delta)^{-3}]\,. \tag{S5}$$

As can be seen from Eq. (S5), the retardation effects between the cavity field and atomic variables are included.

II. EXTERNAL MOTION OF ATOMS

In this section we derive the force for the external degrees of freedom, including friction and noise. We will end up with a classical description of the particles' external degrees of freedom and derive a Langevin equation for the momenta of the particles.

The force on the j-th atom $\hat{F}_j$ is given by

$$\hat{F}_j = \frac{d}{dt}\hat{p}_j = \hbar k\sin(k\hat{x}_j)\frac{g}{2}(\hat{\sigma}_j^+\hat{a} + \hat{a}^\dagger\hat{\sigma}_j^-) + \hat{\mathcal{N}}_j^{\text{pump}}\,, \tag{S6}$$

where $\hat{\mathcal{N}}_j^{\text{pump}}$ represents the random force due to recoil of the incoherent pumping process.
Substituting Eq. (S5) into the above equation , we have

$$\begin{aligned}\frac{d}{dt}\hat{p}_j \approx{}& \hbar k\sin(k\hat{x}_j)\frac{\Gamma_C}{2}\left(-i\hat{\sigma}_j^+\hat{J}^- + i\hat{J}^+\hat{\sigma}_j^-\right) - \hbar k\sin(k\hat{x}_j)\frac{\Gamma_\Delta}{2}\sum_{l=1}^{N}\cos(kx_l)\left(\hat{\sigma}_j^+\hat{\sigma}_l^- + \hat{\sigma}_l^+\hat{\sigma}_j^- - \beta_1\hat{\sigma}_j^+\frac{d}{dt}\hat{\sigma}_l^- - \beta_1^*\frac{d}{dt}\hat{\sigma}_l^+\hat{\sigma}_j^-\right)\\ &- \sin(k\hat{x}_j)\frac{\Gamma_C}{2}\sum_{l=1}^{N}\frac{\eta}{2}\left[\sin(k\hat{x}_l),\hat{p}_l\right]_+\left(\hat{\sigma}_j^+\hat{\sigma}_l^- + \hat{\sigma}_l^+\hat{\sigma}_j^- + \beta_2\hat{\sigma}_j^+\hat{\sigma}_l^- + \beta_2^*\hat{\sigma}_l^+\hat{\sigma}_j^-\right) + \hat{\mathcal{N}}_j\,,\end{aligned} \tag{S7}$$

where $\left[\hat{A},\hat{B}\right]_+ = \hat{A}\hat{B}+\hat{B}\hat{A}$ is the anticommutator and the coefficients are

$$\Gamma_\Delta = \frac{g^2\Delta/2}{\kappa^2/4+\Delta^2},\quad \beta_1 = \frac{\kappa}{\kappa^2/4+\Delta^2}+i\frac{\kappa^2/4-\Delta^2}{\Delta(\kappa^2/4+\Delta^2)},\quad \beta_2 = i\frac{\kappa^2/4-\Delta^2}{\kappa\Delta},\quad \eta = \frac{4\omega_r\Delta}{\kappa^2/4+\Delta^2}. \tag{S8}$$

Here $\hat{\mathcal{N}}_j = \hat{\mathcal{N}}_j^{\rm cav}+\hat{\mathcal{N}}_j^{\rm pump}$ is the sum of the noise processes originating from the cavity output $\hat{\mathcal{N}}_j^{\rm cav}$ and repumping $\hat{\mathcal{N}}_j^{\rm pump}$. In the first line of equation (S7) we neglect β_1 because in the steady state superradiance regime it holds that $|\beta_1|\langle\hat{\sigma}_j^+\frac{d}{dt}\hat{\sigma}_l^-\rangle \sim \frac{w}{\kappa}\langle\hat{\sigma}_j^+\hat{\sigma}_l^-\rangle \ll \langle\hat{\sigma}_j^+\hat{\sigma}_l^-\rangle$. This has also been checked numerically. Therefore we get

$$\frac{d}{dt}\hat{p}_j = \frac{d}{dt}\hat{p}_j^0+\hat{\mathcal{N}}_j, \tag{S9}$$

where we define the force without noise as

$$\begin{aligned}\frac{d}{dt}\hat{p}_j^0 \approx{}& \hbar k\sin(k\hat{x}_j)\frac{\Gamma_C}{2}\left(-i\hat{\sigma}_j^+\hat{J}^- + i\hat{J}^+\hat{\sigma}_j^-\right) - \hbar k\sin(k\hat{x}_j)\frac{\Gamma_\Delta}{2}\sum_{l=1}^{N}\cos(kx_l)\left(\hat{\sigma}_j^+\hat{\sigma}_l^- + \hat{\sigma}_l^+\hat{\sigma}_j^-\right)\\ &-\sin(k\hat{x}_j)\frac{\Gamma_C}{2}\sum_{l=1}^{N}\frac{\eta}{2}\left[\sin(k\hat{x}_l),\hat{p}_l\right]_+\left(\hat{\sigma}_j^+\hat{\sigma}_l^- + \hat{\sigma}_l^+\hat{\sigma}_j^- + \beta_2\hat{\sigma}_j^+\hat{\sigma}_l^- + \beta_2^*\hat{\sigma}_l^+\hat{\sigma}_j^-\right).\end{aligned} \tag{S10}$$

We work at the detuning $\Delta=\kappa/2$ so that η is maximized and β_2 vanishes. As a result we obtain

$$\frac{d}{dt}\hat{p}_j^0 \approx \hbar k\sin(k\hat{x}_j)\frac{\Gamma_C}{2}\left(-i\hat{\sigma}_j^+\hat{J}^- + i\hat{J}^+\hat{\sigma}_j^- - \hat{\sigma}_j^+\hat{J}^- - \hat{J}^+\hat{\sigma}_j^-\right) - \sin(k\hat{x}_j)\frac{\Gamma_C}{2}\sum_{l=1}^{N}\frac{\eta}{2}\left[\sin(k\hat{x}_l),\hat{p}_l\right]_+\left(\hat{\sigma}_j^+\hat{\sigma}_l^- + \hat{\sigma}_l^+\hat{\sigma}_j^-\right). \tag{S11}$$

The first term on the RHS of Eq. (S11) represents forces originating from the adiabatic component of the cavity field, while the second term represents the frictional force arising from retardation effects. The noise term $\hat{\mathcal{N}}_j$ in equation (S9) gives rise to momentum diffusion due to quantum noises associated with incoherent processes. So we derive the equations of motion for the second moments of momenta,

$$\frac{d}{dt}\left\langle\hat{p}_j\hat{p}_l\right\rangle = \left\langle\hat{p}_j^0\frac{d\hat{p}_l^0}{dt}\right\rangle + \left\langle\frac{d\hat{p}_j^0}{dt}\hat{p}_l^0\right\rangle + \Gamma_C\hbar^2k^2\langle\sin(k\hat{x}_j)\sin(k\hat{x}_l)\hat{\sigma}_j^+\hat{\sigma}_l^-\rangle + w\delta_{jl}\hbar^2k'^2\overline{u^2}\langle\hat{\sigma}_j^-\hat{\sigma}_l^+\rangle, \tag{S12}$$

where δ_{jl} is the Kronecker delta, and $\overline{u^2}$ is the second moment of the dipole radiation pattern, *i.e.*,

$$\overline{u^2} = \int_{-1}^{1}duN(u)u^2 = \frac{2}{5}, \tag{S13}$$

where we have taken the dipole pattern $N(u)=\frac{3}{2}|u|\sqrt{1-u^2}$.
We treat the external atomic motion classically under the assumption that the momentum width of the particles $\sqrt{\langle p^2\rangle}$ is larger than the single photon recoil $\hbar k$. So we make the mapping $\langle\hat{p}_j\rangle\to p_j$ and $\langle\hat{x}_j\rangle\to x_j$. As a result this leads to

$$\frac{d}{dt}p_j = \frac{d}{dt}p_j^0+\xi_j^p, \tag{S14}$$

with

$$\frac{d}{dt}p_j^0 = \hbar k\sin(kx_j)\Gamma_C\left(\mathrm{Im}[\langle\hat{\sigma}_j^+\hat{J}^-\rangle]-\mathrm{Re}[\langle\hat{\sigma}_j^+\hat{J}^-\rangle]\right) - \sin(kx_j)\Gamma_C\sum_{l=1}^{N}\eta\mathrm{Re}[\langle\hat{\sigma}_j^+\hat{\sigma}_l^-\rangle]\sin(kx_l)p_l, \tag{S15}$$

where ξ_j^p is the classical noise acting on the momentum of j-th atom and $\langle\xi_j^p(t)\xi_l^p(t')\rangle = D^{jl}\delta(t-t')$. The diffusion matrix D^{jl} can be computed by making quantum-classical correspondence for the second moments. According to Eq. (S14),

$$\frac{d}{dt}\langle p_jp_l\rangle = \left\langle p_j^0\frac{dp_l^0}{dt}\right\rangle + \left\langle\frac{dp_j^0}{dt}p_l^0\right\rangle + D^{jl}. \tag{S16}$$

We use symmetric ordering of quantum operators for the quantum-classical correspondence, *i.e.*, $\frac{1}{2}\left\langle\left[\hat{p}_j,\frac{d\hat{p}_l}{dt}\right]_+\right\rangle \to \left\langle p_j\frac{dp_l}{dt}\right\rangle$. Matching Eq. (S12) and Eq. (S16), we get

$$D^{jl} = \Gamma_C\hbar^2k^2\sin(kx_j)\sin(kx_l)\mathrm{Re}[\langle\hat{\sigma}_l^+\hat{\sigma}_j^-\rangle] + w\delta_{jl}\hbar^2k'^2\overline{u^2}\langle\hat{\sigma}_j^-\hat{\sigma}_l^+\rangle. \tag{S17}$$

Therefore, we could simulate the external motion of atoms with Eq. (S14) and the equation of motion for x_j

$$\frac{d}{dt}x_j = \frac{p_j}{m}\,. \tag{S18}$$

The classical noises ξ_j^p with diffusion matrix D^{jl} make sure that we have the right second order moments for momenta.

III. INTERNAL DYNAMICS OF ATOMS

For the complete simulation of the atomic variables we also need to derive an equation for the internal degrees of freedom. In this section we will derive the equations of motions for the spins in which we drop third-order cumulants. For the internal dynamics of atoms in a superradiant laser, it is sufficient to keep the first order term in Eq. (S5),

$$\hat{a}(t) \approx -i\frac{\Gamma_C}{g}\hat{J}^- - \frac{\Gamma_\Delta}{g}\hat{J}^- + \hat{\mathcal{F}}(t)\,. \tag{S19}$$

Here, retardation effects are not included because they give rise to corrections that are of higher order and their contribution is negligible. This was also checked numerically. The adiabatic elimination of the cavity field leads to an effective quantum master equation for the atomic spins only

$$\frac{d}{dt}\rho = \frac{1}{i\hbar}[\hat{H}_{\rm eff},\rho] + \Gamma_C\mathcal{L}[\hat{J}^-]\rho + w\sum_{j=1}^{N}\int_{-1}^{1} duN(u)\mathcal{L}[\hat{\sigma}_j^+ e^{i\vec{k}'\cdot\vec{x}_j}]\rho\,, \tag{S20}$$

where the Hamiltonian $\hat{H}_{\rm eff} = -\frac{\hbar\Gamma_\Delta}{2}\hat{J}^+\hat{J}^-$ describes the coherent coupling between each pair of atoms, and the collective decay [term $\Gamma_C\mathcal{L}[\hat{J}^-]$ in Eq. (S20)] leads to dissipative coupling. We want to emphasize that this atomic master equation is not sufficient for the external degrees of freedom, which are treated in section II separately, and for which retardation effects are not negligible.

The spin degrees of freedom of atoms scale exponentially with the number of atoms. To solve Eq. (S20), we thus use a semiclassical approximation that is applicable to large atom numbers in the steady-state superradiance [S1, S2]. Cumulants for the expectation values of spin operators are expanded to second order. Because of the U(1) symmetry, $\langle\hat{\sigma}_j^\pm\rangle = 0$. Therefore, all nonzero observables are expanded in terms of $\langle\hat{\sigma}_j^+\hat{\sigma}_j^-\rangle$ and $\langle\hat{\sigma}_j^+\hat{\sigma}_l^-\rangle$ ($j \neq l$). Their equations of motion can then be found from the effective master equation,

$$\begin{aligned}
\frac{d}{dt}\langle\hat{\sigma}_j^+\hat{\sigma}_j^-\rangle &= w(1-\langle\hat{\sigma}_j^+\hat{\sigma}_j^-\rangle) - \frac{1}{2}(\Gamma_C + i\Gamma_\Delta)\cos(k\hat{x}_j)\langle\hat{J}^+\hat{\sigma}_j^-\rangle - \frac{1}{2}(\Gamma_C - i\Gamma_\Delta)\cos(k\hat{x}_j)\langle\hat{\sigma}_j^+\hat{J}^-\rangle,\\
\frac{d}{dt}\langle\hat{\sigma}_j^+\hat{\sigma}_l^-\rangle &= -w\langle\hat{\sigma}_j^+\hat{\sigma}_l^-\rangle + \frac{1}{2}(\Gamma_C + i\Gamma_\Delta)\cos(k\hat{x}_j)\langle\hat{J}^+\hat{\sigma}_l^-\hat{\sigma}_j^z\rangle + \frac{1}{2}(\Gamma_C - i\Gamma_\Delta)\cos(k\hat{x}_l)\langle\hat{\sigma}_l^z\hat{\sigma}_j^+\hat{J}^-\rangle\\
&\approx -\Big(w + (\Gamma_C + i\Gamma_\Delta)\cos^2(k\hat{x}_j)\langle\hat{\sigma}_j^+\hat{\sigma}_j^-\rangle + (\Gamma_C - i\Gamma_\Delta)\cos^2(k\hat{x}_l)\langle\hat{\sigma}_l^+\hat{\sigma}_l^-\rangle\Big)\langle\hat{\sigma}_j^+\hat{\sigma}_l^-\rangle\\
&\quad + \frac{1}{2}(\Gamma_C + i\Gamma_\Delta)\cos(k\hat{x}_j)(2\langle\hat{\sigma}_j^+\hat{\sigma}_j^-\rangle - 1)\langle\hat{J}^+\hat{\sigma}_l^-\rangle + \frac{1}{2}(\Gamma_C - i\Gamma_\Delta)\cos(k\hat{x}_l)(2\langle\hat{\sigma}_l^+\hat{\sigma}_l^-\rangle - 1)\langle\hat{\sigma}_j^+\hat{J}^-\rangle,
\end{aligned} \tag{S21}$$

describing the population inversion and spin-spin correlation respectively. In deriving Eq. (S21), we have dropped the third-order cumulants. In the simulations we integrate (S14), (S18) and (S21) simultaneously.

[S1] D. Meiser and M. J. Holland, Phys. Rev. A **81**, 033847 (2010); *ibid.* **81**, 063827 (2010).
[S2] Minghui Xu, D. A. Tieri, E. C. Fine, J. K. Thompson, and M. J. Holland, Phys. Rev. Lett. **113**, 154101 (2014).

Conclusions & outlook

Summary of results

This thesis investigates long-range interactions, acting on atomic external and/or internal degrees of freedom. Those interactions are induced by a common coupling to a lossy cavity mode. The major part of this thesis considers atoms that are exposed to a transverse coherent laser drive (Chapters 1-6), while the latter is replaced by an incoherent drive in Chapter 7. These setups represent driven-dissipative long-range interacting systems, realized in cavity quantum electrodynamics.

For the case of laser-driven atoms in an optical cavity, this work contains the explicit derivation of a self-consistent theory that treats the cavity field fully quantum-mechanically [74]. Such an approach is crucial below the self-organization threshold, when the atoms form a homogeneous spatial distribution and the scattered photons destructively interfere, such that the cavity field is close to the vacuum[1] [67].
The treatment in this thesis relies on a semiclassical limit for the atomic motion, in which a time-scale separation between the dynamics of atomic motion and cavity field can be identified [74, 96]. This is consistent when the rate of photon losses κ is much larger than the recoil frequency ω_r of the atoms, $\kappa \gg \omega_r$. This approach delivers a Fokker-Planck equation for the atomic motion only, the intracavity (quantum) field being eliminated quasiadiabatically and in a consistent manner. Inspection of the steady state of this Fokker-Planck equation[2] shows that the final atomic momentum distribution is a Gaussian whose width can be identified with

[1] Therefore, it complements several theoretical studies that assume a large intracavity photon number (semiclassical limit for the cavity field) [43, 45, 66], which is arguable in this regime.

[2] The steady state is determined analytically only in the limit $NU \ll \kappa$ [64, 77, 88], with N the number of atoms and U the dynamical Stark shift.

a temperature, in accordance to former treatments [43]. It is worth to point out that, in the present approach, temperature is not an external parameter [66], but the result of photon scattering processes associated to the driven-dissipative dynamics in the long-time limit. The steady state, interestingly, obeys the form of a canonical distribution, characterized by a long-range interacting Hamiltonian and a temperature [64, 77]. This implies that the driven-dissipative dynamics, in the long-time limit, drives the system to thermal equilibrium, allowing for the appliance of standard concepts of statistical mechanics. By defining a convenient order parameter Θ [66] and an explicit mapping of the free energy to a Landau model [76], the transition to spatially ordered patterns has been identified as a second-order phase transition [77].

The dynamics at steady state has been studied by numerical simulations[3] [36, 82, 83]. On the one hand, those studies have focused on the stability of the Bragg gratings [77]. The statistics of its residence time (trapping times [75]) has been analysed, including the characterization of the time scale (jumping times) required for the dynamical switching [45] between Bragg gratings. While this switching between spatial patterns for laser-driven atoms is induced by thermal fluctuations, we have shown that a deterministic (desired) switching can be tailored by a proper phase choice of an additional cavity laser drive [87]. On the other hand, for the case of laser-driven atoms, the properties of the light field, which give information on the spatial density [67, 97], have been analysed in detail. This analysis includes the intracavity photon number, the photon statistics and spectrum of the cavity output [64, 77, 88]. For the considered setup, remarkable similarities can be identified in observations with atoms in the ultracold regime [67, 72, 98, 99].

This thesis further provides new insight in the onset of self-organization, observed after a quench (sudden change in the laser intensity, for instance) from the homogeneous into the ordered phase in the driven-dissipative system [64, 78]. The long-range character of the intrinsically present dissipative forces [89] is crucial for the features that we observe in the long-term dynamics. First, after a fast relaxation, that can be well described by a Vlasov instability [35, 88, 100, 101], the system evolves into a prethermalized stage, being characterized by a non-Gaussian (non-thermal) momentum distribution. This initial dynamics can be well approximated by a mean-field dynamics, derived from a mean-field treatment [78, 88]. Even though this mean-field description well captures both the initial dynamics and the steady state (for large atomic ensembles), it fails in predicting the long-term behavior in the relaxation dynamics towards steady state. It has been verified that the peculiar long-range character of the dissipative

[3] In this thesis, numerical simulations have mainly been performed with MATLAB.

dynamics can push the system even further away from equilibrium, ultimately leading to larger relaxation time scales than those of the mean-field approach [78, 88]. Furthermore, we have shown that, in a properly defined thermodynamic limit [64], these features persist and even longer relaxation times are expected when increasing the size of the atomic ensemble [78].

On the basis of these findings we identify several questions, which we discuss in the following.

Open questions & Outlook

Besides the assumption of thermal atoms in a bad cavity, summarized by the condition $\kappa \gg \omega_r$, the steady state of self-organization has been derived in the regime far from optical bistability, $|NU| \ll \kappa$. While effects of those virtual scattering processes scaling with U have been discarded in the derivation of the analytical steady state, they have been taken into account in a consistent manner in the numerical simulations, at the same footing as retardation effects [77]. Taking into account further corrections in this optomechanical coupling (in the adiabatic cavity limit) results in cavity-mediated forces which can not be derived from a conservative potential [18]. The resulting nonlinear dynamics might result in a steady state that does not fulfill detailed balance, thus being out-of-equilibrium. Optical bistability [24] is expected to be observable for large field intensities and can result in oscillatory behavior. Similar observations have been made in theoretical studies for a laser-driven BEC in the regime $|NU| \simeq \kappa$ [73].

Indeed, a series of experiments for an ensemble of laser-driven atoms has been realized in the ultracold regime, loading a Bose-Einstein condensate into a resonator [37, 47, 67, 70, 72, 102]. Here, the transition to a grating can be mapped to a Dicke model and with it to a second-order phase transition [37, 38, 47]. In comparison to the model of thermal atoms in this thesis, remarkable qualitative (and to some extent quantitative) agreement is found, for instance, for the intracavity photon number, the photon statistics or the spectrum at the cavity output [67, 72]. At least, this implies the question in how far matter-wave coherence is crucial for the observed phenomena [103]. The analogies are indeed surprising, since the semiclassical model is outside the regime of validity in the ultracold realm [74]. Nevertheless, in the experiments performed in Refs. [37, 47, 67, 72] at the ETH in Zürich, the condition $\kappa \gg \omega_r$, for which the semiclassical model predicts thermal equilibrium in the long-time limit, is met. In this treatment and for such a large atomic ensemble ($N \approx 10^5$), however, relaxation times towards steady state in the order of several seconds are expected [78]. Such experimental time scales are hardly accessible due to other loss processes which have not been accounted for in this model.

This arises the question in how far the steady state, predicted by the semiclassical model and due to the dissipative dynamics, can be reached in those experiments. Furthermore, phase diagrams are often recorded by (slow) ramps in the intensity (or detuning) [37, 104]. In the semiclassical regime, as has been shown, (sudden) changes in the control parameter usually result in the creation of metastable states that, only in the long-time limit, evolve towards steady state [78]. Evidence of such metastable states might play a role in recently measured hysteresis behaviors [104]. We remind that the dynamics is governed by the interplay of long-range dispersive and dissipative forces, the latter scaling the rate for reaching the ultimate steady state. The semiclassical model reveals that both dispersive and dissipative forces scale with the laser intensity, while the dissipative ones can be suppressed by large laser detunings ($|\Delta_c| \gg \kappa$ [104]), resulting in even more prolonged relaxation times. In this regime, it would be interesting to verify whether prethermalization due to conservative (dispersive) forces might be dominant.

Bibliography

[1] E. A. Cornell and C. E. Wieman, *Nobel Lecture: Bose-Einstein condensation in a dilute gas, the first 70 years and some recent experiments*, Rev. Mod. Phys. **74**, 875 (2002).

[2] W. Ketterle, *Nobel lecture: When atoms behave as waves: Bose-Einstein condensation and the atom laser*, Rev. Mod. Phys. **74**, 1131 (2002).

[3] D. J. Wineland and W. M. Itano, *Laser cooling of atoms*, Phys. Rev. A **20**, 1521 (1979).

[4] S. Stenholm, *The semiclassical theory of laser cooling*, Rev. Mod. Phys. **58**, 699 (1986).

[5] P. D. Lett, W. D. Phillips, S. L. Rolston, C. E. Tanner, R. N. Watts, and C. I. Westbrook, *Optical molasses*, J. Opt. Soc. Am. B **6**, 2084 (1989).

[6] C. N. Cohen-Tannoudji, *Nobel Lecture: Manipulating atoms with photons*, Rev. Mod. Phys. **70**, 707 (1998).

[7] W. D. Phillips, *Nobel Lecture: Laser cooling and trapping of neutral atoms*, Rev. Mod. Phys. **70**, 721 (1998).

[8] S. Chu, *Nobel Lecture: The manipulation of neutral particles*, Rev. Mod. Phys. **70**, 685 (1998).

[9] R. Grimm, M. Weidemüller, and Y. B. Ovchinnikov, *Optical Dipole Traps for Neutral Atoms*, Adv. At. Mol. Opt. Phys. **42**, 95 (2000).

[10] H. J. Metcalf and P. van der Straten, *Laser cooling and trapping of atoms*, J. Opt. Soc. Am. B **20**, 887 (2003).

[11] I. Bloch, J. Dalibard, and W. Zwerger, *Many-body physics with ultracold gases*, Rev. Mod. Phys. **80**, 885 (2008).

[12] P. Horak, G. Hechenblaikner, K. M. Gheri, H. Stecher, and H. Ritsch, *Cavity-Induced Atom Cooling in the Strong Coupling Regime*, Phys. Rev. Lett. **79**, 4974 (1997).

[13] P. W. H. Pinkse, T. Fischer, P. Maunz, and G. Rempe, *Trapping an atom with single photons*, Nature **404**, 365 (2000).

[14] P. Domokos and H. Ritsch, *Mechanical effects of light in optical resonators*, J. Opt. Soc. Am. B **20**, 1098 (2003).

[15] J. McKeever, J. R. Buck, A. D. Boozer, A. Kuzmich, H.-C. Nägerl, D. M. Stamper-Kurn, and H. J. Kimble, *State-Insensitive Cooling and Trapping of Single Atoms in an Optical Cavity*, Phys. Rev. Lett. **90**, 133602 (2003).

[16] P. Maunz, T. Puppe, I. Schuster, N. Syassen, P. W. H. Pinkse, and G. Rempe, *Cavity cooling of a single atom*, Nature **428**, 50 (2004).

[17] K. Murr, *Large Velocity Capture Range and Low Temperatures with Cavities*, Phys. Rev. Lett. **96**, 253001 (2006).

[18] H. Ritsch, P. Domokos, F. Brennecke, and T. Esslinger, *Cold atoms in cavity-generated dynamical optical potentials*, Rev. Mod. Phys. **85**, 553 (2013).

[19] M. Aspelmeyer, T. J. Kippenberg, and F. Marquardt, *Cavity optomechanics*, Rev. Mod. Phys. **86**, 1391 (2014).

[20] J. Larson, S. Fernández-Vidal, G. Morigi, and M. Lewenstein, *Quantum stability of Mott-insulator states of ultracold atoms in optical resonators*, New J. Phys. **10**, 045002 (2008).

[21] A. T. Black, J. K. Thompson, and V. Vuletić, *Collective light forces on atoms in resonators*, J. Phys. B **38**, S605 (2005).

[22] B. Nagorny, Th. Elsässer, and A. Hemmerich, *Collective Atomic Motion in an Optical Lattice Formed Inside a High Finesse Cavity*, Phys. Rev. Lett. **91**, 153003 (2003).

[23] S. Gupta, K. L. Moore, K. W. Murch, and D. M. Stamper-Kurn, *Cavity Nonlinear Optics at Low Photon Numbers from Collective Atomic Motion*, Phys. Rev. Lett. **99**, 213601 (2007).

[24] S. Ritter, F. Brennecke, K. Baumann, T. Donner, C. Guerlin, and T. Esslinger, *Dynamical coupling between a Bose-Einstein condensate and a cavity optical lattice*, Appl. Phys. B **95**, 213 (2009).

[25] M. Xu, D. A. Tieri, E. C. Fine, J. K. Thompson, and M. J. Holland, *Synchronization of Two Ensembles of Atoms*, Phys. Rev. Lett. **113**, 154101 (2014).

[26] E. Tesio, G. R. M. Robb, G.-L. Oppo, P. M. Gomes, T. Ackemann, G. Labeyrie, R. Kaiser, and W. J. Firth, *Self-organization in cold atomic gases: a synchronization perspective*, Phil. Trans. R. Soc. A **372**, 20140002 (2014).

[27] C. von Cube, S. Slama, D. Kruse, C. Zimmermann, Ph. W. Courteille, G. R. M. Robb, N. Piovella, and R. Bonifacio, *Self-Synchronization and Dissipation-Induced Threshold in Collective Atomic Recoil Lasing*, Phys. Rev. Lett. **93**, 083601 (2004).

[28] R. Bonifacio and L. De Salvo, *Collective atomic recoil laser (CARL) optical gain without inversion by collective atomic recoil and self-bunching of two-level atoms*, Nucl. Instrum. Methods Phys. Res., Sect. A **341**, 360 (1994).

[29] G. Labeyrie, E. Tesio, P. M. Gomes, G.-L. Oppo, W. J. Firth, G. R. M. Robb, A. S. Arnold, R. Kaiser, and T. Ackemann, *Optomechanical self-structuring in a cold atomic gas*, Nature Photonics **8**, 321 (2014).

[30] G. R. M. Robb, E. Tesio, G.-L. Oppo, W. J. Firth, T. Ackemann, and R. Bonifacio, *Quantum Threshold for Optomechanical Self-Structuring in a Bose-Einstein Condensate*, Phys. Rev. Lett. **114**, 173903 (2015).

[31] P. Münstermann, T. Fischer, P. Maunz, P. W. H. Pinkse, and G. Rempe, *Observation of Cavity-Mediated Long-Range Light Forces between Strongly Coupled Atoms*, Phys. Rev. Lett. **84**, 4068 (2000).

[32] F. Dimer, B. Estienne, A. S. Parkins, and H. J. Carmichael, *Proposed realization of the Dicke-model quantum phase transition in an optical cavity QED system*, Phys. Rev. A **75**, 013804 (2007).

[33] R. Bachelard, T. Manos, P. de Buyl, F. Staniscia, F. S. Cataliotti, G. De Ninno, D. Fanelli, and N. Piovella, *Experimental perspectives for systems based on long-range interactions*, J. Stat. Mech. (2010) P06009.

[34] M. P. Baden, K. J. Arnold, A. L. Grimsmo, S. Parkins, and M. D. Barrett, *Realization of the Dicke Model Using Cavity-Assisted Raman Transitions*, Phys. Rev. Lett. **113**, 020408 (2014).

[35] A. Campa, T. Dauxois, and S. Ruffo, *Statistical mechanics and dynamics of solvable models with long-range interactions*, Phys. Rep. **480**, 57 (2009).

[36] J. A. Acebrón, L. L. Bonilla, C. J. Pérez Vicente, F. Ritort, and R. Spigler, *The Kuramoto model: A simple paradigm for synchronization phenomena*, Rev. Mod. Phys. **77**, 137 (2005).

[37] K. Baumann, C. Guerlin, F. Brennecke, and T. Esslinger, *Dicke quantum phase transition with a superfluid gas in an optical cavity*, Nature **464**, 1301 (2010).

[38] D. Nagy, G. Kónya, G. Szirmai, and P. Domokos, *Dicke-Model Phase Transition in the Quantum Motion of a Bose-Einstein Condensate in an Optical Cavity*, Phys. Rev. Lett. **104**, 130401 (2010).

[39] D. Nagy, G. Szirmai, and P. Domokos, *Critical exponent of a quantum-noise-driven phase transition: The open-system Dicke model*, Phys. Rev. A **84**, 043637 (2011).

[40] P. Horak and H. Ritsch, *Scaling properties of cavity-enhanced atom cooling*, Phys. Rev. A **64**, 033422 (2001).

[41] H. W. Chan, A. T. Black, and V. Vuletić, *Observation of Collective-Emission-Induced Cooling of Atoms in an Optical Cavity*, Phys. Rev. Lett. **90**, 063003 (2003).

[42] A. Vukics and P. Domokos, *Simultaneous cooling and trapping of atoms by a single cavity-field mode*, Phys. Rev. A **72**, 031401(R) (2005).

[43] W. Niedenzu, T. Grießer, and H. Ritsch, *Kinetic theory of cavity cooling and self-organisation of a cold gas*, Europhys. Lett. **96**, 43001 (2011).

[44] O. S. Mishina, *Cavity cooling of an atomic array*, New J. Phys. **16**, 033021 (2014).

[45] P. Domokos and H. Ritsch, *Collective Cooling and Self-Organization of Atoms in a Cavity*, Phys. Rev. Lett. **89**, 253003 (2002).

[46] D. Meiser and M. J. Holland, *Steady-state superradiance with alkaline-earth-metal atoms*, Phys. Rev. A **81**, 033847 (2010).

[47] K. Baumann, R. Mottl, F. Brennecke, and T. Esslinger, *Exploring Symmetry Breaking at the Dicke Quantum Phase Transition*, Phys. Rev. Lett. **107**, 140402 (2011).

[48] K. J. Arnold, M. P. Baden, and M. D. Barrett, *Self-Organization Threshold Scaling for Thermal Atoms Coupled to a Cavity*, Phys. Rev. Lett. **109**, 153002 (2012).

[49] M. Buchhold, P. Strack, S. Sachdev, and S. Diehl, *Dicke-model quantum spin and photon glass in optical cavities: Nonequilibrium theory and experimental signatures*, Phys. Rev. A **87**, 063622 (2013).

[50] Emanuele G. Dalla Torre, S. Diehl, M. D. Lukin, S. Sachdev and P. Strack, *Keldysh approach for nonequilibrium phase transitions in quantum optics: Beyond the Dicke model in optical cavities*, Phys. Rev. A **87**, 023831 (2013).

[51] L. M. Sieberer, M. Buchhold, and S. Diehl, *Keldysh Field Theory for Driven Open Quantum Systems*, preprint arXiv:1512.00637 (2015).

[52] M. C. Cross and P. C. Hohenberg, *Pattern formation outside of equilibrium*, Rev. Mod. Phys. **65**, 851 (1993).

[53] M. J. Bhaseen, J. Mayoh, B. D. Simons, and J. Keeling, *Dynamics of nonequilibrium Dicke models*, Phys. Rev. A **85**, 013817 (2012).

[54] M. Antoni and S. Ruffo, *Clustering and relaxation in Hamiltonian long-range dynamics*, Phys. Rev. E **52**, 2361 (1995).

[55] K. Jain, F. Bouchet, and D. Mukamel, *Relaxation times of unstable states in systems with long range interactions*, J. Stat. Mech. (2007) P11008.

[56] M. Joyce and T. Worrakitpoonpon, *Quasistationary states in the self-gravitating sheet model*, Phys. Rev. E **84**, 011139 (2011).

[57] Y. Levin, R. Pakter, F. B. Rizzato, T. N. Teles, and F. P. C. Benetti, *Nonequilibrium statistical mechanics of systems with long-range interactions*, Phys. Rep. **535**, 1 (2014).

[58] T. M. Rocha Filho, A. E. Santana, M. A. Amato, and A. Figueiredo, *Scaling of the dynamics of homogeneous states of one-dimensional long-range interacting systems*, Phys. Rev. E **90**, 032133 (2014).

[59] S. Gupta and D. Mukamel, *Slow Relaxation in Long-Range Interacting Systems with Stochastic Dynamics*, Phys. Rev. Lett. **105**, 040602 (2010).

[60] P.-H. Chavanis, F. Baldovin, and E. Orlandini, *Noise-induced dynamical phase transitions in long-range systems*, Phys. Rev. E **83**, 040101 (2011).

[61] B. Olmos, I. Lesanovsky, and J. P. Garrahan, *Facilitated Spin Models of Dissipative Quantum Glasses*, Phys. Rev. Lett. **109**, 020403 (2012).

[62] P. H. Chavanis, *The Brownian mean field model*, Eur. Phys. J. B **87**, 120 (2014).

[63] C. Nardini, S. Gupta, S. Ruffo, T. Dauxois, and F. Bouchet, *Kinetic theory of nonequilibrium stochastic long-range systems: phase transition and bistability*, J. Stat. Mech. (2012) P12010.

[64] S. Schütz and G. Morigi, *Prethermalization of Atoms Due to Photon-Mediated Long-Range Interactions*, Phys. Rev. Lett. **113**, 203002 (2014).

[65] R. Frisch, *Experimenteller Nachweis des Einsteinschen Strahlungsrückstoßes*, Zeitschrift für Physik **86**, 42 (1933).

[66] J. K. Asbóth, P. Domokos, H. Ritsch, and A. Vukics, *Self-organization of atoms in a cavity field: Threshold, bistability, and scaling laws*, Phys. Rev. A **72**, 053417 (2005).

[67] F. Brennecke, R. Mottl, K. Baumann, R. Landig, T. Donner, and T. Esslinger, *Real-time observation of fluctuations at the driven-dissipative Dicke phase transition*, PNAS **110**, 11763 (2013).

[68] S. Fernández-Vidal, G. De Chiara, J. Larson, and G. Morigi, *Quantum ground state of self-organized atomic crystals in optical resonators*, Phys. Rev. A **81**, 043407 (2010).

[69] A. T. Black, H. W. Chan, and V. Vuletić, *Observation of Collective Friction Forces due to Spatial Self-Organization of Atoms: From Rayleigh to Bragg Scattering*, Phys. Rev. Lett. **91**, 203001 (2003).

[70] R. Mottl, F. Brennecke, K. Baumann, R. Landig, T. Donner, and T. Esslinger, *Roton-Type Mode Softening in a Quantum Gas with Cavity-Mediated Long-Range Interactions*, Science **336**, 1570 (2012).

[71] F. Piazza and P. Strack, *Quantum kinetics of ultracold fermions coupled to an optical resonator*, Phys. Rev. A **90**, 043823 (2014).

[72] R. Landig, F. Brennecke, R. Mottl, T. Donner, and T. Esslinger, *Measuring the dynamic structure factor of a quantum gas undergoing a structural phase transition*, Nature Communications **6**, 7046 (2015).

[73] F. Piazza and H. Ritsch, *Self-Ordered Limit Cycles, Chaos, and Phase Slippage with a Superfluid inside an Optical Resonator*, Phys. Rev. Lett. **115**, 163601 (2015).

[74] S. Schütz, H. Habibian, and G. Morigi, *Cooling of atomic ensembles in optical cavities: Semiclassical limit*, Phys. Rev. A **88**, 033427 (2013).

[75] P. Domokos, P. Horak, and H. Ritsch, *Semiclassical theory of cavity-assisted atom cooling*, J. Phys. B **34**, 187 (2001).

[76] L. D. Landau and E. M. Lifshitz, *Statistical Physics* (Pergamon, Oxford, U.K., 1958).

[77] S. Schütz, S. B. Jäger, and G. Morigi, *Thermodynamics and dynamics of atomic self-organization in an optical cavity*, Phys. Rev. A **92**, 063808 (2015).

[78] S. Schütz, S. B. Jäger, and G. Morigi, *Dissipation-assisted prethermalization in long-range interacting atomic ensembles*, submitted to Phys. Rev. Lett.; see also arXiv:1512.05243 (preprint), *Relaxation after quenches in systems with photon-mediated long-range interactions* (This manuscript has been substantially revised during the review process).

[79] M. Joyce, J. Morand, and P. Viot, *Attractor nonequilibrium stationary states in perturbed long-range interacting systems*, Phys. Rev. E **93**, 052129 (2016).

[80] W. P. Schleich, *Quantum Optics in Phase Space* (Wiley-VCH, Berlin, 2001), First edition.

[81] H. Risken, *The Fokker-Planck Equation* (Springer-Verlag, Berlin, 1989), Second edition.

[82] W. Rümelin, *Numerical Treatment of Stochastic Differential Equations*, SIAM (Soc. Ind. Appl. Math.) J. Numer. Anal. **19**, 604 (1982).

[83] P. E. Kloeden and E. Platen, *Numerical solution of stochastic differential equations* (Springer-Verlag, Berlin, 1992), First edition.

[84] G. Hechenblaikner, M. Gangl, P. Horak, and H. Ritsch, *Cooling an atom in a weakly driven high-Q cavity*, Phys. Rev. A **58**, 3030 (1998).

[85] R. M. Sandner, W. Niedenzu, and H. Ritsch, *Subrecoil cavity cooling towards degeneracy: A numerical study*, Europhys. Lett. **104**, 43001 (2013).

[86] V. Vuletić and S. Chu, *Laser Cooling of Atoms, Ions, or Molecules by Coherent Scattering*, Phys. Rev. Lett. **84**, 3787 (2000).

[87] W. Niedenzu, S. Schütz, H. Habibian, G. Morigi, and H. Ritsch, *Seeding patterns for self-organization of photons and atoms*, Phys. Rev. A **88**, 033830 (2013).

[88] S. B. Jäger, S. Schütz, and G. Morigi, *Mean-field theory of atomic self-organization in optical cavities*, accepted for publication in Phys. Rev. A; see also arXiv:1603.05148 (preprint).

[89] J. K. Asbóth, P. Domokos, and H. Ritsch, *Correlated motion of two atoms trapped in a single-mode cavity field*, Phys. Rev. A **70**, 013414 (2004).

[90] M. Joyce, J. Morand, F. Sicard, and P. Viot, *Scaling Quasistationary States in Long-Range Systems with Dissipation*, Phys. Rev. Lett. **112**, 070602 (2014).

[91] M. Xu, S. B. Jäger, S. Schütz, J. Cooper, G. Morigi, and M. J. Holland, *Supercooling of Atoms in an Optical Resonator*, Phys. Rev. Lett. **116**, 153002 (2016).

[92] D. Meiser and M. J. Holland, *Intensity fluctuations in steady-state superradiance*, Phys. Rev. A **81**, 063827 (2010).

[93] T. Salzburger and H. Ritsch, *Atomic Self-Trapping Induced by Single-Atom Lasing*, Phys. Rev. Lett. **93**, 063002 (2004).

[94] T. Salzburger, P. Domokos, and H. Ritsch, *Theory of a single-atom laser including light forces*, Phys. Rev. A **72**, 033805 (2005).

[95] T. Salzburger and H. Ritsch, *Lasing and cooling in a finite-temperature cavity*, Phys. Rev. A **74**, 033806 (2006).

[96] J. Dalibard and C. Cohen-Tannoudji, *Atomic motion in laser light: connection between semiclassical and quantum descriptions*, J. Phys. B **18**, 1661 (1985).

[97] H. Habibian, S. Zippilli, and G. Morigi, *Quantum light by atomic arrays in optical resonators*, Phys. Rev. A **84**, 033829 (2011).

[98] B. Öztop, M. Bordyuh, Ö. E. Müstecaplıoğlu, and H. E. Türeci, *Excitations of optically driven atomic condensate in a cavity: theory of photodetection measurements*, New J. Phys. **14**, 085011 (2012).

[99] M. Kulkarni, B. Öztop, and H. E. Türeci, *Cavity-Mediated Near-Critical Dissipative Dynamics of a Driven Condensate*, Phys. Rev. Lett. **111**, 220408 (2013).

[100] J. Barré, F. Bouchet, T. Dauxois, S. Ruffo, and Y. Y. Yamaguchi, *The Vlasov equation and the Hamiltonian mean-field model*, Physica A **365**, 177 (2006).

[101] T. Grießer, H. Ritsch, M. Hemmerling, and G. R. M. Robb, *A Vlasov approach to bunching and selfordering of particles in optical resonators*, Eur. Phys. J. D **58**, 349 (2010).

[102] J. Klinder, H. Keßler, M. Wolke, L. Mathey, and A. Hemmerich, *Dynamical phase transition in the open Dicke model*, PNAS **112**, 3290 (2015).

[103] S. Rist and G. Morigi, *Homodyne detection of matter-wave fields*, Phys. Rev. A **85**, 053635 (2012).

[104] R. Landig, L. Hruby, N. Dogra, M. Landini, R. Mottl, T. Donner, and T. Esslinger, *Quantum phases from competing short- and long-range interactions in an optical lattice*, Nature **532**, 476 (2016).

Danksagung

Mein besonderer Dank gilt Prof. Dr. Giovanna Morigi, insbesondere für die Möglichkeit eine Doktorarbeit über dieses Thema zu schreiben, ihr Vertrauen und ihre Hingabe, mich wissenschaftlich zu fordern und zu fördern. Ein ständiger Wegbegleiter, sowohl auf als auch neben dem Platz, war für mich Christian, ich wünsche dir weiterhin viel Erfolg! Ich danke vor allem Hessam und Simon, nicht zuletzt für zahlreiche inspirierende wissenschaftliche Diskussionen. Zudem konnte ich mich sehr glücklich schätzen, dass ich eine lange Zeit ein Büro mit Susanne teilen durfte. Sie war stets hilfsbereit und aufmerksam, meine Kollegen dürften diese Ansicht mehr als teilen. Unter diesen möchte ich mich, in Besonderem für die jüngere Zeit, bei Ralf, Luigi, Katharina und Florian bedanken. Auch meine Anfangszeit wurde mir durch die herzliche Unterstützung von Jens und Sergey leicht gemacht. Insgesamt hatte ich das Vergnügen eine sehr offene, eingeschworene und sympathische Arbeitsgruppe anzutreffen, nicht zuletzt durch unvergessene Maiausflüge. Einen großen Anteil an diesem Zustand hatte ohne Zweifel Marc Bienert, Essenszeiten sollten eingehalten werden. Ein dickes Dankeschön für die intensive Zeit sowohl an Cecilia, Endre, Oxana, Mossy, Mauricio, Rick und Bruno als auch an Rebecca, Tim, Andreas, Tristan, Timo und Sascha. Es ist klar, dass solche Gruppen nicht ohne bürokratischen Beistand funktionieren können, wie er von Monika Francois und Ingeborg Michel in herzlicher Form gegeben wurde.
Für einen angeregten wissenschaftlichen Austausch während der letzten Jahre danke ich insbesondere Wolfgang, Francesco, Cesare, Reza, Matthias Wolke, Malte Henkel und Giovanni Manfredi. Great thanks to Minghui and Murray Holland for your kind hospitality!
Für die Begleitung und Unterstützung, besonders in schwierigeren Zeiten, danke ich meinen Eltern Eva und Georg als auch meinen Brüdern Michael und Markus. Ich bin sehr froh, dass wir einander haben. Gute Freundschaften sind selten und unersetzlich, danke Marco und Sebastian. Ich habe keine Ahnung, ob ich so viel Geduld und Verständnis mit mir in nicht selten stressigen Phasen hätte aufbringen können, umso mehr danke ich Katja dafür, dass sie es getan hat und nicht zuletzt durch Unterstützung im Alltag in jeglicher Hinsicht zum Abschluss und möglichen Gelingen dieser Arbeit beigetragen hat.